Analysis and Modelling of Massive MIMO Mobile Channels with Beam Selection

Henry George Brice

A dissertation submitted to the University of Bristol in accordance with the requirements for the award of the degree of Doctor of Philosophy in the Faculty of Engineering, Department of Electrical & Electronic Engineering

June 2023

Word count (excluding references, appendices and list of contents): 47,422

Abstract

The demand for capacity within existing mobile networks continues to increase as more subscribers and more devices communicate and as data-rich applications become more popular. The evolving 5G telecommunications standards aim to respond to such demand. A promising approach to increasing capacity and reliability within the context of 5G is Massive Multiple-Input Multiple-Output (MIMO) where many transmit antennas are used relative to the number of users, thus providing a greater opportunity to use the spatial characteristics of the channel for spatial diversity and multiplexing.

This thesis presents an analysis of the propagation environments of Massive MIMO. Factors specific to Massive MIMO are investigated, including slow-fading across arrays and spherical wavefronts, as well as standard measures for wireless communications systems. A study of dynamic Massive MIMO channels is also presented, showing how channels vary in time within busy environments. A time-series model based on the channel condition number is proposed for a statistics-based simulation of the channel. The propagation studies described in this thesis inform the investigation of different practical applications of Massive MIMO technology. One such application is related to the synchronisation process within 5G systems, where synchronisation blocks consisting of the physical broadcast channel and synchronisation signals are sent by the base station to allow users to obtain synchronisation information when connecting to a network. Each block can be sent with a different beam configuration, the collection of which forms a grid of beams over the coverage area. The optimal grid of beams varies by coverage area, so this thesis presents a study to obtain such configurations through a combination of practical network data, propagation models and statistical distributions of users, creating a data set of user distributions with optimal beams.

These data then form the basis for the development of a method to simplify the selection of beam configurations. The final chapter describes a study of the effects of beamforming on Massive MIMO performance, comparing beamforming systems with systems that are dependent only on the multipath propagation characteristics of the environment within which the system operates. The study is based on 3D ray-tracing propagation models of Bristol, built from open-source map data. The Marzetta

approach to Massive MIMO downlink transmission using different forms of linear processing, which makes no reference to specific beam configurations, is modelled and the performance analysed in relation to the Error Vector Magnitude, which provides an indication of modulation schemes that can be supported and therefore the expected throughput. The results are compared to similar systems with beams directed towards the mobile users, as well as other systems employing a beamforming strategy.

Dedication and acknowledgements

This work is dedicated to my mother, with thanks for her unfailing support and encouragement.

I would like to thank my supervisors Professor Mark Beach and Dr Geoff Hilton, for their support, guidance and advice during my research.

I would also like to thank my colleagues and fellow students in the Communication Systems and Networks Group for their companionship and collegiality.

I am grateful to my colleagues at BT for their understanding and encouragement as I continued my studies alongside working in the Self-Learning Networks Group, and particular thanks go to the head of the research group Arjun Parekh.

Finally, my heartfelt gratitude to my friends and family for their practical and emotional support over the years. Special mention goes to Matthew Taylor and Zaki Ahmed, without whose advice and inspiration this work would not have been possible.

Author's declaration

I declare that the work in this dissertation was carried out in accordance with the requirements of the University's *Regulations and Code of Practice for Research Degree Programmes* and that it has not been submitted for any other academic award. Except where indicated by specific references in the text, the work is the candidate's own work. Work done in collaboration with, or with the assistance of, others, is indicated as such. Any views expressed in the dissertation are those of the author.

SIGNED 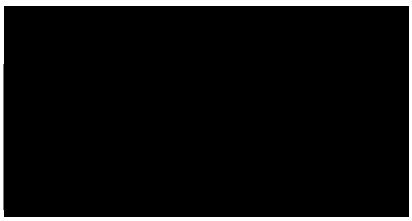 DATE 30 June 2023

Contents

List of figures

List of tables

Glossary of acronyms

AIMM	Autonomous Industrial Mobile Manipulators
AoA	Angle of arrival
AoD	Angle of departure
AM	Amplitude modulation
AP	Antenna port
BER	Bit error-rate
BS	Base station
COST	European Cooperation in Science and Technology
CSI	Channel state information
dB	Decibel
dBm	Decibels per minute
DCN	Demmel condition number
EVM	Error vector magnitude
FDD	Frequency division duplexing
FM	Frequency modulation
GO	Geometrical optics
GPS	Global positioning system
GSCM	Geometry-based stochastic channel models
iid	independent and identically distributed
KPI	Key performance indicator
Lidar	Light detection and ranging
LoS	Line of sight
LTE	Long-term evolution
MDT	Minimisation of drive test
MIMO	Multiple-input Multiple-output
ML	Machine learning
MaxL	Maximum likelihood
MMSE	Minimum mean squared error
MNO	Mobile network operator
MPC	Multi-path component

MRT	Maximum ratio transmission
MS	Mobile station
OFDM	Orthogonal frequency-division multiplexing
OFDMA	Orthogonal frequency-division multiple access
O-RAN	Open radio access network
PAL	Phase alternate line
PBCH	Physical broadcast channel
pdf	Probability density function
PSS	Primary synchronisation signal
PU	Primary user
PWM	Pulse width modulation
QAM	Quadrature amplitude modulation
QoS	Quality of service
RACH	Random-access channel
RF	Radio frequency
RMS	Root mean square
RSRP	Reference signal received power
RSRQ	Reference signal received quality
RSSI	Received signal strength indicator
SA	Simulated annealing
SCN	Standard condition number
SC-FDMA	Single-carrier frequency division multiple access
SINR	Signal to interference plus noise ratio
SIR	Signal to interference ratio
SNR	Signal to noise ratio
SS	Synchronisation signal
SSS	Secondary synchronisation signal
SS Block	Synchronisation signal block
SVD	Singular value decomposition
TDD	Time division duplexing
ToA	Time of arrival

UE	User equipment
ULA	Uniform linear array
VR	Visibility region
WiMAX	Worldwide Interoperability for Microwave Access
ZF	Zero-forcing

List of symbols

1_{kn}	Indicator function (1 when k = n, 0 otherwise)
$A_n(\Theta)$	Beam pattern
$D_n(\Theta_k)$	Relative directivity of beam
$D_{Rayleigh}$	Rayleigh distance
h_{ij}	Response between the i^{th} and j^{th} receive and transmit antennas respectively
I_k	Inter-beam interference
N_0	Transmit power noise term
N_r	Number of receive antennas
N_t	Number of transmit antennas
$p_s(s_1, \dots, s_{N_t})$	Distribution of input symbols $\boldsymbol{s}$ for each N_t transmit antennas
R_k	Data rate
$\boldsymbol{R}_{ss}$	Covariance matrix
s_j	Symbols transmitted from the j^{th} transmit antenna
y_i	Received signal at the i^{th} antenna
z_i	Noise signal at the i^{th} receive antenna
B_k	Lage scale fading between k^{th} terminal and BS
θ_r	Receive antenna elevation angle
θ_t	Transmit antenna elevation angle
λ_n	N^{th} eigenvalue
ρ_{dl}	Downlink SINR
ρ_k	Distance from cell centre to user k
ϕ_r	Receive antenna azimuth
ϕ_t	Transmit antenna azimuth
A	Amplitude
$\boldsymbol{a}$	Spatial signature
B	Shift operator
C	Channel capacity
c	Speed of light

d	Distance
$\boldsymbol{f}$	Precoding vector
$\boldsymbol{F}$	Precoding matrix
G	iid random fading matrix
$\boldsymbol{H}$	Channel matrix
$h(t)$	Complex impulse response
$H(X)$	Shannon entropy of random variable X
I	Identity matrix
$I(X:Y)$	Mutual information between random variables X and Y
j	Imaginary unit
J	Antenna weightings
k	Mobile user
$\boldsymbol{L}$	Lower triangular matrix
L	Largest distance between two antenna elements in an array
n	Index of refraction
N	Number of beams
$\emptyset(B)$	Autoregressive operator
P	Transmit power
$\boldsymbol{Q}$	Orthogonal matrix
$\boldsymbol{q}$	Information bearing transmit signal vector
R	Correlation matrix
$\boldsymbol{s}$	Transmit signal vector
U	Eigenbases
v	Time series within autoregressive moving average process
$\boldsymbol{v}$	Beam selection vector
W	Bandwidth
w	Random drawing from a fixed distribution
$\mathcal{X}$	RSRP matrix
$\boldsymbol{y}$	Receive signal vector
$\mathcal{Y}$	Beam selection matrix
$\boldsymbol{z}$	Noise vector

$\boldsymbol{z}$	Optimisation parameter
$\boldsymbol{Z}$	Normalised channel estimate
α	Path loss exponent
$\boldsymbol{\gamma}$	Channel estimates
δ	Delta function
Δ	Normalised separation of antenna elements
η	Power control coefficient
θ	Incident angle
ϑ	Phase angle
$\Theta(B)$	Moving average operator
λ	Wavelength
σ	Variance
τ	Arrival time
Φ	Incoming wave angle of incidence
Ω	Power coupling matrix

1: Introduction

Throughout the history of electronic communication, the question of how to develop communications infrastructure that is able to meet the performance demands of its users and potential users has been a relevant concern, and one that has only increased up until the present day. The ability of a network to meet demand by providing a sufficient level of possible data throughput is known as its capacity, a key concept within telecommunications research. Related to this is the concept of spectral efficiency, which is discussed later in this thesis.

At the dawn of the use of wireless systems to communicate electronically, early radio transmitters were greatly limited in terms of their available frequency range and, due to limitations in the circuitry of the time, because of their inability to occupy a narrow bandwidth within the available frequency range [1].

While such a situation may have been barely acceptable right at the start of the use of electronic communications, when the number of total users was very limited due to the cost and availability of equipment, it soon became apparent that such a situation would not be sustainable. Beginning in the 1910s, radio users that were not safety critical were required to occupy higher frequencies and to not cause interference with other stations on lower frequencies [2]. Research was conducted to attempt to cause existing types of transmitters to occupy less bandwidth and to display increased frequency stability; however, the increasing availability of thermionic valves greatly advanced this process [3]. Such components can be used to create circuits that provide continuous waves for transmission and modulation, with modulation being motivated by the requirement for audio transmission and broadcasting [4].

This serves to illustrate some crucial components in determining the capacity of a radio system. Although the notion of capacity would not be formalised for many years, it is already apparent that the capacity of a wireless telecommunications system is related to the bandwidth available to it and to the bandwidth demands of the mode or modulation scheme that it employs. It is also related to the demand, in terms of the number of telecommunication system users who wish to communicate, and the size of the messages that they wish to send and receive.

The advances in manufacturing for electronic components and in circuit design allowed for the use of higher frequencies, which provided both additional bandwidth, meaning that more users could occupy radio spectrum at the same time, and later the opportunity for transmission requiring wider bandwidth, as is the case, for example, in FM broadcasting. Both the increase in the number of users and the increase in the bandwidth requirements of transmission modes require a corresponding increase in capacity of the telecommunications. The re-use of spectrum is now of particular importance, as is the study of techniques can be developed to do this effectively.

The bandwidth consumption of modulation schemes has long been of concern for designers of telecommunications systems, especially as the requirement for voice and other audio communications developed. The original form of audio modulation, Amplitude Modulation (AM), was based on mixing an audio signal with a carrier wave, creating a signal consisting of a carrier wave whose signal varied in a way that corresponded with the original audio signal, which could then be covered from the carrier by the receiver. It was discovered [5] that, while such signals were made up of a carrier wave and two sidebands, it was possible to recover the original audio from only one sideband. Such an insight was able to reduce the bandwidth requirements for voice transmission, with the drawback that more sophisticated and expensive receivers were required to recover the transmitted signal. Such advances in reducing bandwidth can be seen in other early examples of modulation schemes. Frequency Modulation (FM), for example, was developed as a way of reducing noise within transmissions by modulating a carrier by varying its frequency, rather than its amplitude [6]. While the form of modulation used for broadcasting required considerably more bandwidth compared with standard AM, it was discovered that it was possible to transmit lower fidelity signals could be transmitted using lower bandwidth by limiting the frequency deviation, considerably lowering the bandwidth requirements.

Following World War II, a major advance in the understanding of telecommunications systems was initiated by the development of Information Theory, discussed in more detail in chapter 2 of this thesis. Information Theory describes communications in terms of statistical principles [7] and presents a formal definition of the information capacity of a communications channel. One of the major implications of this theory is

that there is an upper limit on the capacity of any communications channel, and that it is possible to express what this limit is according to certain assumptions about the channel. It formalised the notion that, when data symbols are transmitted as part of some code, that the symbol that is used should be related to the probability of such a symbol occurring, and that doing so could lead to more efficient use of the channel resources in a way that approached the capacity of the channel.

The insights from Information Theory led to a large amount of research into the development of coding schemes that could achieve the greatest data rate possible for a given telecommunications system. However, it would not be for several decades that a coding scheme that reached the capacity limit predicted by information theory was discovered [8].

Following the development of information theory and the adoption of increased use of digital coding schemes, rather than modulated analogue audio signals, modulation schemes used within a digital context became more common [9]. For example, while quadrature amplitude modulation (QAM) had been used within analogue systems, such as phase alternate line (PAL) colour TV, it also become popular within digital mobile networks [10]. QAM makes use of two carrier signals that are separated by a 90-degree phase shift. The phase angle within the complex plane can then be described by the relative differences in amplitude between the two carrier waves. In digital communications, the complex plane is divided into segments representing the digital symbol being transmitted. This increases the number of bits per carrier that can be transmitted, thus improving the capacity of systems employing such a modulation scheme.

These considerations related to capacity formed an increasingly significant part of the development of mobile telecommunications networks. Early mobile telephone systems operated as extensions of the public telephone networks [11] and operated in a similar way to other private mobile radio networks, except that individual radio telephones could be called using a telephone number that was assigned to them, with the terminals acting as an extension of the telephone network with which they were associated.

The next generations of mobile telephone communications systems, while marking the increase in frequency band usage, and hence available bandwidth, introduced

the notion of cellular communications [12]. Such an approach divides the coverage area of a network into cells, further divided into sectors, to which a user connects to access the network. Each cell would have its own limited coverage area, allowing for different cells to occupy the same frequency and bandwidth resources, a feature advantageous for the optimisation of the capacity of the network. Some cells in the network would overlap with one another, since mobile network operators (MNOs) would seek to provide network coverage across the service area, and it is not practical to create a precise boundary where one cells coverage ends and another begins. This overlap necessitates attention in the design process of the network, to reduce potential interference between cells, thus reducing network performance. It is also necessary to consider how users connect to the cells, and under what conditions they will change to a different cell. The introduction of cells to wireless communications networks is an example of how systems can be designed to re-use available radio spectrum.

The Long-Term Evolution (LTE) standards, which began to be introduced to public networks around 2010, comprised several features that are relevant to the efficient use of what had become, by that time, an increasingly crowded radio spectrum [13]. The scheme for providing multiple-access to the network, in this case orthogonal frequency division multiple access (OFDMA) was introduced to the downlink of mobile networks to provide higher data rates than existing schemes, while a related scheme, single-carrier frequency division multiple access (SC-FDMA) provided a more efficient method for the uplink side, combined with improved power consumption performance. The LTE standards also allowed for flexibility in the modulation scheme used, with several possible options available in both the uplink and the downlink. This allows for the selection of a modulation scheme that is more appropriate for the channel conditions. Additionally, LTE provided more flexibility in specifying bandwidth usage and in subcarrier spacing, which allowed for greater optimisation depending on channel conditions and also the bandwidth requirements of the services, which by then had extended beyond only voice calls to other forms of multimedia data. Greater flexibility within application of the standards was also represented in LTE's ability to support both time division duplexing (TDD) and frequency division duplexing (FDD), again allowing for the most efficient use of bandwidth resources.

One of the main characteristics within the LTE standards was the ability of mobile networks conforming to these standards to make use of multiple antennas to improve spectral efficiency, which describes the data throughput in terms of bandwidth resources. This represented the introduction of Multiple-Input Multiple-Output (MIMO) technology within public cellular mobile networks. MIMO is described in more detail in the following chapter. MIMO, as introduced in LTE, consisted of a maximum of four transmit and four receive antennas. The presence of multiple antennas at the receive and transmit end of the link allows for the use of spatial diversity, where multipath propagation is used to reduce fading experienced within the system, and spatial multiplexing, which allows multiple users to occupy the same bandwidth and frequency resources. Such technology would continue to form part of developing mobile networks, and a greater increase in the possible number of receive and transmit antennas, in the form of Massive MIMO, became part of the 5G standards, and this technology forms a major part of the topic of research for this thesis.

The necessity, from the perspective of the MNOs, for a continued increase in the capacity requirements of mobile networks originates from several sources. The number of mobile subscribers increased dramatically in the 2000s as more people obtained mobile telecommunications devices. However, since the end of that decade, the total number of subscribers has remained reasonably constant, suggesting that number of possible subscribers in the UK has reached its maximum value as a proportion of the total population. Indeed, the number of subscribers is now larger than the size of the population, indicating that many individuals subscribe more than once to the services of an MNO (Figure 1) [14].

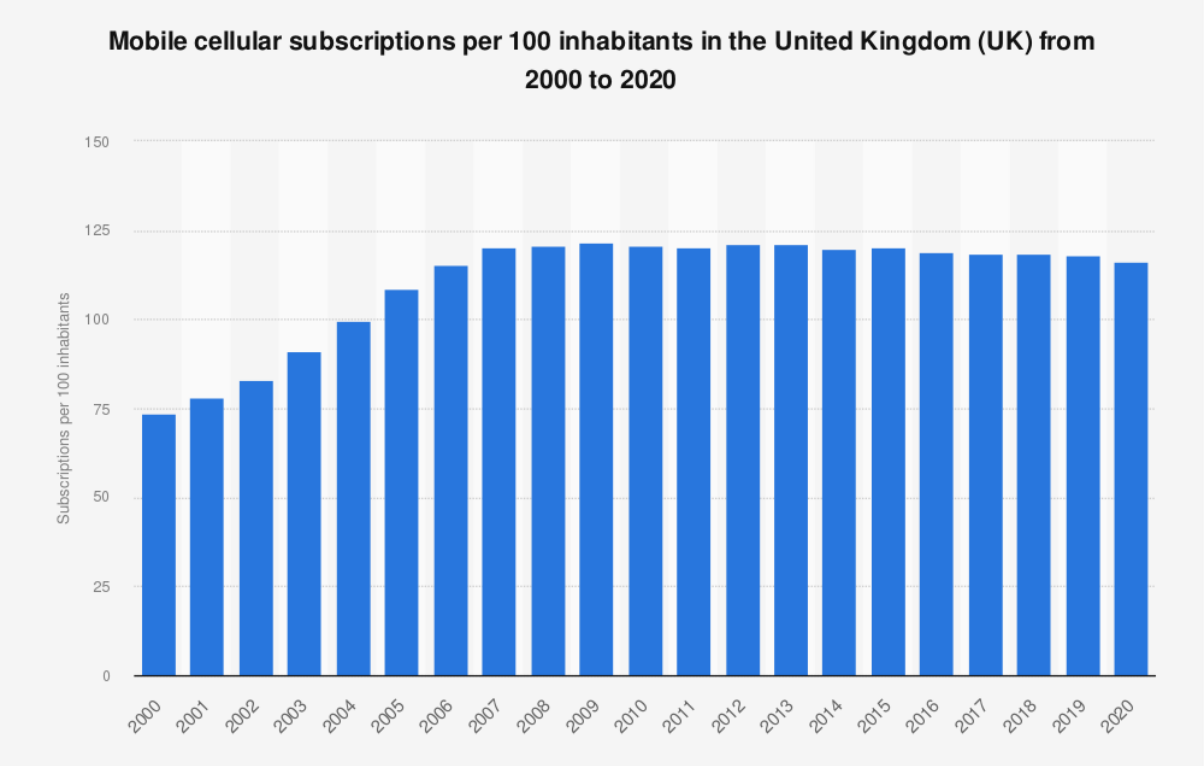

Figure 1: Mobile cellular subscriptions per 100 inhabitants in the United Kingdom (UK) from 2000 to 2020 [14]

Even though the total number of subscribers has remained fairly constant, the total consumption of data within mobile networks has not. In fact, the data demand on networks has increased greatly since 2010 (Figure 2) [15]. This increase in demand corresponds with increased usage of data rich applications within mobile networks, and the expectations of users to be able to access such applications. Consumption of digital video services and calls are a major contributing factor to the increase in data demand [15].

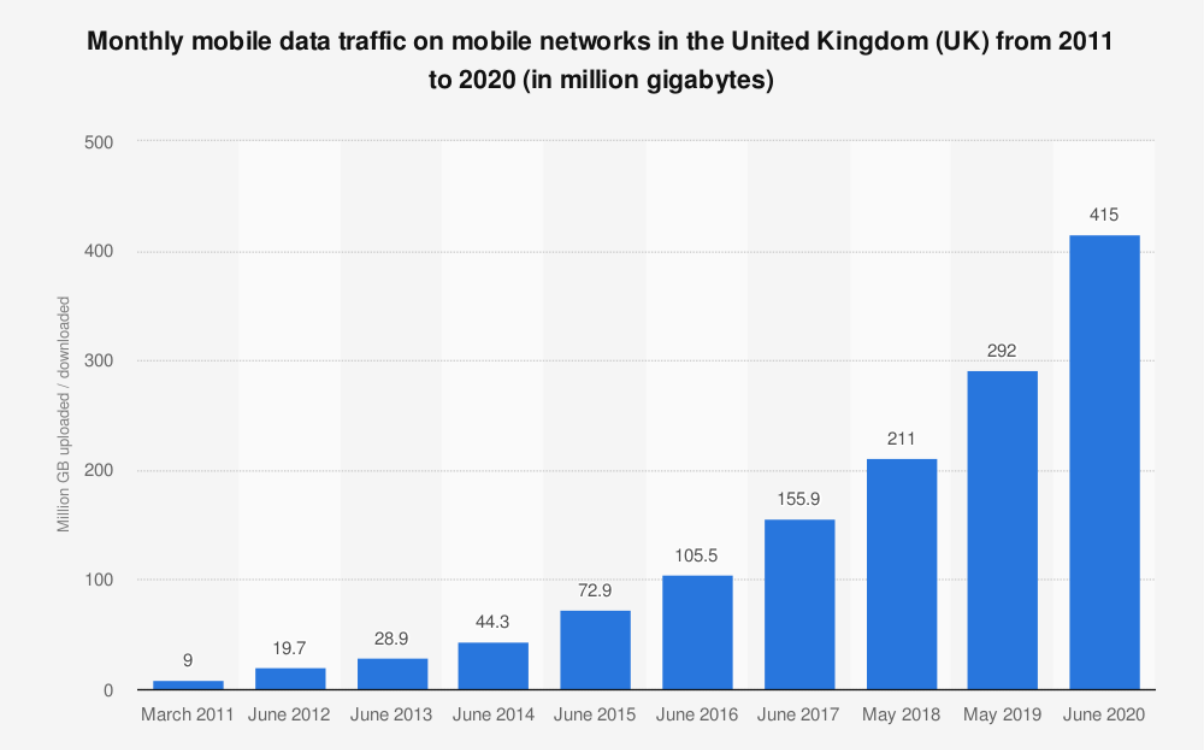

Figure 2: Monthly mobile data traffic on mobile networks in the UK from 2011 to 2020 in million gigabytes [15]

The data demand on networks is not expected to decrease in the coming years, and is actually expected to continue to accelerate. This is due not only to continued demand for data rich applications but is also influenced by the tendency for users to rely on the mobile network for services that, in the past, were more the domain of the fixed network [16]. Likewise, the increasing number of connected devices through the so-called Internet of Things (IoT) will further increase demand upon existing networks. Furthermore, 5G standards organisations anticipate a range of new and novel applications that will also affect demand being placed upon mobile networks.

1.1 Aims

The aim of this research is to identify important features within Massive MIMO channels and to apply these to create verified models that are useful for the design and deployment of networks that employ this technology. The contributions from this research are outlined below.

1.2 Research Contributions

The use of Massive MIMO within 5G networks and beyond requires the availability and understanding of suitable propagation models. This requirement is discussed in more detail in the following chapters. The main research contributions of this thesis are as follows:

- The verification of the effectiveness and importance of the use of spherical wave models when considering the design of Massive MIMO systems (section 3.8).
- The features of how Massive MIMO networks change within dynamic environments, along with how this affects the ability of the network to support multiple users (section 3.10).
- The proposition of how these features can be modelled using statistical techniques (section 3.13).
- A method for assigning broadcast beams from Massive MIMO arrays based on simple propagation models (section 4.6).
- An algorithm that allows for the fast allocation of broadcast beams within networks, that avoids the need for exhaustive searches and that could be implemented in a variety of different contexts (section 4.9).
- Information about how the concentration of a user distribution affects the allocation of the beams and the efficiency of the algorithms used (section 4.10).
- A proposal for how the relative performance of beamforming approaches with Massive MIMO can be compared with standard spatial multiplexing approaches (section 5.7.1).
- Showing that, in some environments, large variations in user position can result in only small angular changes from the perspective of the base station (BS), therefore limiting the effectiveness of beamforming under some circumstances (section 5.7.3).

1.3 Publications

Patent:

Enhanced Beam Selection for Synchronisation coverage optimisation within Mobile Networks. Filed 17 March 2023. Application numbers: EP23162563.3

GB2303906.8.

Upcoming conference paper:

Massive MIMO Beam Selection in 5G Networks using Simulated Annealing Methods. Submitted to IEEE Personal Indoor and Mobile Radio Communications (PIMRC) Conference 2023.

Conference papers:
Brice, H., Mellios, E. and Beach, M. “Analysis and Modelling of Massive MIMO Mobility Channels,” ICT, Saint-Malo, France, 2018.

Harris, P, Hasan, WB, Brice, H, Chitambira, B, Beach, M, Mellios, E, Nix, A, Armour, S & Doufexi, A, 2017, ‘An Overview of Massive MIMO Research at the University of Bristol’. In: Radio Propagation and Technologies for 5G (2016). Institution of Engineering and Technology

Other publications and presentations

Brice, H., Mellios, E. and Beach, M. “Analysis and Modelling of Massive MIMO Channels.” Presentation at CDT Conference, Bristol, September 2018.

Brice, H., Mellios, E. and Beach, M. “Analysis and Modelling of Massive MIMO Channels.” Poster presentation at Cambridge Wireless, Bristol, September 2018.

Brice, H., Mellios, E. and Beach, M. “Models for Massive MIMO Mobility Scenarios.” Presentation at CDT Conference, Bristol, September 2017.

Brice, H., Mellios, E. and Beach, M. “Models for Massive MIMO Mobility Scenarios” Presentation and Temporary Document at IRACON COST meeting, Graz, Austria, 13-14 September 2017.

Brice, H., “Massive MIMO Propagation Models.” Presentation and Temporary Document at IRACON COST meeting, Durham, UK, 4-6 October 2016.

Brice, H., Mellios, E. and Beach, M. “Massive MIMO Propagation Models.” ‘Elevator Pitch’ presentation at CDT Conference, Bristol, September 2016.

Brice, H., “Massive MIMO Propagation Models.” Presentation at UK URSI Festival of Radio Science, Manchester, UK, 16 December 2015.

1.4 Thesis Structure

This thesis begins with an overview of the relevant background research in chapter 2, preceded by an explanation of MIMO technology and the types of system models that are typically used in its descriptions. This explanation provides the theoretical background required for the research presented within this thesis. The overview of

research begins with a review of the relevant propagation models that are often used in the analysis of Massive MIMO channels. Some known issues and limitations with these approaches are then presented to provide a motivation for the research presented in the thesis. A more general description of Massive MIMO research is then presented to illustrate the state of the art and to provide a broader context for the work that is presented.

Chapter 3 presents an extensive review of Massive MIMO channels through the use of deterministic ray-tracing simulations. This includes an overview of standard parameters used to describe these channels and how the addition of more antennas (which are present within Massive MIMO technology) can affect these parameters, and how certain features such as large-scale fading become more significant with the introduction of larger arrays. The use of plane wave models is compared with the use of spherical wave models, and it is shown that a spherical wave approach can provide greater insight into the performance of Massive MIMO channels. The review of these Massive MIMO channels demonstrates how the structure of the channel can vary over time within urban environments and leads to the development of a time-series model for describing this effect.

One of the main features of Massive MIMO arrays is their ability to direct energy towards specific locations within a coverage area. This has implications for both the coverage of a mobile network and for the potential performance in terms of spectral efficiency. Chapter 4 discusses the implications in terms of coverage, presenting previous research in this area and presenting a method for effectively managing coverage within a network that employs Massive MIMO technology.

Chapter 5 discusses the management of the Massive MIMO arrays in terms of throughput and related parameters, by considering how the use of beamforming can affect the network performance either positively or negatively. The description of a method for analysing this performance is presented along with results for different types of propagation environments.

2: Sub-6GHz Massive MIMO Technology

The term Massive Multiple-Input Multiple-Output (Massive MIMO) is associated with several types of system in the research literature but, in the context of this research thesis, it signifies a MIMO wireless telecommunications system operating below 6GHz and where there is a large number of antenna elements at the BS relative to the number of UEs.

The development of accurate and efficient propagation models is essential for the design of mobile networks in order to provide a simulation of the electromagnetic environment. Several propagation models have been developed within the context of standard MIMO, including deterministic models such as ray-tracers and EM-solvers, Geometry based models and stochastic models that attempt to predict the performance of a system based on the statistical features of the channel. There are also hybrid models that combine the features of geometric and stochastic models.

These propagation models can be further classified into physical models that attempt to approximate the features of the environment itself and analytic models that attempt to model the channel matrix directly without reference to any particular channel, a popular example being correlation-based methods.

This chapter sets out to provide a background to the types of methods that have been used to model MIMO systems, along with their advantages and disadvantaged. An overview of some of the research related to later chapters of this thesis is also provided.

2.1 MIMO

In its most general sense, Multiple-Input Multiple-Output communications refer to the use of multi-path propagation to provide an enhanced channel capacity and/or enhanced reliability through the use of multiple antennas at both the input and the output of the channel [17].

The process of using multi-path to improve channel capacity is known a spatial multiplexing [18] and the process of improving reliability is known as spatial diversity [19]. The standard architecture for MIMO systems is different depending on whether the system is designed for multiplexing or diversity.

Spatial multiplexing involves a process where, following encoding and a serial-to-parallel conversion process, the resulting separate bit streams are modulated before being sent to an individual antenna element. The aim is for the receiver to be able to correctly separate the transmitted signals, after they arrive at the receiver having followed different propagation paths. The received signals are sent through a spatial multiplexing decoder that enables each of the received signals from the different paths to be analysed separately. Each of the signals are then demodulated in parallel before being passed through a parallel-to-serial converter to obtain the original bit stream (that is likely to be contaminated with errors). This bit stream can then be decoding using error correction techniques in order to recover the desired information bits. A diagram of this process is shown in Figure 3.

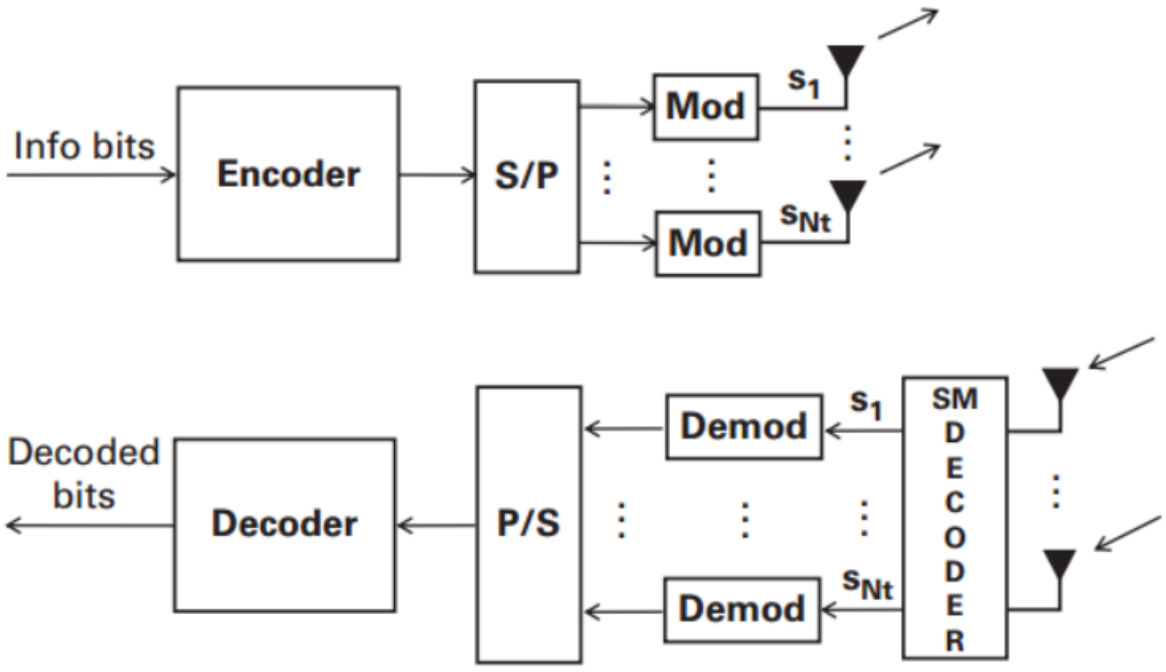

Figure 3: The process of spatial multiplexing. The upper part of the diagram shows the process for transmission and the lower part of the diagram shows the process for reception. An explanation of the various blocks is provided in the text [20]

As with the architecture for spatial multiplexing, the process for spatial diversity begins with the encoding of information bits followed by these encoded bits being

passed through a serial-to-parallel converter. The parallel bit streams, which each contain the coded bit stream, are then modulated and the output symbols are sent to the separate antennas so that each of the modulated signals can be transmitted over a particular multipath component. These signals are then received at the antennas of the receiver, which then undergo space-time decoding. The recovered signal is then demodulated and finally decoded using standard techniques in order to recover the original information bits. This process is demonstrated in Figure 4.

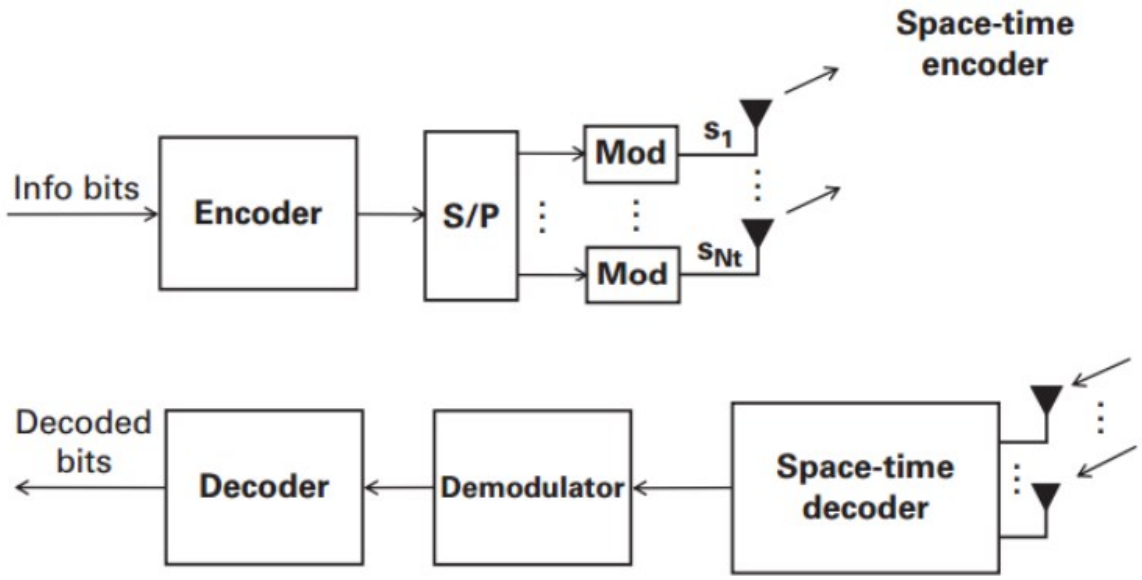

Figure 4: The process of spatial diversity. The upper part of the diagram shows the process for transmission and the lower part of the diagram shows the process for reception. An explanation of the various blocks is provided in the text [20]

2.2 System Model

The basic model for a MIMO system can be considered in terms of a channel matrix, which can be used to describe the mathematical relationship between each of the antennas present in the system [21]. The narrow-band channel (that is, where the bandwidth is below the correlation bandwidth) can be described by the mathematical expression [20].

$$y_i = \sum_{j=1}^{N_t} h_{ij} s_j + z_i \tag{2.1}$$

For i = 1, …, Nr where Nr refers to the number of receive antennas. In the above expression, y_i refers to the received signal at the i[th] receive antenna, N_t refers to the number of transmit antennas, h_{ij} is the response between the i[th] and j[th] receive and transmit antennas respectively, s_j refers to the symbols transmitted from the j[th] transmit antenna and z_i refers to the noise signal at the i[th] receive antenna. In matrix form, this equation can be expressed as

$$\boldsymbol{y} = \boldsymbol{Hs} + \boldsymbol{z} \tag{2.2}$$

Where $\boldsymbol{H}$ is called the channel matrix and is of dimension $N_t \times Nr$.

The channel capacity for a MIMO channel, as for any channel, is defined as the maximum mutual information between the input and the output of the channel [22]

$$C = max_{p(x)} I(X:Y) \tag{2.3}$$

For the input distribution $p(x)$. Here X refers to the channel input and Y refers to the channel output with I(X:Y) being the mutual information between X and Y defined as

$$I(X:Y) = H(X) + H(Y) - H(X,Y) \tag{2.4}$$

where the function H is defined as the Shannon entropy or average information

$$H(X) = -\sum_{x \in \mathrm{X}} p(x) log_2 p(x) \tag{2.5}$$

for the probability space X. An equivalent form for the mutual information is

$$I(X:Y) = H(X) - H(X|Y) \tag{2.6}$$

where $H(X|Y)$ is the conditional entropy

$$H(X|Y) = \sum_{x \in \mathrm{X}} \sum_{y \in \mathrm{Y}} p(y,x) log_2 p(x|y)$$

(2.7)

For the probability spaces X and Y.

The expression for channel capacity can be adapted to define the MIMO channel capacity more specifically as

$$C = max_{p_s} H(\boldsymbol{y}) - H(\boldsymbol{y}|\boldsymbol{s})$$

(2.8)

Where the maximum mutual information is found for each possible distribution $p_s(s_1, \dots, s_{N_t})$ of the input symbols $\boldsymbol{s}$ for each of the N_t transmit antennas. From the definition $\mathbf{y} = \boldsymbol{Hs} + \boldsymbol{z}$ it can be observed that $\boldsymbol{Hs}$ is fixed for a given channel and that the noise term $\boldsymbol{z}$ is responsible for random variations in $H(\mathbf{y}|\boldsymbol{s})$, therefore the formula for the MIMO channel capacity can be simplified to

$$C = max_{p_s} H(\boldsymbol{y}) - H(\boldsymbol{z}).$$

(2.9)

The specific expression of the MIMO capacity formula for real valued signals and expressed in bits per second while assuming Gaussian noise (see [20] for the derivation) is found to be

$$C = W log_2 \left| \boldsymbol{I} + \frac{1}{\sigma^2} \boldsymbol{H} \boldsymbol{R_{SS}} \boldsymbol{H^T} \right|$$

(2.10)

For noise variance σ. Here $\boldsymbol{I}$ refers to the identity matrix and $\boldsymbol{H^T}$ to the transpose matrix of $\boldsymbol{H}$. The matrix $\boldsymbol{R_{SS}}$ refers to the covariance matrix for the transmitters defined as the expected value

$$\boldsymbol{R_{SS}} = \mathrm{E}(\mathbf{s}\boldsymbol{s^T}).$$

(2.11)

The development of accurate and efficient propagation models is essential for the design of mobile networks in order to provide a simulation of the electromagnetic environment from which the channel matrix can be obtained or to model the channel matrix directly.

2.3 Singular Value Decomposition

Much of this thesis is focussed on the types of propagation effects that are likely to be relevant within practical Massive MIMO systems. However, to assess the usefulness of any propagation model within this type of practical system, it is necessary to understand how the system makes use of features of the propagation environment to obtain the desired increase in SE. The investigations described in chapter 5 of this thesis compare the use of standard beamforming methods for targeting different users from an array compared with a spatial multiplexing approach with the same type of array. When using a spatial multiplexing approach, it would be ideal for the number of data streams to equal the number of antennas on the BS array, but this is often not possible due to correlations between the different channels, which impair the ability of the BS to separate out the different spatial streams. In such a situation, it is necessary for the BS and UE to coordinate to allow for the use of the maximum number of possible spatial streams. According to Ren et al [23], this is usually achieved through the use of Singular Value Decomposition (SVD). This method of providing the maximum number of possible data streams has long been used within MIMO systems, however, as the number of BS antennas has gradually increased with the introduction of new standards for mobile networks, this process has also become more complex and thus there has been a large amount of research focussed on improving the efficiency of algorithms that apply the SVD method for precoding and decoding signals within multipath environments, and also in relation to other signal processing and non-telecommunications applications where the same method is used. See, for example, Abed-Meraim [24] for a description of an algorithm designed to address the problem of increased complexity. The optimisation of SVD is beyond the scope of this thesis, however SVD is used as part of the simulation of Massive MIMO channels and is therefore discussed here. An SVD method generates weights that are applied at the antenna ports for precoding at the transmit end and combining at the receive end of the link. In the singular value expression [25]

$$H = U \Sigma V^T \tag{2.12}$$

The transmit precoding weights are described by matrix $\boldsymbol{V}$, whose dimensions are defined by the number of transmit antennas $N_t \times N_t$, and the receive combining weights are described by matrix $\boldsymbol{U}$, whose dimensions are defined by the number of receive antennas $N_r \times N_r$. The aim of the SVD method for precoding and combining is to obtain matrices $\boldsymbol{U}$ and $\boldsymbol{V}$ such that the channel can be described in terms of the singular value matrix $\boldsymbol{\Sigma}$ instead of the usual channel matrix $\boldsymbol{H}$.

$$\Sigma = U^T(U\Sigma V^T)V = U^T HV \tag{2.13}$$

The matrix $\boldsymbol{\Sigma}$ has the same dimensions as the channel matrix $\boldsymbol{H}$, but contains values only along its diagonal, the total number of which are equal to either the number of receive or transmit antennas, whichever is less. This allows the totality of the channels to be expressed as a single column vector, containing the gain of each of the spatial streams. The total capacity can then be calculated by obtaining the capacity for each data stream as though it were a standard SISO channel, with the total capacity obtained by finding the summation of the capacity values.

2.4 Relevant Types of Propagation Models

Several propagation models have been developed within the context of standard MIMO, including deterministic models such as ray-tracers and EM-solvers, Geometry based models and stochastic models that attempt to predict the performance of a system based on the statistical features of the channel. There are also hybrid models that combine the features of geometric and stochastic models. These propagation models can be further classified into physical models that attempt to approximate the features of the environment itself and analytic models that attempt to model the channel matrix directly without reference to any particular channel, a popular example being correlation-based methods.

2.4.1 Ray-tracing for MIMO

Ray-tracing is a useful type of deterministic physical model that considers the propagation channel in terms of a collection of individual rays within a well-defined geometric environment, corresponding to a real-world environment within which a

mobile network will be deployed [26]. The technique involves the modelling of each path between each mobile and BS antenna. Each path is represented by a ray, analogous to a ray of light following the laws and features of classical optics such as reflection and refraction. Ray-tracing systems that have been used to model outdoor MIMO channels include various characteristics such as “building reflection, building rooftop diffraction, building corner diffraction, building scattering, terrain scattering, and combinations of the above” [24]. The ray-tracing system, while providing an accurate model of the channel, is limited in terms of the computational expense required to model all the rays and to simulate a complex propagation environment. It is certainly possible to reduce the expense by reducing the number of rays modelled, reducing the complexity of the terrain or by reducing the number of simulated effects, but this can pose a significant problem for MIMO (and perhaps even more so for Massive MIMO) systems because of the contribution of many rays of often low power in comparison to the more prominent components.

The University of Bristol is known for its expertise in the area of ray-tracing for mobile communications, having developed software that models individual rays in both indoor and outdoor environments using three-dimensional vector analysis with image generation in two-dimensions [27]. In addition to the optical properties of the rays such as reflection and diffraction, the ray-tracing system can also account for the effects of polarisation and antenna patterns. It is known that, due to the computation costs associated with ray-tracing, that optimisation techniques are necessary for viable ray-tracing methods when considering large numbers of antenna elements and associated rays such as in Massive MIMO systems. The University of Bristol has responded to such a requirement by developing models that combine ray-tracing with optimisation methods [28]. In addition to the already established features, this model also includes techniques for reducing path loss, the more accurate modelling of scattering effects from rough surfaces and for increasing the processing speed of rooftop diffraction effects. Various optimisation techniques are performed at the beginning of the algorithm during the data-base processing stage in order to accelerate the ray-path finding process without any loss of accuracy and several electromagnetic calculation techniques are applied to the rays once the trees have been generated. Outdoor measurements have been performed and an average path-loss error of 2 decibels (dB) was observed.

2.4.2 Geometry-Based Stochastic Models

A geometry-based stochastic channel model (GSCM) is similar to a ray-tracing model in the sense that objects are located in space acting as scatters with which a path interacts according to the properties of the object (known as a Scatterer). However, unlike the ray-tracing model, which is deterministic as the objects are placed according to archived locations in a database that correspond with actual physical locations, a GSCM will place the scatterers randomly based on statistical distributions of the placement of objects according to known data corresponding with, for example, an inner-city or a rural environment. Such a model has the advantage of being able, at least some of the time, to model dynamic environments in an accurate way seeing as certain mobile objects such as cars and trains are distributed in a random fashion within a propagation environment [29]. GSCMs also have the advantage of having all the relevant information contained within the distribution of the scatterers, so that correlations between various outputs does not complicate the model. In addition, the movement of mobile stations (MS) can be incorporated into the model and the effects of slow fading and the disappearance of paths as a result of blocking by buildings or other large objects and their reappearing can be implemented in a relatively straightforward manner, which allows for the long-term correlation of the channel to be implemented in straightforward way according to Molisch *et al* [30].

It is known that far-scattering effects (which is to say the scattering from distant objects such as buildings or geographical features) lead to increased temporal and angular dispersions and thus are significant for MIMO systems. These effects will continue to effect Massive MIMO systems and could perhaps be even more significant; however, to the author's knowledge, it would seem that little practical work has been done to this effect at this time.

The implementation of such a model with relevant statistical models has been proposed by Molisch *et al* [30]. The proposed configurations here are valid for BSs with several elements and include local scatters clustered around the MS and a cluster of far scatters located at a distance and directions according to the relevant statistical properties (Figure 5). Such a model can also incorporate the effects of moving MSs.

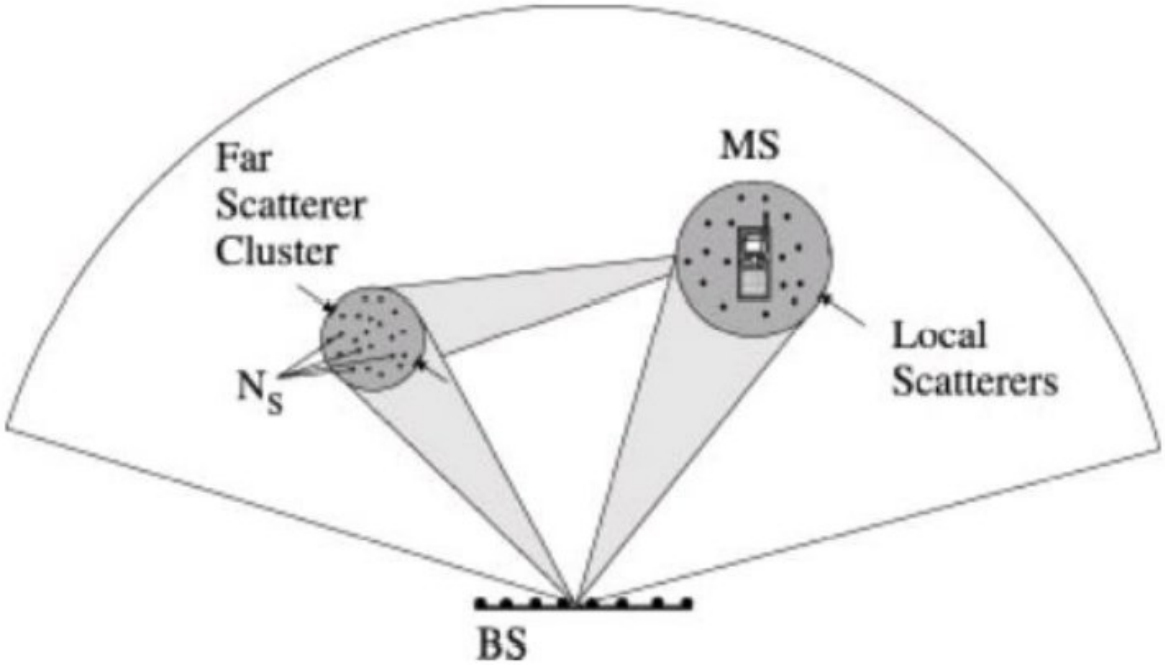

Figure 5: Propagation model incorporating local and far scatterers [29]

2.4.3 Cluster Models for MIMO and Adaptations for Massive MIMO

This subsection considers specific implementations of models that make use of the clusters containing scatterers for the modelling of MIMO channels. An example of such a model, which itself falls within the category of GSCM, is the COST2100 model proposed in 2012 [31] that is an extension of earlier European Cooperation in Science and Technology (COST) models. A graphical representation of the operation of the COST2100 model is shown in Figure 6.

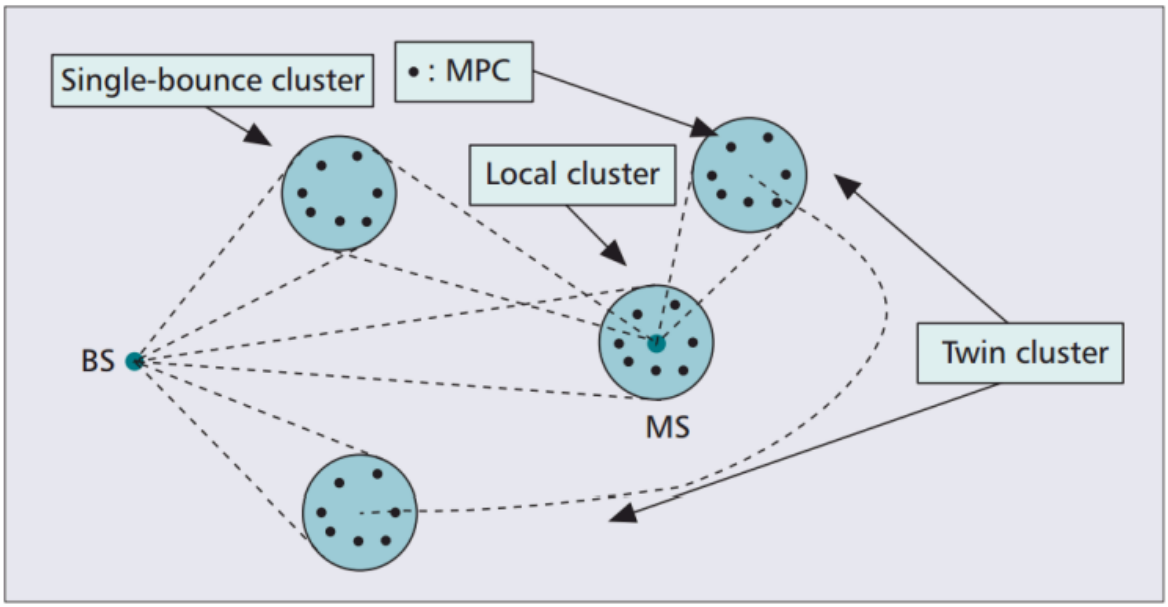

Figure 6: Graphical representation of the COST2100 Model [31]

In COST2100, each cluster has an associated visibility region (VR). When an MS enters a VR, the associated cluster begins to become visible to the MS. The process of the cluster gradually becoming visible to the MS is associated with a so-called 'VR-gain' associated with a number from 0 to 1. The cluster becomes completely visible to the MS as it moves further into the VR. Several types of clusters are defined in the model in order to simulate the various types of propagation associated with various objects in terms of their relation between the MS and BS that would be present within an environment. The authors of the paper that introduced this channel model describe its effectiveness to characterise stochastic environments in multi-link MIMO scenarios [31]. They also list a number of possible extensions but acknowledge drawbacks in terms of the current state of parameterisation and validation efforts as well as the need for more advanced channel estimation methods and more measurement campaigns, something that would seem to apply to Massive MIMO in particular.

An extension to the COST2100 has been proposed to incorporate the effects observed within Massive MIMO channel measurement campaigns [32]. COST2100 was extended in several ways although one of the main adaptations for Massive MIMO was the provision for the fact that, in these systems with very large BS arrays, different elements are likely to be within different VRs. In addition, elements within

the same VRs may have different VR gains so that any one element may ‘see’ the associated cluster to a greater or lesser extent. This provision is illustrated graphically in Figure 7.

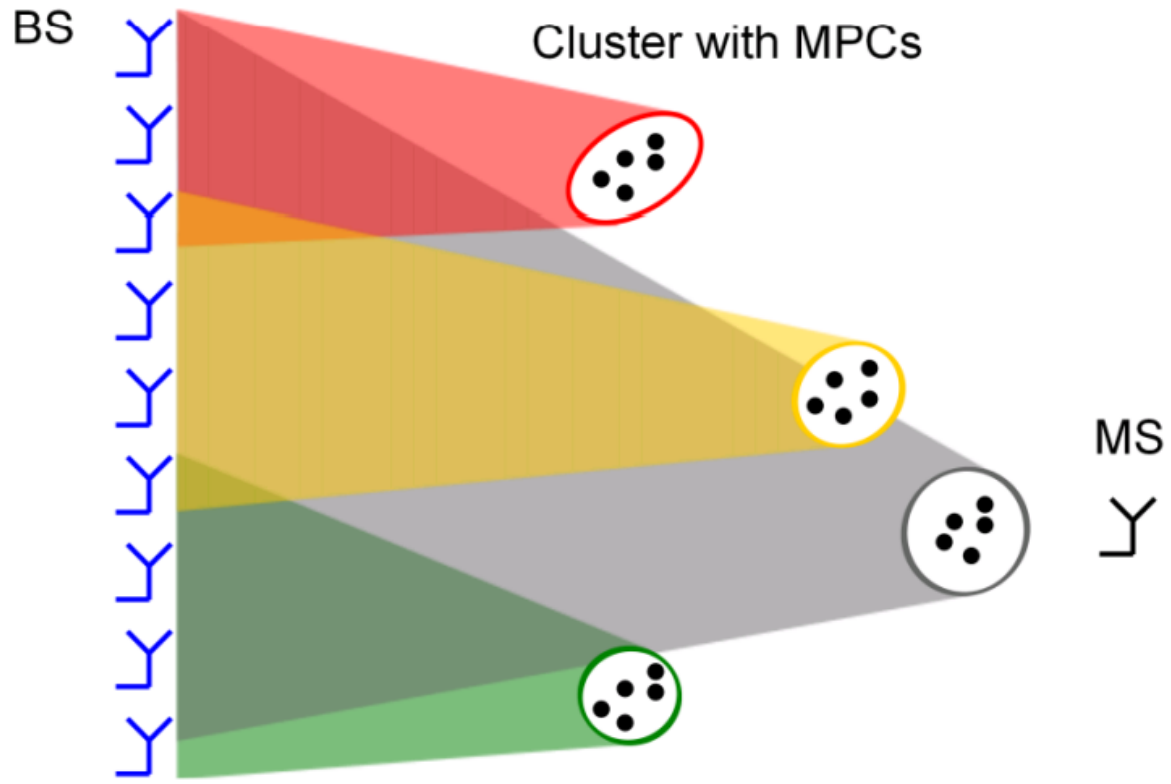

Figure 7: Provision for elements of large arrays occupying different VRs in COST2100 extension [32]

The authors of the COST2100 extension for Massive MIMO [32] provide for an extension in three dimensions, which is identified as being especially important for Massive MIMO channels, particularly for scenarios involving large arrays where different elements are located at different heights (such as rectangular and cylindrical array) and where parts of the large array are located closer to surrounding objects.

Polarisation is also considered within the extension because Massive MIMO arrays sometimes have the elements polarised in different directions in order to aid the separation of users. The COST2100 also introduces VR-gain functions for individual MPCs, which are often not visible in entire VRs in Massive MIMO systems.

2.4.4 The 3GPP Spatial Channel Model

The 3GPP SCM is an important tool in MIMO research that contains both a Calibration Model and a System Simulation Model [33]. The calibration mode is not intended for propagation modelling of MIMO as such but rather provides a simplified model than can be used for the specific purpose of comparing the implementation of algorithms to determine whether they are equivalent by appealing to a 'calibration channel.' The Simulation Model, on the other hand, is a model that includes parameters that are supposed to model suburban macro, urban macro and urban micro cells and can be used to simulate actual MIMO systems. This is a type of GSCM that is based upon the parameters shown in Figure 8.

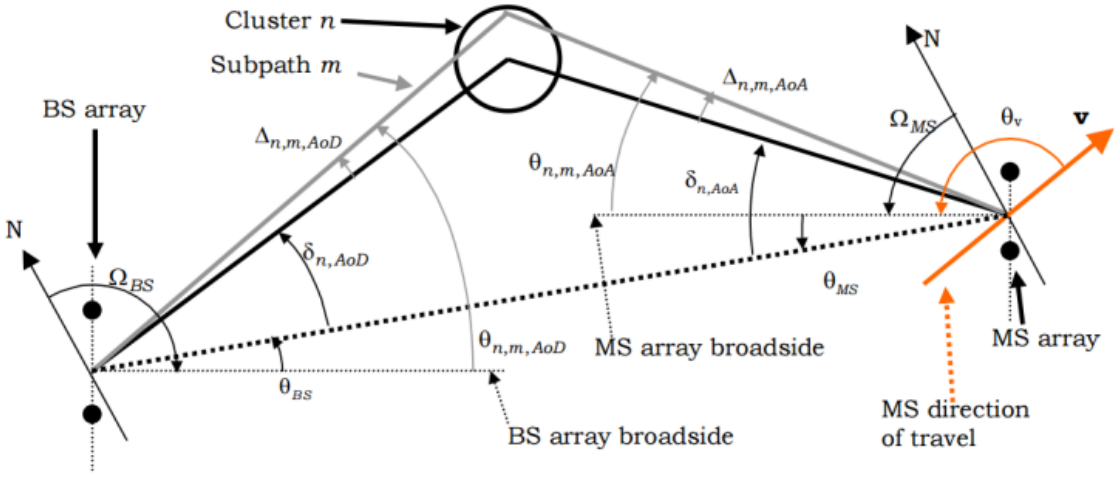

Figure 8: Parameters for the 3GPP model [33]

The MSs are placed randomly within a given cell and the movements (including speed and direction) and the orientations of the arrays are also determined randomly. The path loss components are determined from the parameters given in the COST models. The standard 3GPP SCM only supports bandwidths of 5MHz, has a limited range of applicable frequencies and, although an extended version exists that supports wider bandwidths, neither the original nor extended model contains an indoor scenario [34].

In the year 2020, following a series of meetings, the 3GPP consortium agreed to extend the existing approved channel model so that it is applicable to more broadband systems. In practice, this means that the 3GPP channel model should be

applicable to systems operating anywhere between 500MHz and 100GHz. The development of this model has proceeded such that the new channel models are broadly aligned with previous models designed to apply below 6GHz whilst also taking into account the findings of recent measurement campaigns. The general features of this updated channel model are described in this section. The requirements for this standard model, in a general sense, include the support of all of the typical scenarios that are currently considered by MNOs in the design of the RAN, namely: urban microcell street canyon, urban macrocell, indoor office, rural macrocell, and indoor factory environments. Bandwidth is required to be supported up to 10% of the centre frequency of 2GHz, whichever value is lower. Mobility is also required to be supported at both ends of the link as well as large arrays based on a far field assumption and also that the channel is stationary over the size of the array, an assumption that may not be accurate within Massive MIMO channels within dynamic environments, if the array is large enough such that the channel statistics vary across different elements.

The model in general features elements that can be divided into two sections, the first of which deals with the fundamental elements of a radio propagation system and the second of which addresses additional features and anomalies that may be present within a system and that may need to be considered to obtain sufficient accuracy of the calculated outputs. The second section consists of a series of channel models taking into account the effects of phenomena such as doppler shift, user rotation, ground reflections and interference sources and a series of models that can be used for link-level evaluations. The first section describes the antenna modelling, path-loss models and the fast-fading model, the latter of which is of particular interest to the research in this thesis, which focusses largely on propagation effects in relation to the H-matrix, which describes the response between BS and UE terminals and can be generated from a fading model. 3GPP also describes the parameters that are assumed in each of the different types of deployment scenarios for the MNOs, such as the BS antenna height and, for indoor environments, the room layout.

The BS antenna is always described in the 3GPP standards in terms of a cross-polarised panel array as shown in Figure 9, where each element can be either single or dual polarised.

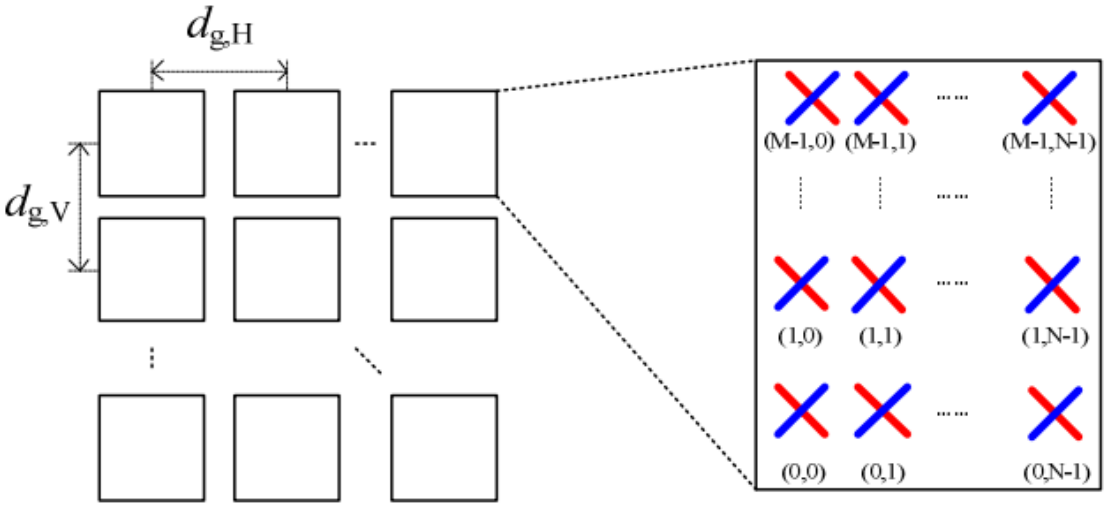

Figure 9: The standard description of the MIMO antenna array within the current 3GPP wideband channel model.

The path loss between BS and UE elements is described according to a set of formulas that correspond to the set of deployment scenarios. Additionally, formulas are provided for the probability that an LoS link occurs within each of these scenarios.

The process for developing the channel coefficients within the H-matrix is defined by the process shown in Figure 10 (XPR refers to the cross-polarisation ratio).

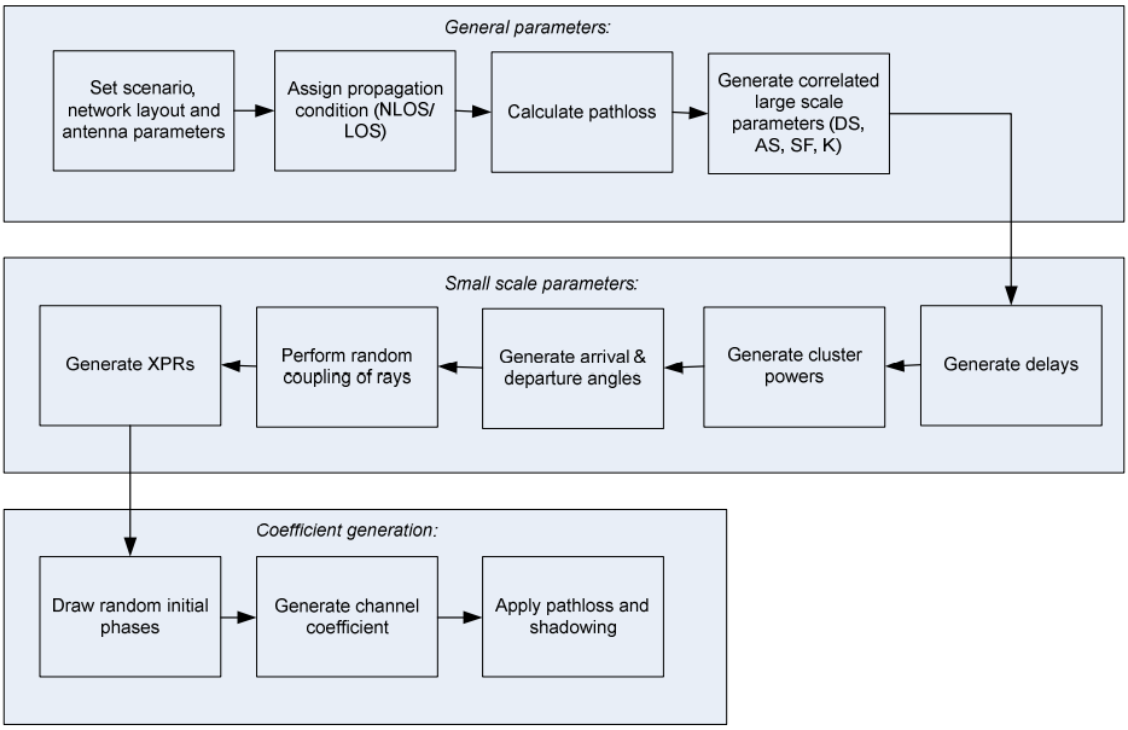

Figure 10: The general process for obtaining the channel coefficients for a MIMO channel according to the current 3GPP wideband channel model [35]

Formulas are provided for the generation of the H-matrix for both LoS and NLoS links.

2.4.5 WINNER-II Channel Models

The WINNER-II model, which developed out of the WINNER model (which, in turn, was developed from the 3GPP SCM followed by its extended version) with extended features, provides two types of propagation models. These are the generic model and a simplified clustered delay line model [36]. The model itself has been developed thanks to an extensive collaboration effort including several measurement campaigns throughout Europe. The result is a full GSCM model based on real-world data that is used to determine channel parameters stochastically for a range of scenarios while antenna geometries and field patterns can be selected manually by the user [37]. The model makes use of a ray-tracing approach where the rays are summed along with SSPs including delay and power level to resolve the channel.

Clusters are considered as collections of rays (Figure 11) and it has been noted that the dependence on angles between antennas and objects could be a specific problem for Massive MIMO, as these angles can change across large antenna arrays.

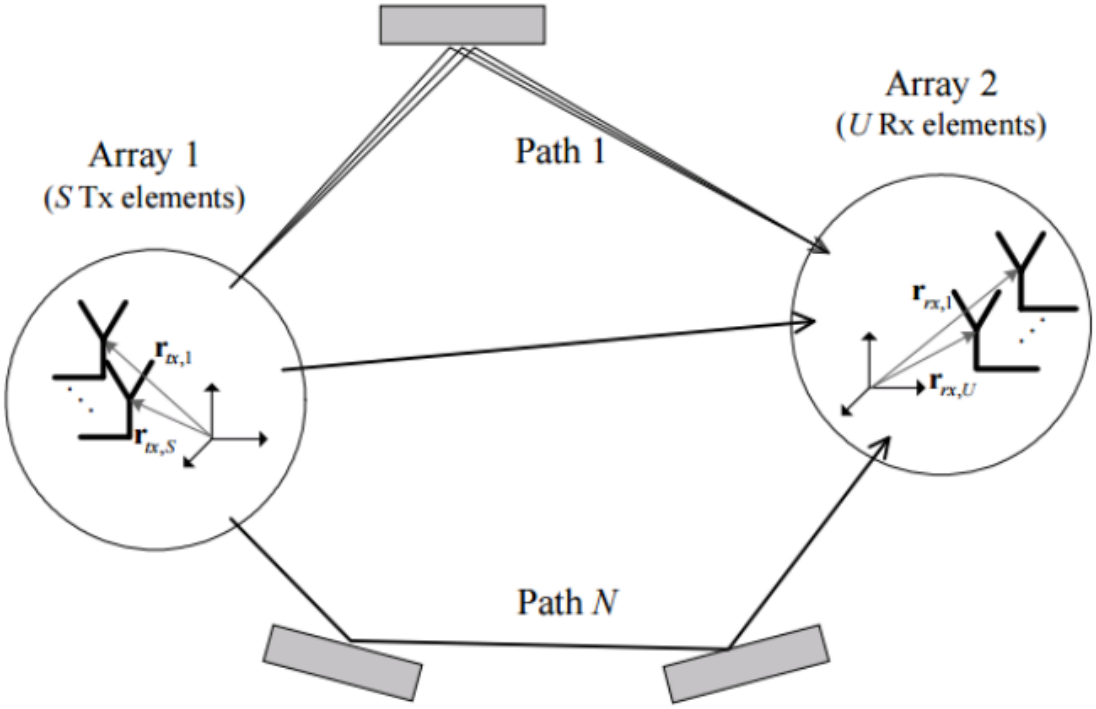

Figure 11: Overview of the WINNER-II Channel Model [37]

2.4.6 IEEE Models

Several models that can be used for MIMO systems have been included within IEEE Standards [38]. These include the TGn model of IEEE 802.11, which can be used for indoor environments with an operational frequency of 2GHz or 5GHz. IEEE 802. Standard 16a contains channel models for fixed macrocelluar mobile networks, where the MS antenna is installed on a rooftop, operating at 2.5GHz with a bandwidth of between 2 and 20MHz.

2.4.7 Correlation Models

The class of propagation models known as ‘correlative models’ do not attempt to model the features of the channel itself but rather attempt to model the correlation between transmit and receive antennas according to statistical properties, thereby

making these models further examples of stochastic models, but without a geometric component. A standard approach to the modelling of mobile channels is the independent and identically distributed (iid) Rayleigh model whereby a series of random variables with Gaussian distributions are used to model the effects of channel fading, which is assumed to be roughly uniform throughout the channel. Measurement campaigns have shown that such a model is not sufficient for the modelling of Massive MIMO channels [39].

A possible extension to the iid model that has become very popular in the research literature is the Kronecker model [39]. The channel (H) is defined in terms of the correlation matrices for both the transmit and receive end of the link as

$$H = \frac{1}{\sqrt{tr\{R_{RX}\}}} R_{RX}^{1/2} G (R_{TX}^{1/2})^T \tag{2.14}$$

Where $R^{\mathrm{T}}X = E\{H^T H^*\}$is the transmit side correlation matrix with H^T as the transpose channel matrix and H^* as the conjugate channel matrix. $R_{RX} = E\{H^H H\}$ is the correlation channel matrix the receive side and G is the iid random fading matrix of circularly symmetric complex Gaussian identities with zero mean and unity variance. Although this is a popular method, it is known to underestimate MIMO channel capacity and is thus likely to be problematic for the modelling of Massive MIMO channels [40].

The Weischelberger model is a further extension that introduces the notion of coupling between link ends. The channel matrix is given by

$$H = U_{RX}(\tilde{\Omega} \circ G) U_{TX}^T \tag{2.15}$$

where Ω̃ is the element-wise square root of the power coupling matrix Ω and ∘ refers to a Schur-Hadamard multiplication. URX and UTX are the eigenbases from eigenvalue decompositions of R_{TX} and R_{RX}. Ω specifies the coupled energy between eigenvectors of each side of the link and is defined as

$$\Omega = E\{U_{TX}^H H U_{RX}^* \circ U_{TX}^T H^* U_{RX}\}$$

(2.16)

This approach is more accurate than the Kronecker model but requires the availability of additional information obtained from measurement campaigns or a full correlation matrix of the channel.

2.4.8 Extended Saleh-Valenzuela model

The Extended Saleh-Valenzuela model occupies a class of physical channel models where each of the physical parameters (such as time of arrival (ToA), angle of arrival (AoA), and angle of departure (AoD)) are determined entirely by reference to statistical parameters without reference to any particular geometry associated with a propagation environment [41]. This model was developed for MIMO and extended the original SV model by adding AoA parameters, whereby it was shown that the capacity probability density functions (pdfs) and pairwise element pdfs from measured channel data could be matched. This model has further been extended to incorporate some of the characteristics of Massive MIMO, something which is discussed in more detail later in this report. It should be noted that SV models are characterised by their treatment of MPCs as clusters.

2.4.8 Zwick Models

The Zwick model [42] was proposed as a response to the observation that, while clustering effects tend to occur within MPCs in rural and outdoor urban environments, these are generally not observed, at least to not such a strong extent, within indoor environments. Since the SV model operates by clustering together MPCs, a new model is proposed that, like the SV model, determines physical parameters based entirely on statistical parameters without any reference to any specific geometry. Like the SV model, it determines departure and arrival angles in a stochastic manner. The Zwick model considers each MPC individually and uses a Stochastic Process to determine their appearance and disappearance within the propagation environment.

2.4.9 Finite-Scatter Model

The finite-scatter model is an example of an analytic propagation-based model whereby the channel matrix is modelled in terms of the propagation parameters rather than through correlations between transmit and receive elements as is the case with correlation-based models [43]. The finite-scatter model uses the concept of

multi-path propagation to model individual rays within a propagation environment. Unlike standard ray-tracing however, these rays are defined for the propagation environment without any reference to particular antenna elements or array geometries, thus allowing the model to describe the propagation between any pair of elements, allowing for single and multiple-bounce propagation.

2.4.10 Maximum Entropy Model

The maximum entropy model is an information theoretic model that serves to provide guidance with regard to the construction of a MIMO model based on system parameters that happen to be available at the time [44]. The process is founded on the principle of maximum entropy and the consistency criteria, which requires that, given two channel models with the same state of knowledge regarding the channel, the same result should be obtained.

2.4.11 Virtual Channel Representations

Virtual channel representations of MIMO channels have also been investigated [45]. These representations form an ‘intermediate’ virtual model between the idealised statistical representations and the geometric representations of other models and capture “the essence of physical modelling and provides a simple geometric interpretation of the scattering environment.” The obtained virtual channel matrix serves as the channels uncorrelated spectral representation and, via various techniques, key parameters and channel statistics such as diversity and capacity can be characterised.

2.5 Known Issues

Some of the types of models described in the previous section were developed for MIMO, rather than Massive MIMO, systems but can, at least in theory, be extended to Massive MIMO channels. However, there are several known issues that are specific to Massive MIMO and do not apply to standard MIMO channels. Thus, the use of these models for Massive MIMO are likely to give results that are not useful. In the next section, a review of recent attempts to address these issues through the development of models that are specific to Massive MIMO. This section discusses some of the issues themselves that should be addressed in relation to developing such models. It should be noted that, especially due to the lack of Massive MIMO measurement campaigns, this section may not provide an exhaustive list of all the

significant features of Massive MIMO channels that would be relevant from the perspective of propagation models and that the recent attempts to develop Massive MIMO models may not adequately address each of these features. It should be noted that the features mentioned here apply to the physical channel of Massive MIMO systems in general and do not represent specific issues inherent in certain models (such as the observation of different BS elements occupying different VRs within the COST2100 model, as discussed earlier).

2.5.1 Slow Fading Across Large Arrays

The BS arrays for Massive MIMO are potentially very large. Thus, a situation may arise, for example, where part of the array is in the shadow of a nearby object such as a building and part of it has a clear LoS link with a MS. Current MIMO models tend to view the BS array as a point and thus do not consider the slow fading across the array. There have been some attempts to investigate this effect so that it can be incorporated into physical propagation models. For example, in Aulin, 2015 [46], it was shown, via an evaluation of cell spectral efficiency using a derived closed-form expression for the downlink received signal to interference ratio (SIR) assuming such large-scale fading, that a higher cell spectral efficiency can be obtained in comparison with what would be expected from conventional MIMO models. Further theoretical analysis has been provided [47] on the effect of large-scale fading within Massive MIMO systems. In particular, this paper analysed the ergodic achievable rate for an uplink Massive MIMO system and showed that the achievable rate is largely determined by the large-scale fading for both perfect and imperfect CSI within an urban environment. There amount of work that has been done in this area is limited and the development of models that provide for the effects of large-scale fading is a particularly important area for further research.

2.5.2 Spherical/Plane Wave Assumptions

It has been shown [48] already that certain types of standard MIMO systems operating over short range are not well characterised using standard MIMO models relying on an assumption of a plane wave-front from the BS array as these models tend to underestimate the channel capacity by failing to model accurately the relatively strong line of sight (LoS) component within short-range LoS links. Thus, spherical wave alternatives [49] have been proposed in order to increase the

accuracy of models at the expense of added computational complexity. In response to these observations, theoretical work was conducted to determine analytically the distance from the BS at which a plane-wave assumption can be made, considering that the spherical wave model converges towards a plane wave model with increased distance [50].

The spherical-wave model assumption has been incorporated into various Massive MIMO specific models that have been published in the academic literatures and which are discussed in the next section of the literature review. In addition, a theoretical analysis of the spherical wave-model has been provided [50]. As with the case of large-scale fading across large arrays, it has been shown that a spherical wave front (Figure 12), while seeming problematic at first, can actually provide advantages for telecommunications systems. An advantage to the spherical wave front is that spatial separation between closely spaced MSs becomes possible in situations that would be challenging if a plane-wavefront were present.

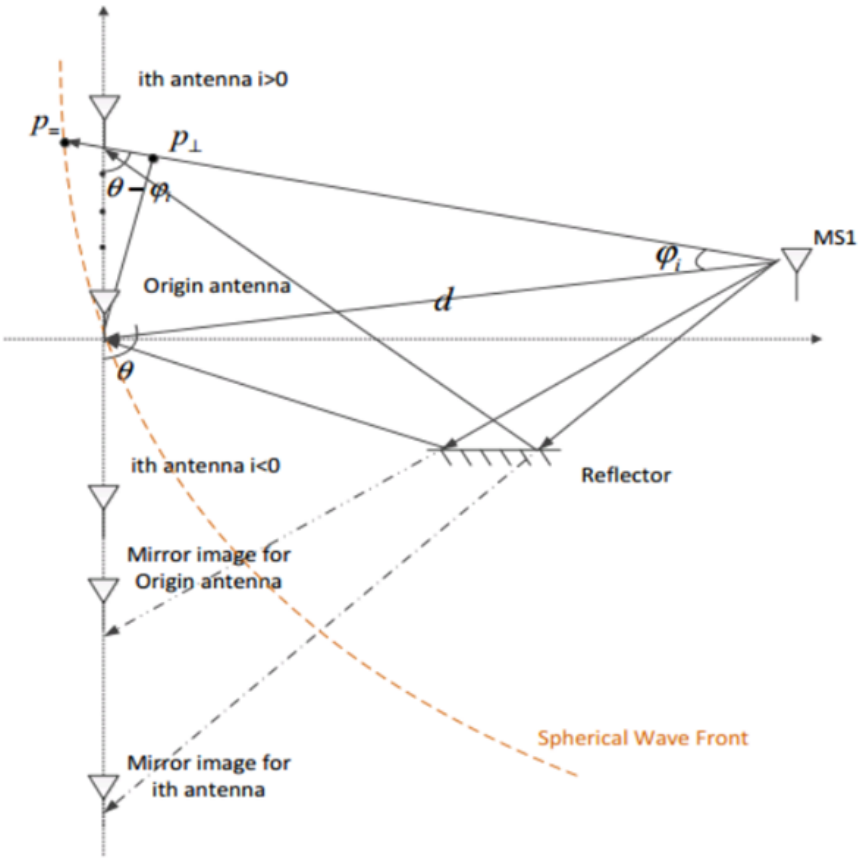

Figure 12: Principle of a spherical wave model [50]

2.5.3 Multi-Path Components (MPCs) at BS

Due to the potentially large dimensions of the BS array, it cannot be assumed that the MPCs will arrive at the same angle at each of the elements [38]. In addition, and in particular for the case of 3D arrays, the elevation angles of the MPCs needs to be incorporated into any model that wishes to provide an accurate view of the Massive MIMO channel. Gao's extension to the COST2100 model includes these three-dimensional considerations [32].

2.5.4 Underestimation of channel capacity in correlation models

It has been generally acknowledged that correlation-based models (such as the Kronecker Model) are characterised by a tendency to significantly underestimate channel capacity in Massive MIMO channels, especially in those with strong LoS components [51]. Although extensions of existing correlation models have been proposed, such as the Weichselberger model, these tend to require a lot of information about the channel (that may not be available) and are also computationally costly. Thus, further research into viable correlation-based propagation models is important.

2.5.5 Viability of some MIMO models has not been applied to Massive MIMO

Some of the models for standard MIMO models may, with significant modifications, be applicable to the simulation of Massive MIMO channels. Some of MIMO models have already been extended in this way, for example, there has been interest in extending the Extended Saleh-Valenzuela model for outdoor Massive MIMO scenarios [52] but, to the author's knowledge, no extension has been provided for this model's indoor equivalent (the Zwick model).

2.5.6 Lack of measurement campaigns

There is a widely accepted dearth of Massive MIMO measurement campaigns, which is a problem when attempting to verify Massive MIMO propagation models. For example, the authors of the original COST2100 model state this as a specific limitation of the theoretical and computational work [31]. There has also been practically no work in the obtaining of dynamic Massive MIMO channels with moving objects such as cars and pedestrians, largely because measurement campaigns (see the relevant section of this review) have been conducted using 'virtual arrays' that may, for example, consist of one element moving along a track, thus requiring

that the environment remain static during the campaign. Other aspects of the channel that should be investigated include the effect of far scatterers such as mountains and distant buildings on the channel.

2.6 Development of Models specifically for Massive MIMO

The development of models specifically for Massive MIMO has become an area of interest for the academic literature only within approximately the past two years. This section reviews some attempt to develop channel models that are specifically intended to work for Massive MIMO channels, even though a lack of measurement campaigns may make their effectiveness difficult to determine.

There have been some attempts to develop correlation-based models for Massive MIMO. For example, a novel Kronecker based model [53] has been proposed to incorporate a stochastic process that models the scatterer sets on the array axis. This is significant because, as shown in Figure 13, not all elements see the same scatterers as the others.

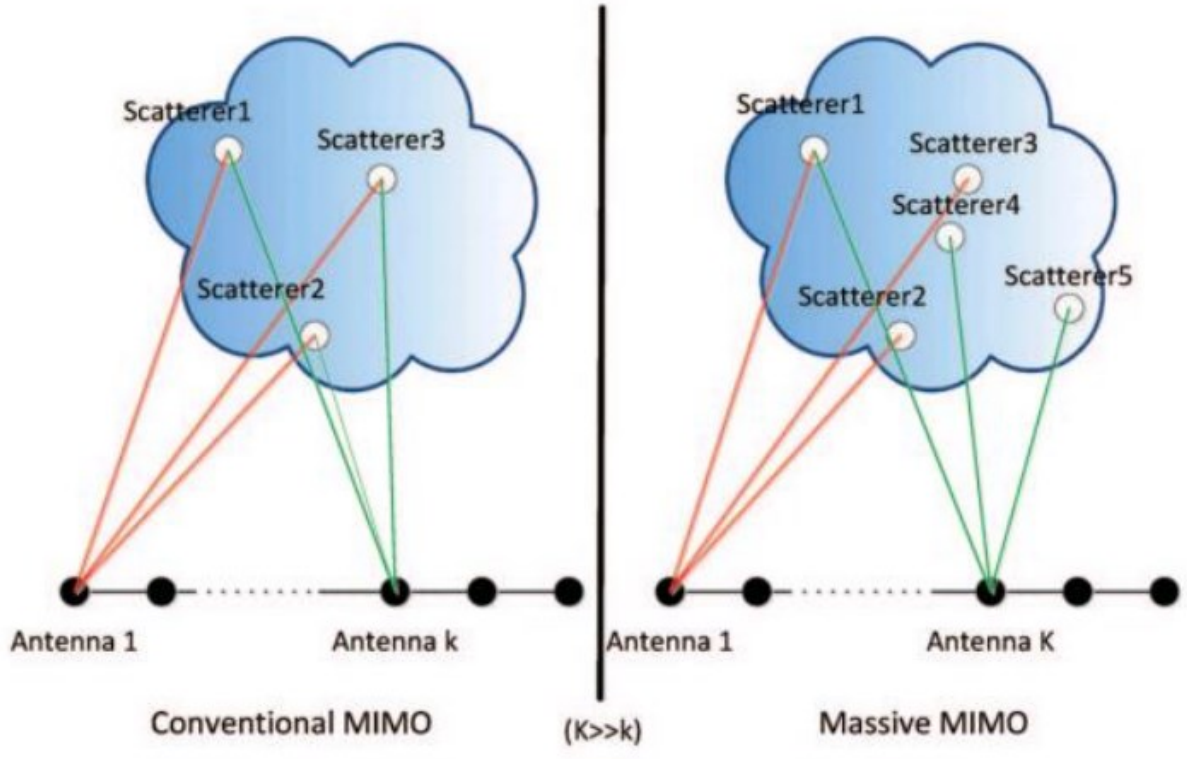

Figure 13: Representation of how different scatterers are seen by different antenna elements [53]

Following research in standard MIMO channel models, there has been interest in hybrid models that incorporate features from both geometric and stochastic model. Such GSCMs include a multi-confocal ellipse two-dimensional channel model that incorporates a spherical wave assumption with a stochastic process to model the evolution of the scatters on the antenna axis [53] Another example of such a model is a proposed three-dimension 3D two-cylinder regular-shaped geometry-based stochastic model for non-ionospheric Massive MIMO scattering channels. This model incorporates non-stationary properties stochastically and places all scatters on the surface of a cylinder [54].

There has been some ray-tracing work conducted within the context of statistical ray-based models. These include a comparison of a measurement campaign with a raylaunched simulation incorporating a spherical wave assumption [55] and an investigation of the effectiveness of ray-based models has been conducted [56]. Both of these investigations suggested that ray-tracing based methods are particularly useful for the modelling of indoor environments.

Theoretical work has included sum-rate analysis for Massive MIMO in urban environments [57] as well as investigations into finite scatterer, Mutual Information effects on information capacity in Massive MIMO [58,59].

2.7 Summary of Experiments with Large Arrays

Even though there is a generally acknowledged lack of data from measurement campaigns for Massive MIMO channels, there have been several relevant campaigns conducted, some using virtual Massive MIMO arrays. This section provides a summary of recent propagation studies involving practical experiments with large arrays, although such studies have largely been limited to static environments. The studies are listed by the locations of the research groups that conducted them. All of the systems mentioned here were used to conduct experiments below 6GHz in order to correspond with the interest of this PhD project.

2.7.1 Bell Labs, Germany

Bell Labs have used a type of rotating system to simulate a cylindrical array [60]. In Figure 14, the figure on the left shows the system from the side and the figure on the right shows the system from the top.

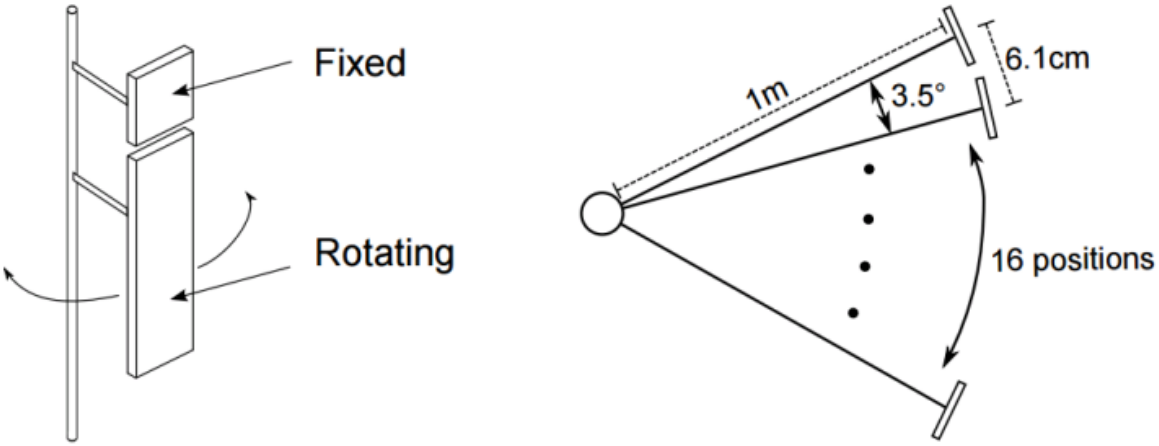

Figure 14: Bell Labs' Virtual Array [60]

The system contains a rotating section and a fixed section. In the experiments, seven antennas are attached to the rotating section and one antenna is attached to the fixed section. The single fixed antenna is placed at a sufficient distance from the other antennas so that reflections are avoided and can be used to calculate carrier phase offset between different measurements. The rotating section is moved between 16 positions in order to simulate a 112-element cylindrical array. Measurements were conducted in an outdoor environment using two single antenna receivers placed two metres apart on top of a car and with the transmit array located on top of a building.

2.7.2 Beijing Jiaotong University, China

The Institute of Broadband Wireless Mobile Communications has used a mechanical system to simulate a linear Massive MIMO array that involves running a bi-conical along a track [61]. Figure 15 shows the array (top-left).

Figure 15: Beijing Jiaotong University's propagation environment [61]. Clockwise from top left: transmitter, stadium environment, location of users within stadium.

A measurement campaign was conducted within a stadium environment as shown in the other parts of the figure. The red dots in the lower part indicate the location of receive bi-conical antennas. The environment was kept fairly static due to the time required to move the transmit antenna across the track. An R&S SMBV100A signal generator was used as a transmitter with an appropriately synchronised receiver.

2.7.3 Aalborg University, Denmark

In terms of the setup of the users and the BS array, the measurement campaign at Aalborg University [62] seems to be somewhat more similar to our measurement

campaign conducted with 112 antennas attached to a wooden block. The measurement campaign involves the use of many monopole antennas at the transmit array (64 in this case) and eight users with handset type transceivers each with two antennas. The users are arranged within an indoor environment (including a staircase) for several types of scenario (including both LoS and non-line-sight configurations). The measurements themselves were conducted using a correlation-based channel sounder.

The 64 monopole antennas are divided into eight sets of eight antennas. The antennas in each set are placed in a line with half-wavelength spaces and with two dummy elements placed at each end to provide balanced properties among the active elements. There were three configurations for these sets of elements that can be seen in the Figure 16. The first involves the sets of antennas being placed along a two-metre plank, the second involves the sets of antennas being placed further apart along an eight-metre plank and the third involves the sets of antennas being placed parallel to one another to form a square array.

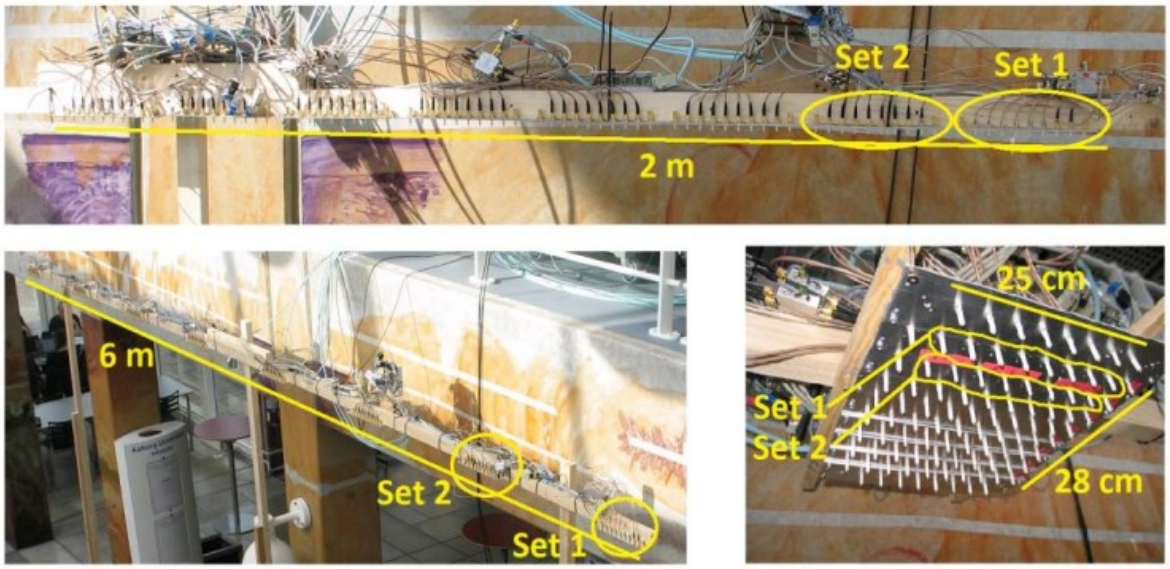

Figure 16: Aalborg University: indoor measurements using array configurations. Clockwise from top: large linear array, compact array, very large linear array [62]

2.7.4 University of Stuttgart, Germany

Measurement campaigns have been conducted in both indoor laboratory environments and outdoor environments using an adaptable array of 64 patch antennas [63]. The patch antennas are collected in groups of eight and can be connected to form either a linear array or an 8x8 rectangular array with half wavelength spacing in both configurations. The antenna and its configurations are represented in Figure 17.

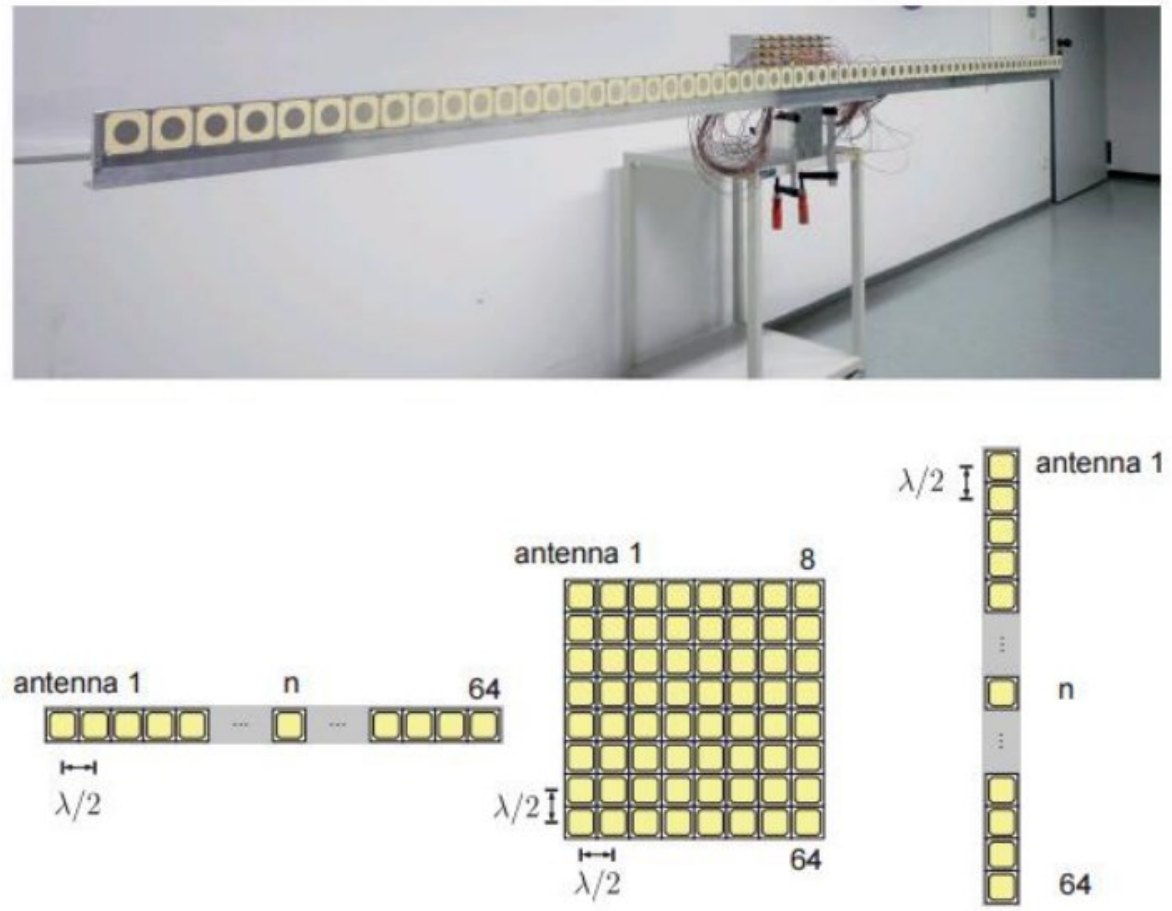

Figure 17: University of Stuttgart patch arrays [63]

The base-station antenna is driven by eight parallel FPGA based radio frequency (RF) front ends. According to the referenced paper, these RF front ends are proprietary and were all packaged in a single in-house remote radio head. The receiver is composed of two ground-plane antennas with an R&S TSMW Universal Radio Network Analyser.

2.7.5 University of Southern California, USA

A group from the University of Southern California [64] have conducted a measurement campaign in Cologne in Germany using a virtual spherical array that is similar to the one used by Bell Labs. A MIMO MEDAV RUSK channel sounder was used to obtain the channel measurements and a stacked polarimetric uniform circular patch array attached to a vehicle was used for the MS.

2.7.6 Lund University

Several measurement campaigns have been conducted to investigate propagation scenarios involving large arrays at Lund University. The measurement campaigns have been enabled by a MIMO Channel sounder produced by MEDAV [65] shown in Figure 18.

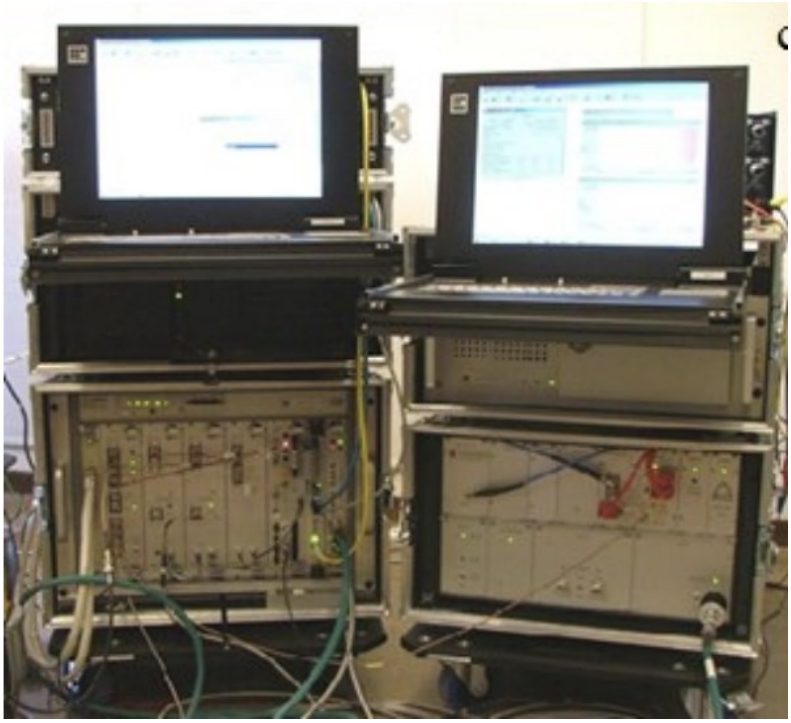

Figure 18: Lund University channel sounder [66]

The purpose of the channel sounder is to obtain the impulse response of MIMO channels and can be used (according to medav.de) to perform real-time channel sounding and propagation analysis. Direction of arrival (DoA), direction of departure (DoD), Doppler spread data and other parameters can be estimated in high

resolution during measurement campaigns. The channel sounder used by Lund University is capable of operating within a bandwidth of up to 240MHz in the 300MHz, 2GHz and 5GHz bands.

The measurement campaigns at Lund University have used different types of arrays designed to operate at 2.6GHz, including a uniform cylindrical array and a uniform linear array as shown in Figure 19 [67].

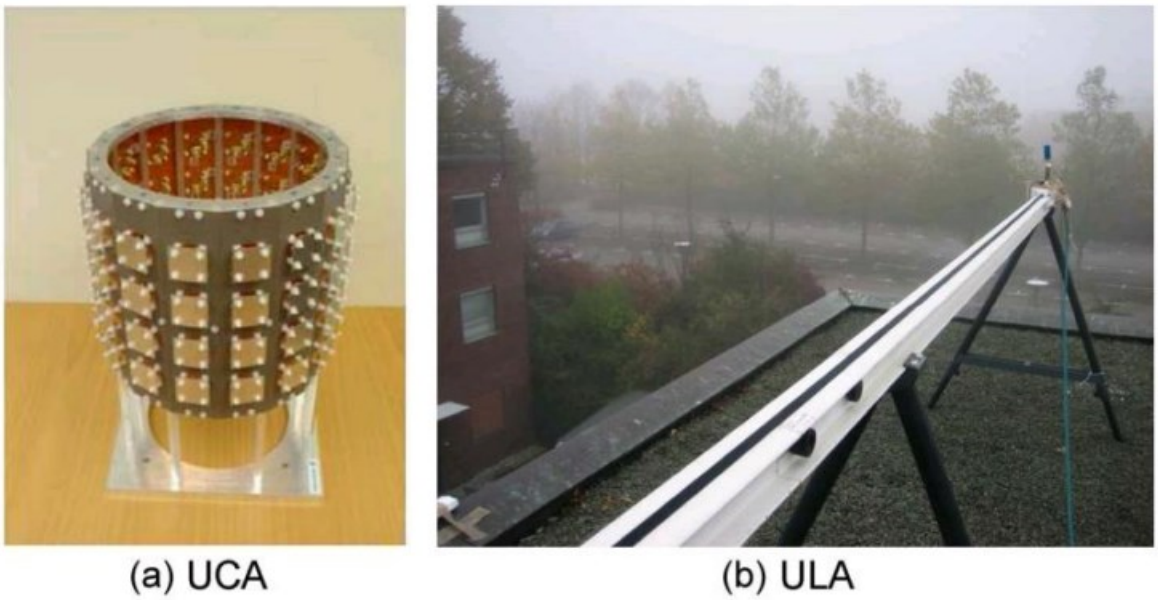

Figure 19: Lund University arrays [67]

The Uniform Cylindrical Array (UCA) is a compact Massive MIMO antenna that consists of four stacked circles of 16 dual-polarised patch antenna arrays. Researchers at Lund have noted some drawbacks with using a compact design, namely higher antenna correlation and poorer angular resolution. However, the UCA has the advantage of being able to resolve incoming waves in two dimensions. The uniform linear array (ULA) consists of a ‘virtual’ 128 element array that is simulated by moving a vertically polarised omnidirectional antenna across a rail in 128 equidistant positions. The ULA is known to provide superior angular resolution in comparison with the more compact array.

During a recent measurement campaign, the MEDAV channel sounder was used with the UCA and an HP 8720C Vector Network Analyser was used with the ULA. A

mobile omnidirectional antenna was moved around an outdoor campus environment to represent MSs. The arrays were placed on a roof and several measurement sites were used to represent LoS and non-LoS scenarios with users placed closely together and scenarios where the users are placed far apart.

More recently, collaborative research was conducted with the University of Bristol using a 4x25 Massive MIMO array [68].

2.7.7 Georgia Institute of Technology, USA

The following example of a measurement campaign is less recent and uses fewer antenna elements than the previous examples. Nevertheless, it may still be of interest both for the type of setup that was used and for its relevance to spherical and plane-wave model comparisons.

The Smart Antenna Research Laboratory has a system like the one shown in Figure 20 for simulating Massive MIMO arrays [48].

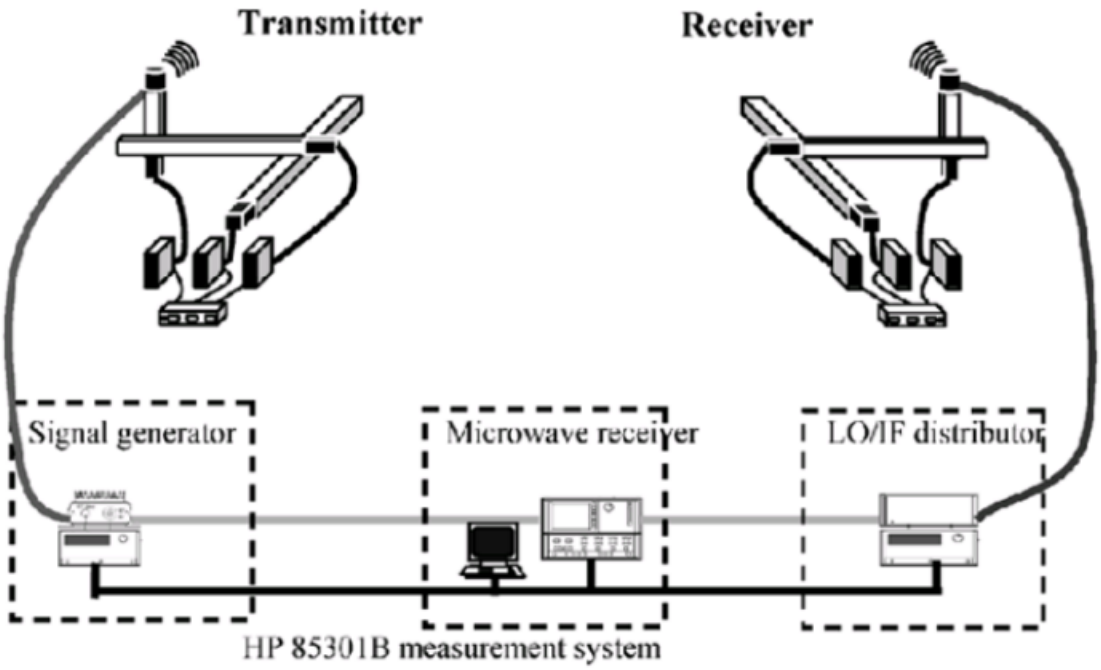

Figure 20: Smart Antenna Research Laboratory virtual arrays and measurement system [48]

A single antenna for the receiver and transmitter is attached to a mechanical system that moves the antenna according to pre-defined spacing in order to simulate a

linear, rectangular or cubical array. The HP85301B antenna pattern measurement system is used to capture the frequency response of the channel. Experiments have been conducted for LoS indoor environments where both the parameter estimations and capacity measurements were captured. These experiments have shown that plane wave models tend to underestimate channel capacity.

2.8 Current Work in Massive MIMO

2.8.1 Overview of Massive MIMO Research

Massive MIMO presents a large number of possible research direction so, as part of a literature review, the key areas of research interest are discussed here. The discussion will begin with a general overview of various areas of research, as presented by Lu *et al* [69] and will be followed by a discussion of some of the Information Theory topics that have been explored in the literature, some of which may be very relevant to research into channel modelling due to the profound links with concepts such as channel capacity (where one of the main purposes of Massive MIMO is to increase capacity).

Massive MIMO systems rely in a very fundamental way on multi-path propagation and thus on the understanding of the state of a channel in order for the system to know how to make use of the multi-path environment. This knowledge of the channel is known as the Channel State Information (CSI) and is required to be present at the BS. As would be expected, there has been much interest in the investigation of methods for obtaining this information and several methods have been proposed to this effect. The general strategy tends to involve the use of a pilot sequences to understand the CSI but this process is complicated if different frequencies are used for the uplink and downlink. Jose et al [70] have proposed a TDD based method where channel reciprocity is assumed and thus only information about the uplink is required to determine the relevant information. FDD remains an area for investigations, but there are some problems associated with the issue of obtaining CSI data for both the uplink and the downlink. Minimum Mean Squared Error (MMSE) approaches are also popular approaches for obtaining the CSI data and have shown to be able to obtain near-optimum performance [69]. Nguyen [59] has also proposed a compressive sensing approach to obtaining the CSI data.

The issue of signal detection is a vast subject that is beyond the scope of this report but there has been a strong interest in the research community into the investigation of the types of receivers that could be used within Massive MIMO systems and Hoydis [71] has provided some comparisons of different detection techniques for Massive MIMO channels.

The issue of pilot contamination is another significant challenge with regard to Massive MIMO. As mentioned earlier, the obtaining of CSI data normally necessitates the use of the sending of pilot sequences to the MSs in order to obtain relevant information about the channel. Ideally the 'pilot channels' associated with each cell of the network would be orthogonal to each other but, due to the limited amount of available bandwidth, the large number of users and the large number of transmit antennas, this cannot always be assumed. There is therefore a problem in obtaining accurate CSI data because the associated channel vectors of users with different (but nonorthogonal) pilot channels become correlated. There has been much research interest in the development of techniques to mitigate the effects of pilot contamination [72]. For example, Jose *et al* [70] have proposed a method for reducing the effect of pilot contamination through the use of a MMSE precoding technique based on a joint-cell approach that was shown through numerical results to outperform a single cell approach. Appaiah *et al* [73] proposed an approach that involved changing the time frame in which each pilot signal occurred for each cell, so that pilot sequences in neighbouring cells did not occur within the same time frame.

There are issues related to energy use that are significant to Massive MIMO. The use of cheaper and less power-consuming components is seen as a general advantage of Massive MIMO although there is still research to be done with regard to power trade-offs and comparisons with other types of communications systems [69].

2.8.2 Information Theory Research

Much of the current work related to Massive MIMO channels tends to take a more theoretical and Information Theory centred approach. Some of the basics relating to the Information Theory approach to MIMO (such as channel capacity) have been previously discussed; however, for a more detailed discussion of Information Theory topics, the reader is directed towards the paper by Rusek *et al* [74].

There was a significant amount of theoretical groundwork that led to the increased interest in Massive MIMO as a way of resolving challenges to the next generation of mobile networks. Already in 1998, Foschini and Gans [75] provided a theoretical demonstration of how multiple antennas at both the transmitter and the receiver can increase channel capacity for a single user case with narrow bandwidth, which is to say less than the coherence bandwidth. This theoretical proof underlies much of the motivation for the development in massive MIMO since the numbers of antennas at both ends of the channel were shown to be highly significant. Some numerical computations of these early results are available in the 1999 paper by Telatar [25].

There has been a long-standing interest in multiple-access channels for multi-user networks and there is a large body of work with regard to algorithms that can approach channel capacity for this configurations. An example of this is the algorithm proposed by Wei Yu *et al* [76], which takes an approach based on the classic 'water-filling' problem. It was shown that, through this method, it was possible to allocated power to each of the mobile users in such a way that capacity was attained.

There is still an open question regarding the MIMO broadcast channel and the actual theoretical capacity associated with it (even though algorithms exist that are shown to achieve performance within the region of the expected channel capacity). The 2003 paper by Caire and Shamai [77] is often cited as a main foundation for research into achievable rates through broadcast channels. The 2005 paper by Sharif and Hassibi [78] also provides an overview of the various approaches that have been taken towards the MIMO broadcast channel. In addition, Caire discusses the 'sum rate capacity' (which is the total transmission rate of all users) of the MIMO broadcast channel and how this is achievable through the use of so called 'dirty paper coding,' which is a type of non-linear precoding that has proved very popular with MIMO communications in general even though, with the increase in antennas in Massive MIMO systems, non-linear methods are often preferred due to their reduced complexity [70]. Vishwanath [76] provides a more computationally efficient method for achieving the 'dirty paper' achievable capacity region and Weingarten showed in 2006 [80], through the application of the 'dirty paper coding' technique to the Gaussian MIMO broadcast channel that the capacity region is indeed reached.

Various non-optimal pre-coding schemes are also available such as an extension of the Tomlinson-Harashima precoding technique [81]. A 'nesting lattice' approach for

an interference channel is also discussed by Zamir et al [82]. Another coding technique based on the long established ‘channel inversion’ technique is presented by Peel [83].

A very significant result from the theoretical work by Foschini and Telatar is that it is possible to increase the capacity of a channel (whilst not necessarily reaching its capacity) even when the CSI data are not known at the transmitter. This was shown theoretically by Zheng, Tse and Medard [84] who demonstrated that the capacity of the channel can be scaled as long as the channel coherence interval is not too short without any knowledge of the CSI at both the transmitter and the receiver.

There had been a lot of early interest in the use of scheduling algorithms with relation to the MIMO broadcast channel: however, in 2004, Hochwald *et al* [85] showed that the throughput gain as a result of the use of such algorithms actually decreases as the number of antennas increase.

2.8.3 Massive MIMO Detection

Massive MIMO systems present some specific challenges related to the detection of signals at the receiver. More specifically, different sequences of transmitted symbols may be arriving at a receiver at different angles due to multi-path propagation. The task is to recover a vector $\boldsymbol{s}$, representing a sequence of transmitted symbols, from the received signal

$$\boldsymbol{y} = \boldsymbol{H}\boldsymbol{s} + \boldsymbol{z} \tag{2.17}$$

Where $\boldsymbol{H}$ is the channel matrix, defined as an $m \times n$ matrix (with m and n being the number of transmit and receive antenna elements) (see Figure 21, [86]). The vector $\boldsymbol{z}$ is a random noise term.

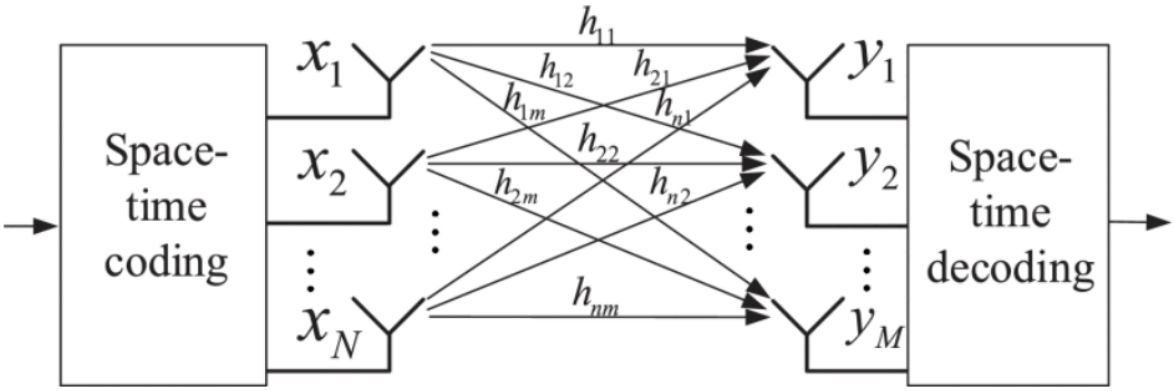

Figure 21: Basic Massive MIMO architecture showing composition of channel matrix [86]

Some common detection methods:

2.8.4 Maximum likelihood

The problem, for elements of $\boldsymbol{s}$ belonging to a finite alphabet S is

$$\min_{s \in S} \|\boldsymbol{y} - \boldsymbol{H}\boldsymbol{s}\|. \tag{2.18}$$

This is expressed in the form of a maximum likelihood problem. The channel matrix $\boldsymbol{H}$ can be decomposed (using QL decomposition) to $\boldsymbol{QL}$ where the matrix $\boldsymbol{L}$ is lower triangular. Doing so enables the problem to be re-expressed as

$$\min_{s_k \in S}\{f_1(s_1) + f_2(s_1, s_2) + \cdots + f_n(s_1, \ldots, s_n)\} \tag{2.919}$$

Where

$$f_k(s_1, \ldots, s_k) \approx \left(\widetilde{y_k} \sum_{l=1}^{k} L_{k,l} s_l\right)^2 \tag{2.20}$$

While noting that $\tilde{\boldsymbol{y}} \approx \boldsymbol{Q}^T \boldsymbol{y}$.

This can be visualised in the following tree diagram1 (Figure 22) [87].

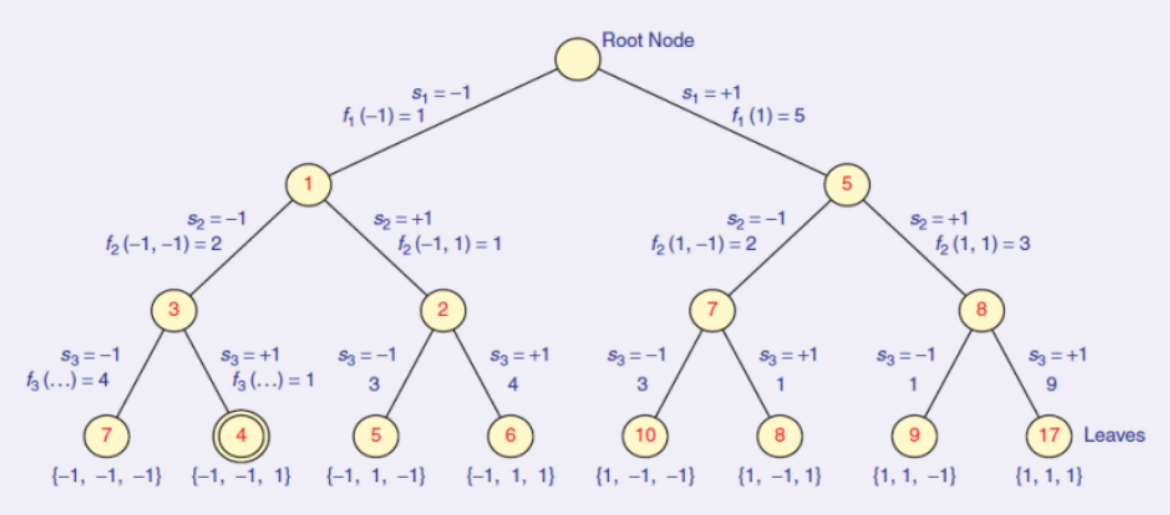

Figure 22: Tree diagram showing maximum likelihood decoding [87]

The idea is to select arbitrary values for the received symbol s_k at each edge along with the value of the function f_k. Each node is assigned the cumulative value for each of the preceding values of f_k and the most likely transmitted vector is the one that corresponds to the overall lowest cumulative value. Following this process will return the transmitted symbol vector with a low error dependent upon the accuracy of our knowledge of $\boldsymbol{H}$ and the noise characteristics.

The question now is how this problem can be solved more efficiently, given that it would be extremely computationally complex to solve all of the values in the tree and then simply select the lowest value when a large number of antennas are present in the system. Several common approaches have been used to solve this problem in practical environments with lower complexity, which are discussed briefly in this document. One problem with these methods is that, even though they can provide computationally efficient solutions, they are more prone to error than maximum likelihood estimation. Machine learning (ML) techniques have been applied to attempt to increase detection efficiency while retaining computational efficiency.

2.8.5 Zero-Forcing (ZF)

Standard Zero-Forcing (ZF) detection begins by framing the detection problem in a similar way to maximum likelihood detection [87]. However, unlike in maximum likelihood detection when the receive vector was assumed to belong to a defined finite alphabet, ZF detection requires only that the receive vector $\boldsymbol{s} \in Rn$. The

minimisation problem is thus expressed as

$$\tilde{\boldsymbol{s}} \approx \arg\min_{s \in R^n} \|\boldsymbol{y} - \boldsymbol{H}\boldsymbol{s}\| = \boldsymbol{L}^{-1}\tilde{\boldsymbol{y}} \tag{2.21}$$

where L is a lower triangular matrix. Once the minimisation process has been completed, the resultant vector is projected onto the space of possible vectors from the library, and the final estimation obtained by:

$$\hat{s}_k = \arg\min_{s_k \in S} |s_k - \tilde{s}_k|. \tag{2.22}$$

ZF provides a more efficient form of detection than that offered by MaxL detection, however it is less accurate and can only be regarded as reliable under certain types of channel conditions, namely when the channel matrix is well conditioned (i.e. near to full rank).

2.8.6 Minimum Mean Squared Error (MMSE)

The reason that ZF performs poorly in the cases where the channel matrix is not well condition is because the detection process, when projecting the calculated receive values onto the constellation of possible values, fails to take into account the noise correlations within the received symbols. A standard alternative method for detection when ZF is not viable is MMSE detection, which reformulates the problem to take account of the noise correlations:

$$\tilde{\boldsymbol{s}} = \arg\min_{s} \|\boldsymbol{y} - \boldsymbol{H}\boldsymbol{s}\|^2 + \frac{N_t}{\sigma}\|\boldsymbol{s}\|^2 = \boldsymbol{H}^{\boldsymbol{H}}(\boldsymbol{H}\boldsymbol{H}^H + \frac{N_t}{\sigma}\boldsymbol{I})^{-1}\boldsymbol{y} \tag{2.23}$$

Where N_t is the number of transmit antennas and σ is a suitably calculated noise term. The effect of this is to find the expected value $E(\boldsymbol{s}|\boldsymbol{y})$, which is then projected onto the constellation of possible transmit symbols.

Other detection methods not discussed here include ZF with Decision Feedback and Sphere Detection.

2.8.8 Spherical Wavefront Research for Massive MIMO

A number of papers have been published relating specifically to the issue of spherical wavefronts in the modelling of Massive MIMO channels. The channel model proposed by Jianzhi Li *et al* [88] is based upon a consideration of spherical wavefronts following analysis of results of an indoor measurement campaign involving omni-directional dipole antennas for both receive and transmit. As with other campaigns, a virtual array was used to simulate the configuration of a Massive MIMO array by moving the transmit antenna mechanically over several minutes to obtain the CSI as though a full-size array were used.

As discussed in other sections of this thesis, it is common to consider a geometric channel model as the links between transmit and receive antennas with one or more scatters located at some point between the two antennas. It is noted by Jianzhi Li *et al* [88] that the plane wave model can be considered valid when the distance between an antenna and a scatter is less than the Rayleigh distance

$$\mathrm{D}_{\mathrm{Rayleigh}} = \frac{2\mathrm{L}^2}{\lambda} \tag{2.24}$$

Where L is the largest distance between two antenna elements in the array and λ is the carrier wavelength. It was noted, from this assumption, that the indoor environments considered could lead to the situation where some of the users are in a position such that the plane wave assumption could be considered valid and some were not and therefore it was necessary to consider a model that always assumes the spherical wavefront. An approach to the question of when spherical wavefront assumptions are necessary is presented in this section of the thesis, thus helping to refine the decision-making process for when a plane-wave model would be appropriate, although this is often determined exclusively from the definition of the Rayleigh distance.

It was observed that, for the indoor environment, it is possible, by considering elevation and azimuth angles of arrival, to determine the presence of a spherical wavefront. A plane wavefront is observed when there is a clear and uniform angular offset to the array and a spherical wavefront where this is absent and the MPCs arrive in a more seemingly random fashion. The array that contained a greater

number of horizontal elements showed a greater presence of spherical wavefronts within the azimuth plane and the array containing a greater number of vertical components showed a greater presence of these wavefronts in the elevation plane. The observations of the presence of spherical wavefronts leads to the development of an extension of a standard cluster based Massive MIMO channel model to include 3D spherical wavefronts, which is described in the paper.

Some direct comparisons between the capacity resulting from a channel matrix obtained by a spherical wavefront assumption and a channel matrix obtained from a plane wavefront assumption have been presented. This includes Tamaddondar and Noori [89] where channel matrices are obtained for spherical and plane wave assumptions and capacity results compared. It is noted that non uniform distances between antenna elements could be applied in such a way that obtaining orthogonality between the sub-channels is still possible, even when some users are within the Rayleigh distance.

The research presented is concerned with non-uniform linear arrays, as these are the types of arrays that are likely to experience the largest change between the two elements at the each of the far ends of the arrays. The plane wave example shows a number of mobile users placed in parallel to a non-uniform linear array between the two end elements but at a variety of different distances from the array. It is not clear what the distances are and therefore whether the users are within the Rayleigh distance or not. The plane wave channel matrix is then obtained for the described scenario.

A similar scenario is then described but with the channel matrix obtained using a spherical wave assumption. The capacity of the channel is then determined using the standard Shannon formula and the results show that, on average, there is a significant different between the capacity calculated using a plane wave model compared with the capacity calculated using a spherical wave model, with the plane wave model underestimating the capacity compared with the spherical wave model when users are placed close to the BS (and are thus more likely to be located within the near field). It is observed that, when the mobile users move further away from the BS array, the spherical and plane wave models begin to converge until they predict approximately the same channel capacity.

The same format of results is presented for non-uniform linear arrays with different numbers of elements. These results show that, when the array consists of fewer elements, the difference between the two types of model is less; however it is still observed that the spherical wave model predicts greater capacity than the plane wave model and that the capacity predicted by the models converges as the users move further away from the BS array. This convergence occurs more quickly for arrays with a greater number of elements. It is also observed that the initial different in capacity between the two models is greater as the number of BS elements increases.

A similar convergence occurs when the number of users is varied. In the previous examples, the number of mobile users was 10. However, when the number of users is increased, the difference in capacity predicted by the two types of models is increased (with the spherical wave model still predicting higher capacity). As before, the capacity predicted by the two types of model converges as the users move further away, with this occurring much more quickly with the smaller number of users (Figure 23).

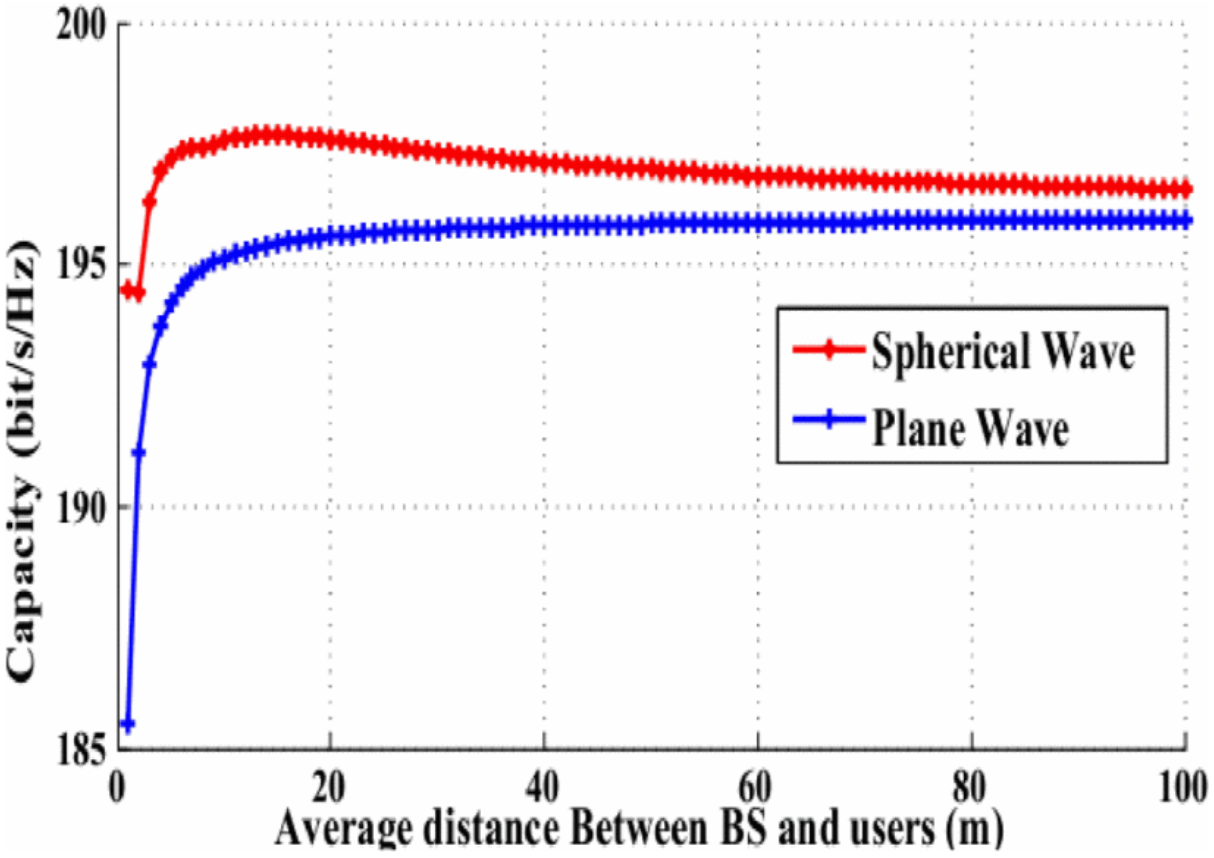

Figure 23: Capacity estimated by spherical and plane wave models [89]

A parabolic approximation of spherical wavefronts has been investigated by Lopez, Wang and Feng [90]. It was identified by the authors, as with others, that the plane wavefront assumption may not be valid for Massive MIMO arrays because of both near-field and environmental effects. The authors refer to the near filed effects as being those that occur when a user is located within the Rayleigh distance of the array, leading to effects such as variations in angles of arrival across the array that make the spherical wavefront assumption invalid. The environment effects refer to the large-scale parameters that affect large arrays, such as the shadowing that can occur that varies across the array, something that has also been investigated as part of this thesis.

The model proposed by the authors is intended to address the issue of the variation of AoA variation across the array, an effect observed through measurement campaigns. Crucially, they also mention the high level of complexity required for a spherical wave model, as this requires the simulation of all of the paths between the transmitter and receiver. The paths may be modelled deterministically using a ray-tracing system with map data or geometrically and stochastically by modelling the appearances of clusters within a model. The use of a parabolic approximation is intended to reduce the complexity and a stochastic method is proposed to more accurately simulate the appearance of clusters.

Jiang *et al* [91] have discussed the impact of a spherical wavefront assumption on both LoS and non-LoS propagation scenarios. This is in the context of vehicle-to-vehicle communications using Massive MIMO, for which the authors propose a novel channel model. This model, incorporating the spherical wavefront assumption, is proposed to address what the authors describe as the changeable vehicle shapes in 3D space and the failure of other methods to take account of the impact of spherical wavefront assumptions on channel statistics. The changeable vehicle shapes must be taken into account, according to the authors, to account for the changing geometry of the arrays required to achieve Massive MIMO communications in purely vehicular environments. Furthermore, it is noted that the use of a plane wavefront assumption is unable to take account properly of the 3D geometry of the types of arrays that would be used in vehicular communications.

The authors have identified a lack of comparisons in the research literature of the performance of different areas of the 5G mmWave spectrum. They have attempted

to address this lack by conducting measurement campaigns that obtain the same types of measurement for the same types of environments and configurations at several different mmWave frequencies bands, names at 11, 16, 28 and 38GHz. The measurements were taken within an indoor office environment and comparisons are provided for the power delay, power azimuth and power elevation profile. The power azimuth profile described the power arriving at an antenna as a function of the azimuth angle and the power elevation profile provides the same power metric but as a function of the elevation angle instead of the azimuth angle. The measures investigated at different frequencies also include the root mean square (RMS) delay spread, the azimuth angular spread and the elevation angular spread. These final two measures refer to the spread of the MPCs at the receive antenna and, as they give a sense of the multi-path richness of the environment, are important in determining the suitability of the channel provided by the configuration for spatial multiplexing with Massive MIMO.

Even though the research described is concerned with mmWave Massive MIMO, which is generally outside of the scope of this thesis, it investigates some of the so-called ‘new Massive MIMO properties’ as part of the analysis, including the effects of spherical wavefronts. The analysis also includes an investigation of the cluster birth-death property and the non-stationarity property. The clusters seen from the perspective of a Massive MIMO array, which are responsible for the scattering of MPCs, may not be visible from each of the antenna elements within the array, especially in propagation scenarios involving large arrays or complex spatial environments. This spatial property can be modelled as a markov process, describing the appearance and disappearance of clusters across the array. The non-stationarity property refers to the fact that, for large arrays, the wide sense stationary assumptions for the array may not be valid. The implication of this is that certain properties that could ordinarily assumed to be the same across the entire array, such as LoS receive power, may not be valid for the Massive MIMO scenarios. The research describes the change of received power for the LoS received power across the array and the change in azimuth AoA. In each case, the property is seen to vary significantly across the array. However, the functions describing the power and azimuth angles relative to the antenna element of the array are significantly different depending on the chosen frequency band, even though the propagation environment

is the same for each time measurements were taken. The following graph (Figure 24) shows an example of how the received power varied across the array:

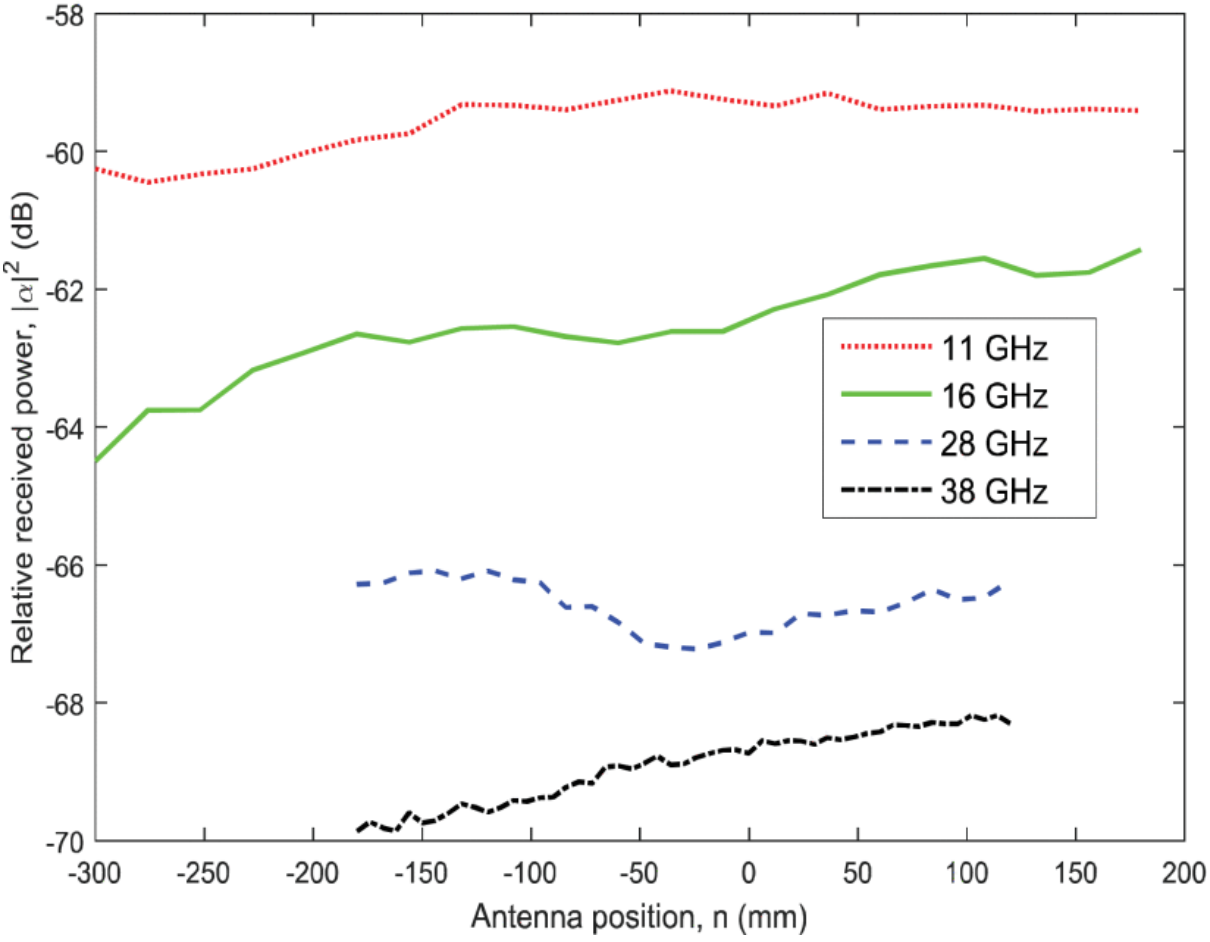

Figure 24: Variation of received power for antenna elements across array at different frequencies

The SAGE algorithm, which assumes a plane wavefront, was used by the researchers to obtain various properties investigated as part of this research. The researchers were, however, still able to use the algorithm to investigate the spherical wavefront effect by dividing the array into several sections and obtaining results, with the sections each small enough to ensure that the transmit antennas were beyond the Rayleigh distance and that it was possible to make a comparison of the spherical wavefront properties across the elements of the antenna when comparing the results obtained within different sections. The comparison is obtained by using a sliding window to obtain the gradual changes that occur across the array. The spherical wavefront properties relate to the MPCs arriving at each antenna element of the

array and the researchers show the variations of the azimuth angles of the components vary from one end of the array to the other and the variations of the elevation angles of the components. The analysis of each of these spherical wavefront properties demonstrate the importance of assuming spherical wavefronts, as the variations were seen to vary sometimes by about twenty degrees from one end of the array to the other.

It is notable that, even though algorithms such as SAGE and RiMAX that assume planar wavefronts are often used to estimate the properties of MPCs within a channel, there have been attempts to obtain algorithms that are based on spherical wavefronts. These algorithms have proposed for estimating the properties of the MPCs within Massive MIMO channels, where a spherical wavefront may be required, and as an alternative to obtaining properties based on the spherical wavefront assumptions by using the method described previously using a sliding window with a plane wavefront assumption. One such example of a spherical wavefront-based method for channel estimation is proposed by Chen et al (2016), who discuss the use of this approach with regard to the localisation of clusters [92].

The performance of the spherical wavefront approach to localisation was discussed and the results of simulation presented by the researchers. Firstly, the root-mean-squared estimation error was presented by considering a path with a set elevation angle-of-arrival and then determining the error of the estimated path for different azimuth angles of arrival. It is shown that the error is greatest for all elevation angles-of-arrival when the transmit antenna is located in the same plane as the array (that is at zero and 180 degrees). The error decreases to its lowest value at an azimuth angle of around 90 degrees, at which point it begins to increase again. Higher elevation angles lead to greater error but, for elevation angles lower than 20 degrees and azimuth angles between 20 and 160 degrees, the error is less than two percent and even less for low signal to noise ratio (SNR) scenarios.

The evaluation of the spherical wavefront approach to channel estimation and localisation was aided by data from an outdoor measurement campaign that, as with the comparisons of the properties of mmWave band for Massive MIMO, were conducted at mmWave frequencies. While these frequencies are outside of the scope of this thesis, the analysis of spherical wavefronts is relevant. The researchers present results from the original power spectrum with delay compared with the AoA.

The published paper does not provide a detailed comparison of the SAGE algorithm against the algorithm with the spherical wavefront assumption, how it does mention that the plane wavefront assumption tend to underestimate the power spectrum by about 30dB whereas the spherical wavefront assumption underestimates it by about 10dB, therefore offering an improvement. A more detailed comparison of spherical and plane wavefront assumptions in the estimation of multi-path properties would be an area for further investigation. The researchers also present a summary of the results of the location of scatterers using a spherical wavefront assumption. They identify that scatterers are successfully located, which is to say that they correspond with the physical location of objects on the rooftop where the measurement campaign was conducted. However, they also show that sometimes the images of the scatters are located instead of the scatterers themselves, which is still useful for understanding the contribution of the scatterers but not useful for accurately locating the physical objects responsible for scattering within a Massive MIMO propagation environment. A more detailed comparison of spherical wavefront and plane wavefront approaches in identifying the location of scatterers, and the tendency of each approach to select the images of scatters instead of the scatters themselves, is not presented and would be an area for further research. Figure 25 shows the localisation of scatters (or the images of scatterers) using the spherical wavefront model:

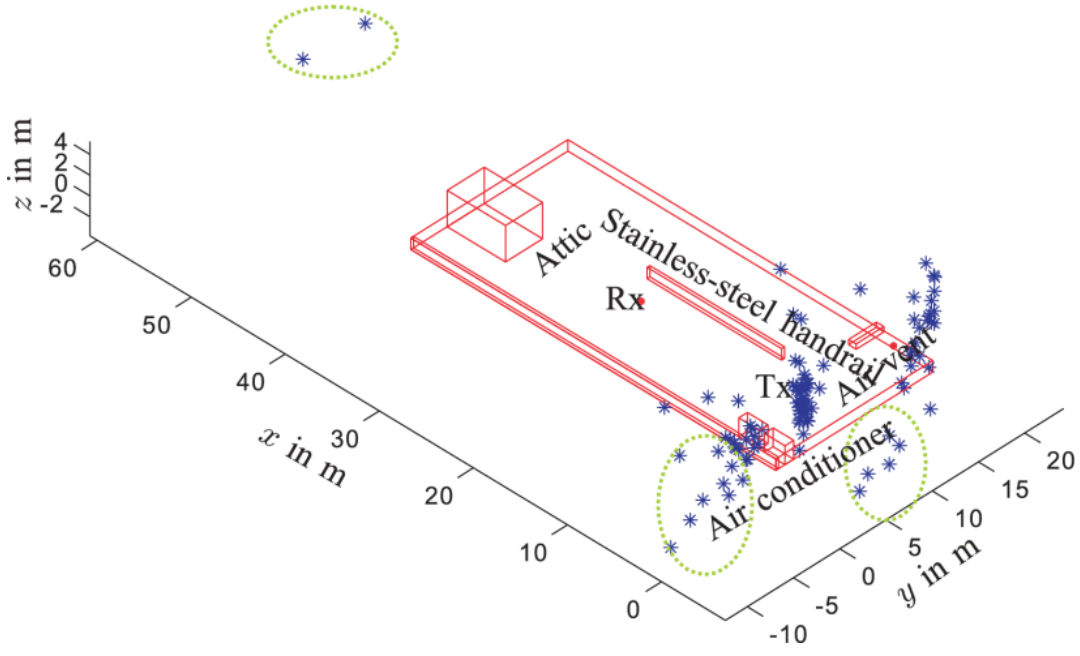

Figure 25: The localisation of scatters or their images using the spherical wavefront model

Much of the interest in spherical wavefront approaches to Massive MIMO can be traced back, if one considers citations in more recent papers, to the development of a two-dimensional channel model by Wu [93] that assumes a spherical wavefront instead of the more usual plane wavefront in order to address the address the observation that scatterers for Massive MIMO arrays can often not be assumed to be within the Rayleigh distance. As well as proposing a channel model for Massive MIMO, the authors also conducted a comparison of plane and spherical wavefronts within such channels. The proposed model is an ellipse model and the effects of the spherical wavefront assumption on LoS and non-LoS links. The authors also introduce an algorithm to model the appearance and disappearance of clusters. This algorithm includes a model of the changes that can be observed spatially across the antenna array, where some antenna elements can see certain clusters while others can see other clusters. It also includes incorporates a model of how clusters appear and disappear over time. Various statistical properties of the proposed Massive MIMO model are also presented.

One of the key results in terms of spherical wavefronts presented by the authors is the change in angles of arrival that occurs gradually from one end of the array to the other. This is explained as part of the effect of the spherical wavefront due to the transmit and receive elements or, more commonly in non-LoS channels, the clusters not being outside of the Rayleigh distance. This raises the question of whether there is a certain class of Massive MIMO channel where the clusters can be assumed to be in a position where the assumption of elements being outside of the Rayleigh distance can be maintained. The authors also discuss the received power difference from one end of the array to the other and how this would appear to be approximately proportional to the correlation between elements.

Figure 26 shows an example of the power spectrum for angles of arrival across the array:

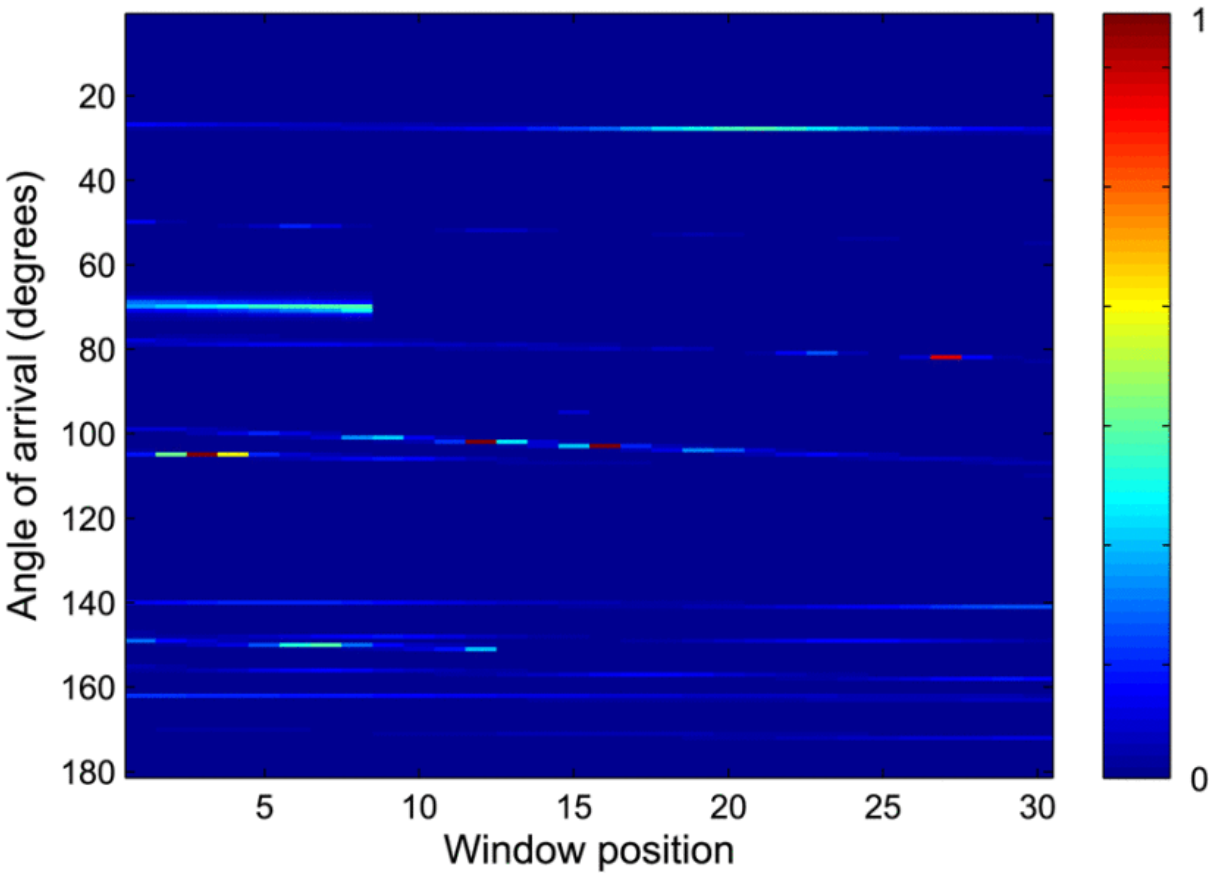

Figure 26: An example of the power spectrum for angles of arrival across the array

2.9 Conclusion

This literature review has provided an overview of propagation models for Massive MIMO, a key enabling technology for the future 5G telecommunications systems. Following an explanation of the general background theory that will be relevant for the considering of Massive MIMO, the concept of MIMO communications was introduced in terms of both single and multi-user contexts. The understanding of standard MIMO is important because it forms the foundation of much of the ideas related to Massive MIMO, such as spatial multiplexing and spatial diversity, even though Massive MIMO represents new challenges of its own from a channel point of view that are not present in Massive MIMO due to the much greater quantity of transmit and receive antennas.

The introduction to standard MIMO systems led into an explanation of the Channel matrix in terms of its mathematical expression. The channel matrix represents the response between each of the antennas within a MIMO system and will be crucial for

the modelling of a MIMO channel. The general mathematical explanation was followed by a review of some of the general approaches that are used for the numerical modelling of the channel matrix, beginning with models that are purely deterministic through the consideration of the geometry of the specific environment in question, proceeding to models that use a statistical understanding of the propagation environment combined with a geometrical interpretation (thus providing useful information about the channel within certain standard types of environments, such as offices, city centres and suburban scenarios). Models based only on a statistical understanding of the propagation scenario without any geometrical considerations were also discussed briefly.

The discussion of the general approaches to the modelling of the channel matrix were followed by a more detailed explanation of some of the main channel models that are used to model MIMO systems, specifically the WINNER-II model and the 3GPP spatial channel model. The angular parameters of the models were presented along with information about the specific scenarios that the channels can model from a statistical perspective. The need for verified propagation models that can be used for the design of Massive MIMO systems was also discussed.

An overview of current research interests in Massive MIMO was provided followed by a more detailed explanation of current theoretical research related to the Massive MIMO channel. It was seen that much of the current work is of a theoretical (specifically Information Theory related) nature and that this is likely to prove of importance to the research project due to a strong interest in increasing channel capacity and spectral efficiency.

3: Ray-Tracing for Massive MIMO Channels

The purpose of this chapter is to introduce the deterministic methods for the modelling of Massive MIMO channels that are used throughout the research described within this thesis. These methods are introduced partly through the illustration of various examples that are especially representative of the kinds of phenomena that are expected to be present within many Massive MIMO channels. In particular, the use of antenna arrays that are much larger than antenna systems typical of mobile networks is considered as an important element in the modelling of these channels. This consideration leads to the requirement for any realistic Massive MIMO based propagation model to account for the changes in how the channel appears from the perspective of different points on the antenna array. Such changes that occur across the array can be associated with certain observations. For example, slow fading across the array is potentially highly significant within Massive MIMO channels involving large arrays when compared with smaller arrays, where these kinds of effects may often be negligible. This large-scale fading may occur when, for example, a large array is orientated towards a particular service area but where this is some obstruction blocking the LoS path from the array to the users. Because of the dimensions of the array, it is possible that such an obstruction blocks only the LoS paths from some of the elements of the array, but not all of the elements, thus potentially leading to a situation where the channel characteristics look very different from the perspective of one end of the array when compared to the other.

The observations of the changing channel conditions as seen across large arrays leads to the question of the appropriateness of planar wavefronts when considering the propagation models used for Massive MIMO based networks. It may be necessary, for example, to favour a spherical wavefront-based model, where the propagation paths between each antenna are considered on an individual basis, rather than assuming an arriving wavefront where the differences between array elements are represented only by phase shifts. Essentially, the ray-tracing described in this chapter provides such a spherical model, though at higher computational expense than may be suitable for some applications.

A significant implication of the research presented in this chapter is in relation to mobility scenarios, where the users follow routes around the cell area. Here, such mobility is modelled through the use of discrete time steps where the user equipments (UEs) occupy a neighbouring location on the time-step after the current step close to the current position. Mobility in terms of handover is not considered in this chapter, however it is observed that very significant changes can occur in the propagation channel within the cell. This then affects how well the channel can support multiple spatial streams though the lack of rank-deficiency within the channel correlation matrix (since the ideal propagation scenario would involve a full-rank correlation matrix). The relative ability of the channel to support the separate streams can be considered as a one-dimensions channel condition time-series. This time-series is discussed within this chapter, and it is shown that such a series is amenable to modelling using well-established statistical methods. Correlation can be due, at least in part, to mutual coupling between the antenna elements, as illustrated by Lu, Hui and Bialkowski in 2008 [94]. This thesis, however, does not consider this as a separate effect.

3.1 Theoretical background of ray-tracing

The research described in this thesis is largely based on two separate ray-tracing engines, the first of which is an in-house ray-tracing system developed within the University of Bristol. The second system is a third-party system developed by Recom software. The first system became unavailable after a system upgrade and a modified version was found to contain inconsistencies within the generated data.

Ray-tracing is a general technique for simulating optical effects that is based on notions with geometrical optics (GO). GO is a well-established area of physics that involves the study of the behaviour of light according to certain simplifying assumptions. The simplification allows for the obtaining of useful predictions regarding how light would be expected to propagate within a medium, whilst not requiring, in many situations, the finding of solutions to Maxwell's Equations, which describe the laws of electrodynamics governing the propagation of light in a classical sense, or the use of quantum electrodynamics, which describes the interaction of light with materials by describing the dynamics of photons [95].

GO, in the context in which the ray-tracing is applied within this thesis, achieves the simplification of the dynamics of light by developing an abstraction known as a 'ray.' In the case of a narrow beam of light or laser beam, it is intuitive to understand how light could be described as a ray, however GO and ray-tracing can be used to create predictions about all forms of light, and indeed for electromagnetic energy propagating at other frequencies and within a wide variety of conditions. This is often achieved by using several rays as contributing to the dynamic of the electromagnetic energy.

Each ray is subject to certain principles that make up GO. These include reflections from surfaces, where the angle between the incident and reflected ray is determined by the arrival angle and the geometry of the surface. Refractions are also considered, which involve a change in direction of the ray as it is seen to pass from one material to another, each with a different refraction coefficient. The refraction is modelled according to Snell's Law

$$n_1 \sin\theta_1 = n_2 \sin\theta_2 \tag{3.1}$$

Where n_1 and n_2 are the indices of refraction and θ_1 and θ_2 are the angles between the normal to the surface and the incident and refracted rays.

While ray-tracing is based primarily on the principles of GO, it also incorporates some other elements to its calculations of the dynamics of electromagnetic element that do not form part of GO. For example, ray-tracing engines often provide the option to consider diffraction as part of the computations, which allows for the consideration of rays moving around buildings and other structures as well as for the effects of scattering within certain types of environments.

The ray-tracing engine at the University of Bristol dates back to the year 2000 [96] and was part of an effort within research to address the requirements of propagation models for small cell networks, which, at the time, were gaining increased attention as a possible way to address the growing demands being placed upon existing mobile networks through the increased use and popularity of cellular telephones. Around this time, it was common to use empirical propagation models for the design of mobile networks. These models were developed from data obtained through

measurement campaigns, where measurements would be taken at various locations within an environment that represented the type of scenario. Statistical methods such as regression analysis were then used to obtains reasonably simple 'inverse square' type rules that would provide an approximation of field strength as the distance from the BS antenna increased. While these types of methods are still used in mobile network planning, in combination with other methods, it was observed at the time that these methods did not provide sufficient accuracy for small cell networks. MNOs had previously emphasised the importance of maximising coverage, and this priority was reflected in the types of propagation models that were employed and the emphasis place on large 'macrocells,' with BSs often placed at the highest locations possible. The use of small cells would require a much more thorough understanding of the propagation environment, due to the need to focus more on the complexities of the coverage area and the presence of many cells that would potentially be overlapping. In addition, there was a gradual shift in emphasis by MNOs away from coverage and towards capacity, and this would need to be considered within the process of designing the RAN.

The goal of the University of Bristol ray-tracing system, as with other ray-tracing systems, is to use the described methods to obtain the 'complex impulse response' of the received signal

$$h(t) = \sum_{n=1}^{N} A_n \delta(t - \tau_n) \exp(-j\vartheta_n) \tag{3.2}$$

Where the CIR, $h(t)$, is made up of a summation of amplitudes,A_n corresponding to a phase angle ϑ_n at arrival time τ_n.The ray-tracer functions according to a method based on the 'method of images,' whereby an image table is generated of each location of the image of the BS. This is achieved by considering all surfaces present as possible reflectors. It is possible to create this image table by considering every possible combination of reflection, transmission and diffraction to create a path through each reflector and then obtaining a location for the BS from the perspective of the UE. Once these locations have been obtained, it is possible to find the paths between each UE and each BS image. The computation is made more rapid by

introducing the concept of an ‘illumination zone,’ which is the area for which a certain order of reflection can give a valid path (Figure 27).

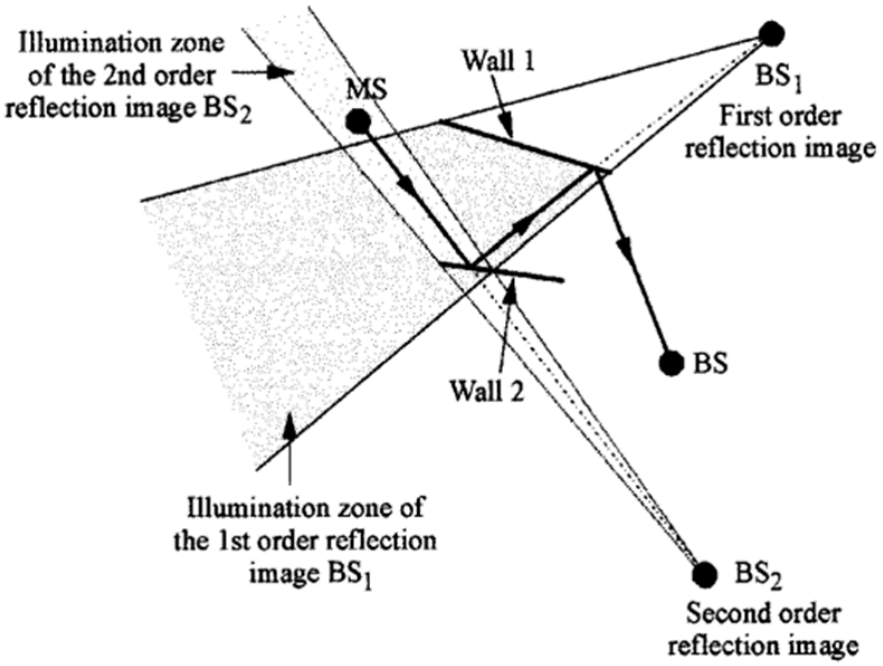

Figure 27: Illumination zones from base station (BS) images [97]

The specific method used by the proprietary Remcom software is described within the documentation [98] and includes the use of a ‘shooting and bouncing ray method’ to initially trace the paths without reference to specific field points, followed by an ‘eigenray’ method, which constructs the ray paths between the transmitters and receivers. However, many ray-tracing systems are based fundamentally on a ‘ray launching’ algorithm, where rays are sent out from the UE at a series of angles with their paths traced. A ray is accepted if a certain power threshold is reached. There are ways of making this process faster, such as the one described relating to the University of Bristol ray-tracing system.

3.2 Discussion of ray-tracing system used in this research

The ray-tracing system used by the University of Bristol, which forms the basis for much of the research presented in this chapter is based on light detection and ranging (lidar) data representations of outdoor locations. Lidar data refers to a technique of using reflected energy passed over land to determine the distance of

the objects on the ground, with the time taken for pulses to return indicating the location. Such data are available for regions around the city centre of Bristol and is used to provide a representation of the environment, including buildings and foliage.

The lidar data are translated into a representation for the system that approximates the layout of the land. This representation for the ray-tracer is only approximate and is based on a series of squares containing the information regarding the height of the feature of the land, which is not defined in the system, but which could include a tree, for example, or a building. To illustrate this, consider the two photos in Figures 28 and 29. The first shows an area of land in the centre of Bristol from a satellite photograph. The second shows how the ray-tracer 'sees' this terrain, in other words how the ray-tracing system interprets these terrain data. As can be seen, the ray-tracer has only a general block interpretation of the terrain, with the colours in the image indicating height. This representation, however, does mean that simulated ray-trace results do correspond approximately to a realistic interpretation of the Bristol urban environment. It should be noted that the shapes here, in addition to the height information, include horizontal and vertical edges that are used to model diffraction with the centre of tiles used for scattering and the shapes themselves used for reflection [28].

The process of ray-tracing includes "building reflection, building rooftop diffraction, building corner diffraction, building scattering, terrain scattering, and combinations of the above" [28] and supports three dimensions. Firstly, the lidar data are pre-processed, after which the ray-finding process is used to identify all possible paths between transmit and receive antennas. An electromagnetic calculation process is then applied to each ray, which uses several electromagnetic propagation models including hybrid scattering models and foliage loss models.

Functioning of the ray-tracer system

The ray-tracer allows the user to specify a point at which an antenna element would be located. This point is associated with a function describing the antenna pattern which is used for calculating the gains associated with each ray. The following example demonstrates this principle.

A portion of Bristol city centre is selected to provide an example of a dynamic urban environment (Figure 28). The area chosen is Cabot Circus, located to the east of the

inner-city area, known as an area with a large amount of traffic and potential for congestion. The transmit antenna is placed on a large building near the main road. In order to show the effect of the rays rather than the gains at the antenna, an isotropic radiation pattern (with unity gain in each direction) is chosen to provide an impression of the environment, although specific simulated and measured antenna patterns (obtained through an anechoic chamber) can also be used in the system. The location of the antenna is indicated by a dot and arrow on the map, with the arrow indicating the reference direction for the antenna, although this is not relevant for a pattern with equal gain in each direction, such as is used here.

Figure 28: Aerial image of Cabot Circus, Bristol (located at grid co-ordinates: 51.4585° N, 2.5853° W). Figure shows an area approximately 1200m x 640m. The white rectangle indicates the area that is represented by Figure 29

A high-quality satellite image of the region can be used to provide a detailed impression of the terrain, although it should be noted that the lidar data used within the ray tracer are based on terrain data that were collected several years ago and thus are not completely accurate, due the changes to the urban environment that have occurred since then. Most of the buildings, however, remain the same and it is reasonable to assume that the terrain has not changed significantly. Therefore it is

possible to gain an impression of the propagation characteristics within this type of environment. If a more precise model is required, it would be necessary to investigate the extent to which any new buildings had altered the propagation environment. The area in this example includes a large and popular shopping centre, that was still under construction but was substantially complete, when the lidar data were assembled. The terrain, as seen by the ray-tracer comprises a series of blocks, as shown in Figure 29, which approximately correspond with the features of the terrain shown in the satellite image. In the ‘block representation,’ the blue squares represent buildings with the lighter shades representing higher building levels and the darker squares representing buildings of lower height. Foliage is represented by yellow squares with the shade representing the density. Note that the representation of a ‘high street’ shopping area is shown on the left, comprising mainly buildings that vary in height with a walking area that forms a cross, the centre of which corresponds with the centre of the high street area. This walking area appears as empty space in the default dark blue colour within the representation. There are also various gaps between the shop building and where vehicle parking areas are located, also represented by the same colour. Several city trees are present in this area, represented by the yellow/green blocks. To the south of this is a park area, represented by an increase in foliage with the yellow/green blocks and to the east is a mixed residential and commercial area, with a combination of foliage and building data. The area between these east and west regions is a large main road, shown in dark blue in this representation.

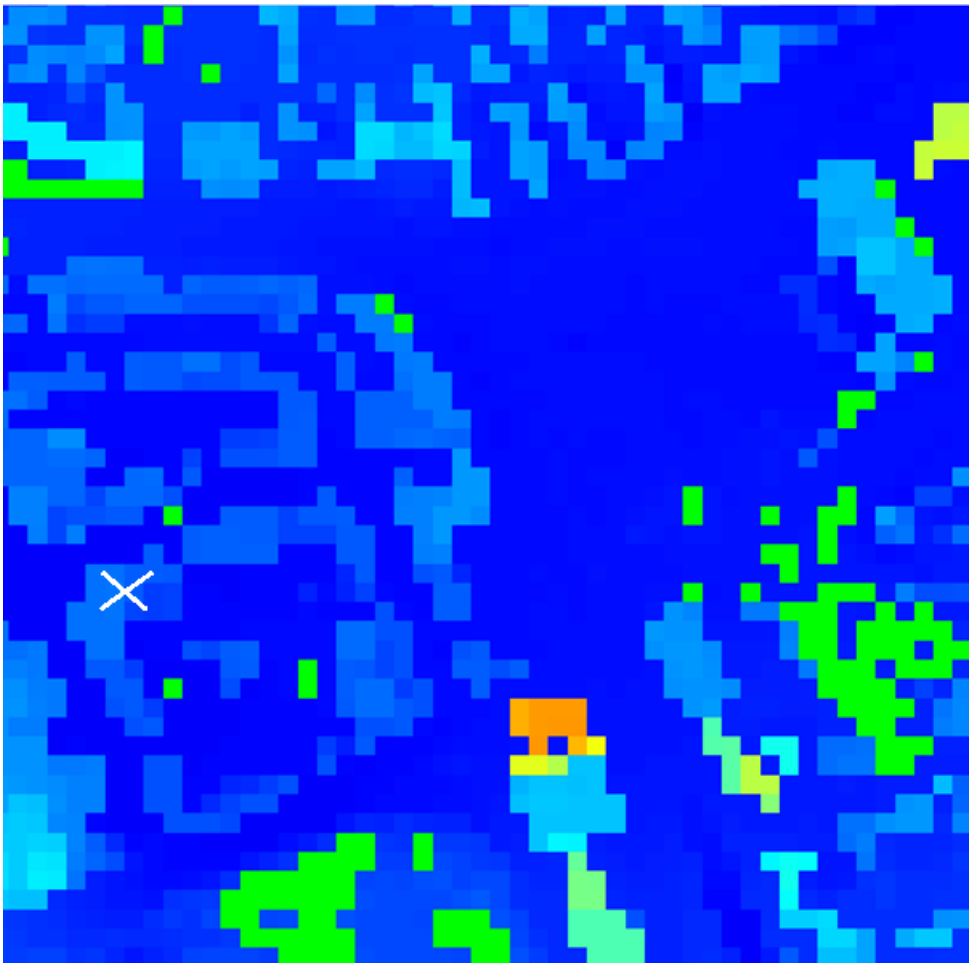

Figure 29: Satellite image of Cabot Circus, Bristol as represented by lidar data used in the ray tracing system. The blue shades represent buildings with the lighter shades showing greater height. Orange and yellow represent tall foliage, while green indicates low foliage. The white cross represented the location of the BS, orientated so that zero degrees is towards the east (which is towards the right-hand side in this image).

3.3 Plane Wave Models

The plane wave model is derived from an analytical investigation of the geometrical properties of an idealised linear array in a purely LoS environment. As such, it has often been assumed that this model represents an accurate representation of Massive MIMO systems in environments that are generally LoS (i.e. with few reflectors). It is likely that this observation is more relevant to mmWave above 6GHz because such frequencies generally only work well in LoS environments. Multipath components may be more relevant to lower frequency Massive MIMO even when the system is LoS. The model is developed by considering a linear array of equally spaced antenna elements from the perspective of a single point source antenna.

Here (following Tse and Viswanath, 2005 [99]) the impulse response for antenna element i is

$$\mathrm{h_i} = \exp\left(\frac{-\mathrm{j}2\pi\mathrm{d_i}}{\lambda_c}\right)$$

(3.3)

Where d_i is the distance in metres between the source and array antenna and λ_c is the carrier wavelength in free space. This expression for the response assumes that $d_i/c \ll 1/W$ where W is the carrier bandwidth.

The channel response is given in the usual way by combining the channel vector with the transmit symbol (of which there is just one value in this case) and adding to a noise term. The distances d_i between transmit and receive antennas are given by

$$d_i = d + (i-1)\Delta_t\lambda_c cos\ \Phi$$

(3.4)

With d being the distance from the transmit to the first (that is the nearest) antenna in the array and Δ_t being the normalised separation of the antenna elements normalised to the carrier wavelength. In this expression Φ is the angle of incidence of the incoming wave. So, on this assumption, the first channel response for the antenna element closest to the transmit source is

$$\mathrm{h_1} = \exp\left(\frac{-\mathrm{j}2\pi\mathrm{d}}{\lambda_c}\right)$$

(3.5)

and the remaining responses for $N = 2\ \ldots N$, where N is the number of antenna elements in the array, is

$$\mathrm{h_n}\ = \mathrm{h_1}\ \exp\left(-\mathrm{j}2\ \pi\Delta_\mathrm{t}(n-1)\ \cos\Phi\right).$$

(3.6)

Noting that the spacing between the antenna elements is fixed in the described scenario. The implication of these plane wave assumptions is that any capacity gain is due only to signal gain and not to any spatial multiplexing. The individual responses can be combined into the signal vector **h** and the capacity given as follows, showing the form of capacity gain that is obtained

$$C = log\left(1 + \frac{P\|\mathbf{h}\|^2}{N_0}\right) \tag{3.7}$$

Where P is the transmit power and N_0 is the noise term.

3.4 Spherical Wave Model

In two dimensions, considering again the point source transmit antenna with the linear array of receive elements, the wavefront should be considered in a spherical form to capture more precisely the geometry of the propagation environment. The wavefront would be considered as propagating in all directions with a simple example of an isotropic source, although radiation patterns should be considered for more realistic scenarios. Effectively, the spherical wave model, rather than assuming a uniform phase shift across the receive array, would consider the arrival of the wavefront from all possible paths with the distances defined between the transmit element and the receive element in question. In a complex propagation environment, that is one involving reflectors instead of just a LoS link, these distances may vary even though the paths arrive at the same antenna element.

A way of applying the spherical wavefront model is to model the paths using a ray-tracing system. There are several possible approaches to ray-tracing, where paths between transmit and receive antennas are calculated and various propagation models applied to take account of path loss, diffractions, reflections and how these relate to certain types of environmental features such as foliage and buildings. The approach used by the system at the University of Bristol works by creating an ‘imaging table’ for each of the transmissions by considering all possible permutations of wall reflections, transmission and diffractions [100] which is then stored to compute the channel characteristics at each location. The incoming rays at each location are then combined to provide the impulse response of the received signal. The implementation of the model includes taking account of wall conductivity, permittivity, and thickness in order to improve the accuracy of the model. Using this technique allows for the comparison of spherical and plane wave models by creating a scenario and obtaining the channel response under a spherical wave assumption. This response can then be compared with a directly computed implementation of the plane wave model. It should be noted that the plane wave model by itself is best

compared with an implementation of the model taking place in an open space without many reflectors. In the presence of many reflectors, it would be expected that the plane wave model would create inferior results compared with the spherical wave model, but that this could possibly be improved by the inclusion of reflectors within the plane wave model.

3.5 Plane Wave Models with Reflectors

As discussed elsewhere in this thesis, part of the aim in the development of Massive MIMO is to be able to use the effects of multipath propagation to obtain a degree of freedom gain through the ability to separate the signals obtained from the transmit and receive antenna arrays. The plane wave model described in a previous section can be extended to take account of reflectors that are used to provide a representation of multipath propagation. In practical scenarios, reflections occur thanks to the presence of various objects, such as buildings, trees and vehicles, and reflectors in a plane wave model provide an abstraction of these effects.

The extension to a plane wave model with reflectors can be visualised by considering a scenario in two dimensions with transmit and receive arrays placed in parallel with each other at a significant distance apart with a reflector placed at right angles at some point between the two and either above or below the arrays (in two dimensions) (Figure 30). The reflector is considered as a straight line of a certain length. For each element of the transmit array, a mirror image can be considered that is located in the same plane as the array and at a distance double that of the distance to the plane of the reflector (and in the same direction). It is then possible to consider a second transmission source by the receive array at the mirror image of the first transmission source. Considering a straight line drawn directly between the transmit and receive elements, this second mirror image source is taken into account only when the line passes between the two ends of the reflector.

The plane wave model is extended in the example described in the previous paragraph by considering wavefronts arriving from the two sources in the same way as in the example with no reflectors. The received response at the antenna is obtained by adding the responses formed by each wavefront, in other words determining the superposition of the wavefronts.

Here are some results from some MATLAB experiments where plane wave models are compared with spherical wave models for a linear 128x8 Massive MIMO LoS link operating at 3.5GHz with the following parameters [49]:

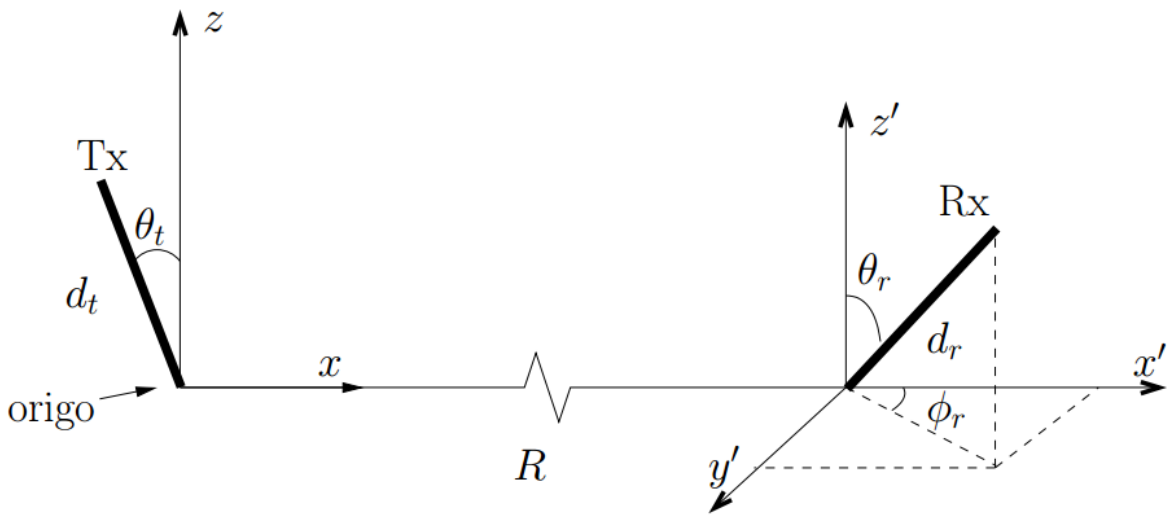

Figure 30: Co-ordinate system for transmit and receive arrays [49]

Where the specific parameters are defined as follows:

θ_t	0.5236rad
Θ_r	0.7854rad
Φ_r	0.1745rad
d_t	0.043m (half wavelength spacing)
d_r	0.043m

The distance R is not defined for the plane wave model and is varied in the spherical wave model to investigate how distance affects the accuracy of the plane wave model in comparison with the spherical wave model.

We begin by considering the plane wave model where, extending Bohagen's 2x2 MIMO scenario, the spatial signature for the receiver is

$$\boldsymbol{a_r} = \left[1 \quad e^{j\frac{2\pi}{\lambda}d_r \cos\alpha_r} \quad e^{2j\frac{2\pi}{\lambda}d_r \cos\alpha_r} \quad \ldots \quad e^{Mj\frac{2\pi}{\lambda}d_r \cos\alpha_r}\right]^T \tag{3.8}$$

Where M is the number of receive antennas. The spatial signature for the transmitter $\boldsymbol{a_t}$ is defined in the same way but where M is replaced with N, the number of transmit antennas. The H-matrix is then obtained from the spatial signatures as

$$\boldsymbol{H} = \boldsymbol{a}_r \boldsymbol{a}_t{}^T \tag{3.9}$$

Unlike in the case of the plane wave model, the spherical wave model requires us to consider the distance between each of the transmit antenna elements and each of the receive antenna elements:

$$\boldsymbol{H_{m,n}} = e^{j\frac{2\pi}{\lambda}d_{m,n}} \tag{3.10}$$

The matrix representing the distances between each antenna element is defined in a supplementary text by Bohagen [101] as:

$$\begin{aligned} d_{m,n} &= \|a_m^r - a_n^t\| \\ &= [(R + md_r sin\theta_r cos\phi_r - nd_t sin\theta_t)^2 + (md_r sin\theta_r sin\phi_r)^2 \\ &+ (md_r cos\theta_r - nd_t cos\theta_{t)}{}^2]^{1/2} \end{aligned} \tag{3.11}$$

Plots of the mean-squared error for the imaginary part of the H-matrix from 1 to 100 and from 0.1 to 1 are shown in Figures 31 and 32:

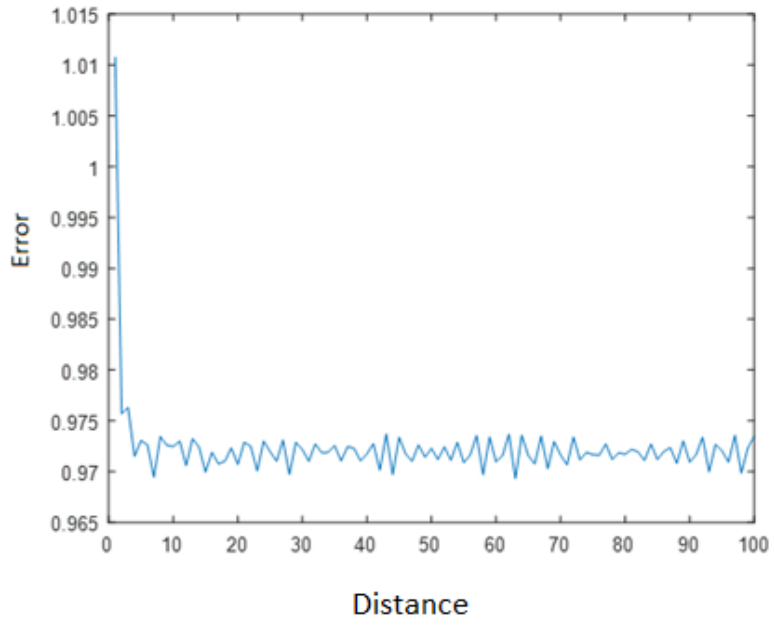

Figure 31: Mean-squared error for the imaginary part of the H-matrix from 1 to 100 m

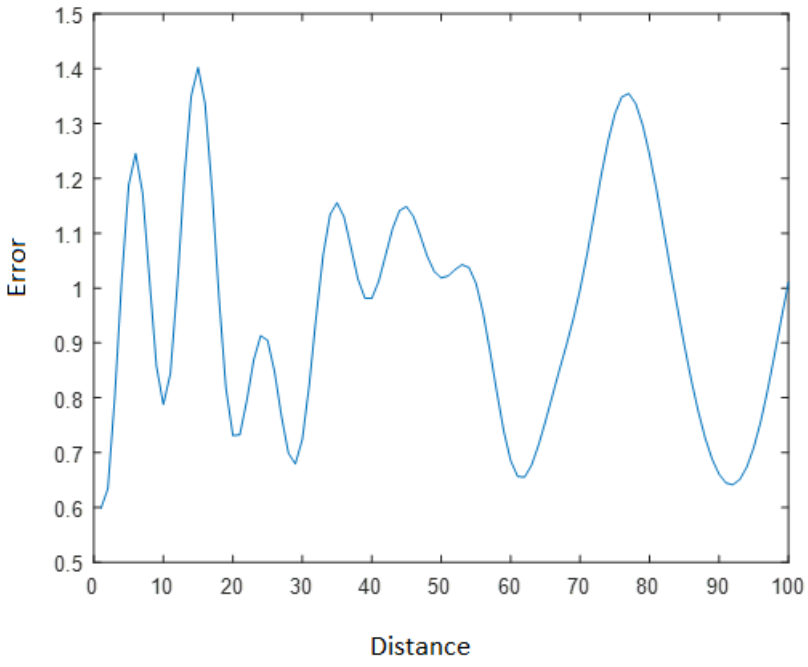

Figure 32: Mean-squared error for the imaginary part of the H-matrix from 0.1 to 1 m

3.6 Analysis of large arrays

The BS arrays for Massive MIMO are potentially very large. Thus, a situation may arise, for example, where part of the array is in the shadow of a nearby object such as a building and part of it has a clear LoS link with a MS. An example of a situation

where slow fading across an array contributes in a highly significant way to the performance on the channel is shown in Figure 33. Here, a linear array operating at 3.51GHz with half wavelength spacing with total distance between the first and last element of 5.3975 metres is located near a tower of Bristol Cathedral. A MS is located near to the north edge of College Green such that part of the linear array is visible and part of it is concealed by the tower.

Figure 33: Array based at Bristol Cathedral serving College Green (51.4517° N, 2.6006° W). The area shown is approximately 120 m north to south and 180 m east to west.

The power delay profile for the link between the MS and the end element of the antenna at the side that is visible and provides a strong LoS link is shown in Figure 34. The multipath environment is shown in Figure 35.

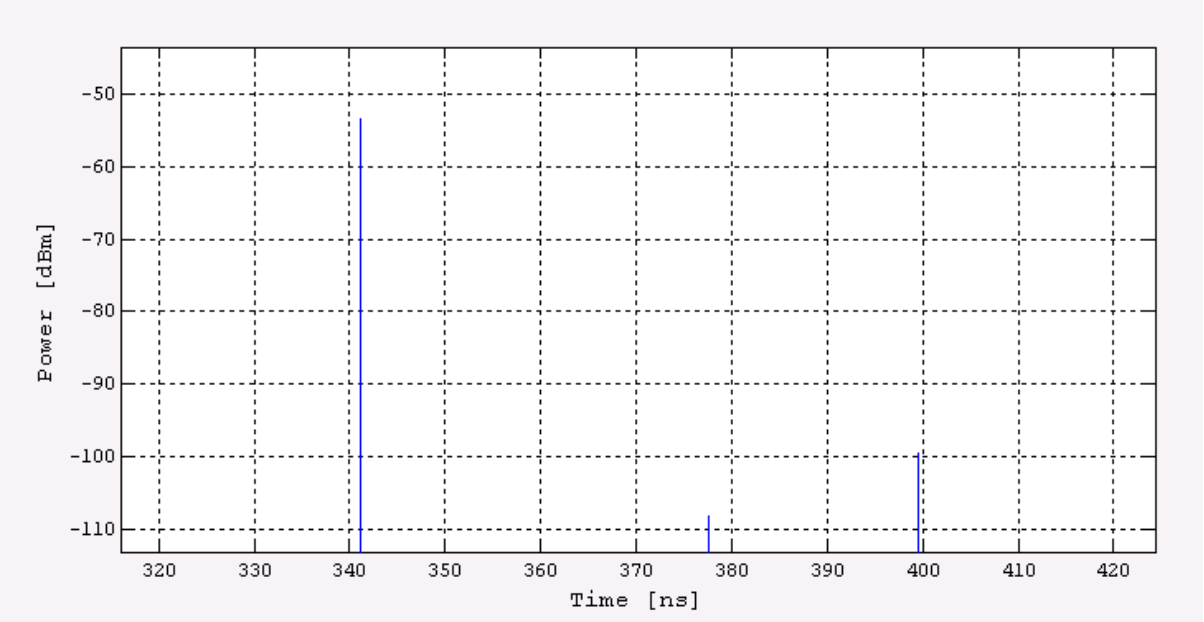

Figure 34: The power delay profile for the link between the MS and the end element of the antenna at 30 dBm (decibels relative to one milliwatt) with isotropic transmitters and receivers.

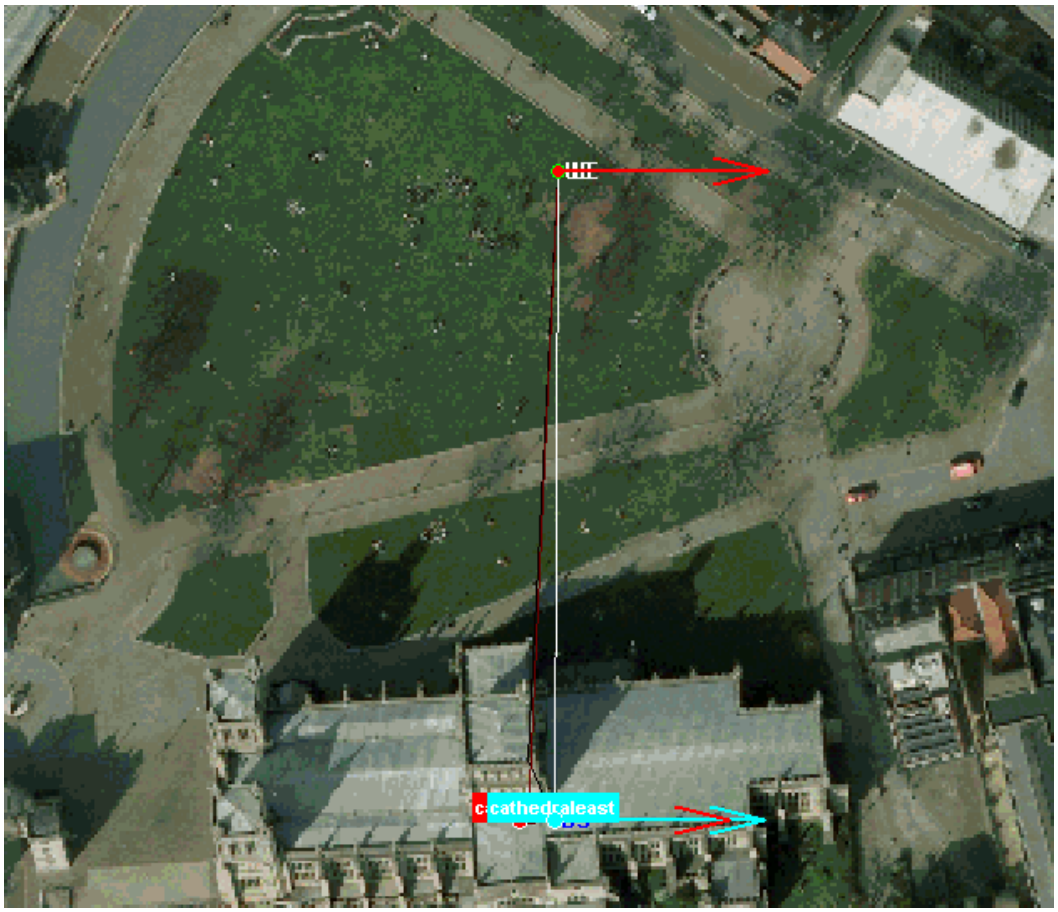

Figure 35: Multi Path Environment for first element of array. Area shown is College Green (51.4517° N, 2.6006° W). The area shown is approximately 120 m north to south and 180 m east to west.

The results shown in Figure 34 can be contrasted with those for the link between the MS and the end element of the array that is not visible. The associated rays indicate a much richer multipath environment for this case, as illustrated in Figures 36 and 37.

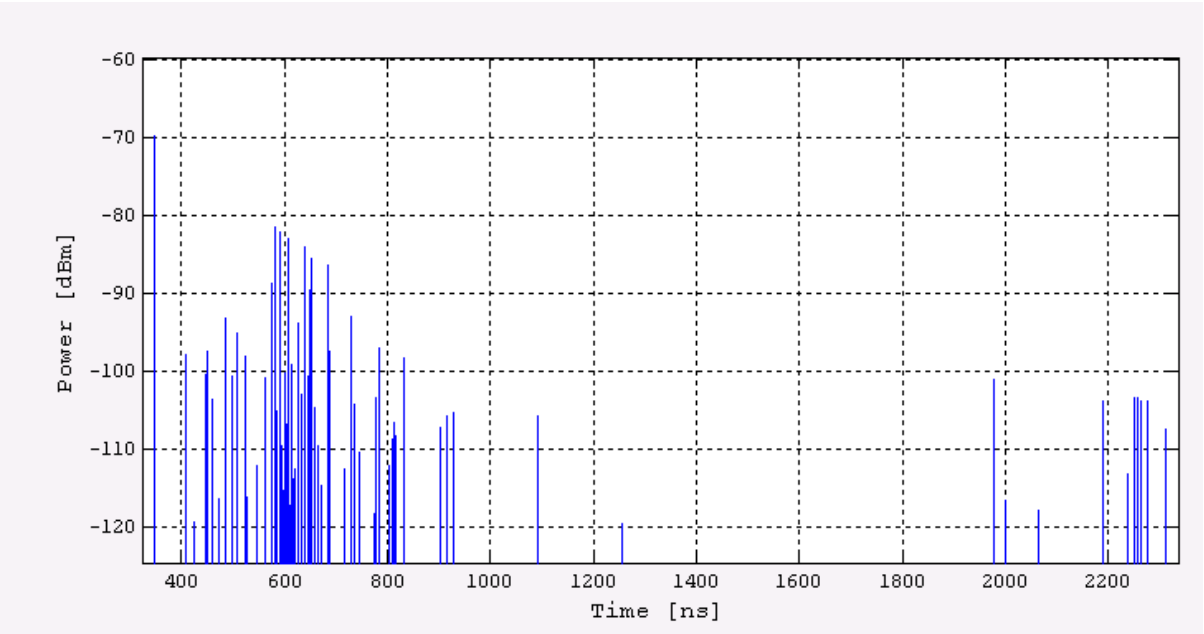

Figure 36: Power delay profile for array antenna elements obscured by tower. Transmit power 30 dBm.

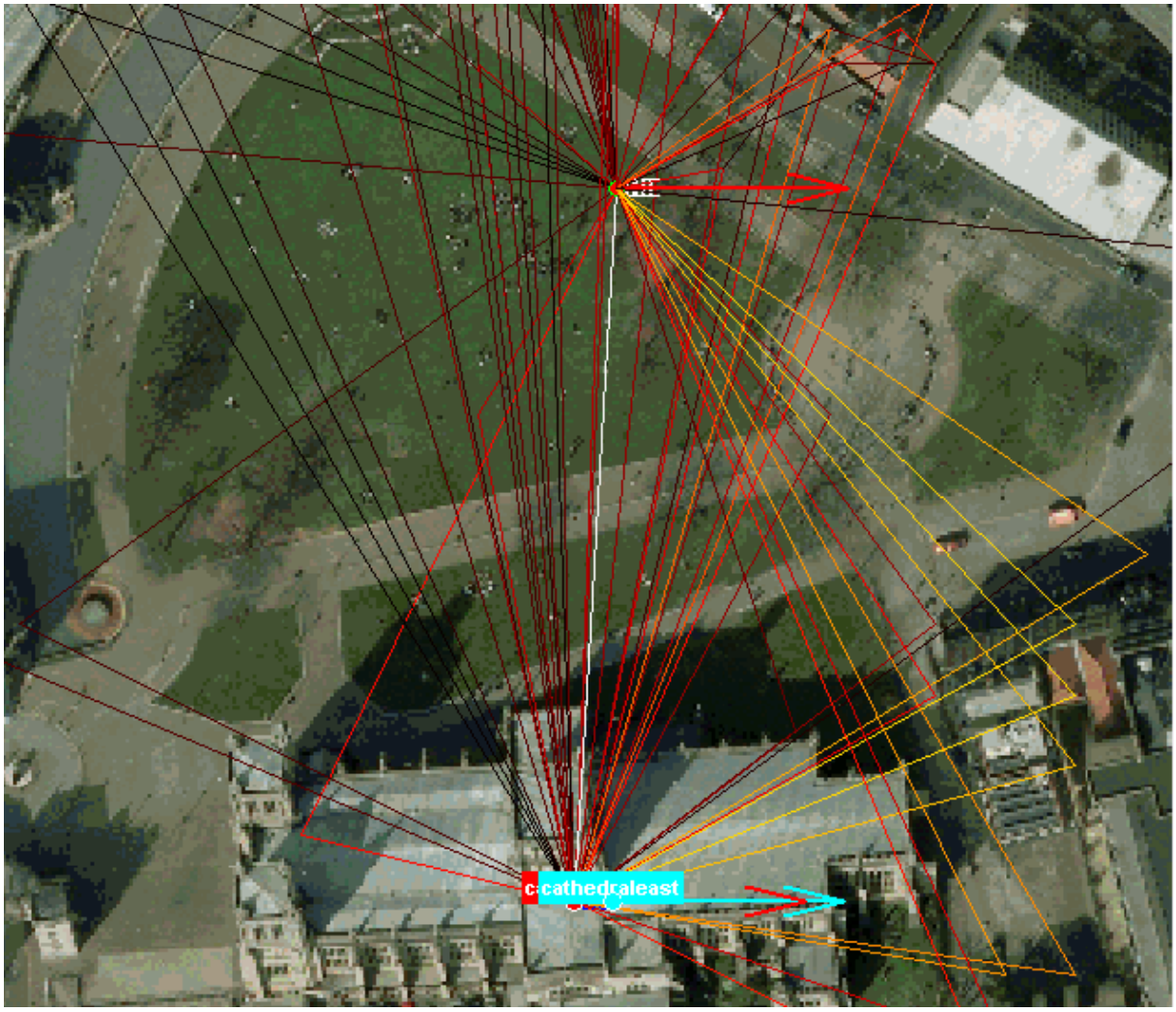

Figure 37: Multipath components between UE and element of BS obscured by tower. Area shown is College Green (51.4517° N, 2.6006° W). The area shown is approximately 120 m north to south and 180 m east to west. The white line indicates the principal component with the darker shades representing the less significant components.

3.7 MPCs at BS Array

Due to the potentially large dimensions of the BS array, it cannot be assumed that the MPCs will arrive at the same angle at each of the elements. In addition, and in particular for the case of 3D arrays, the elevation angles of the MPCs needs to be incorporated into any model that wishes to provide an accurate view of the Massive MIMO channel. A more specific example of this effect can be demonstrated by considering the same linear array placed near the Cathedral tower but with the position of the MS and the antenna changed slightly so that no part of the array is visible via a LoS link to the MS (Figure 38). The rays to the first element are shown

in Figure 39 and the rays to the final element are shown in Figure 40 in order to represent the differences.

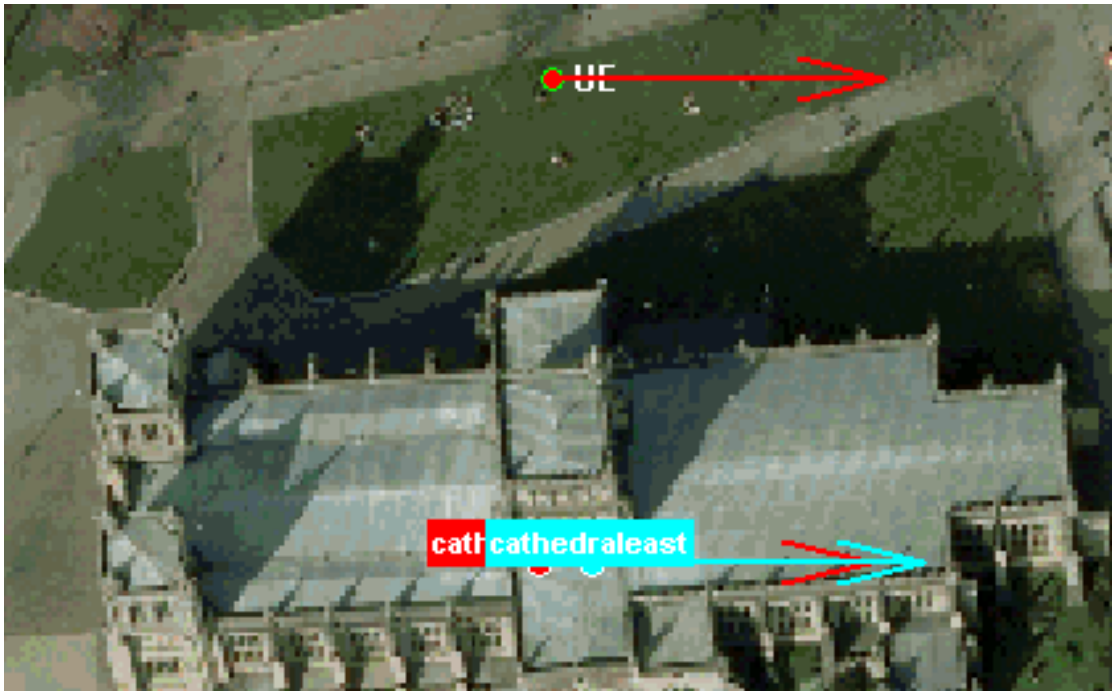

Figure 38: Position of UE in the shadow of Bristol Cathedral. (51.4517° N, 2.6006° W). The area shown is approximately 50 m x 100 m.

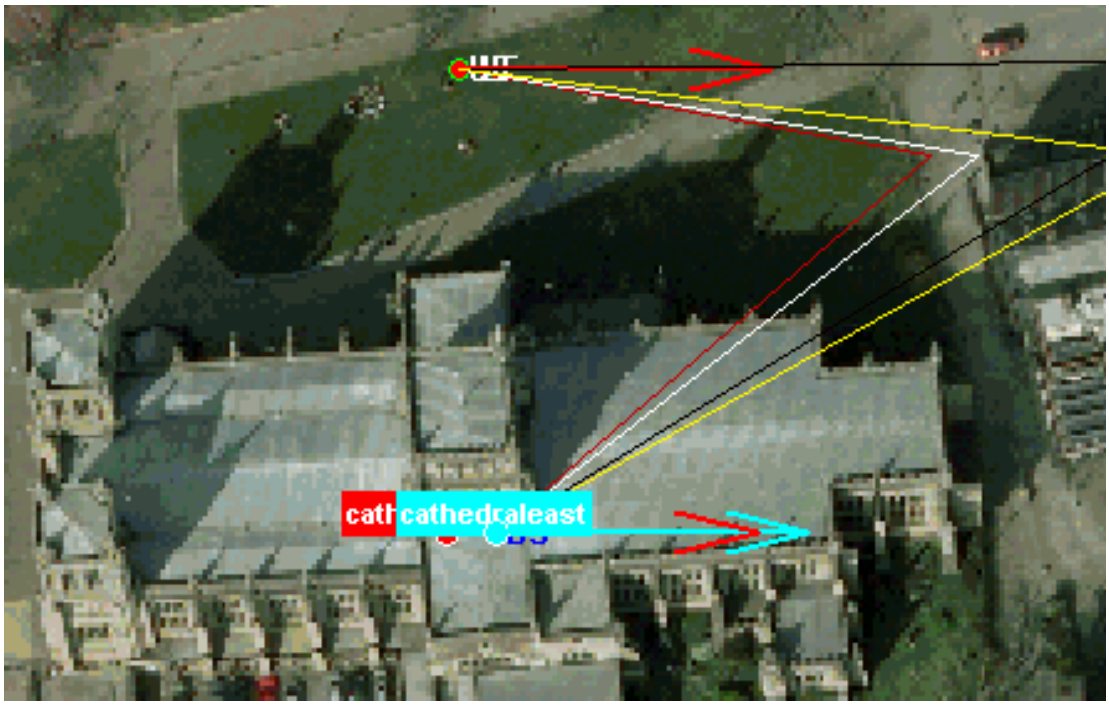

Figure 39: MPCs to first element of BS array

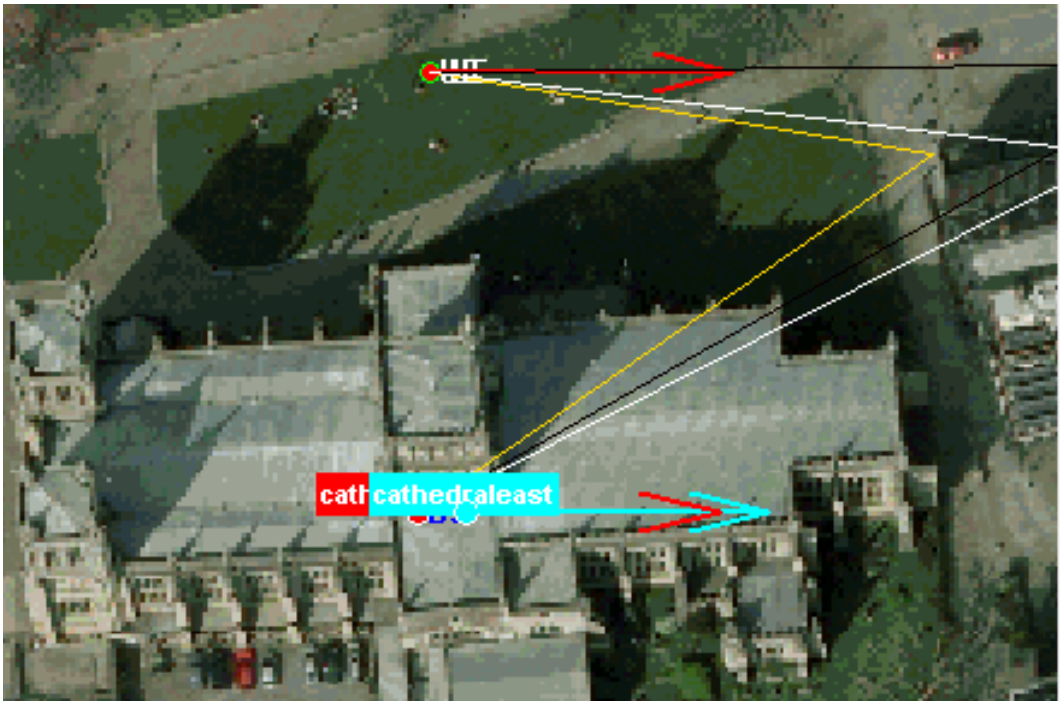

Figure 40: MPCs to last element of BS array

The elevation and azimuth angles for the first element (Figure 41) and the last element (Figure 42) illustrate that there is a difference in these angles across the array, which should be considered in propagation models.

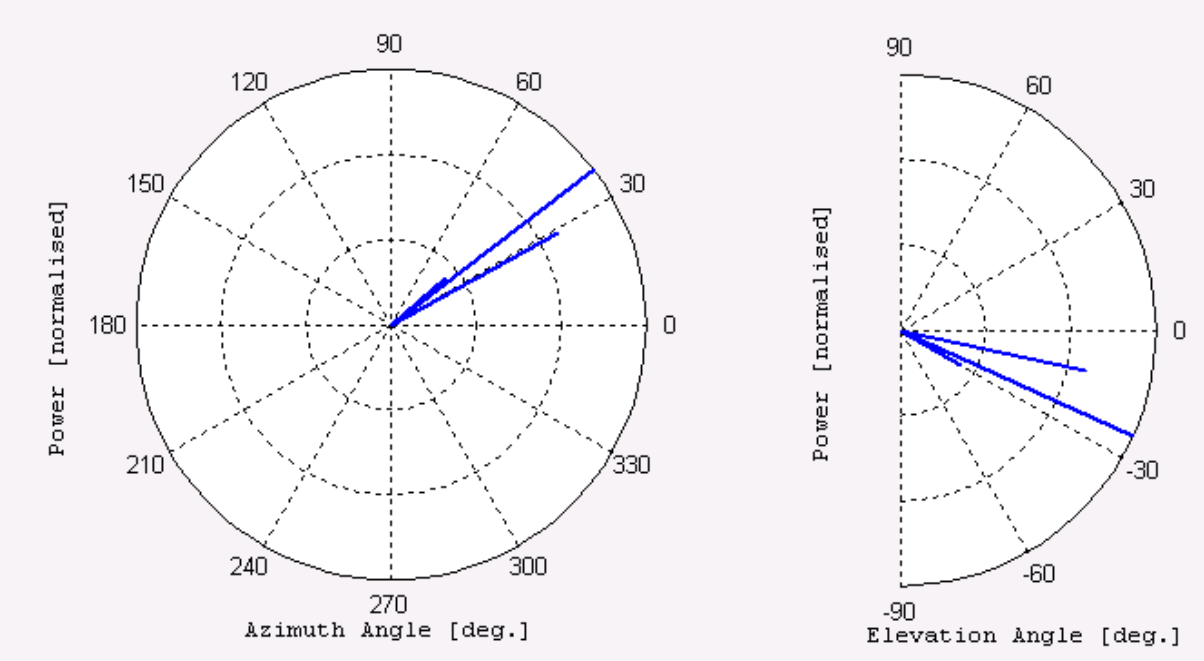

Figure 41: Elevation and azimuth angles for the first element. The scaling shows normalised power with the outer circle representing the maximum receive power.

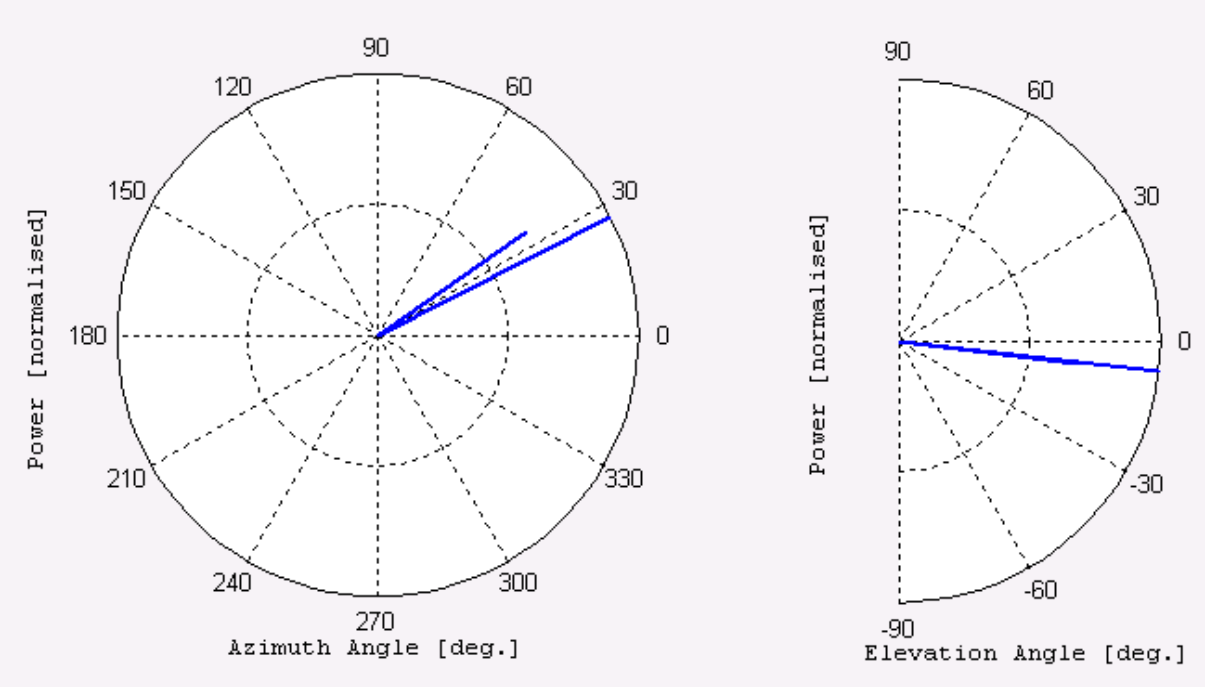

Figure 42: Elevation and azimuth angles for the last element. The scaling shows normalised power with the outer circle representing the maximum receive power.

3.7.1 Example of variations across a Massive MIMO Array

The following plots show how the RMS Delay Spread and Average Power vary across a linear 128 Massive MIMO array at 3.5GHz as seen from a MS in a non-LoS environment (Figure 43). This configuration is represented as follows:

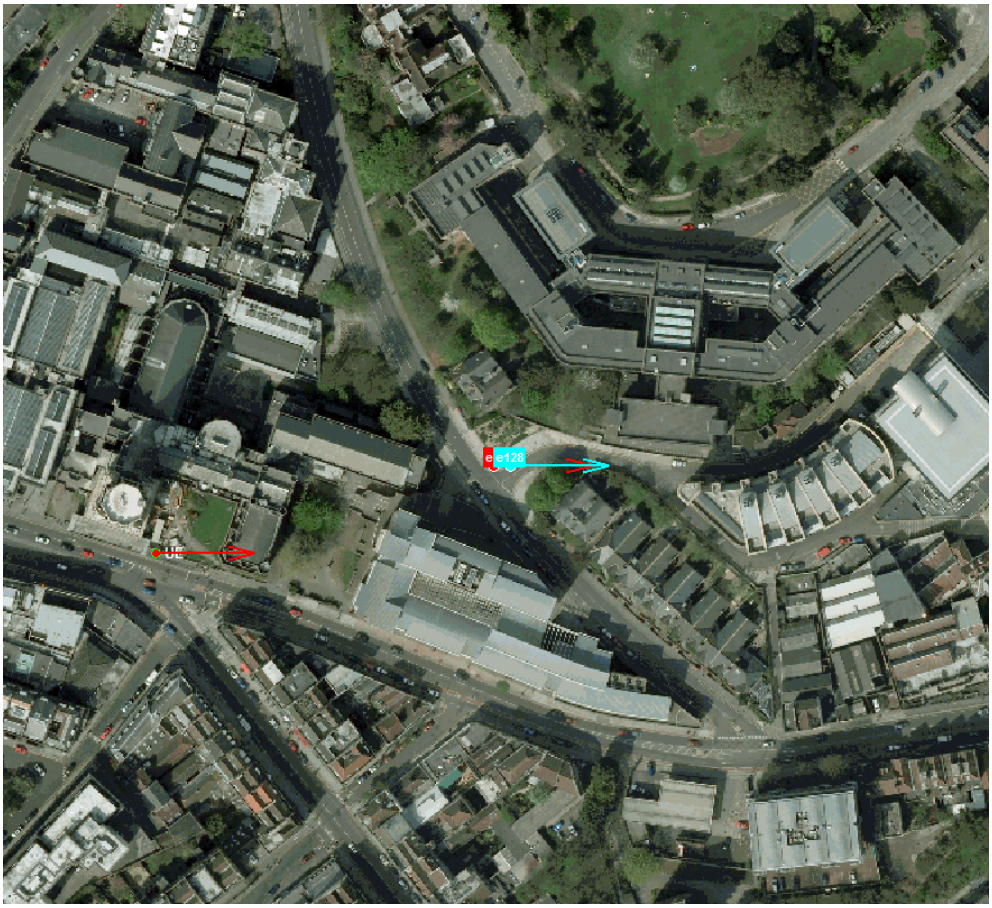

Figure 43: Location of BS near Bristol University Campus. Area shown is approximately 275 m from north to south and, from east to west, 300 m (51.4563 N, 2.6042 W)

The RMS delay spread (in nanoseconds) as seen by the MS from BS antenna 1 (furthest left) and antenna 128 (furthest right) is shown in the following graph (Figure 44).

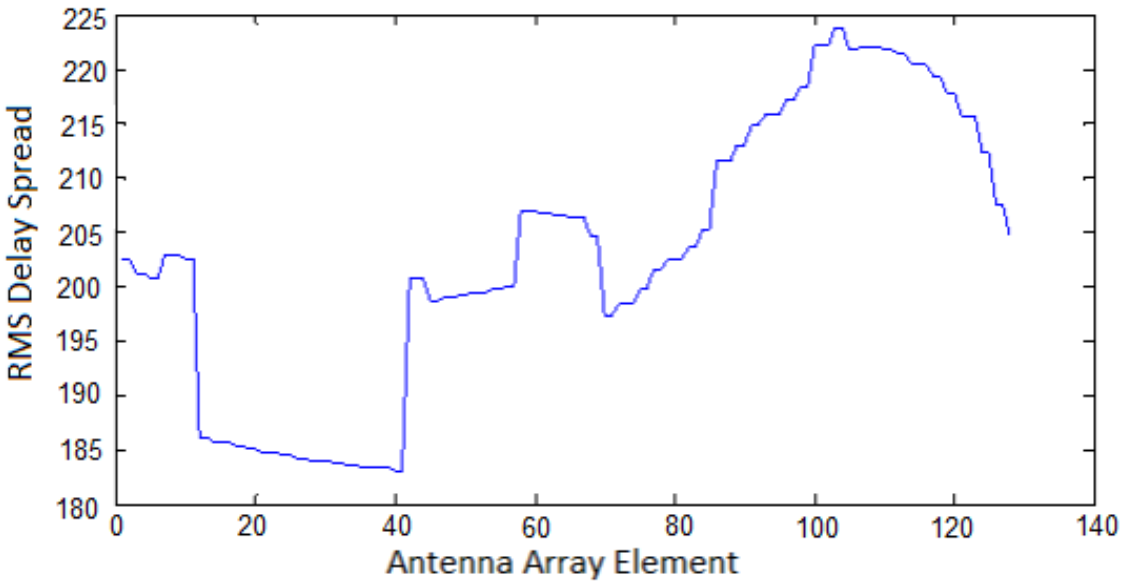

Figure 44: RMS delay spread (in nanoseconds) as seen by the MS from BS antenna 1 and antenna 128

The average power (in dBm) from BS 1 to 128 is presented in the following graph (Figure 45):

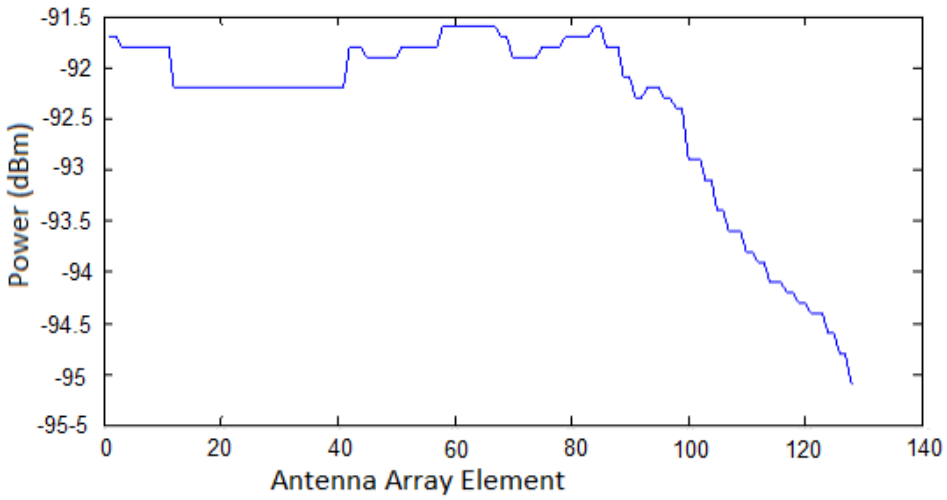

Figure 45: Average power (in dBm) from BS 1 to 128

3.8 Other parameters

3.8.1 Derivation of channel condition

In addition to parameters that are often used within the context of propagation models (such as delay spread, coherence bandwidth and k-factor) there are also

some more insightful metrics that can be used to describe both channel and correlation matrices within the context of Massive MIMO. Examples of such parameters include various types of condition numbers, which are investigated in later chapters as part of this project but will be discussed here from a general and theoretical standpoint.

3.8.2 Condition Numbers

The Condition Number of a matrix is a way of describing the 'rank deficiency' of that matrix. In other words, it can be considered as a measure of how far a matrix is from being 'full rank' where each of the column vectors are orthogonal to each of the others. The aim of defining a Condition Number is to express this feature of a matrix using one single-dimensional parameter. Each definition is limited in some way and it would seem a non-trivial problem to capture rank deficiency in an economical way.

3.8.3 Standard Condition Number

The Standard Condition Number (SCN) definition of the Condition Number has been discussed extensively within the context of Massive MIMO, such as in Ngo, Larsson and Marzetta [102]. The criteria for what is described as 'favourable propagation' is obtained when all the channel vectors (the columns h of the channel matrix) are pairwise orthogonal, which is to say that the quantity ${h_i}^H h_j$is zeros when $i \neq j$ and the square of the norm of h_k with $i = j = k = 1, \dots K$ where $K$is the number of single antenna terminals. Thus, ideally, the channel correlation matrix $H^H H$ is a diagonal matrix with elements being the square of the norm of the channel going from 1 to K across the diagonal of the matrix. The eigenvalues of $H^H H$ can be arranged in descending order such that $\lambda_1 \geq \lambda_2 \geq, \dots, \lambda_S$. The SCN is defined as

$$SCN = \frac{\lambda_1}{\lambda_s} \tag{3.12}$$

The value of the SCN is seen to be one in the ideal 'favourable propagation' condition described above. However, this ideal scenario that cannot be reached in practice due to the limitations of practical equipment. Thus, the SCN can be considered as providing an indication of how far away the system is from the ideal

scenario, in other words, the further away from one the value of the SCN, the further away from the ideal scenario the system is from a propagation perspective.

From a practical perspective, however, the SCN has some very significant limitations, as assumptions are implied that are unlikely to be reached in practical settings. The main limitation is that, in the ideal propagation scenario, the value of the SCN will only be 1 if each of the channel vectors shares the same norm. As this will likely not be the case, the SCN will be limited in its accuracy. In particular, its efficacity in describing the state of the channel and the correlation matrix will be limited because it will not be clear which SCN value represents the ideal and what the step changes in the value actually mean in a concrete sense. It is also based only on two eigenvalues and thus the possible significance of the other values will be lost. For example, it may be the case that an unfavourable condition of the channel is present (with two or more channel vectors not being orthogonal) but where the channel is still perfectly useable because of the presence of other orthogonal channels.

Ngo, Larsson and Marzetta [102] have proposed a related channel parameter based on the distance from the ideal form of ‘favourable propagation’ that is somewhat similar to the SCN, however it is not clear that this would provide a great advantage or Massive MIMO analysis due to the complexity of the systems required. In particular, Massive MIMO systems require knowledge of the CSI, with the SNR dependent upon this knowledge, and thus assuming perfect CSI would be unreasonable.

The SCN may still be useful in giving an indication of the change in the system (see later sections on Massive MIMO mobility) and has also found a use in various practical applications related to Massive MIMO that are discussed in the following sections.

3.8.4 Demmel Condition Number (DCN)

The SCN forms part of a series of measures based on the spread of the eigenvalues of a matrix. Another example of such a measure is the Demmel Condition Number (DCN), which, although initially represented in relation to numerical analysis, has found various applications within MIMO based wireless communications, including Massive MIMO [103]. These applications are discussed in the following sections.

The DCN is possibly advantages over the SCN in the sense that it is a representation based on all of the Eigenvalues within a matrix, rather than just the two extremities of the Eigenvalue spread. The definition of the DCN is

$$DCN = \frac{\sum_{n=1}^{N} \lambda_n}{\lambda_1} \tag{3.13}$$

Where N is the total number of eigenvalues of the matrix (not unique eigenvalues, two or more may be equal) and λ_1 is the smallest eigenvalue.

3.8.5 Applications within Massive MIMO and Related Research of Condition Numbers

3.8.5.1 Standard Condition Number

One of a number of applications of the SCN within the context of MIMO communications can be found in the design of channel detection schemes [104]. Detection schemes form an important part of MIMO communications, as reliable detection is necessary to be able to make use of the potential gain from the spatial diversity within the channel. Maximum Likelihood (MaxL) methods are often used as a way of making full use of the diversity of the channel, however schemes are considered computationally expensive. The performance of sub-optimal schemes has been shown to be dependent on the condition of the channel, where schemes tend to perform better with channels with a lower condition (i.e. closer to full-rank and therefore optimal) than with a high condition, and thus the SCN has proved useful when designing and optimising sub-optimal schemes, providing a useful metric to describe an input channel matrix during testing and thus facilitating the optimisation of detection schemes for ‘bad channels’ (i.e. those with high correlation between channel vectors).

The SCN has also been used in the context of Spectrum Sensing, a series of techniques often used to detect a Primary User (PU) within a MIMO system [105]. The SCN finds its use in this area thanks to the interest in eigen-value based techniques within Spectrum Sensing, techniques that an important within the context of MIMO communications because they do not require prior knowledge of the PU signal, something that will mostly not be present to the receiving equipment in MIMO systems. It transpires that the SCN can provide the threshold value for making the

decision as to whether a PU is present. This threshold value is obtained by considering the SCN of both the noise covariance matrix and the received signal covariance matrix. If the latter is greater than the former, then a PU is determined to be present.

3.8.5.2 Demmel Condition Number

Heath, Sandhu and Paulraj [106] have shown that the DCN is directly related to the suitability of channel for spatial multiplexing (as opposed to diversity) operation, with these two modes representing the available techniques for obtaining greater capacity and reliability through MIMO. This observation allows for the design of systems that switch between the two modes rather than, more traditionally, limiting the design to only one mode. This observation was extended through the proposition of a specific technique to perform the switching between the two modes based on the instantaneous channel state [107]. It was shown that a BER advantage can be achieved over single-mode systems. The paper is significant from the point of view of the DCN because it was shown that the DCN is related to a sufficient condition for multiplexing to be more advantageous than diversity, whereas this is not the case for the SCN.

Another example of an application of DCN is in the link adaptation for Worldwide Interoperability for Microwave Access (WiMax) [103,108]. Specifically, the WiMax standards contain specifications for Modulation Rate Adaptation, where the modulation scheme is altered depending on the channel condition. The DCN was chosen as a measure for the channel condition within this paper.

The DCN has also been applied experimentally, for example within standard MIMO indoor measurement campaigns [109]. It was shown from these experiments that the DCN varies dependent upon the locations of the transmit and receive antennas, and different forms of channels were described in terms of the distribution functions of the DCN. These observations are taken further within this thesis by applying them to Massive MIMO mobility scenarios and suggesting models based on these observations. The analysis is concerned, as in other cities, with the suitability of a MIMO channel for either Spatial Multiplexing or Spatial Diversity, and the decision process regarding which should be used [109].

More recently, the DCN has been used as a verification measure for the design of GSCM for mm wave MIMO (mm wave being outside of the scope of this thesis but mentioned here for completeness) [110]. The mm wave analysis was intended, according to the paper, to expand upon the standard channel models, which have not been parameterised at such high frequencies. The model is based on parameterisations from practical measurement campaigns and the DCN analysis was used alongside the channel capacity.

Mlayeh *et al* have investigated several implementations of a switching algorithm for Spatial Diversity and Spatial Multiplexing based on using the DCN as the selection criteria and ones that use knowledge of the SNR as the criteria [111]. The BER performance was used as the measure for choosing the best implementation technique.

3.9 Time evolution of channel condition

The purpose of this section is to demonstrate an observation regarding how channel conditions change within a mobility scenario, and to provide a general indication of how these changes progress within different types of scenarios, such as those that are generally more LoS in nature, or those that are more non-LoS.

Council Building BS Mostly LoS Scenario

The BS array is placed on the top of the council building and the six mobile users move around roughly within the area indicated by the yellow border (Figure 46). The transmit power is 1W.

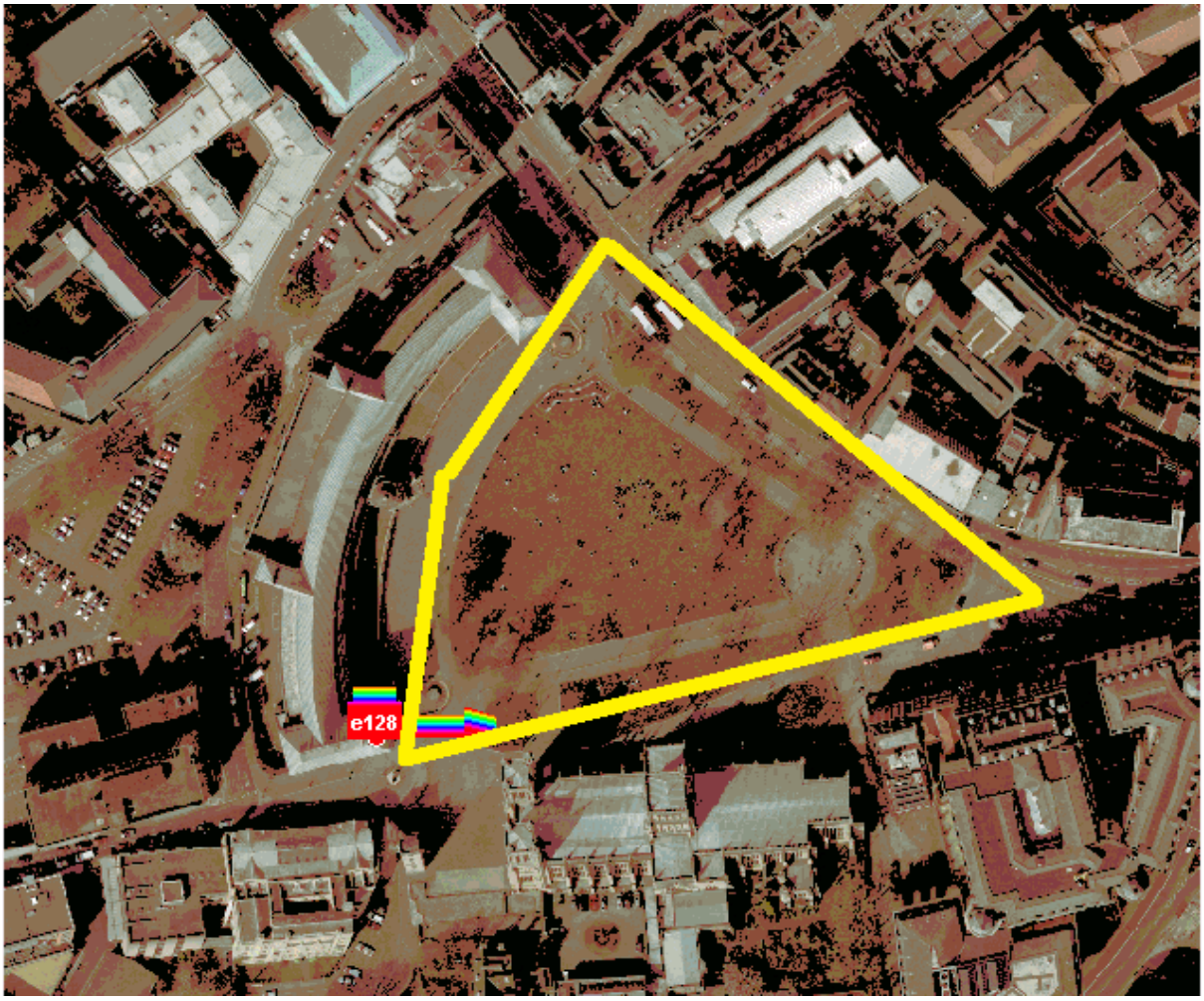

Figure 46: Route of UE around College Green, Bristol, shown by yellow line (total length of route approx. 300 m)

The DCN at each of the first 1000 time steps (representing a standard distance moved by the UEs) is shown in Figure 48. Here it can be observed that the condition of the channel seems to progress through various stages, some of which are marked by increasingly volatile changes in the channel condition. There are also stages where the channel condition is fairly stable for longer amounts of time.

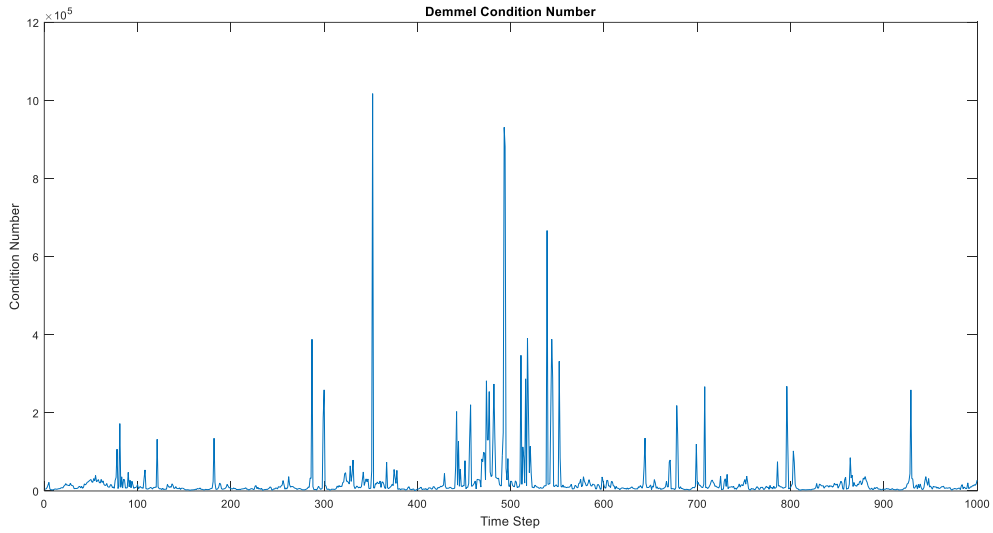

Figure 47: DCN at each of the first 1000 time steps with power at 1W

Mostly non-LoS link

The next link is a mostly non-LoS scenario with the same transmit array (but with power turned up to an unrealistic 10kW in order to reduce the problems associated with the ray-tracer's inability to record lower receive power levels). The mobile users travel up and down the street next to the Aquarium, which is located to the south of the Cathedral. This is a deterministic route where each time step represents a change of five metres.. Once again, various phases in channel condition are observed, including phases where the condition is fairly consistent, and other phases where this is not the case (Figure 48).

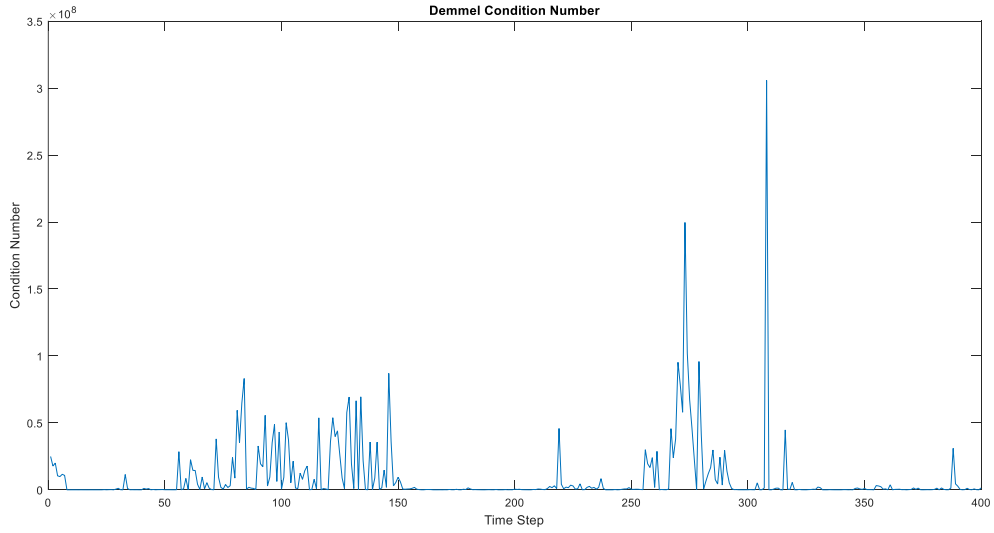

Figure 48: DCN at each of the first 400 time steps with power at 10kW

3.10 K-Factor

K-Factor

It is possible that the investigation of other parameters that are typically used to study the state of the channel may provide further insights on how this observed change in channel condition relates to the state of the channel at any instance in time. The condition number already provides some insight into the state of the channel, as a measure of channel quality. However, by definition, the condition number provides a summary measure for the entire channel, rather than taking into account each transmit and receive antenna element pair. It may be necessary, to understand more fully how the channel condition relates to the physical state of the channel, to study the channel on a more granular level, by considering each pair of elements. An investigation of the larger scale physical parameters is presented later in this chapter (in The Physical Interpretation), However this section provides an introduction to the use of the K-Factor in analysing the state of the channel in relation to the variations with the condition number.

The K-factor is a commonly used metric for describing communications channels. It can be described for any transmit and receive pair of antennas within any environment. Also known as the Rician K-Factor, it is used to provide an indication of the extent to which a communications channels resembles a Rayleigh or Rician channel. A Rician channel resembles a Rayleigh channel, in that the received signal is made up of several multipath components however, in a Rician channel, one of the components is much stronger than the others, and generally represents the LoS component between the transmit and receive antennas. In practice, the distinction between these two types of channels is somewhat subjective for any realistic scenario, so the K-factor is used to provide a comparison.

The K-Factor is defined as the ratio between the square of the amplitude of the ‘direct component,’ which is the strongest component within the link, to the average amplitude for the other components [112]. It is possible to find analytical expressions for the K-factor for various communications scenarios, some of which have been

incorporated into the various wireless standards. A K-factor of zero corresponds to a Rayleigh channel, and the higher the K-factor, the more ‘Rician’ the channel.

The K-factor has formed an essential part of much research and standards work related to Massive MIMO, especially as it has been shown to have a profound effect on the capacity of such communication systems. It has been demonstrated, for example, that improved capacity within MIMO systems is attainable in situations where the exact CSI is not known, but where the BS has knowledge of the K-factor [113]. Additionally, many modern types of wireless devices are designed to operate within environments that are, by their nature, Rician. For example, small cell systems designed to operate over much shorter ranges than macro-cells will often have a strong LoS component present within the communications links. Likewise mmWave links within 5G networks are based on communications links that are mainly LoS. Therefore research has been conducted over the past few decades to study the possibility of accurately simulating Rician environments and to accurately determine the K-factor. For example, Holloway *et al* [114] presented a methodology for creating a Rician propagation environment for any value of K-factor using a reverberation chamber. Taking the other point of view, Lemoine *et al* [115] provide an example where, instead of creating a test environment based on a required K-factor, the directivity of antennas is determined within a reverberation chamber based on a determination of the K-factor, the accuracy of which has become beneficial in designing effective communication systems.

It is possible to estimate the K-factor at the various points within the time-series representing the condition of a channel. For example, considering the time-series shown in Figure 50, where there is a significant variation between the highest and lowest value of channel condition.

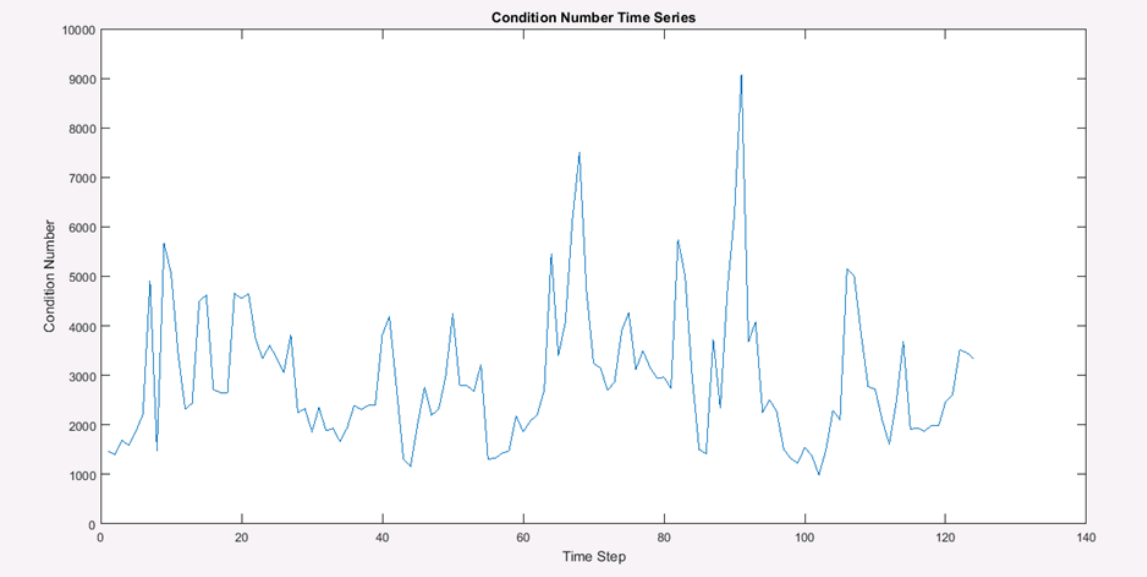

Figure 49: Example of variation of channel condition

The K-factor for each antenna pair at the maximum value of the condition number time series. The x-axis represents the index of the BS antenna element, with the element corresponding to index 1 being at one end of the linear array, and the element for index 128 being at the other end, with the index incrementing as one moves from one element to the next from one end of the array to the other. The y-axis represents each of the six UE antenna elements. The calculated K-factor is shown on the z-axis, creating the surface shown in Figure 50.

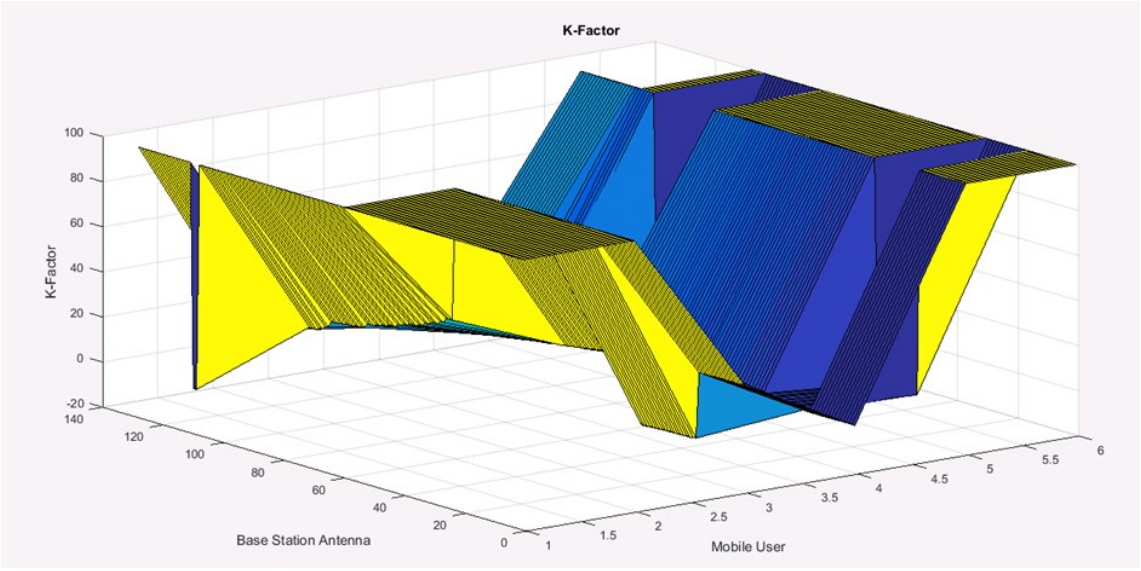

Figure 50: K-factor in dB for pair of BS and UE elements for maximum condition number value

The corresponding surface for the lowest value of condition number is shown in Figure 51.

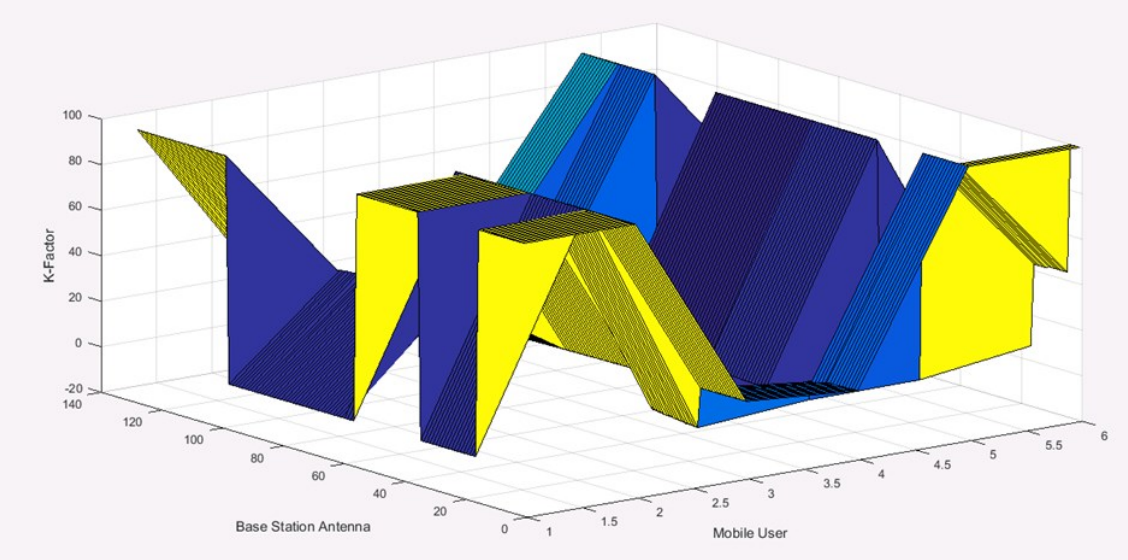

Figure 51: K-factor in dB for pair of BS and UE elements for minimum condition number value

It can be seen that, although the fourth mobile user is associated with a low k-factor at both the high and the low of the channel condition, there are generally more low values at the low value of the channel condition, thus suggesting that, for a lower channel condition, the channel is generally seen as more Rayleigh from the perspective of more of the antenna elements when compared with the higher channel condition.

3.11 Stochastic methods

It is possible to use methods from statistics and time-series analysis to model the evolution of rank-deficiency within a Massive MIMO channel with mobility over time based on ray-tracing data [102,116]. A mobility scenario using the Prophecy ray-tracer is set up. A linear half-wavelength spaced array operating at 3.51 GHz is placed on the council building and six users follow separate and (more or less) LoS paths around College Green. The path of the first user and position of the array is shown in Figure 52.

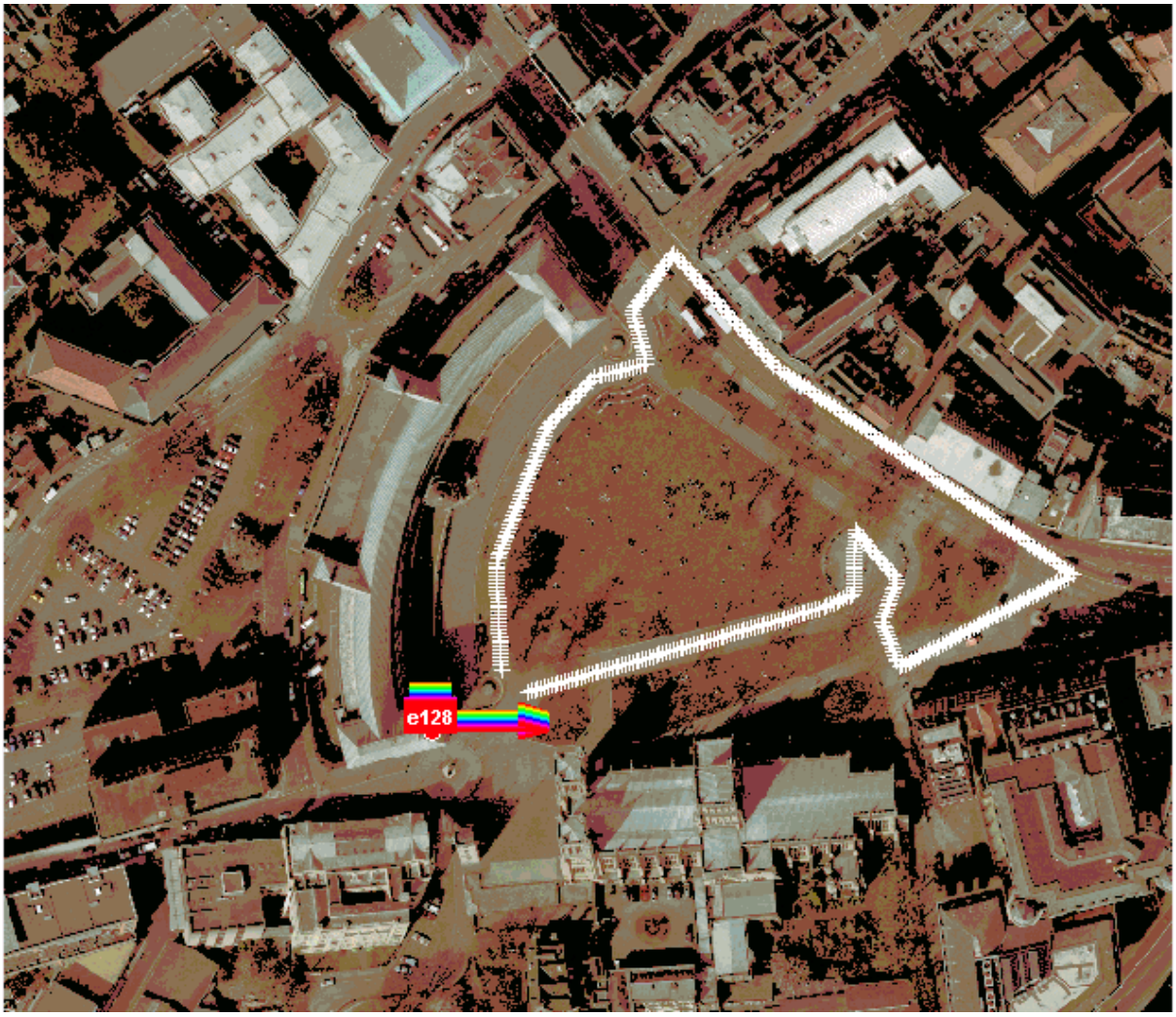

Figure 52: Path of the first user and position of the array, College Green area

At each instance in time the received power from each BS antenna is calculated for each mobile user. These values are then placed into a three-dimensional matrix, which represents the evolution of a two-dimensional matrix in time with the rows indicating the BS antenna and the columns corresponding to the mobile users. It is possible to obtain the channel response H matrix from the power values (expressed as dBm) by converting the values to a linear scale and dividing by transmit power (assuming that all BS antennas are transmitting with the same power). However, this leads to some rounding problems in MATLAB so, for now, let us stay with considering the power matrix in order to demonstrate the feasibility of taking the proposed modelling approach to a Massive MIMO channel. It should also be noted that, again to minimise rounding issues in MATLAB, the transmit power has been set at 70dBm, which is much higher than would be expected in practical systems.

The rank deficiency of a channel is given by the condition number with a high condition number indicating a strongly correlated channel and a condition number close to 1 indicating an orthogonal channel. This value is obtained from the channel matrix H by finding the eigenvalues of $H^H H$ and dividing the largest eigenvalue by the smallest. If we take this approach with the power matrix, we see the 'condition number' evolve in time as shown in Figure 53:

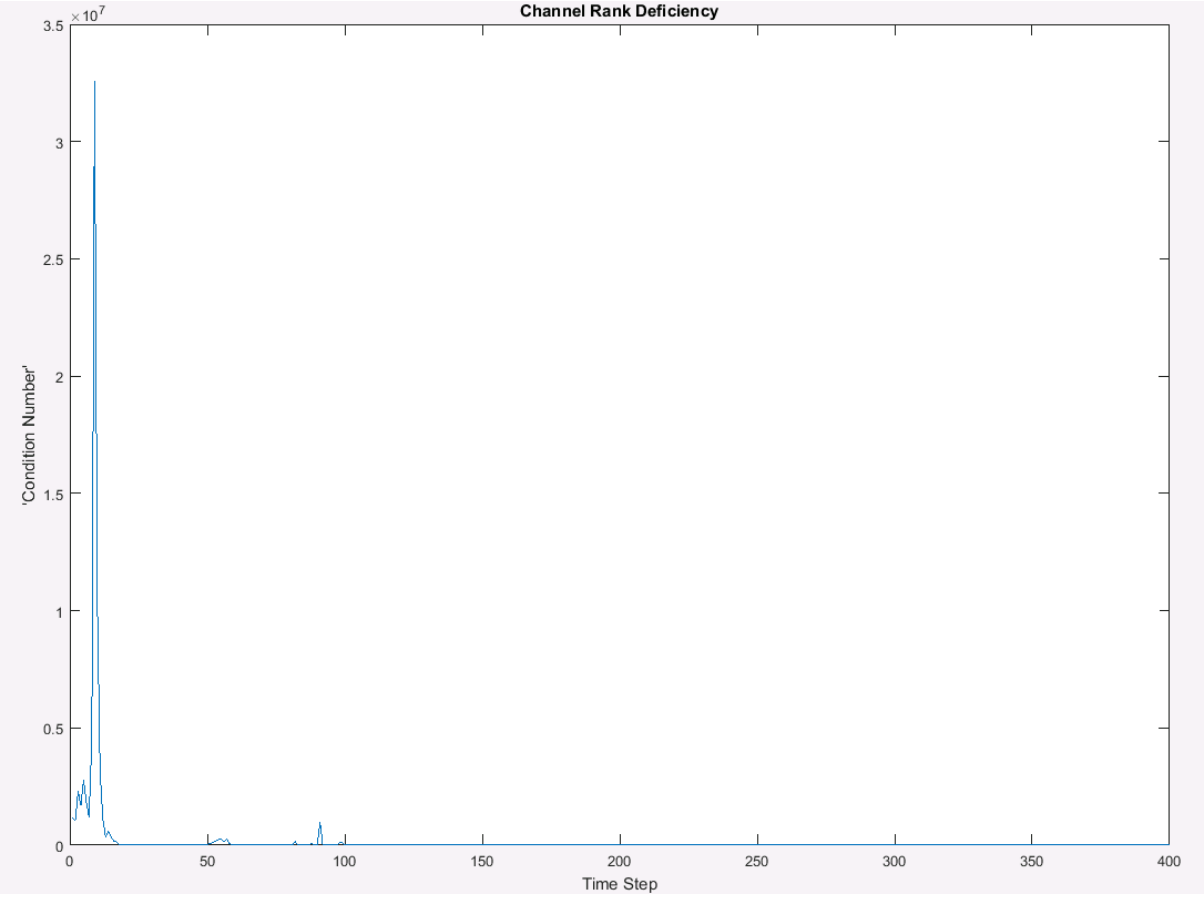

Figure 53: Condition number evolution over 400 time steps

As can be seen, there are high condition numbers at the early time steps, which obscure the values on the rest of the graph, so, for the moment, these will be treated as anomalous and the values after the 100th time step are shown in Figure 54.

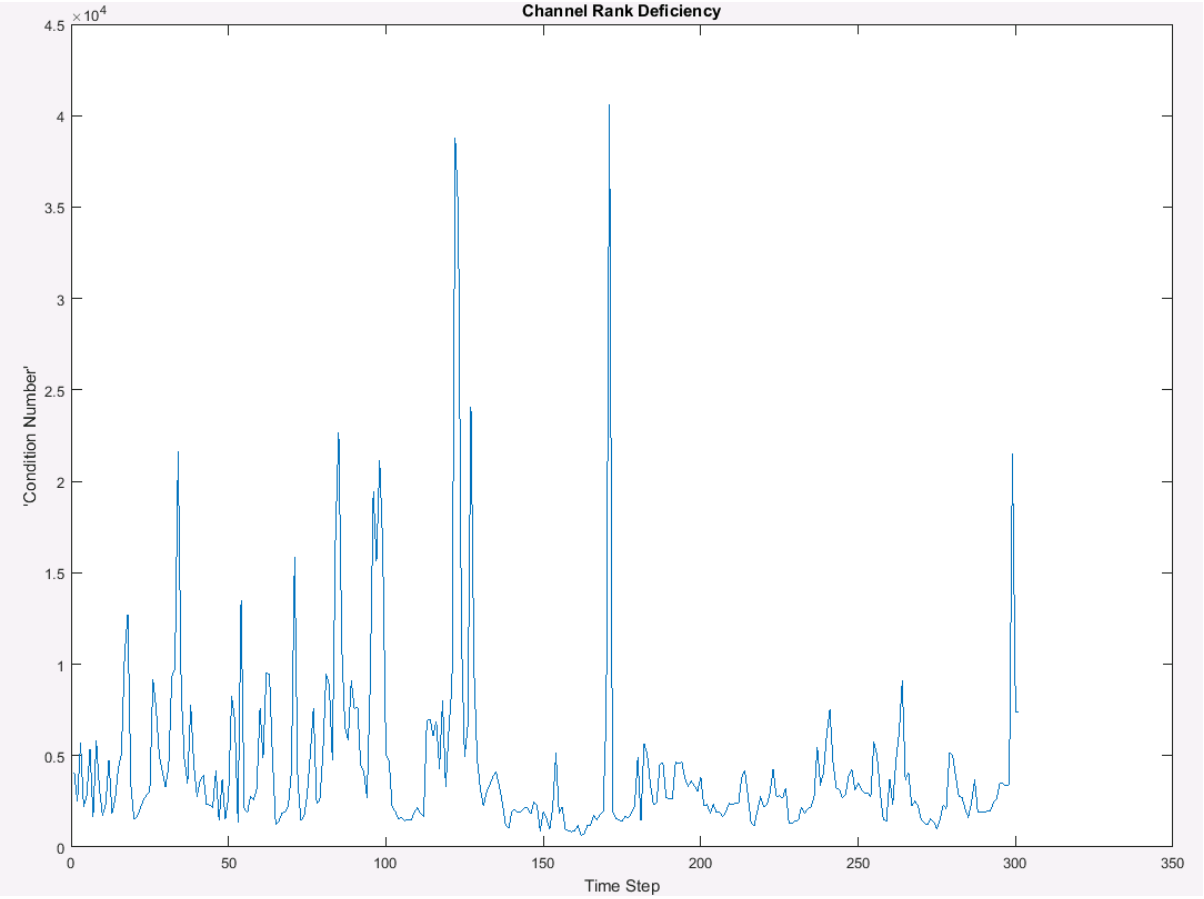

Figure 54: Condition numbers after 100th time step

It would seem feasible, from studying this graph, that, as with the measured data, the condition number goes through defined ‘phases’ that begin and end at specific times. However, this requires further investigation and, for the moment, let us consider the entire data set displayed in the graph shown in Figure 54.

The idea is to attempt to identify a stochastic time series model that may be able to model the condition number. A general form of such a model is given by:

$$\emptyset(B)(1-B)^d v_t = \theta_0 + \theta(B)w_t \tag{3.14}$$

which represents a mixed autoregressive integrated moving average process, with the left-hand side representing the autoregressive part and the right-hand side representing the moving average part, where v_t is the time series and w_t is a random shock taking the form of random drawings from a fixed distribution (usually

considered normal with zero mean) with variance of σ_a^2. B refers to a shift operator with the property that

$$B^n v_t = v_{t-n}.$$

(3.15)

The operators $\emptyset(B)$ and $\theta(B)$ are of orders p and q respectively.

$$\emptyset(B) = 1 - \emptyset_1 B - \emptyset_2 B^2 - \cdots - \emptyset_p B^p$$

Where $\emptyset_1, \emptyset_2, \ldots, \emptyset_p$ are the autoregressive parameters to be determined from the data.

$$\theta(B) = 1 - \theta_1 B - \theta_2 B^2 - \cdots - \theta_q B^q$$

(3.16)

Where $\theta_1, \theta_2, \ldots, \theta_q$ are the moving average weights to be determined from the data. The variable θ_0 may be used to indicate a linear progression (i.e. slope) of the process and $(1 - B)^d$ represents the dth order difference of the time series. A process can be described as being of order (p, d, q).

3.12 Development of stochastic models

The autocorrelations and partial autocorrelations of the time series (condition number) and the first and second differences are investigated in order to identify types of models that might possibly work as reasonable approximations for our data (Figures 55 and 56) In general, an autoregressive process has an autocorrelation function that gradually tails off and a partial autocorrelation function that has a cut-off after a certain number of lags. The opposite is the case for a moving average process and a mixed autoregressive moving average process may be more appropriate if both the autocorrelation and partial autocorrelation functions tail off.

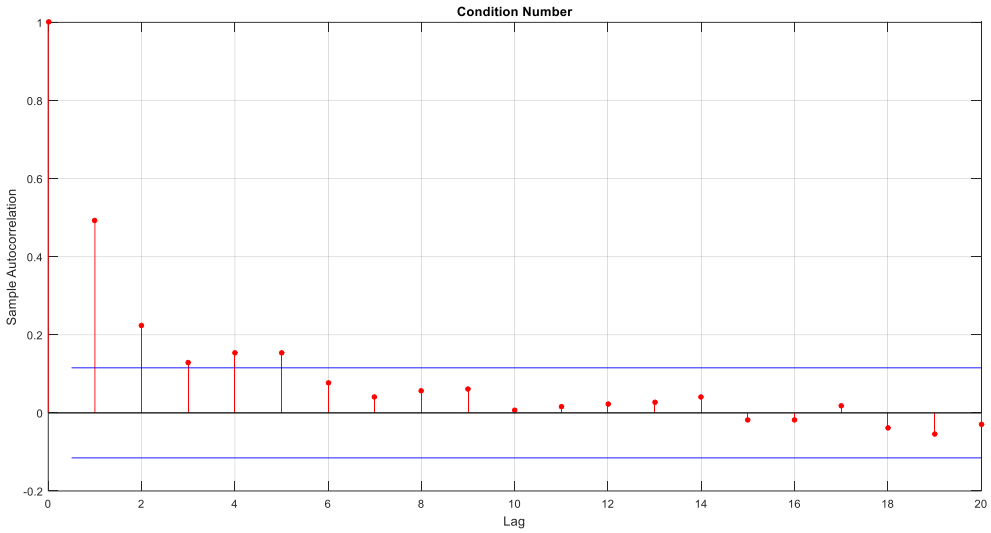

Figure 55: Autocorrelation for condition number

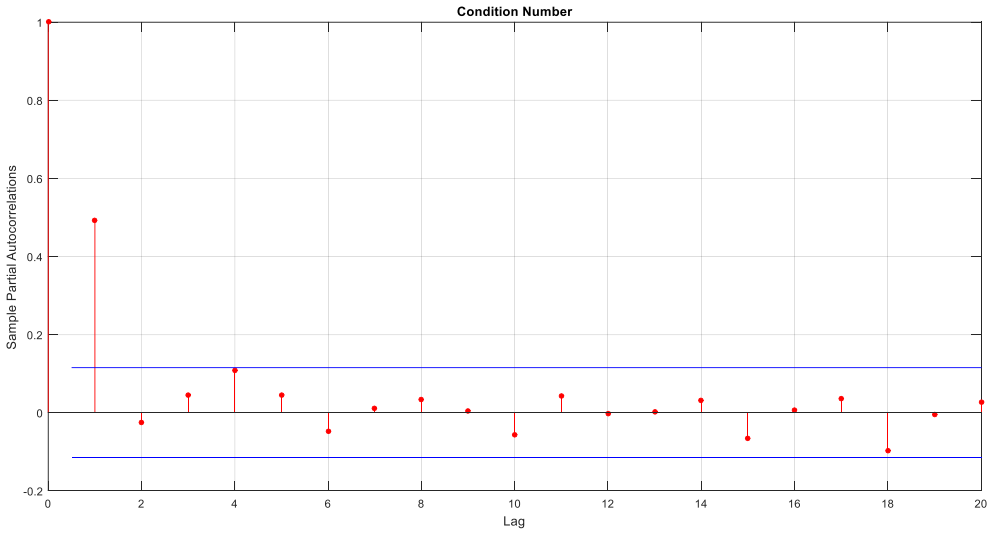

Figure 56: Partial autocorrelation for condition number

These functions suggest that an autoregressive (5,0,0) process may be a reasonable fit (Figures 58 and 59).

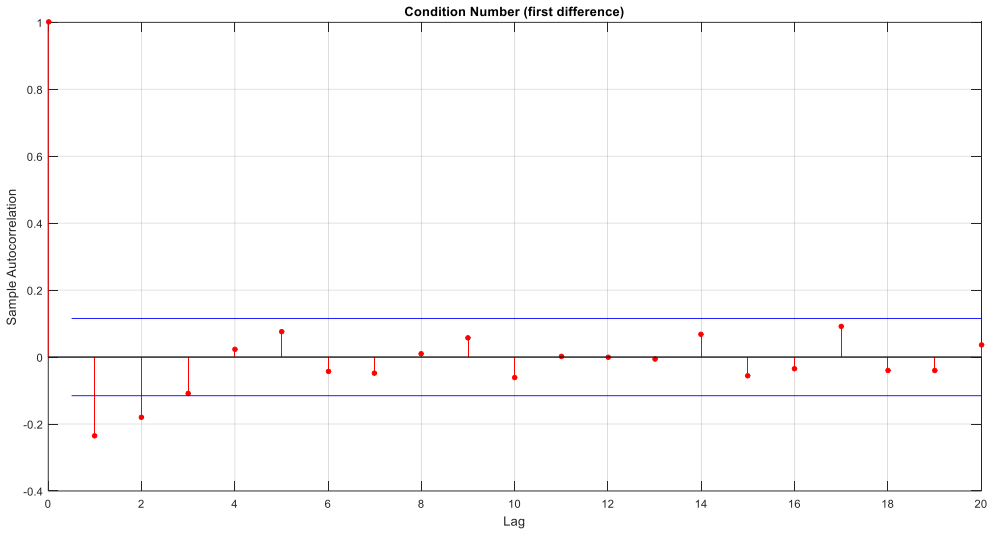

Figure 57: Autocorrelation of first derivative of condition number time series

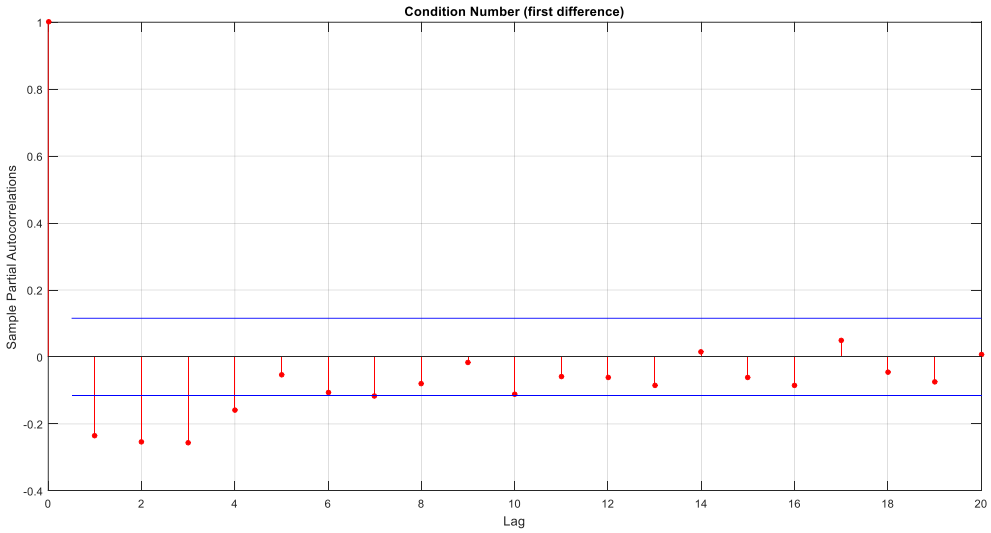

Figure 58: Partial autocorrelation of first derivative of condition number time series

Both of these functions tail off, suggesting a mixed integrated autoregressive moving average process, possibly of the form (2, 1, 4); however the partial autocorrelation function continues to oscillate to levels near the control lines, so this may not be such a good model (Figure 59).

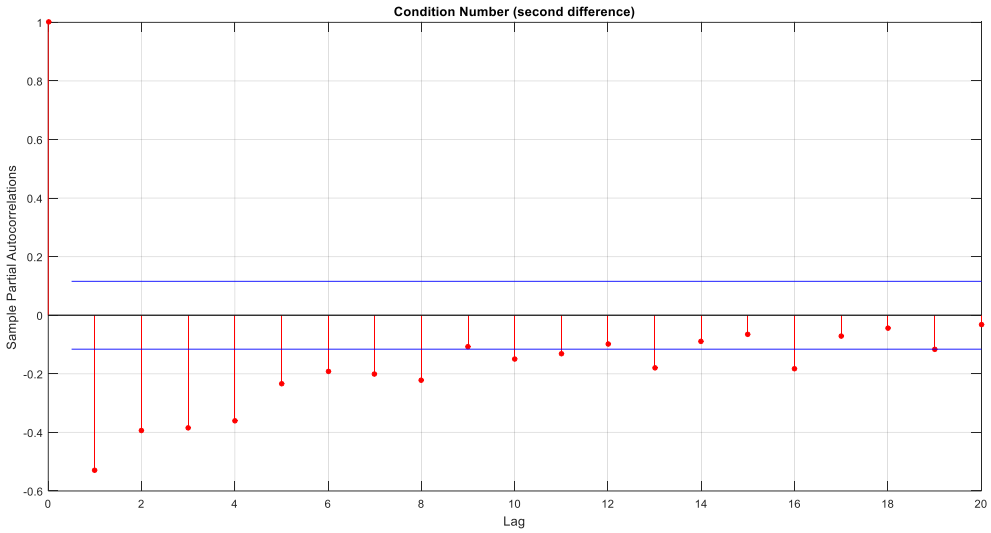

Figure 59: Partial autocorrelation of second derivative of condition number time series

These graphs suggest an autoregressive process of the form (1, 2, 0) as the autocorrelation function cuts off after the first lag. However, the partial autocorrelation function seems to tail off very slowly, so this requires further investigation.

3.13 Change Detection

Change detections refers to a selection of algorithmic techniques for analysing time-series data with the aim of determining both whether some parameter changes during a given time period and the time at which this change occurs. Such algorithms can be determined as being either on-line, where a signal is analysed in real time as it is being received, or offline where the full time-series is already available to the algorithm.

It was observed in previous sections that the time evolution of the channel seems to go through various stages within a mobility scenario, which can be shown by considering the time series of the condition number. It was therefore determined that a change detection algorithm may help to formalise these changes, to determine their statistical distributions and to inform the creation of a statistical model for the channel. Once the change detection algorithm has been applied, it should also be possible to determine the extent to which certain stages are recurring within the time

series, the likelihood of a change occurring in a general sense and the likelihood, given one specific state, of transitioning to another specific state.

It is necessary to determine a specific parameter that, when a change occurs within it that is judged to be significant, would represent a transition within the time series. It was observed informally that, based on an analysis using a ten-tap rectangular window Moving Average filter, the moving average appears to change in accordance with the observed changes in the channel evolution. The moving variance (obtained also using a ten-tap filter), while oscillating throughout the time series, was relatively more consistent than the moving average. Thus the mean average was chosen as the parameter to investigate using the Change Detection algorithm with the interest of locating a change point in the series. The oscillations within the variance could be problematic, as such an approach to Change Detection assumes a constant variance. This could perhaps be addressed when modelling the channel by varying the variance randomly, especially considering that the detection of the transitions can be achieved using the described approach in this paper.

Many different approaches have been taken to Change Detection within different applications [117]. However, in this chapter, an approach is taken based on variable Moving Average filters that is appropriate given the features of the data already discussed. The results presented later in this paper assume a simple square window Moving Average filter but it's possible that accuracy could be improved by using more sophisticated windows within the analysis. The approach functions by stepping through the time series, with t indicating the current location of the time step, and defining two moving average filters, one placed before t and terminating one step prior to this value and the other beginning after t. Initially the windows are both of the same length, requiring the algorithm to begin several steps into the time series. The averages before and after t are then determined and compared. If the two average values diverge by more than a specified threshold value, then the value of t is recorded as a change point. The values prior to t are determined as representing a particular stage within the time evolution of the Massive MIMO channel, which is recorded as stage one and associated with the average value obtained by the filter prior to t. The value of t is then reset to the current value of t plus the length of the filter after the current value of t and the process continued. (It was determined that the value of t should skip several values rather than just being iterated by one

because of a tendency of the algorithm to overstate the presence of a change if this interval is too short. This is because, when in a period of transition, the values of the time series are usually changing significantly and thus the two moving average filters are likely to diverge in any case.) If, once again, the threshold value is exceeded by the comparisons of the mean values before and after t, then the sequence of values between each end of the filter prior to t is regarded as representing stage 2 with its mean value determined by the moving average filter prior to t. This process continues until the end of the time series with the iteration of the stage number.

In the event that the difference between the moving averages before and after t does not reach the defined threshold value after any iteration then the value of t increases by one and the start and end times of the moving average filter after this value (which is of fixed length) increase by one. The start value of the moving average filter (which is of variable length) however, remains fixed and the end value increases by one such that it is now located one step before t. These two new average values are compared. The reason for increasing the length of the moving average filter before t is because, considering that the algorithm has determined that the stage is longer than the previous filter length, an increased filter length will lead to a greater accuracy when determining the mean value for the particular stage of the channel. It should be noted that this algorithm assumes that each stage is at least the length of the original filters. This process of increasing the filter length prior to t continues until the difference between the two average values exceeds the specified threshold value, at which point a change is assumed to have been identified and hence a stage in the Massive MIMO channel. The mean value for this stage, corresponding to the mean value for the variable length filter, is recorded along with the number to be assigned to the stage, which is simply an iteration of the previous stage number. The value of t then increases by the length of the fixed value filter and the variable length filter is returned to the original length, with the end value one step prior to the value of t and the start value determined by the original filter length.

The whole process then continues until the end of the time series is reached, at which point all of the recorded mean values for each stage are rounded to suitably chosen nearest values. The number of unique mean values is then determined, which corresponds to the number of different types of stages that may or may not be reoccurring during the evolution of the channel. Following this, all the transitions

between stages (which is to say a set of 2-tuples with the first value representing a preceding mean and the second value representing a following mean) are assembled. The number of transition types that may occur one or more times during the channel evolution are then determined followed by the probability of each transition occurring.

3.14 Results

The stages that can be determined intuitively can be detected formally by choosing a relatively high value of the threshold value. The divisions in Figure 60 show the transitions that were determined using the algorithm with a threshold value of 20 and, as can be seen, correspond closely with an intuitive judgement about the locations of the transitions.

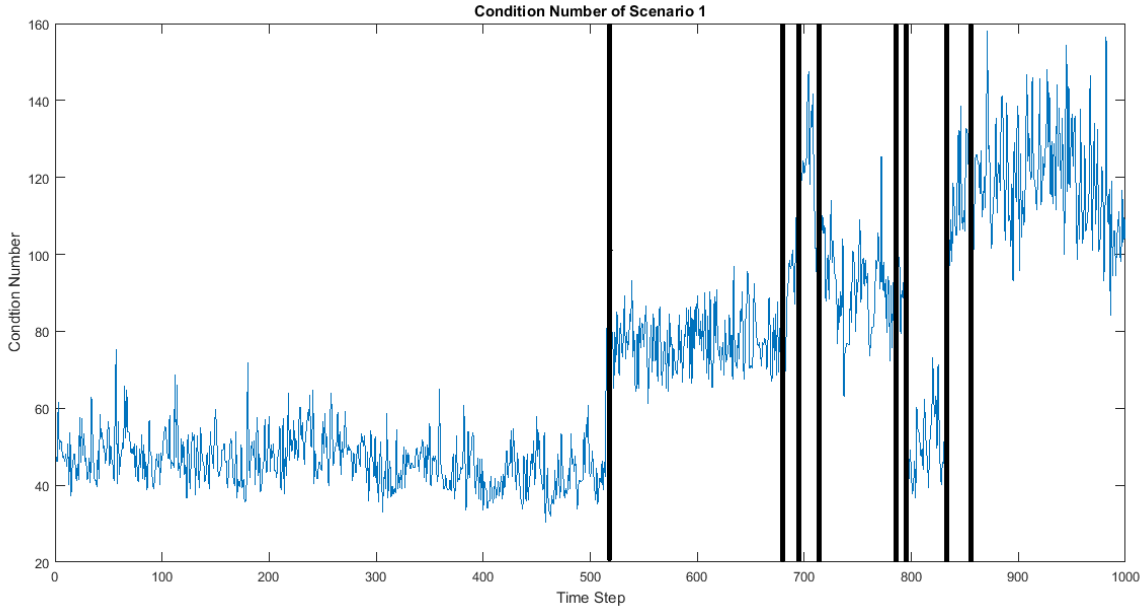

Figure 60: Example of channel condition time series with different phases present. Black lines indicate changes in channel condition

Statistically, however, choosing a lower threshold value may be useful for developing more accurate models. For example, if the same time series is considered as in Figure 60 but with a threshold value of 10 instead of 20, the number of transitions increases from 9 to 17 and these locations are more difficult to determine visually but can be shown to be present using this analysis.

3.15 The physical interpretation

It is not immediately clear what the physical interpretation should be of the observation that the condition of Massive MIMO mobility channel has a tendency to pass through various recurring stages with time. It is also not clear what the definition of ‘stage’ should be and whether this is an appropriate term for the corresponding sections of the channel condition evolution.

The evolution of the channel condition is considered in Figure 61. Note that this is based on a dB interpretation of the channel due to scaling issues with the software (the values are very small and cover a large range). The task is to identify two regions of the channel that appear to be distinct.

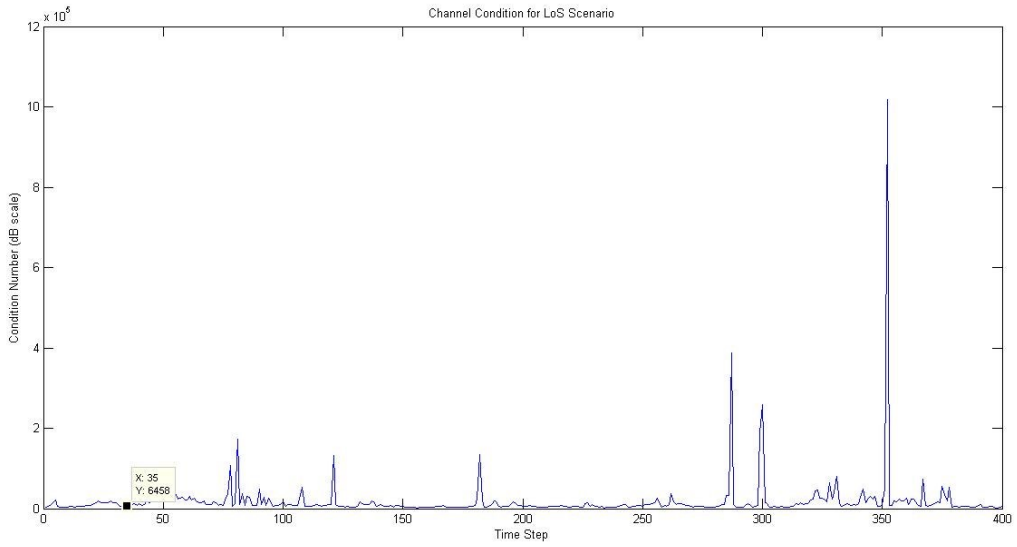

Figure 61: Evolution of the channel condition

A relatively low value at step 35 is chosen and it is decided that this should be compared with a distinct value at time step 352, which represent a large spike within the data. It is quite possible that the condition at step 352 is an outlier, and this needs to be considered as part of the analysis; however, it would seem to be a good choice of value that is far away in terms of value from the value at step 35. To begin, the location of the users at these steps are identified.

The locations of the users at step 35 are shown in Figure 62. The users appear to be paired within three classes (indicated by the yellow circles). These pairs of users represent the one travelling in broadly opposite directions. In all cases, the users are

within around tens of metres of each other. A noticeable difference is observed within the configuration of the users at step 352, where, firstly, each of the users (except for two) are spread out fairly evenly within the measurement area. These four users are highlighted by yellow circles (Figure 63). The other two users, however, occupy virtually the same location (highlighted by the blue circle) within the measurement area.

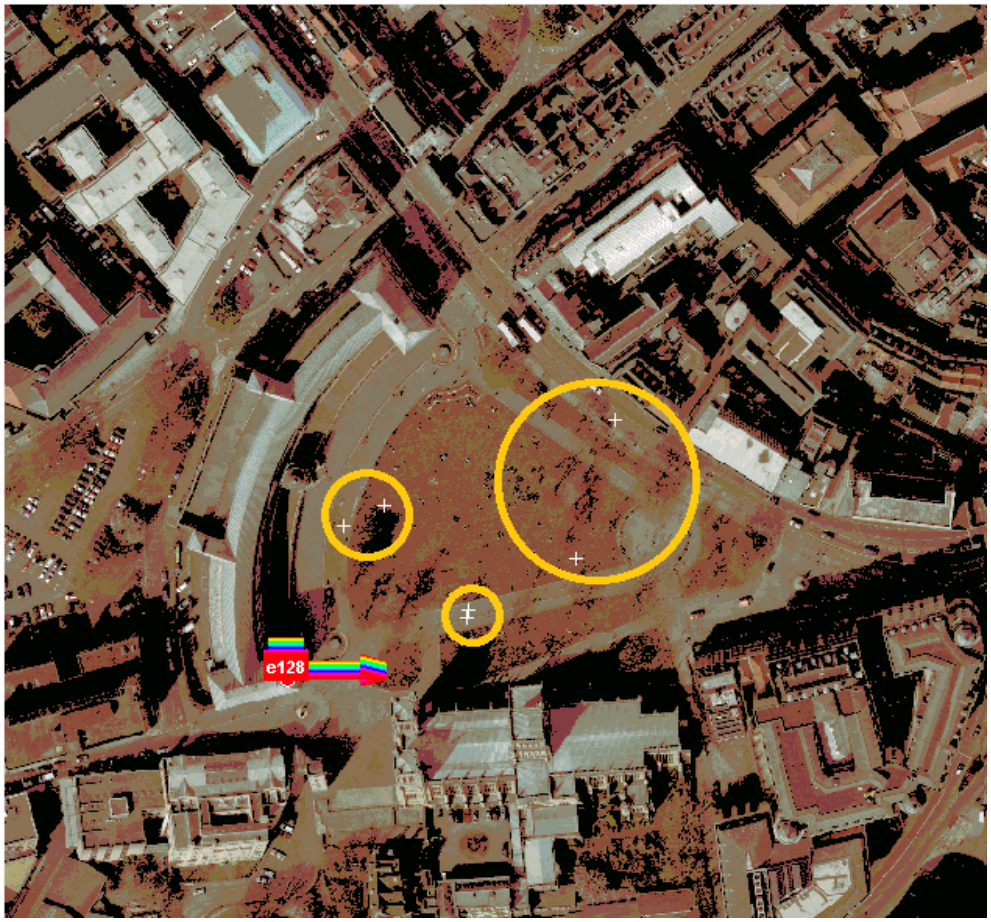

Figure 62: Location of users at step 35

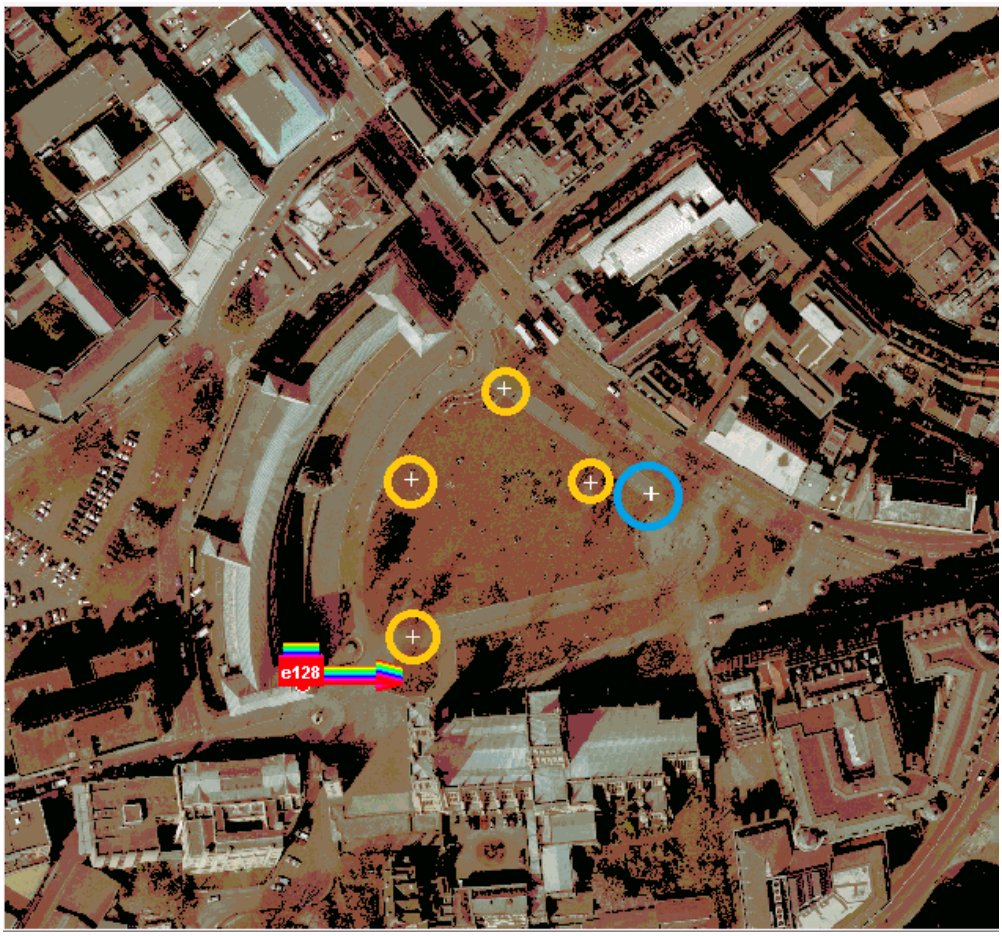

Figure 63: Location of users at step 352

This is an initial analysis of a limited selection of the features of the channel condition evolution, in this case the difference between the spikes and the rest of the data. The analysis of the configuration at points 35 and 352 raises the question of whether the spikes in the data represent overlaps between the locations of the users, however this is evidently not the case following the analysis of steps 50 and 300, two more steps representing a lower value and a spike (Figure 64 and Figure 65). Here the configuration corresponding to the lower value is similar to the corresponding configuration in the time step in the previous example, not surprising given the temporal proximity of the two examples, but with two pairs of users slightly further apart and one pair within ten metres of each other (and notably further apart than in the configuration for step 352). The configuration for step 300, however, diverges from the general features of for step 352, with two pair of users close together, as before, but with the other two users more clearly separated in space rather than occupying virtually the same location. Therefore, the spikes in the channel condition

cannot be said to correspond to a configuration in which two users are occupying a similar location in space.

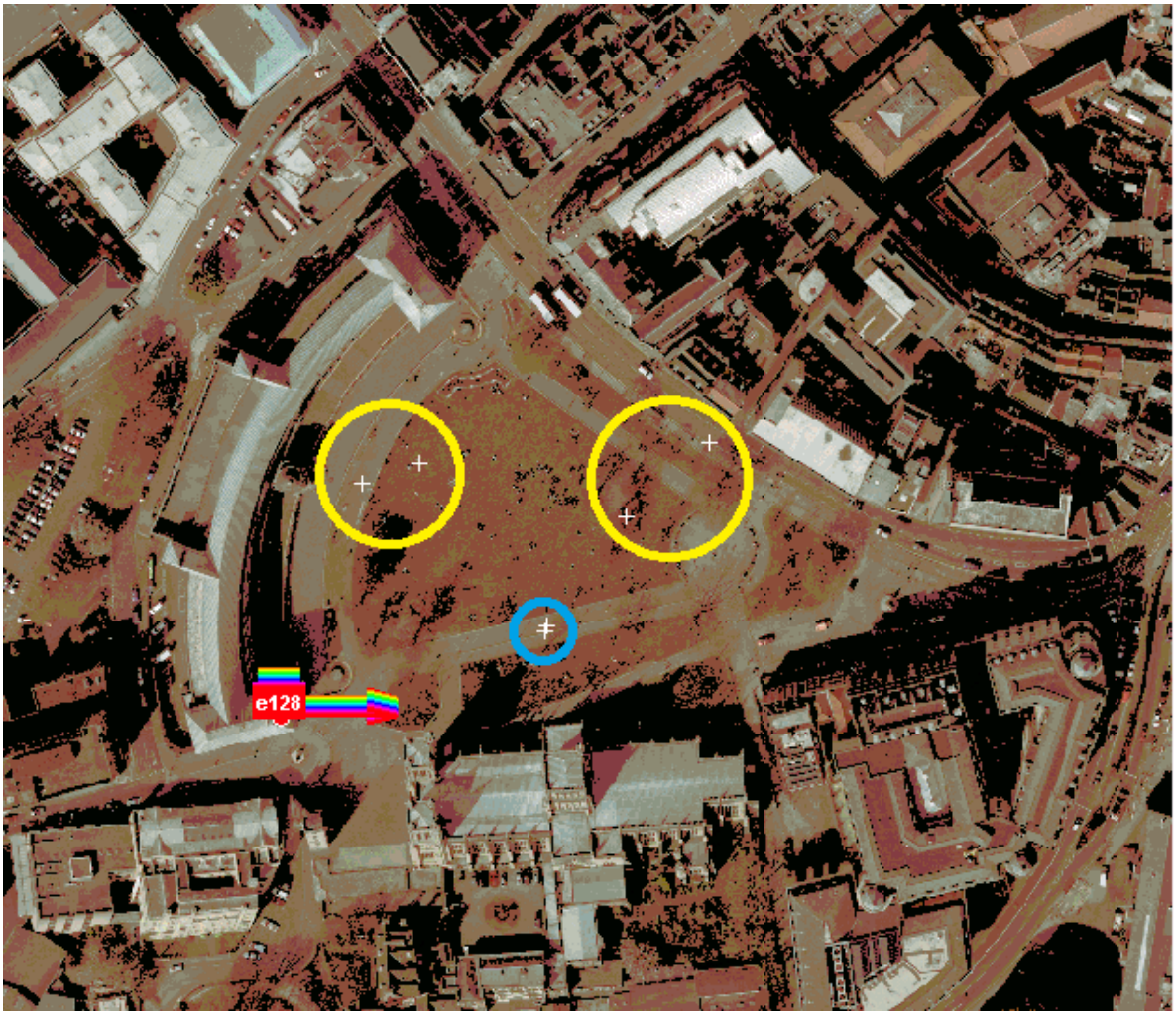

Figure 64: Location of users at step 50

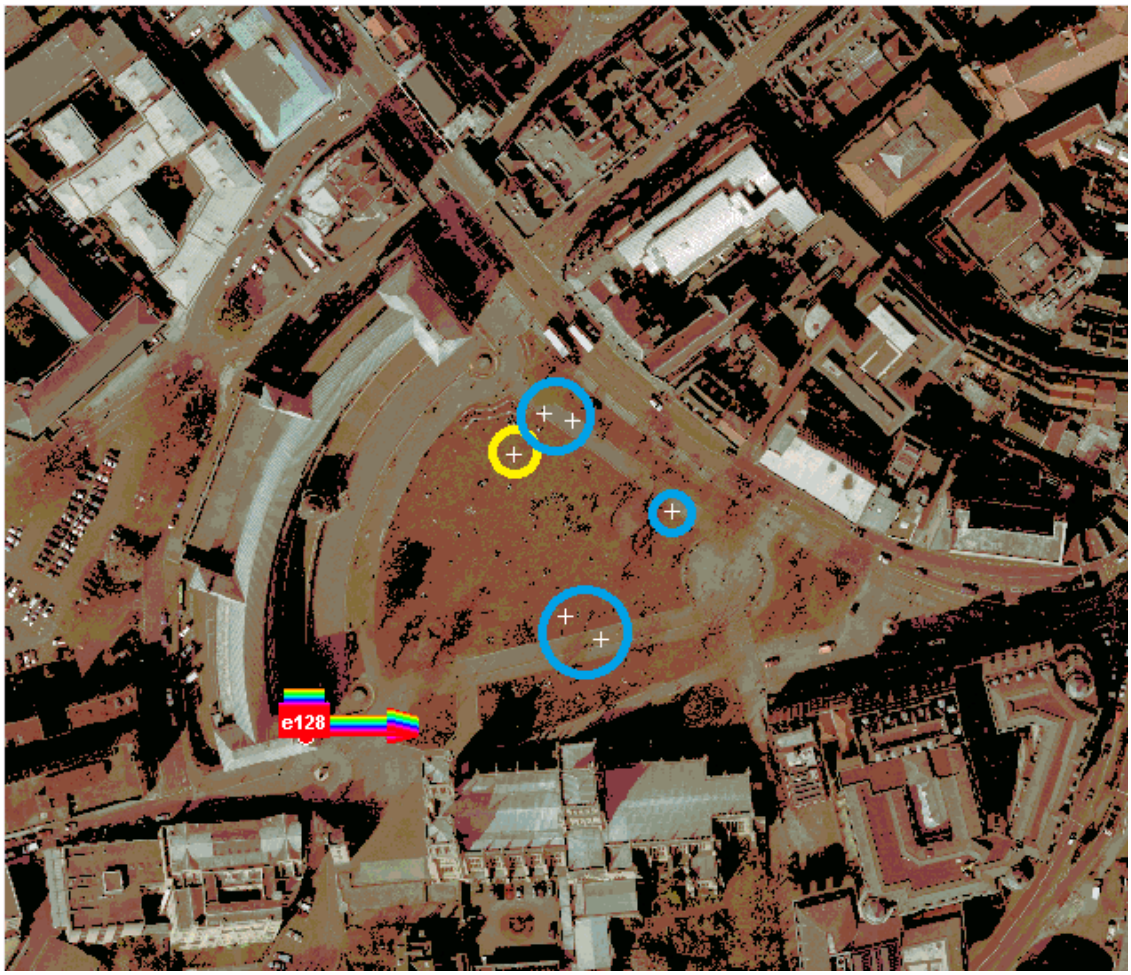

Figure 65: Location of users at step 300

3.16 Conclusion and recommendations for further research.

This chapter has been presented primarily as a representation of the use of ray-tracing for channels involving large antenna arrays such as those required in 5G Massive MIMO networks. As mentioned in the second section of this chapter, two ray-tracing systems have been used as part of the research presented in this thesis, one based on research at the University of Bristol and one proprietary software system. The results presented in this chapter have been based on the University of Bristol system. This system is based upon a 'method of images' approach combined with the principles of 'illumination zones,' instead of a more typical 'ray launching' approach. The proprietary software used in the following chapters does not provide such a detailed explanation of how the rays are created with the software. The first system uses a block representation of an areas from satellite lidar data whereas the

second system uses a three-dimensional block representation from OpenStreetMap data.

The purpose of using ray-tracing has been to demonstrate and investigate some of the physical properties of the channels that require increased attention when compared with channels that do not involve large arrays. Following the presentation of plane-wave models for Massive MIMO, and the changes that are observed from one end of the array to the other under the plane wave assumption, it has been shown that a spherical wave model can provide a much more detailed view of the physical properties of the channel. It has also been shown that, under a more detailed view provided by a spherical technique, there are often significant variations in how the channel is seen from the perspective of each element of the array.

More specifically, it was shown through the use of realistic scenarios within central Bristol that there are large variations in the MPCs in situations where part of the array is obscured from the UE, and therefore where there is no LoS component, and where another part of the array is not obscured and there is an LoS link to the UE. In such scenarios, the obscured part of the array corresponds to a much richer multipath environment compared with the non-obscured part of the array, which sees a more standard Rician channel. These types of differences across the array apply even to arrays that are completely obscured from the UE, though to a lesser extent. Further examples were presented showing the effects of changes across the array within dense urban environments that present strongly multipath propagation environments. It was shown how the RMS Delay Spread varied between elements from the perspective of a static UE, and also how the average receive power from each element varied at the UE.

The observations regarding the changes across the array led to a consideration of how these changes may affect the ability of a Massive MIMO network to support separate spatial streams, and thus obtaining the advantages from increased spectral efficiency for which Massive MIMO was developed. In particular, the question of how this ability would change when there are several users connecting to the network whilst following a route around the cell coverage area was addressed. It has been possible to use the University of Bristol ray-tracing system to simulate these types of scenarios, which are intended to represent the types of dynamics that may be encountered within a busy urban environment with a large amount of vehicle and

pedestrian traffic. The users in such scenarios were set to follow fixed routes, with a snapshot of the scenario being provided at discreet time steps. In theory, it would have been possible to analyse the channel characteristics in the same way as for the static examples presented earlier in the chapter, however doing this would have been unlikely to lead to useful results, as there would have been an extremely large number of rays that would need to be analysed individually. Therefore, it was decided that describing the general channel condition at each step in the simulation would provide a reasonable overview of the state of the channel. Such an approach has the disadvantage of omitting more specific details about how suitable a channel would be in supporting the various spatial streams, however it has the advantage of providing an understanding of how the channel condition changes, and to what extent, over time. Furthermore, it is possible to present the changing channel condition in the form of a one-dimensional time-series, which allows for the use of techniques from time series analysis, signal processing and various statistical methods in interpreting the results.

The channel condition number was selected for analysing the change in channel condition, as this is a standard method for describing the Massive MIMO channels. It was observed that, when represented as a time-series, the channel condition seemed to transition through various phases as the users moved around the cell areas. Some of these phases were characterised by fairly consistent conditions of the channel, whilst some were characterised by more variable conditions. It was not immediately clear as to what these changing conditions corresponded in a physical sense. It did, however, suggest a certain approach to the modelling of the changing channel conditions, namely a statistical representation of the different phases of the channel condition, combined with a method for detecting when the changes between different phases of the channel condition occurred.

A standard method for modelling certain types of time-series data is to use an auto-regressive moving-average process. The suitability of the use of such a process is determined by examining the autocorrelation and partial autocorrelation coefficients of the time-series, as well as its derivatives. Through the obtaining of these coefficients, it was shown that the Massive MIMO channel condition could, in some cases, be simulated using an auto-regressive moving-average process. In addition, the use of change detection methods could sometimes accurately detect the

changes in the time-series that were observed subjectively. It seemed that, in a general sense, the changes of condition within the channel may correspond to how clustered the users are, although this is not always clear.

Further research would be necessary to investigate how the change in channel condition should be interpreted in terms of the physical state of the channel. It is possible that using clustering methods to analyse the user positions may provide advantages when developing this interpretation. Likewise, the ability to more accurately detect changes in conditions would be advantageous. Anomaly detection is an active area of research, and detecting changes in Massive MIMO channel conditions could be an interesting use case for anomaly detection methods.

The change analysis within this chapter has involved six UEs. When these UEs are located close together, there is an increased possibility that the channel conditions from the point of view of a UE will be similar to those seen by another UE. Similar channel conditions from the perspectives of the UEs lead to a decrease in the ability of the Massive MIMO system to support spatial multiplexing, however nearby UEs do not necessarily correspond with higher condition numbers if the physical characteristics of the environment are such that the users can still be separated from the point of view of the BS. In the same way, lower channel condition numbers are not guaranteed just because UEs have a greater spatial separation between them. Nevertheless, if the number of UEs were to increase beyond the six represented in these results, it would be expected that the probability of similar channel conditions from the point of view of the UEs would also increase, leading to a gradually increasing possibility of fluctuations within the condition number time series as the number of UEs increases. The magnitude of this increased possibility is likely to depend on the environment and how rapidly the state of the propagation channel is seen to vary between different regions.

4: Beamforming for coverage optimisation in Massive MIMO systems

There are several ways that Massive MIMO networks can address the issues of limited radio resources in order to meet user demands for service [118]. When located within a dense urban environment, for example, the multipath propagation within the environment tend to cause variations in the angles of arrival, signal strength and phase angles across the array. These variations, combined with appropriated precoding and detection schemes, allow for the use of aggressive spatial multiplexing, where multiple communications channels are able to share frequency and bandwidth resources at the same time. The large number of antenna elements also allow for the directing of energy toward much narrower regions compared with what is possible with smaller arrays. This beamforming is achieved by varying the antenna weights, that is the amplitude and phase angles, across the elements of the array.

The use of ML for the management and optimisation of programme parameters within Massive MIMO algorithms is currently an active area of research, and the interest has only increased thanks to growing use and investigations of disaggregated and Open Radio Access Network (O-RAN) systems, which provide for increased network softwarisation and the deployment of ML applications in near-real time and real time contexts and easier implementation through the use of dedicated ML components within the O-RAN standards for example the near real time RAN Intelligent Controller (RIC) and the non real-time RIC [119].

There is the option to deploy Massive MIMO systems within a variety of contexts that each have different criteria for optimal performance aligning with the related 3GPP standards. This chapter focusses specifically on the questions of coverage as it relates to the synchronisation process within the 5G standards. This process is discussed in more detail in the following section and is dependent upon how beamforming is configured at the BS.

The application of ML to the optimisation of beamforming parameters within Massive MIMO has been approached in a number of different ways. For example, Wang et al

[120] propose a low-complexity, sub-optimal beam allocation algorithm based on fixed beams formed using the Butler method [121]. This, as in this chapter, is a combinatorial optimisation problem, but with the constraint that each beam serves only one user and where the aim is to maximise the sum data rate of the system.

Shafin *et al* [122] take a different approach to applying ML to beam optimisation, by making the beamwidth and angles of the beams the parameters to be optimised. In other words, a set of beam weights is determined, again by formulating an optimisation problem. This paper aims to maximise the Signal to interference plus noise ratio (SINR) at the user by determining the most appropriate beam parameters.

This chapter also describes an approach for beam selection that is based upon optimising the coverage during the synchronisation process for a set of users for whom the spatial distribution is known. The approach involves the adjustment of the beamforming parameters by choosing beams from a defined set according to a defined criterion.

As a precursor, this chapter begins by outlining the necessary and essential synchronisation processes. It then discusses how the propagation models and user distributions are configured to obtain the necessary parameters for finding a solution. Results are then presented following the use of an exhaustive search algorithm, which is shown to be effective but computationally slow. Characteristics of the solution are then discussed that demonstrate that it is possible to find solutions by computing only a small number of the beam configurations, thus significantly increasing the speed of the process. The chapter concludes by demonstrating some methods for obtaining suitable beam configurations more rapidly and describes possible applications for the method described.

4.1 Beamforming

Synchronisation with the RAN, whilst important in previous generations of mobile networks, is especially important within 5G, owing to the time-critical nature of many of the technologies within such networks and the increased number of devices operating with these requirements. For example, TDD technology requires both the BS and the UEs to transmit using the same bandwidth resources, thus making the timing critical at both ends of the link to avoid interference [123]. Likewise, the use of

multiple beams within Massive MIMO technology that are dynamic and not covering the same area, with the same boundaries at the same time, necessitate the use of correct timing at both the UE and the BS end of the link. The synchronisation process is a method within the 5G standards, preceding the transfer of data, that allows the UEs to establish the timing necessary to connect to the network [124].

The synchronisation process allows the UE to detect the time at which a radio frame begins and the time at which an OFDM symbol begins, a process that is achieved by the transmission of a Synchronisation Signal Block (SS Block). This forms part of the process of downlink synchronisation. Uplink synchronisation is the process that allows the UE to obtain timing data for when it should send uplink data. This uplink synchronisation forms part of the random access channel (RACH) process. However, downlink synchronisation remains the focus of this paper because of the relatively cohesive way in which it can be mapped onto the process of beamforming described in the introduction.

The downlink synchronisation process consists of the BS sending several synchronisation signal (SS) bursts, each consisting of a block of data separated by defined timing intervals. The number of SS bursts is currently defined as not being permitted to exceed certain numbers depending on the frequencies being used, with 4 below 3GHz, 8 up to 6GHz and 64 above that. The use of 8 blocks is considered here, as mid-3GHz is typical for 5G BSs; however, it would not be complicated to adapt this to lower numbers of blocks or to different frequency ranges if necessary.

The separation of the SS bursts in 5G are defined in terms of orthogonal frequency-division multiplexing (OFDM) symbols, and each SS Burst is a mapping across four symbols, each of which are mapped across 240 subcarriers, although not all of these subcarriers are used for the transfer of information. The first symbol contains the Primary Synchronisation Signal (PSS), the second and fourth contain the Physical Broadcast Channel (PBCH) and the third contains both the PBCH and the Secondary Synchronisation Signal (SSS).

Each of the SS bursts may be transmitted at the same time that the antenna array at the BS is configured to form the beam according to a pre-determined specification. The effect of this is that, during the synchronisation process, the beam can be made to sweep across a geographic region. The UEs, as part of the process, report back

to the BS the reference signal received power (RSRP) values as an indication of signal quality within the RACH preamble. This allows for a beam to be identified as providing the highest quality link between the BS and the UE. This information, with the process initiated during synchronisation, forms part of the overall beam management framework for 5G communications. Once the beam has been established as best serving a certain set of UEs, the beam refinement process, where beams can be made narrower and more specifically directed, can begin to allow for further data transfer. However, beam refinement is beyond the scope of this chapter.

This chapter now focusses on synchronisation and beam selection from the perspective of coverage. In other words, how can the beams associated with the SS Blocks be best configured to provide the best coverage from the perspective of a BS for a given distribution of users and environment. It is possible to ask this question because the characteristics of the beams (in terms of width, azimuth, elevation and electrical tilt) are not defined and there may therefore be some discretion for the operator to define these, subject to operation considerations.

The method for addressing this problem is discussed further in later sections, however the following assumptions are used as the foundation to this research:

1. The best set of beams for a given BS, operating within an environment and with a defined user distribution, is the one that provides the most even coverage to the users. In other words, each beam serves an equal number of users.
2. A single beam is capable of serving multiple users.
3. There is no maximum number of users that can be served by a BS. This assumption is not realistic, but is reasonable for the studies here as only typical numbers and distributions of users are considered.

Use is made of a MATLAB simulation from the 5G toolbox as the basis for obtaining the RSRP values from users. 5G synchronisation allows for beamforming at both ends of the link, however only beamforming at the BS is considered here. The frequency for the simulation is 3.5GHz, and thus, following the standards, eight synchronisation signal blocks are transmitted, each with an associated beam from the beam set. A user distribution is first defined around a central point with users

distributed between 100 and 1000 metres. The area for sweeping is limited to within a typical tri-sectored region, not accounting for the edges of the beams and the sidelobes. The full waveform and grid for the synchronisation signal bursts is generated and transmitted through a channel. Initially a Rayleigh fading channel. The RSRP values are then reported back from the UEs, with the highest RSRP value corresponding to the selected beams.

The process of simulating the propagation of the waveform through the channel is computationally slow and overly complex for investigating synchronisation coverage. Therefore a more simplified model is used that greatly increases the speed of the simulations.

4.2 Beamforming in MIMO

The use of simplified propagation models is justified both in addressing the issue of complex 5G channel models and in allowing for a clearer formal description of the problem being investigated, a description that is presented in the next section. However, when implementing such a system in an actual network it is likely to be necessary to use a more sophisticated channel model, since a Rayleigh model may not occur often in environments which may be encountered in a practical network. Many 5G channel models are statistical in nature and the following process results in models that are essentially look-up tables. However, it could be argued that the large number of users being considered and the level of granularity make a determined average value at each point within the model acceptable. The level of granularity is related to the dimensions of the environment, and in this case all the environments being considered are outdoors and based on macro-cells with beams that are wide enough to cover several UEs at a time. Thus, less precision is required compared with indoor environments or in situations where beams are narrow enough to serve individual UEs within dense user environments.

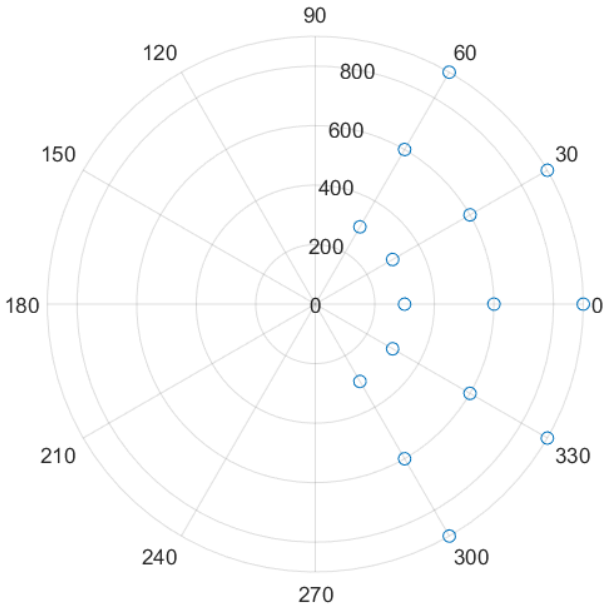

Figure 66: User distributions around BS at centre of graph. The blue circles represent the location where the RSRP value is determined. The concentric circles represent the distance from the BS in metres.

The aim of this approach is to create an RSRP surface that can represent a typically expected RSRP value for each of the possible beams. The users are placed evenly around a BS as shown in Figure 66. Only a third of the total area is occupied with users to simulate a typical tri-sector BS configuration. The range for these examples is set out to 1km, although another value could have been chosen. Additionally an area near to the BS is excluded to avoid near-field effects and complications with overlapping beams. An assumption of this model is that there are no users within the exclusion zone. The waveform model for 5G is then run for each of the beams. On each occasion each user reports back its measured RSRP value for the beam. These reported RSRP values at specific points, correspond to points within a two-dimensional RSRP surface (Figure 67). This surface is then extended to cover the entire area of interest from the point of view of the propagation environment.

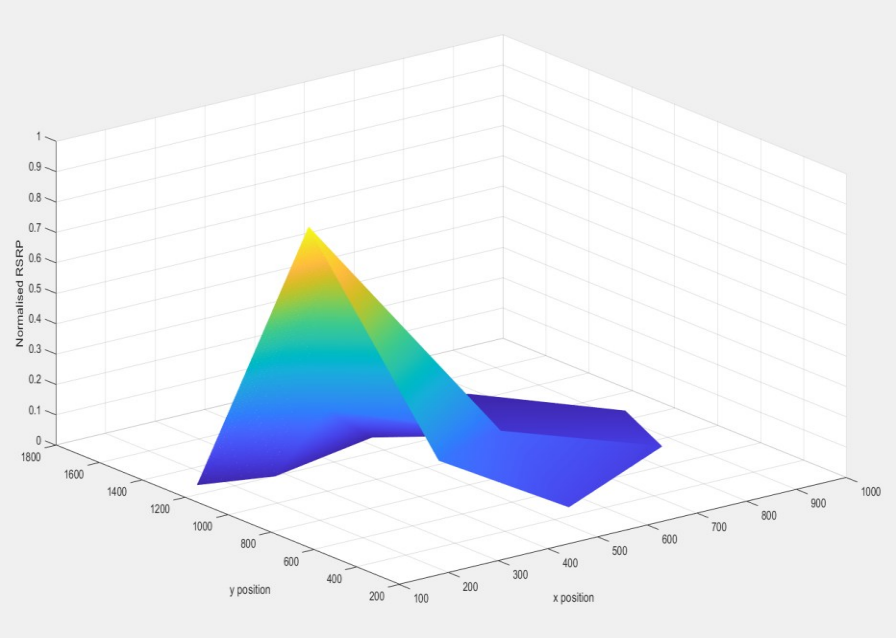

Figure 67: Example of a generated 'normalised RSRP surface' for one beam from the described methods. Each beam will have its own surface, which can be considered as almost synonymous with the beam.

4.3 Scope of Analysis Undertaken

The aim of this section is to discuss some possibilities for approaching the beam optimisation problem as part of this research thesis. It also summarises the data requirements for the project, provides a description of the problem to be solved, and describes some of the resources available and their functionality.

It has been necessary to determine whether a specific method for beam allocation is to be assumed. There are various possibilities when it comes to investigating this area of research such as looking at traffic patterns, applying existing ML methods or attempting to learn an optimal grid of beams.

- Much of the research in the area of applying ML to Massive MIMO beamforming is concerned with using ML to learn the required beam based on some parameter (such as SINR or receive power). These methods assume a specific 'grid of beams' that cover the cell, with the aim being to pick out the beam selected during the synchronisation process.

A second area of interest is to use ML to determine the best parameters of the beams themselves (beamwidth, tilts, elevation and azimuth).

These two areas of interest could be considered to be linked in the sense that several pre-defined grids could be considered, some with narrow and some with wide beams, for example. Then, the ML method is applied with different grids, the results of which are combined and processed to somehow determine which general beam configuration should be used. It may be, for example, that a configuration consisting of several narrow beams in one direction with wider beams in another direction could be optimal in many urban environments, for example when a shopping in centre is located in a certain direction relative to the BS. It would be necessary to have a way to represent numerically how good a certain configuration would be, perhaps related to the number of unused beams within a configuration.

Advantages of using a ML approach include the reduction of time and costs in the case of running physical experiments and the possible reduction of complexity compared with running deterministic simulations.

The aim of this project is to make use of realistic data regarding the distribution of mobile users.

4.4 ML Techniques and prior work

4.4.1 Problem statement 1

Junyuan Wang *et al* [52] have formalised a beam selection problem that can be applied to ML in a way that focusses on learning selected beams from a 'grid of beams' (i.e. a collection of beams covering an entire cell) based on some chosen parameter.

The assumptions of the problem statement described by the authors are that the users are all equipped with a single antenna and are uniformly distributed within a circular cell area. The array is linear with isotropic elements and half wavelength spacing with a collection of beams formed by the Butler method.

$$A_n(\theta) = \frac{\sin\left(0.5N\pi cos\theta - \beta_n\right)}{Nsin(0.5\pi cos\theta - \frac{1}{N}\beta_n)} \tag{4.1}$$

Where

$$\beta_n = \left(-\frac{N+1}{2} + n\right)\pi.$$

(4.2)

Where N is the number of beams, θ is the AoD, and n is the integer index of the beam. The users are distributed around the linear array and served by the beams as shown in Figure 68.

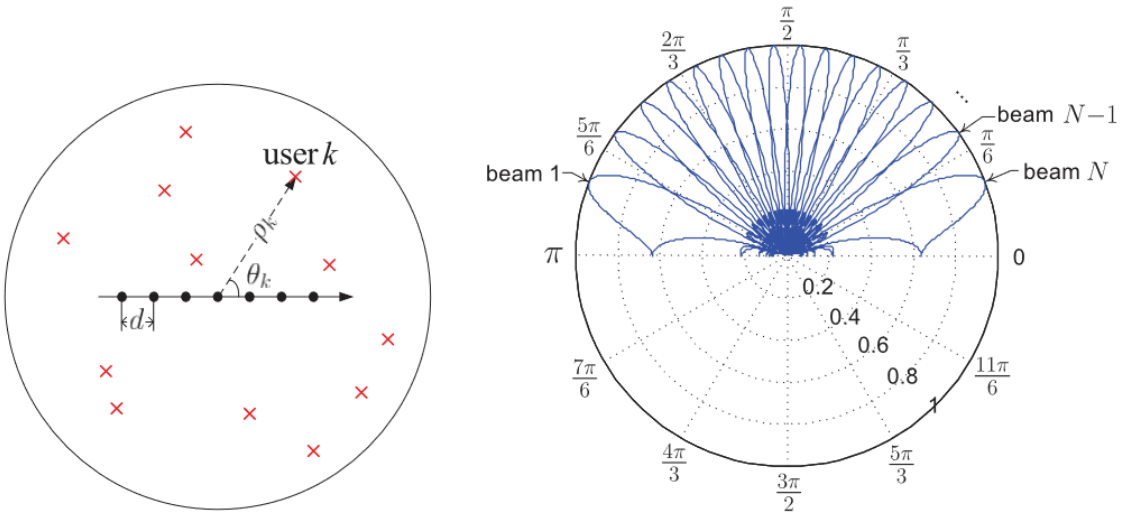

Figure 68: Distribution of users around the linear array with example beam patterns

The receive power is determined for each user k according to a standard path loss model

$$P_k = \sum_{n=1}^{N} 1_{k,n} p_n D_n(\theta_k) \rho_k^{-\alpha}$$

(4.3)

where $1_{k,n}$ is an indicator function indicating the chosen beam (i.e. 1 where beam n is selected for user k and 0 otherwise), p_n is the allocated beam transmit power, $D_n(\theta_k)$ is the relative directivity of beam n, ρ_k is the distance from the cell centre to user k and α is the path loss exponent. A further assumption of the model is that each beam can serve at most one user and that the total transmit power is fixed, with the power allocated to each beam being given by

$$p_n = \begin{cases} \frac{P_t}{N_s}, if \sum_{k=1}^{K} 1_{k,n} = 1 \\ 0, if \sum_{k=1}^{K} 1_{k,n} = 0 \end{cases}$$

(4.4)

Where N_s is the total number of allocated beams. The assumed achievable data rate is

$$R_k = log_2\left(1 + \frac{P_k}{\sigma_0^2 + I_k}\right)$$

(4.5)

Where σ_0^2 is the variance of the noise and I_k is the inter-beam interference

$$I_k = \sum_{j=1, j\neq k}^{K} \sum_{n=1}^{N} 1_{j,n} p_n D_n(\theta_k) p_k^{-\alpha}$$

(4.6)

The aim is then to find

$$\max_{\{1_{k,n}\}\forall k,\forall n} \sum_{k=1}^{K} R_k$$

(4.7)

This problem is slow to solve directly and forms the basis of some research in ML and MIMO beam selection, as discussed later in this thesis.

4.4.2 Problem statement 2

The second problem statement approaches the problem differently, by making the azimuth and elevation beam widths (in addition to the electrical tilt setting) the parameters to be learned through ML techniques. This effectively means that the beams themselves and the configuration of the grid of beams covering the cell are learned, not which beams within the grid are activated and for which users.

Shafin *et al* [122] formulate this approach to beam optimisation by considering a problem of determining a weight vector (which is applied at the BS array to define how the beam is steered towards individual users). The authors consider the

received signal vector for each user k (where the notation m refers to the sector and M) as

$$y_k = \boldsymbol{h}_{m,k}^T \boldsymbol{f}_m s_m + \sum_{\substack{m'=1 \\ m' \neq m}}^{M} \boldsymbol{h}_{m',k}^T \boldsymbol{f}_{m'} s_{m'} + z_{\boldsymbol{k}}$$

(4.8)

Where $\boldsymbol{h}_{m,k}$ is the channel vector between the mth sector and the kth user, s_m is the transmitted signal and $\boldsymbol{f}_m$ is the precoding vector applied to the mth sector. The final term relates to the noise. The aim is to learn the optimal beam pattern for each sector. The interference between sectors must also be considered as part of the selection process.

There is, for each BS with its sectors, a predefined class of J possible weighting vectors for the antenna array

$$J: \{\boldsymbol{j}^1, \boldsymbol{j}^2, \dots, \boldsymbol{j}^J\}$$

(4.9)

Where each of the weightings corresponds to a beam pattern with a specified azimuth, elevation and tilt. The chosen weight corresponds to the sector's precoding vector f. The weight vector is chosen based on the distribution of users.

The choice of weight vector is made based on the following process (noting that the aim of any ML scheme related to this general approach is to learn the weight vectors that result from the described process): firstly the SINR rate for each user is determined for each of the available beam configurations. A threshold SINR value is selected that will be used as the baseline for determining if a user can be said to be connected to the BS or not. The aim is then to compute the set of beams for each sector that maximise the total number of connected users, i.e.

$$\max_{\boldsymbol{f}_1, \boldsymbol{f}_2, \dots, \boldsymbol{f}_M} \sum_{k=1}^{K} 1_{SINR_k > T}$$

(4.10)

Where T is the threshold SINR level and '1' is the indicator function. In other words, this is the total number of connected users that occurs for some set of beam

configurations, with one beam pattern associated to each sector. Finding this set of beams is made more complicated by the fact that there will likely be inter-sector interference, a factor that could affect the number of connected users that is achievable.

It should be noted that the criteria for beam selection is very different compared with the first formulation, because here the aim is to obtain a beam that will serve the largest possible class of users, but in the first formulation each beam served only one user.

This formulation of the problem would seem to be closer to what is described in the Autonomous Industrial Mobile Manipulators (AIMM) use cases specification: however, it may be that this formulation of the problem could be combined with the first formulation. This could work by determining which grid of beam configurations are available to the networks, simulating the channel with user distributions, and then attempting to learn the beams selected through available parameters, repeating this process for each of the possible grid of beams configurations. It would then be necessary to determine which grid should be chosen according to some parameter. Perhaps, for example, the chosen grid would be the one with the fewest number of unused beams.

Determining the grid in this way could help in providing an optimal grid for different environments, as described in the introduction.

4.5.3 Recent Research

There seem to be fewer research outputs related directly to the topic of using ML for SS Block Broadcast Beam optimisation compared with other areas of MIMO research. Much of the relevant literature is from conference proceedings and often assumes the use of mmWave frequencies. There may be opportunities to investigate some of these methods but in the context of frequencies more relevant to the mobile Radio Access Network, as well as to use real data, such as those provided by the ‘average number of connected users’ metric, to provide more realistic data for the development of ML algorithms.

The emphasis of this work is not to attempt to learn which beams are selected as a result of the synchronisation process from a specified grid of beams. Rather it will be to identify the best beam patterns to use from a set of defined possibilities. This

involves identifying a figure of merit to determine which beam pattern should be used. The initial tasks are as follows:

- Identify a selection of beam patterns. The first options will likely be patterns formed from different numbers of active antenna elements, which will correspond to beams of different widths and different total number of main lobes within the beam patterns. The next options could be to rotate the selected beam patterns in various directions. Depending on the metric chosen to identify the favoured beam pattern, it may be possible to infer when a certain azimuth range can be excluded.
- Obtain and pre-process location data of users from the mobile network. These data will be in two dimensions at first, only in the azimuth plane, which is more relevant in situations without high rise buildings. It will be necessary to consider exactly what form these data will take and whether they will include information about buildings within the data or whether the position of the users is presented in terms of radio distance, rather than physical location.
- Modify code so that it can run the simulations with the output required. Determine whether the RSRP measurements and antenna weights or necessary, or whether only the selected beams are necessary.
- Run the simulation and obtain results.

4.5 Simulation Features

5G Simulations for Beam Selection

MATLAB provides, within its 5G simulation toolbox [125], the ability to simulate the synchronisation signal burst process within a 5G Radio Access Network, including beam selection from a defined array and the reported measurements from the user equipment upon which the beam selection is made. This simulation is based on a 2D environment with scatterers; however, it would seem to be based on a fairly simplified representation of antenna geometry and propagation path loss. More details of the environment assumptions are presented later in this chapter, which will present the features of the SSB simulation that are relevant to the research project and discusses the output data provided and how these output data could be made to

more closely resemble realistic data by using practical network data at the simulation input.

The BS array

The transmit array is, by default, an 8x8 uniform rectangular array with a pattern as shown in Figure 69:

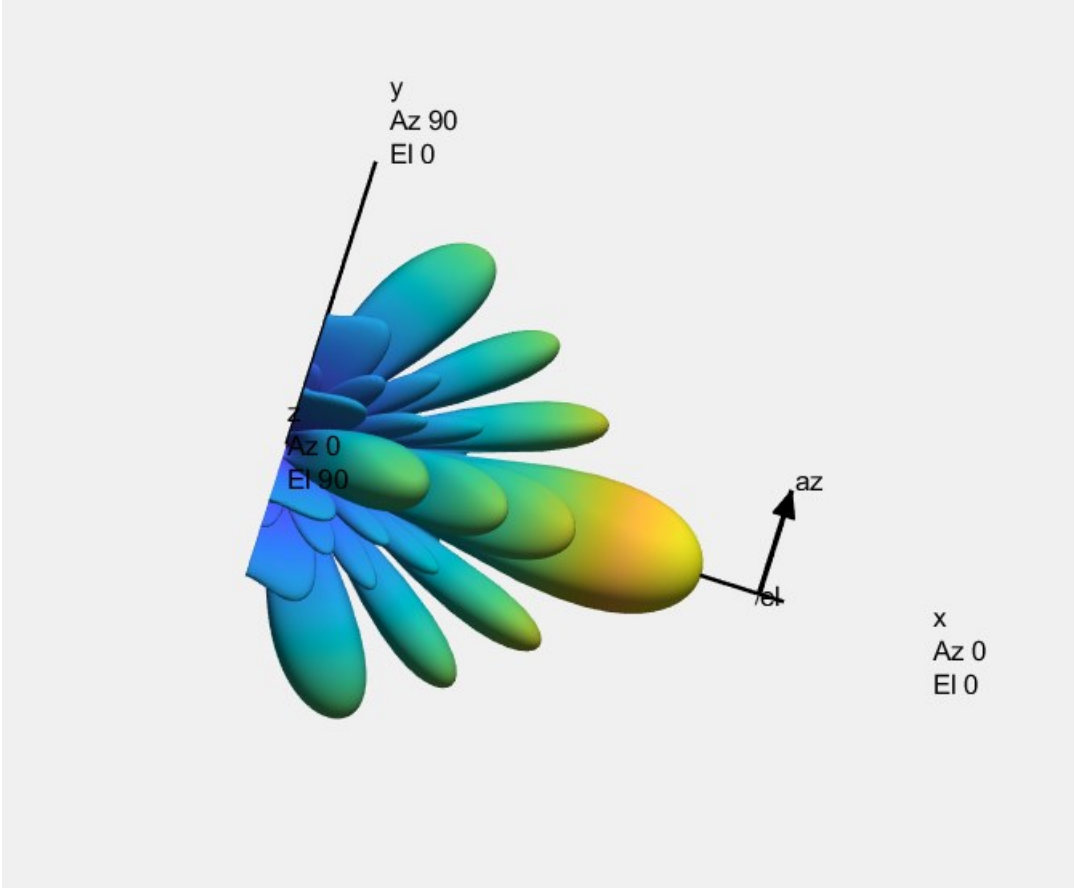

Figure 69: Generated beam pattern for 8x8 uniform rectangular array with equal weights

This array, as can be seen, forms a grid of beams over a sector of the cell. More beams can be added by varying the number of elements:

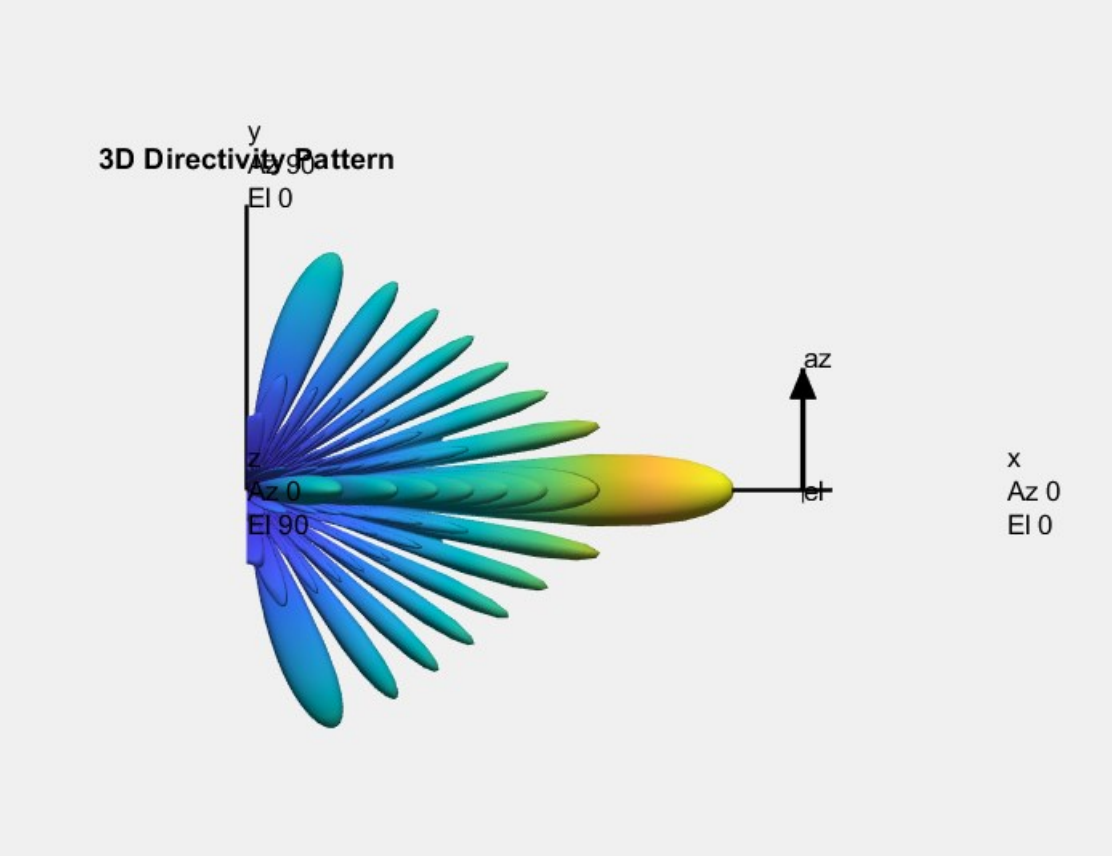

Figure 70: Generated beam pattern for an array with 128 elements

The number of beams is linked to the number of synchronisation signal bursts, and the result of the beam sweeping stage is to create a class of weighting applied across the elements of the array. For example, for an 8x8 array the weightings could result in the beam patterns shown in Figure 71 and Figure 72.

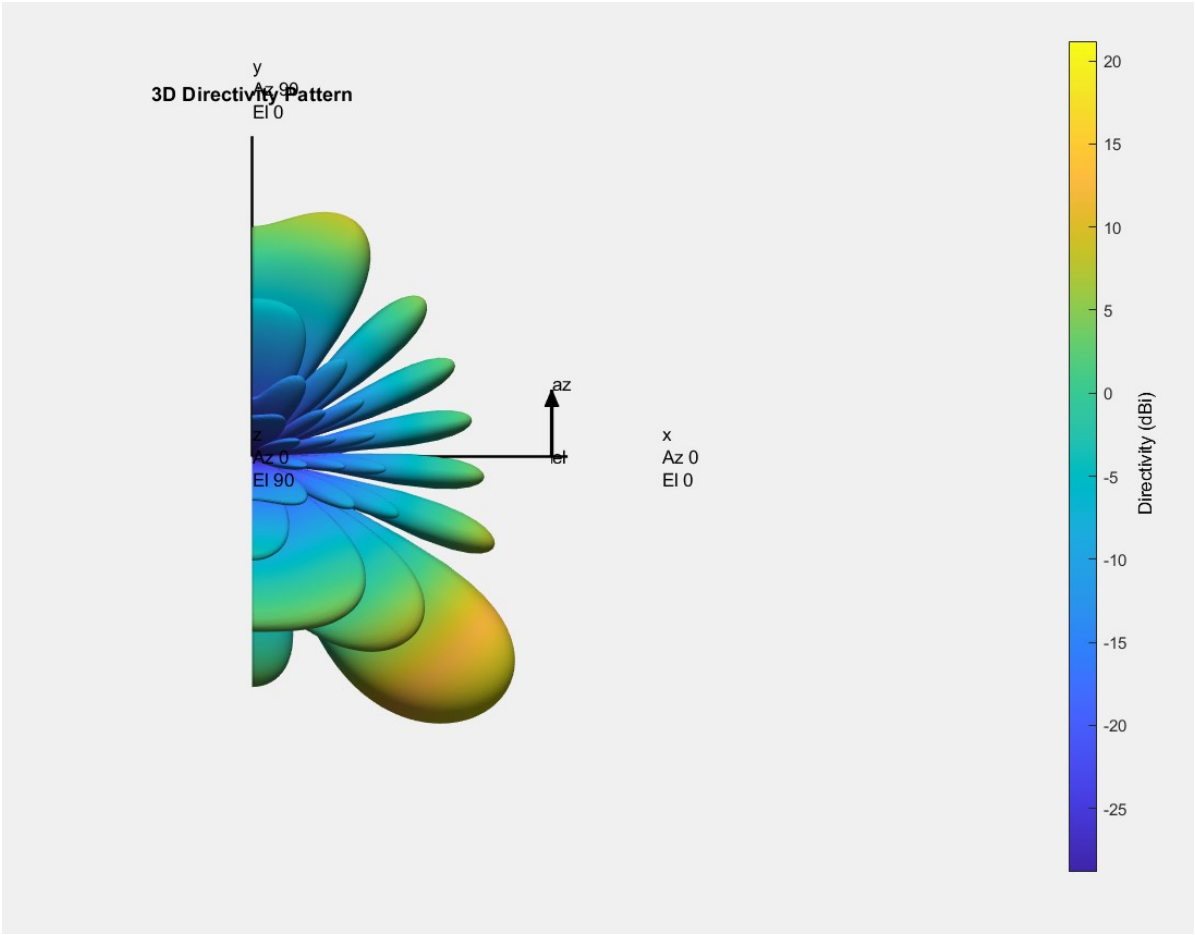

Figure 71: Example generated beam pattern for 8x8 array with applied antenna weights

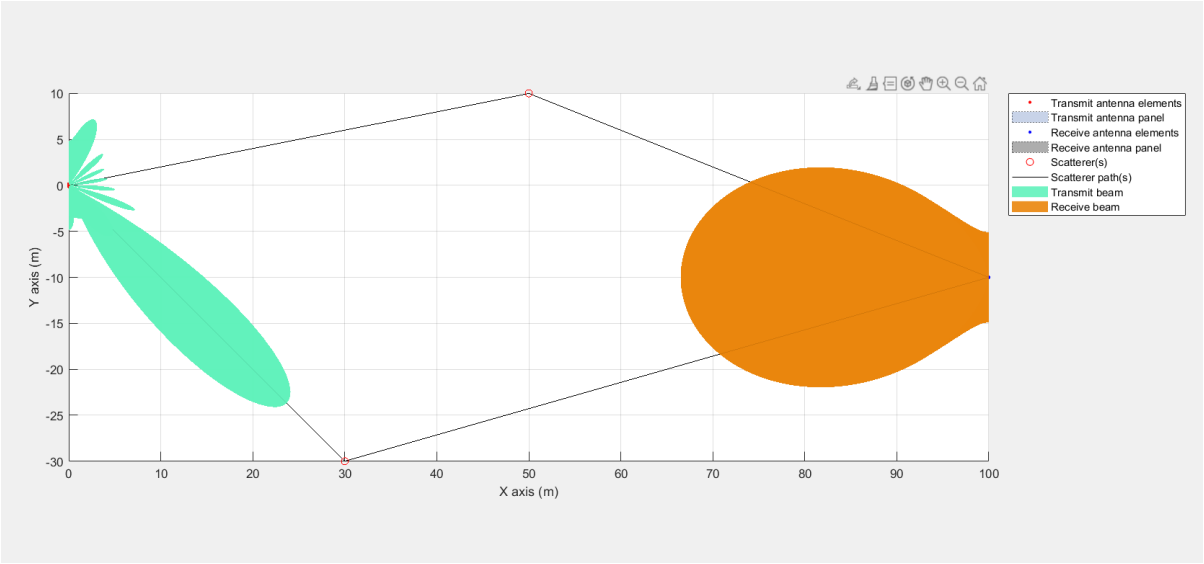

Figure 72: Example generated beam pattern for 8x8 array in 2 dimensions with scatterers and receive array

The weightings for the antenna array are provided as a vector with a number of elements equal to the number of elements in the antenna array. The RSRP measurements are also provided (with the rows and columns referring to the transmit and receive end of the link).

The selection of the beam pair is determined by simply choosing the maximum value from the table. The weights are determined from the array steering vector function dependent upon the angle of the beam that is identified as the best for connecting to the UE.

Placement of UEs

The user equipment can be placed around the grid using cartesian coordinates as shown in Figure 73 and Figure 74 (noting that the circle towards the top of the grid represents a scatterer):

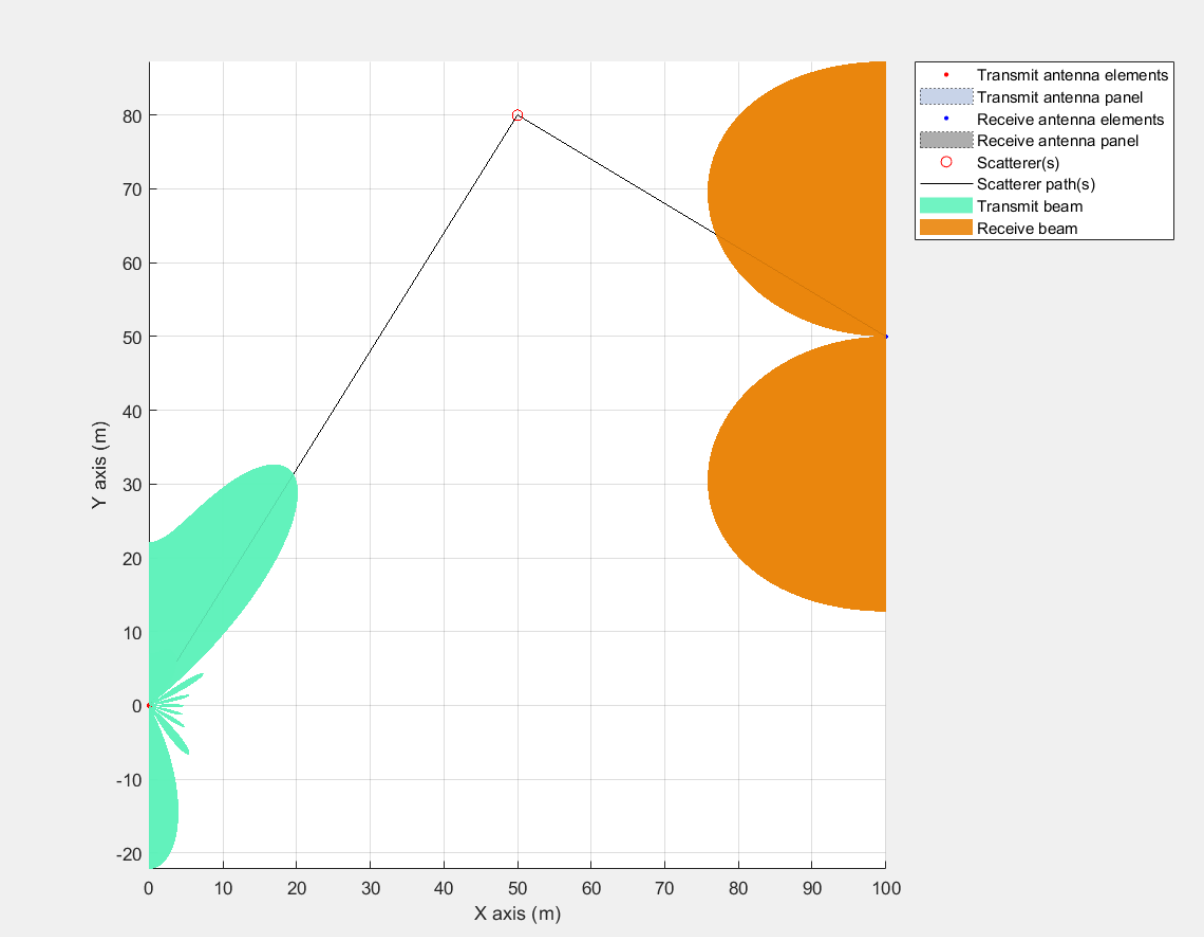

Figure 73: Placement of user in two-dimensional grid with scatterer

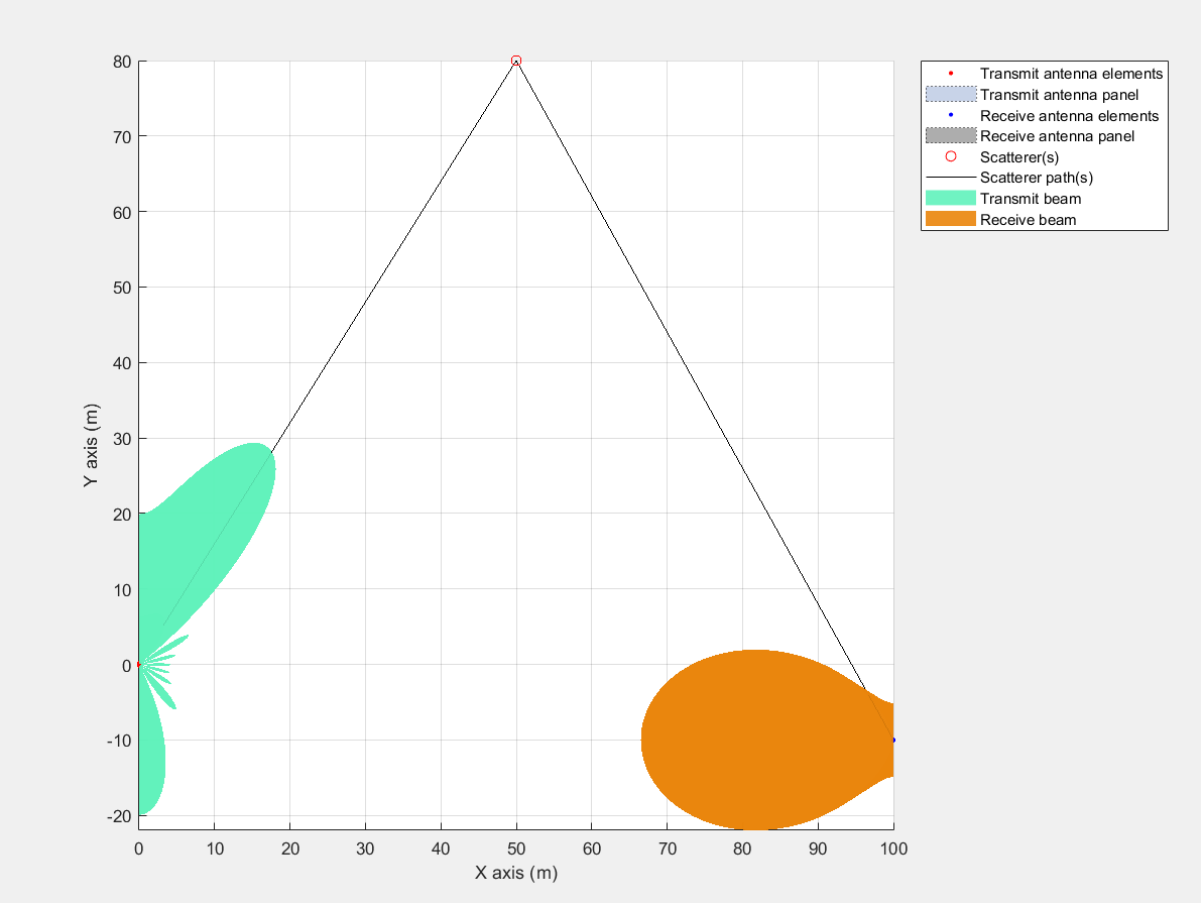

Figure 74: Placement of user in two-dimensional grid with scatterer

In this example, only the placement of one UE is allowed without modification to the software. There are different options available for running the simulation with multiple users. The simplest approach would be to run the simulation several times with the users in different locations. This would mean, however, that one would not obtain the weights for the multiple users, as these would be re-calculated for each user. However, it may be the case that the weightings themselves are not necessary, and it would be possible to develop a ML system based only on the reported RSRP values during the synchronisation process, or even just the list of the selected beams.

Since the beam weightings are obtained from the RSRP and based on the direction of the user relative to the array, it may be possible to collect the RSRP measurements by running the simulation several time and then calculate the approximate locations of the users. This information could then be used to inform the array weightings.

A more complex approach would be to create a beam sweeping simulation for the synchronisation process that captures the RSRP measurements for several users placed on a map. The measurements would be based on assumptions regarding the propagation environment. One advantage of taking this approach would be to overcome limitations in the propagation model that is used within the simulation, which are described later in 'issues with propagation model' section of this document.

Placement of Scatterers

The placement of scatterers is achieved in the same way as the placement of the UEs. These scatterers can be used to approximately represent buildings and other objects within a propagation environment.

Summary of Data Output

The main outputs from the simulation are:

- The RSRP measurements for the combination of receive and transmit beams, presented as an MxN matrix (with M and N being the number of BS and UE beams). The maximum value in the matrix corresponds to the chosen beam.
- The selected beam IDs (in the range 1…M and 1…N) of the selected beams.
- The BS array weightings, as a vector with a number of elements corresponding to the number of antenna elements.

4.6 Mathematical Description of Problem

The generation of the normalised RSRP surfaces allows for the problem to be expressed more precisely as a combinatorial optimisation problem. This formulation is developed with attention specifically to assumption 1 in the opening section, that is to provide even coverage of broadcast synchronisation beams for a given user distribution and environment.

Within a region covered by a 5G BS (i.e. a gNodeB) m user locations (each defined with (x,y) coordinates). It is assumed that a sector is known that corresponds to the coverage area.

The matrix $\mathcal{X}$ is n×m where n refers to the number of possible beams (each with their computed normalised RSRP curves). The quantity n is determined simply by the beams that are being considered, which could be the number of possible beams

given the hardware constraints or those that could possibly be permissible given operation considerations. It may also be defined by the requirements of a specific type of study. For example, if it was necessary to test different types of beam configurations, one might choose a set of beams of one type and a set of beams of a different type, with each set being the same size. The m columns of $\mathcal{X}$ refer to the RSRP values at the user locations.

The r×m matrix $\mathcal{Y}$ is made up of r rows from $\mathcal{X}$, where r is the maximum number of allowed beams (often eight in our examples and r<m), define v_j as the position of the maximum value in column j, that is the row of $\mathcal{Y}$ that contains the maximum value.

Define z_d as the number of times that d appears in $\boldsymbol{v}$ where d=1,…,r. Then find the r rows of $\mathcal{X}$ forming the matrix $\mathcal{Y}$ that minimise the difference between the maximum number contained within z and the minimum number.

$$\max(\boldsymbol{z})\text{-}\min(\boldsymbol{z}) \tag{4.11}$$

The beams that are selected to form the rows in Y provide for the most even coverage amongst the user distribution, as described earlier. Intuitively one is presented with a matrix where the rows correspond to the beams and the columns to the RSRP values specific users. A vector is then created to show the list of beams that provide the best coverage for each user, and the aim is to find the set of beams for which each beam appears in the list with the same frequency as the others.

4.7 Available data

Data Requirements

Location data for the mobile users are a requirement for this research. These could be entirely empirical in nature or a combination of empirical and a statistical data. Data that are generated entirely based on statistical models may not be appropriate, as part of the originality of this research will be based on the use of realistic traffic and locations. Additional information such as performance data could also be useful, though this may be a secondary concern as the first point of interest is the user distributions themselves. Data such as practical RSRP data could be useful for the verification of the accuracy of the distributions used (if these are not based on

precise known locations). For example, it may be possible analyse the range of RSRP values present in the practical network and see if these match the results that are suggested in the simulations, although this may be complicated because of the varying configurations of the beams, which may not match between the practical and simulated environments.

Milton Keynes simulation

The data that are currently available (i.e. data that are simple to access within the research group at present) include the following:

Location data for BSs and the surrounding environment are available (Figure 75). The database also includes coverage maps, which will represent the regions that will form part of the analysis of the beam selection simulations.

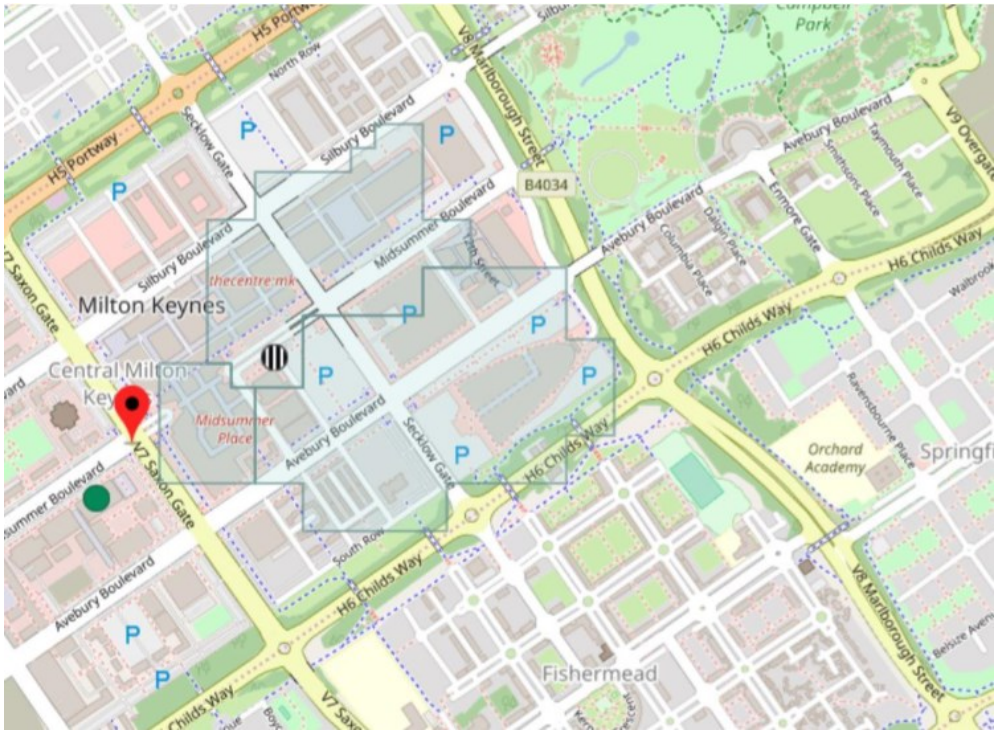

Figure 75: Milton Keynes BS coverage data. The shaded areas represent the coverage for each sector.

A key type of data that could prove very useful and is readily available is the average number of connected user data. As this provides an average value for the number of mobile devices that are connected at any time, this effectively provides the number of users that need to be included in any simulation.

In addition to these network data, there are some traffic data that has been provided by local councils consisting of origin and destination matrices. This could be useful in refining (and possibly simulating) the movement of traffic, although this project will likely focus firstly on beam configurations that do not change too often, so this could be of limited use at first. It is possible that other public domain data could also be useful, as many councils provide these sorts of data in various formats.

Minimisation of Drive Test (MDT) data are also available from the network and are advantageous in that they contain the exact global positioning system (GPS) coordinates for each user (Figure 76). They also contain altitude data, which could be useful if the proposed framework is extended into three dimensions. They also include both RSRP and reference signal received quality (RSRQ) data, which will be potentially useful for the verification of the simulation.

A major disadvantage of MDT data is that not all UEs provide them, as users must give their permission for these data to be transmitted to the network. Additionally, not all mobile operating systems support the collection of these data. It is likely that the availability of these data will only reduce in the future. Also, no information about the features of the geographic environment are provided within the MDT data, that is there is no information about buildings or direct information about the terrain apart from what can be inferred from the GPS coordinates.

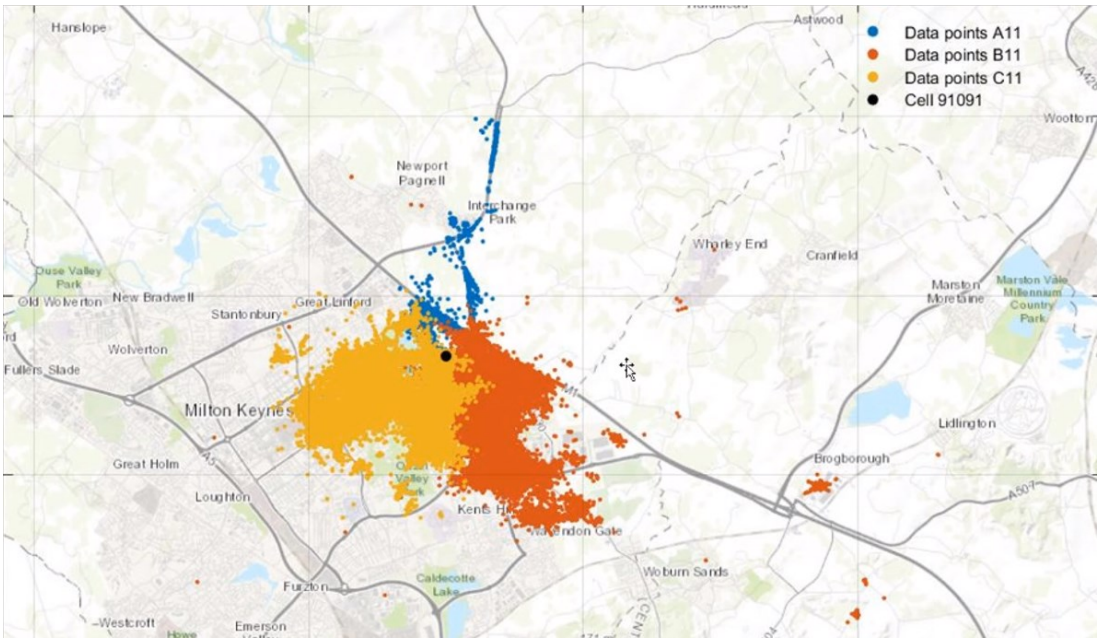

Figure 76: Example location data from MDT (courtesy of Shipra Kapoor)

4.8 Approaches to finding a solution

The most obvious approach to solving the even coverage problem described in the previous section is to use an exhaustive search method. This is achieved by computing the RSRP values from the matrices representing the RSRP surfaces for each of the possible beam combinations from a defined set of beams. This approach, however, is potentially time-consuming. For example, finding eight beams from a set of only 15 require 6435 iterations of possible beam combinations. As shown in this section, this many iterations may not be necessary as sometimes there can be many sets of possible beams that yield very similar distributions. This can be seen in the following example.

Here, 15 beams are selected to be investigated. These are not chosen to be related to a specific example, but rather to view the types of results that can be expected. The beams are chosen to sweep a sector of 120 degrees to the west of the BS. The first eight beams are separated so that the main beam sweeps at equal intervals between -60 and 60 degrees. The final seven are the first beams from the set that sweep at equal intervals between -50 and 50 degrees. The simulation is run according to the RSRP surface method described above, obtaining the normalised RSRP values for each of the users present. The beams and their associated indices are illustrated in Figure 77.

Figure 77: Illustration of beams with their associated indices. The areas within the blue lines indicate the gain shown on circular graphs with the BS located at the centre points.

An exhaustive search method was used to provide a baseline for comparisons with other methods for finding optimal beam configurations and to analyse the features of the variations in user distributions over beams. The ‘distribution over beams’ is the difference described in equation (4.11), which is the difference between the number of users that are served by the beam with the highest number of users and by the beam with the lowest number of users.

The results of the exhaustive search are shown in Figure 78, with the horizontal access representing the combination of eight beams from the set of fifteen. The lower the value on the y-axis, the better the combination of beams in terms of even coverage. It can be seen immediately that the range of user distribution over beams is very large, especially considering that the number of users in this example is limited to 100. It can also be observed that, while the user distributions never reach zero, which would represent the most idea scenario for even coverage, the lowest values of around 11 and 12 are revisited several times, suggesting that computing the RSRP values for all combinations may not be necessary. In this example, specific user data was not used to generate the results, but rather a sample from

identical and independently distributed random variables representing the distance from the BS and the azimuth data.

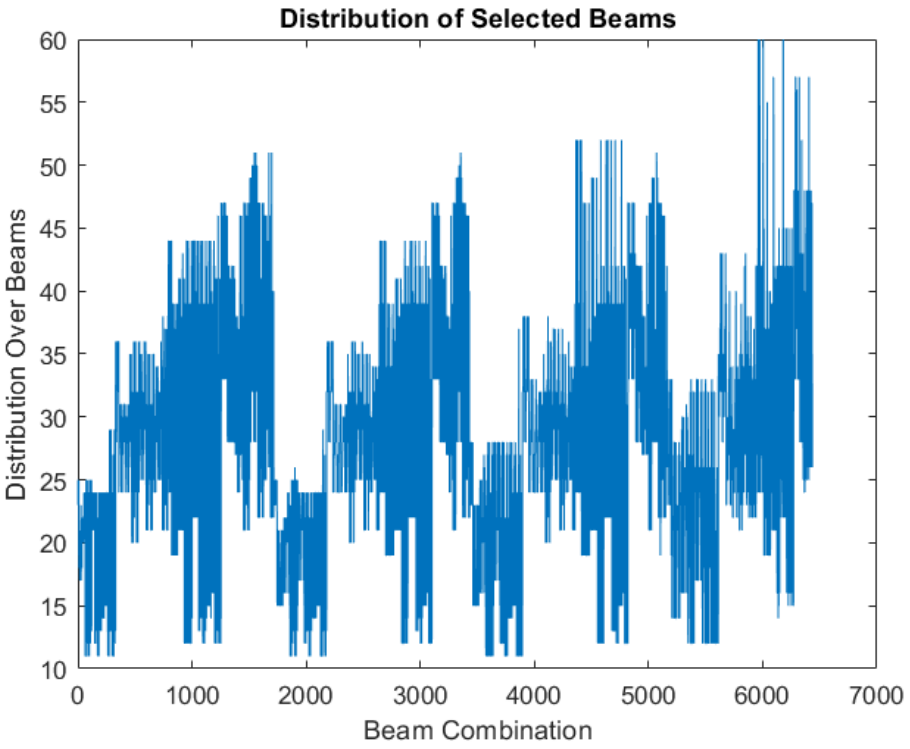

Figure 78: Variation of the distribution of users over the selected beams, as described in the text, for all possible combinations of a set of 15 beams.

4.9 Experimental Results

The problem of finding a minimum value from the beam selections is addressed in this section. The function is discrete, therefore making this a problem in integer linear programming. Unfortunately, this means that many of the standard optimisation algorithms are not appropriate for finding a solution, although simulated annealing (SA), a standard method in optimisation, offers a possibility, as it has often been used for optimisation problems involving discreet data [126]. It should be noted that it may not be necessary to find an actual minimum value, as an approximate minimum value may suffice for practical purposes.

SA, first introduced by Kirkpatrick *et al* [127] is similar to other stochastic search methods where a random point is selected, followed by another point which is rejected if it offers a worse solution or accepted if it offers a better solution, with the process continuing until a minimum is reached. SA extends the process by introducing the possibility that a solution will be accepted even if it is worse

depending on a temperature coefficient that gradually reduces as the algorithm proceeds.

A variety of parameters were used to determine how quickly a minimum value could be found for a beam distribution using such a method. Firstly, the total range to be considered for the beam combinations was limited to 1000, as it has already been determined that a low value has been reached several times within that range. The maximum step size is set to 100 to keep the step size within the range of the data. Table 1 shows the minimum value of the user distribution as obtained with various parameters.

Table 1: Minimum value of user distribution as obtained with various parameters

Maximum Number of Iterations	Initial Temperature	Determined Minimum Value of Distribution
100	10	11
50	10	11
25	10	13
25	100	11
10	100	11

The initial temperature has been seen often to affect the effectiveness of obtaining a reasonable value within the maximum number specified, although this depends on how random numbers appear in the sequence. Figure 79 shows an example of the process of finding the best beam pattern using the SA process described. The blue line represents the sequence of random values at which the distribution of users is measured. This uses the Python random number generator and begins by imitating these pseudorandom numbers, with the variation over time determined by the initial temperature of the algorithm. The other line in the diagram shows the accepted candidate solutions for the beam distribution, which, in this case, obtains the lowest possible distribution.

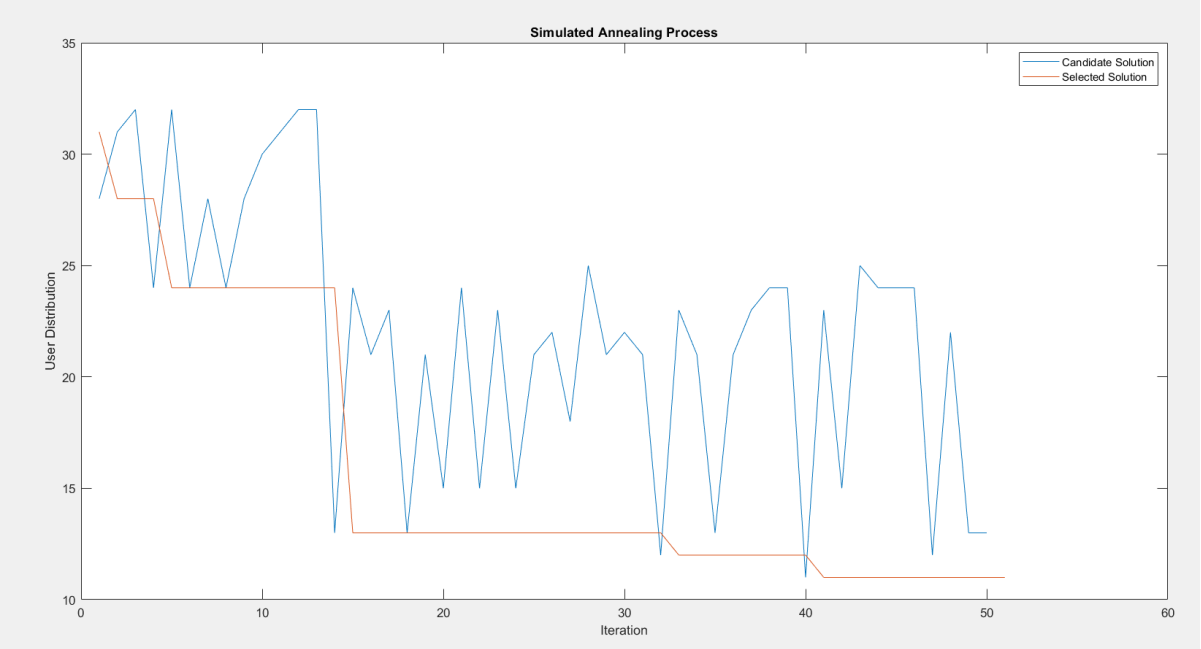

Figure 79: Representation of SA for 15 beams of equal width with temperature of 10. The blue line represents the candidate solutions and the red line represents the accepted solutions.

The previous example was for beams of equal beamwidth. The example in this section is for a set of beams containing beams of different widths. The purpose of such an example is to demonstrate how changing such parameters affects the approach to finding optimal beam configurations and how more complex problems can be addressed when designing mobile networks with beam selection.

In the previous section, the beams were all generated based on an isotropic rectangular phased array with 64 elements, each of which were active in generating the beam. For this example, fourteen beams are chosen with the first eight generated according to the array in the previous example and the final eight generated with only 32 of the elements, forming a square around the central point of the 8x8 square of elements. These eight beams are wider than the original eight beams, however they all point the strongest section of the lobe in the same direction, that is equally spaced in one sector of a typical tri-sectored BS. This time, there are 3003 possible beam combinations, and the distribution for the users is shown in Figure 80.

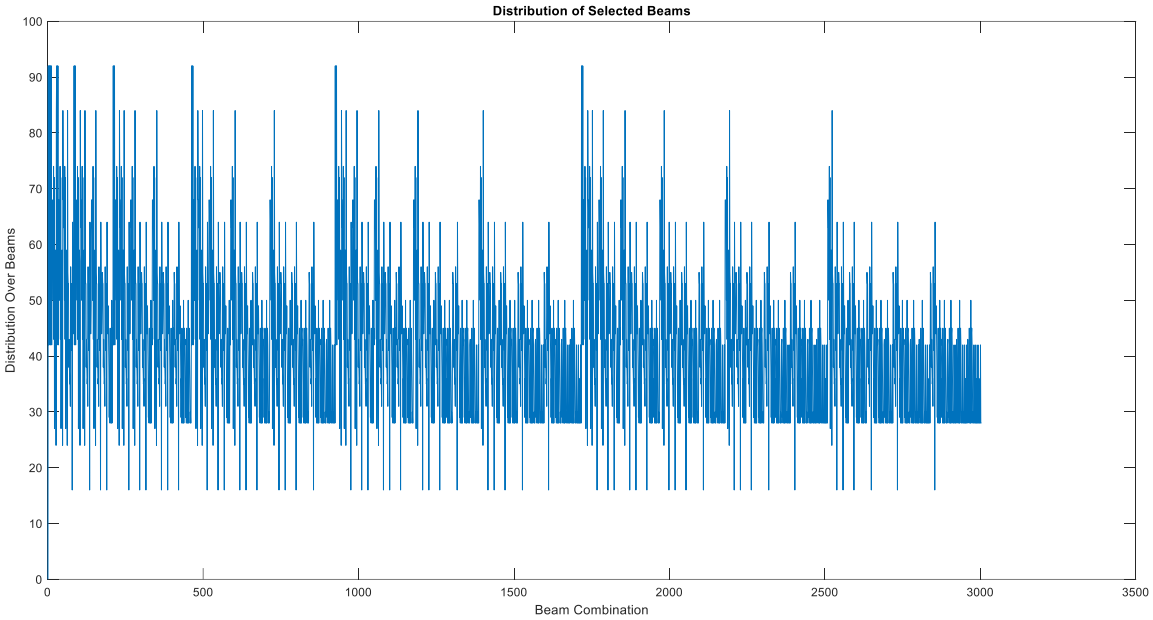

Figure 80: Distribution of beams over users for 14 beams, eight of a narrower width and eight of a wider width.

Once again, the SA process significantly reduces the number of iterations down to 30 with an initial temperature of 100 (Figure 81).

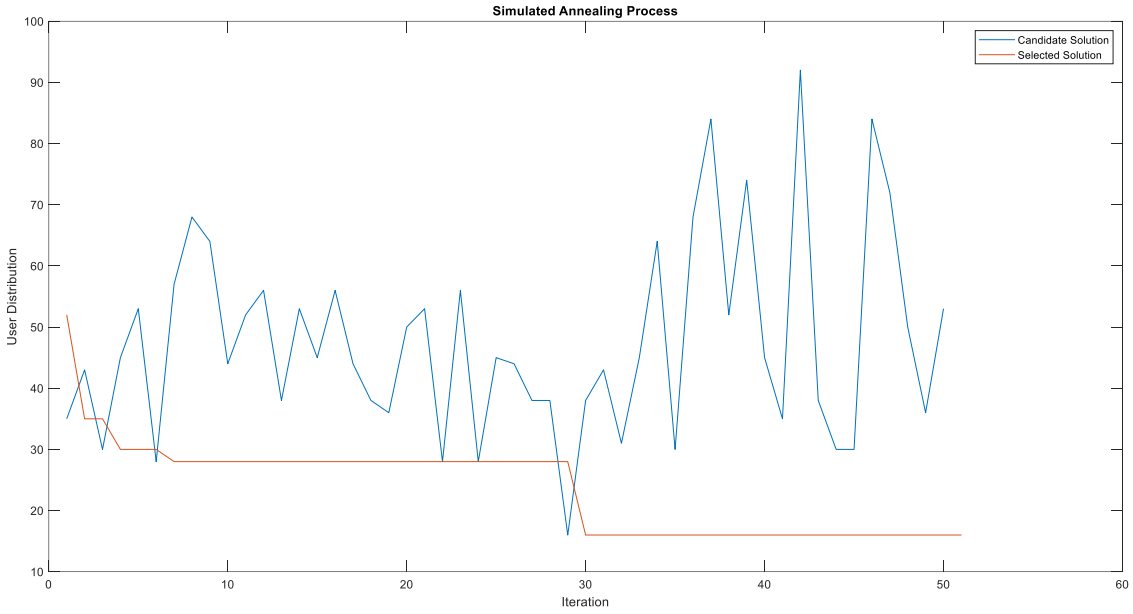

Figure 81: Representation of SA for 14 beams, with eight of one width and eight of another.

The following provides a basic example of the performance of SA using a distribution where users are more clustered in certain directions. Take, for example, the heat map for a BS in Bromley, designed by Timothy Sanmoogen at BT as shown in Figure 82. The map shows the density of connected users within an area, with the scale from blue to red corresponding to low to high density. However, this scale does not correspond to an absolute quantity of users, but is related to the total number of users within the areas. This means that, in the image shown here, the areas coloured red correspond to those areas that had the highest number of users relative to the other areas. The approximate location of the BS with its three sectors is also shown on the map.

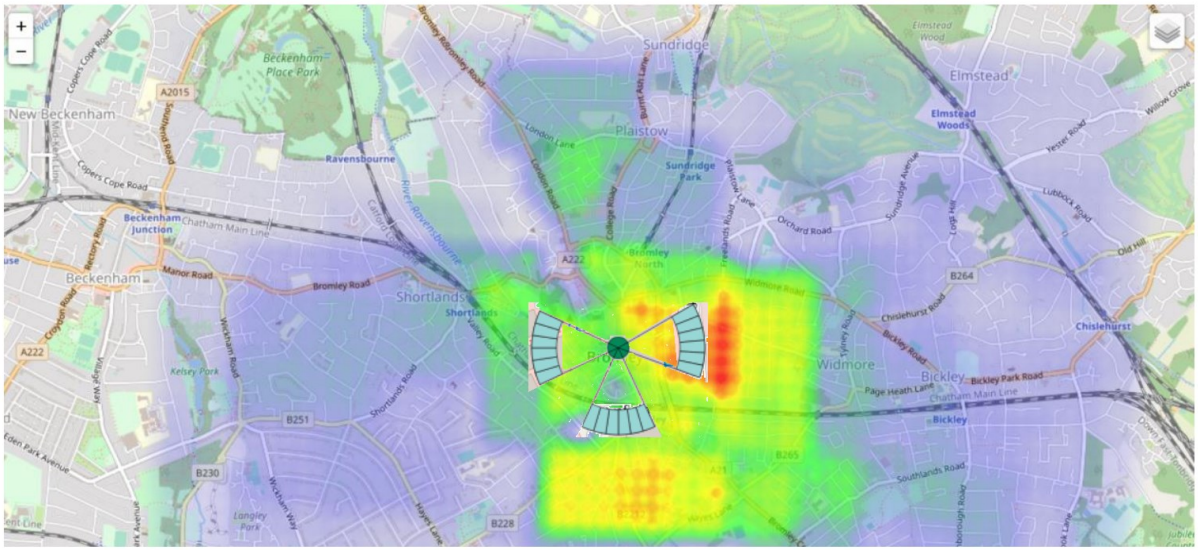

Figure 82: Heat map for BS in Bromley (courtesy of Timothy Sanmoogen)

There is a BS located just to the west of the darker red area of the map, which represents a greater contribution of users. Again, considering a tri-sectored BS, the density of users would vary with a sweep from -60 to 60 degrees (if 0 degrees represented a direction of due east). This can be approximated through a random selection of 100 users with a larger number chosen to occupy a certain section of the total sweep (Figure 83).

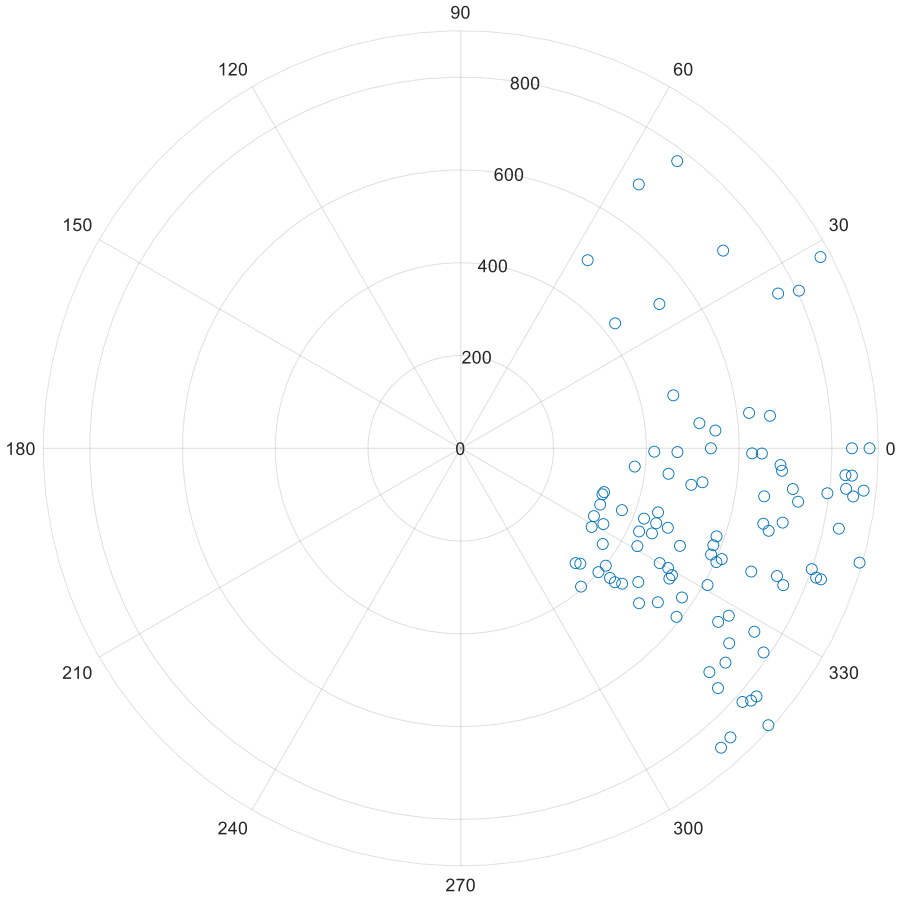

Figure 83: Approximation of user distribution observed in Bromley. The scaling of the concentric circles is indicative only.

Significantly, the distribution of the users over the beams appears to have slightly different characteristics than the distributions for non-clustered random users (Figure 84). The lowest possible value is visited only a few times in comparison with the many times that it was visited for the non-clustered examples. It does, however, reach the next lowest value many more times, but this is quite far away from the lowest value. It may be that, without a sufficiently high temperature or number of iterations, this non-optimal value would be chosen. The specific circumstances would determine if this were a reasonable solution for the selection of beams or not.

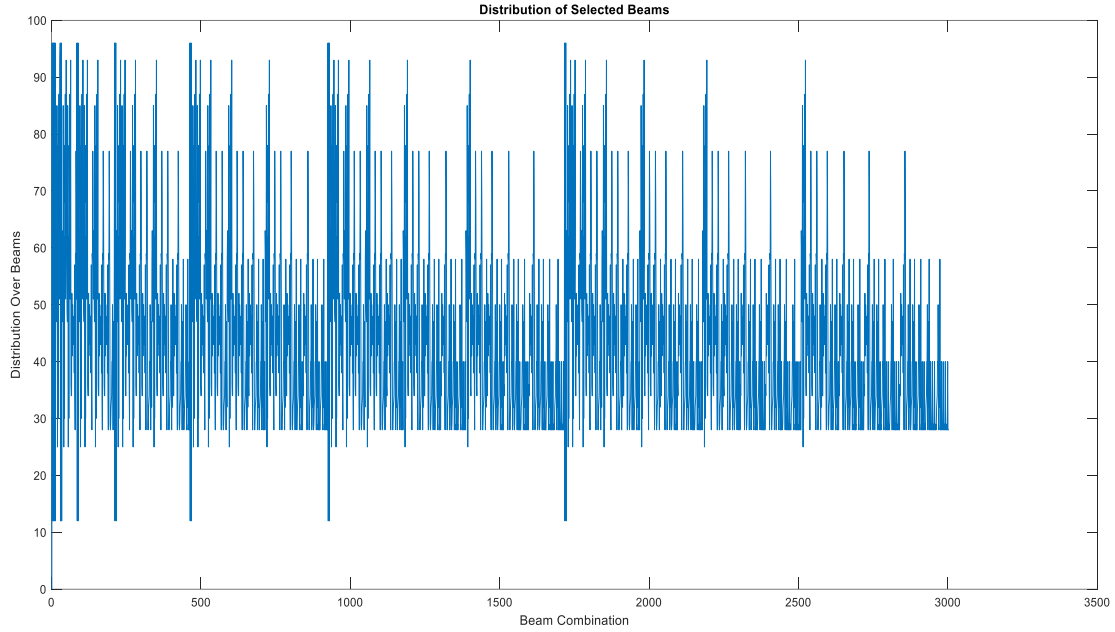

Figure 84: Values for distribution of the users over the beams

Indeed, nearly 200 iterations are required to obtain the correct solution when the initial temperature is set to 100, and nearly 100 iterations to obtain the next closest solution (Figure 85).

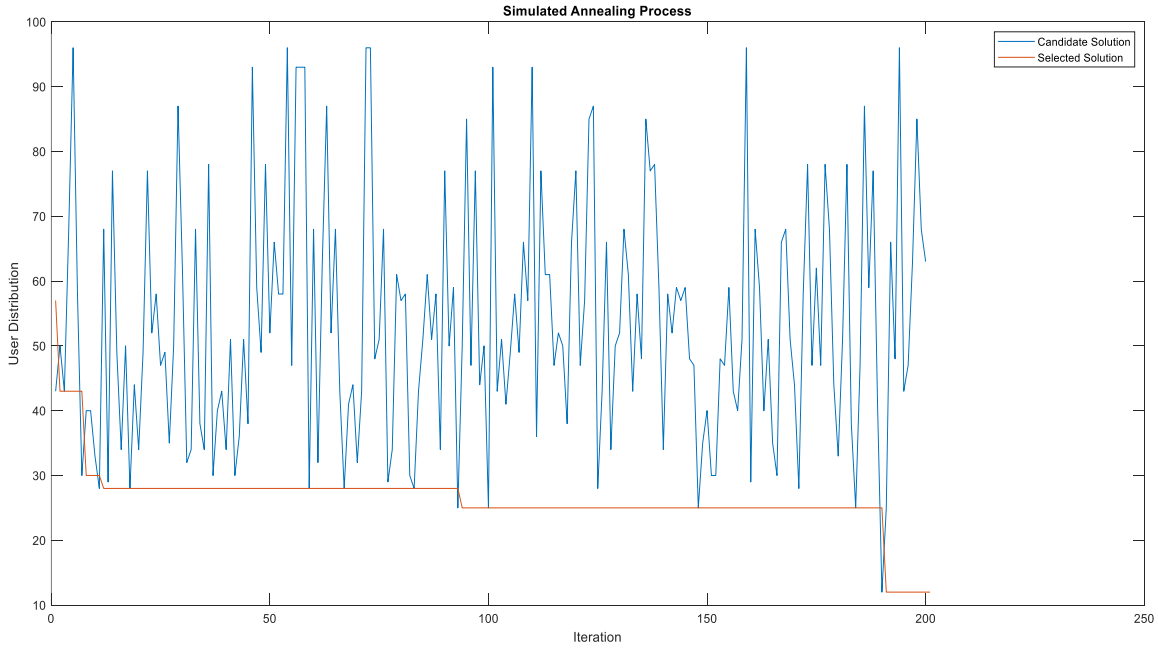

Figure 85: Obtained candidate solutions and selected solutions for SA algorithm

However, setting an initial temperature to 200 allows for a correct solution to be obtained in only seven iterations.

4.10 Network deployment recommendations

From a network deployment and management perspective, the research presented in this chapter has a significant implication.

As described at the start of this chapter, the synchronisation process allows for a sweeping of beams over a coverage area to allow for the initial connection and synchronisation of user equipment. This process precedes the process of establishing data throughput, which is discussed more in the next chapter. The specifics of the beam parameters are not defined in the standards and can, at least in theory, be established by the MNO. However, the number of beams that can be used and tested is limited in both a temporal and physical sense. Physically because of the limitations in hardware and potential difficulties in making changes to the parameters, especially if the site is already in operation. Temporally because, if a large number of candidate beams are used that vary between sweeps, then it will be a length process to obtain signal reports from each user related to each of the candidate beams. It is highly likely, especially in dense urban environments, that the characteristics of the coverage area in terms of the location of user equipment, will have changed several times by the time that results are obtained, by which time such results will not be relevant to the coverage environment.

The advantages that this research brings can be considered in both a real-time and non-real-time sense. The non-real-time sense related to planning and design. As previously discussed, running propagation models is time consuming and the number of beams that an operator may consider could easily be several thousand or more. The examples in this chapter have used simplifications of propagation models using the RSRP surfaces described combined with standard Rayleigh propagation models. This was done due to limited computational resources and because the aim of this study is to investigate potential benefits in the design and management of the beam management process with synchronisation, rather than to investigate the propagation characteristics of specific environments. However, when designing Radio Access Networks in a way that does require the use of more complex

propagation models, these would need to be run only a few times in comparison to the many times that would be needed if run for each possible beam configuration. This is because it has been shown that, from the perspective of coverage, an optimal (or near optimal) set of beams is likely to have been found after only a small number of iterations through the set of candidate beams, relative to the thousands of iterations necessary for an exhaustive search of all the possible candidates.

The application of the process of beam selection discussed in this chapter could potentially be applied with self-learning networks in real time, however this would require further research. This is mainly because of the complexities in applying such concepts to specific network architectures, a process that would require careful investigation, and because of the much higher risks associated with applying optimisation in real time, since a sequence of bad solutions could potentially be very detrimental to network performance, leading to a degradation in user experience that could then lead to financial risks, especially if user experience is consistently worsened, or safety risks if a minimum level of service is not maintained. However, a careful application of beam optimisation methods in real-time could potentially yield great benefits for performance if one considered a scenario such as the following:

Suppose that a mobile BS has access to a large set of potential beams but is using a standard subset of evenly spaced beams of equal width. These eight beams are used for sending the synchronisation blocks to the users wishing to connect to the network. It may be possible to add a threshold condition to the computation architecture responsible for synchronisation, that states, for example, that the user distribution is acceptable below a certain value. In other words, once the beams are such that they are each serving a number of users for which that number of users does not vary between beams by more then a specified amount, then this is acceptable. If, on the first sweep of the beams, this number is not an achieved, then the computational hardware could choose a different set of beams based on the methods described in this chapter. Since such a method has been shown in theory to yield a near optimal solution in a relatively small number of iterations, it should be possible for the BS to obtain its threshold value within a small number of sweeps, which may be fast enough to be useful before a significant change to the user environment. Likewise, when the environment does change, it may be possible to adapt to this environment more quickly than if an exhaustive search of the beams

was necessary, especially if the network operator already obtains knowledge of likely changes, such as changes that usually occur during the evening rush hour. It may then have already determined a set of possible optimal beam from the previous day, or a sequence of previous days, that can then form the initial set of beams, thus making any optimisation even faster.

The way that the problem of beam selection is formulated can suggest certain approaches to finding a solution. For example, it may be that (unlike in the approach taken in this chapter where a known set of beams is defined and the aim is to select a number of beams from the set to serve the UEs) the possible beams are not defined precisely. In this case, it may be of more interest to attempt to discern the shape of the coverage area, and then creating a beam that approximates this required coverage. Such a formulation would lend itself to an approach that begins by focussing on the distribution of users instead of the set of possible beams, and one such approach could be through the adaptation of techniques used within binary search methods, such as a binary slice approach. The binary slice approach to searching may occur when a computer has an array of data that is arranged in ascending order, and there is a requirement to find the data point that is equal to a certain defined target value. The slicing that occurs involves splitting data into two equally sized arrays (or two arrays where one has one additional data entry compared with the other, if the original data has an odd number of entries). This is achieved by determining the midpoint of the array by dividing the array length by two. The data at the midpoint is then checked and, if the data is equal to the target value, then the search is complete. If, however, the data point is less than the target value, then this indicates that the target value is contained in the upper half of the array, and so the lower half of the array is disregarded, and the search process is repeated until the location of the target value is obtained. If the data point is greater than the target value, then this indicates that the target value is contained in the lower half of the array, and so the upper half of the array is disregarded, and the search process repeated.

It is possible that this type of slicing, as applied within search algorithms, could be applied to the problem of beam selection given a known distribution of users. Consider, for example, a group of UEs at random points around a BS, all equal distance away but at different angles from the perspective of the BS. Each UE could

be assigned a number in ascending order starting from 1, with the largest number being equivalent to the total number of UEs. It would then be possible to determine the midpoint, as in the search algorithm, and slice the data into two sets, and then continue this process until the number of sets containing the UEs is equivalent to the number of beams that will be serving the coverage area. Then, for each set of UEs, the associated beam would need to cover an area between the angle of the first UE in the set and the angle of the last UE in the set. This approach could also be extended to two or three dimensions with some rule determining how the UEs would be numbered in the event that two were located at the same azimuth angle from the BS, but at different distances.

This type of binary slice approach could be useful for a situation where the configuration of the BS is sufficiently adaptable so that beams can be generated with required widths and angles to a reasonable degree of precision. The testing of such a method and the comparison with the approach described in this chapter could form the basis of further research. The level of adaptability required within the hardware for a binary slice approach to be viable would need to be investigated. The comparison of the complexity of both approaches would also be of interest and it would be valuable to determine whether one method would be more suitable than the other within different time scales.

4.11 Conclusion

This chapter has presented an approach to determining optimal beam configurations specifically from the perspective of coverage within the synchronisation process for 5G networks employing Massive MIMO. The approach is based on a perspective where a known set of beams is available to the BS, with an unknown set of several beams that will provide the most even coverage for users within any environment. It has been shown that, while an exhaustive search method is both time consuming and computationally expensive, especially for complex environments, it is unnecessary to test the entire set of beams before an optimal or near-optimal solution is found. This is true for standard sets of beams of equal width, and for sets of beams that contain beams of differing widths and azimuths.

This observation is potentially beneficial for MNOs both in the context of network planning and design, and in the context of real-time self-learning networks. In terms of setting up the beam selection, there are a number of key conclusions to be drawn. Firstly, it is possible to save computational resources when running potentially complex propagation models, as the described approach would limit the number of times that running such a model would be necessary for different beam configurations. Secondly, the methods described here could form the basis for faster, more accurate and more efficient optimisation of the network in real-time situations, although specific implementations would be the subject of further research. Thirdly, the number of iterations required to obtain the optimal set of beams would seem to be related to how clustered the users are within the service area. Further research could be conducted to study the effects of user clustering in more depth.

This chapter has been entirely concerned with the question of coverage in 5G networks and has not addressed the issue of data throughput. It has been shown that the use of properly configured beams can provide great benefits from the perspective of network coverage, but the situation may be different from the perspective of data throughput, depending on the environment. This subject forms the basis for the next chapter.

5: Massive MIMO Beamforming Study

The previous chapter discussed the use of beamforming within Massive MIMO as it relates to coverage and synchronisation within 5G. It was shown how an algorithmic method can be used to maximise coverage for a given key performance indicator (KPI) within a cell area; however, the question of spatial channel interference, and the related question of achievable data throughput, was not considered as this is less of a concern when considered in relation to the synchronisation between the UEs and BS. However, these questions become more significant when considering the system as a whole, and in how interference and throughput relate to the way that the beam is formed over the coverage area. This is especially important considering that there is the potential for MNOs to adapt the parameters of the beams that are used at a mobile site; doing this according to a robust method would maximise benefits for both subscribers and MNOs. Subscribers would benefit from better quality of service (QoS) while MNOs would obtain the financial and reputational benefits of running a more efficient network.

Massive MIMO systems do not necessarily require the use of beamforming at all, if this is taken to mean that the direction of the main beam (and possibly side lobes) is adjusted to provide coverage that is optimal according to some definition. It may be, for example, that it is preferable in some scenarios to not apply any beamforming or, in other words, to apply equal weights to all the antenna elements. There are several reasons why this might be preferable, and these are explored in more detail within this chapter. It may be, for example, that the environment already provides sufficient multipath richness such that an adequate diversity of multiplexing gain could be obtained without the need to orient the beam. However, in these scenarios, increasing the gain in the direction of the most significant MPC may still provide an improvement in terms of SINR. Another important reason why it may be preferable to not use beamforming is because of how, in some situations, the use of beamforming will increase noise due to interference. This could happen due to the presence of a nearby transmitter interfering with the uplink signal, if the beam is overlapping both the intended target user and the nearby user. It could also occur due to inter-beam interference, which is more likely to occur in some situation than in others. For

example, in a flat terrain with sparsely separated users, a main beam may be able to serve each user without much overlap. However, in a rapidly changing multipath environment, it could be the case that, even though the users are separated by a great distance, the actual angular separation between beams is much less, meaning that it may not be possible to transmit beams from the Massive MIMO array without them overlapping to an extent that causes unacceptable levels of interference. All of these effects are discussed throughout this chapter.

This chapter begins with an overview of how beamforming is employed within Massive MIMO systems, specifically how a grid of beams is formed across a coverage area by the BS. A section is then devoted to the question of Massive MIMO without beamforming, by discussing the various methods for precoding and combining that are used to benefit from spatial multiplexing, where independent spatial data streams are formed to increase the throughput that could be obtained if there were only one data stream between the BS and the UE. It is noted that there is nothing preventing these techniques from being used in combination with beamforming, just that the methods do not assume the use of any particular form of beamforming. The chapter then continues with discussions on how to evaluate the performance of Massive MIMO systems in the presence of beamforming, and how MATLAB simulates changes in SINR value. The remainder of the chapter presents a case study discussing observed phenomena related to beamforming as obtained through ray-tracing.

5.1 Antenna Set-up

Virtual Massive MIMO antennas were used as part of this study, obtained from the Remcom [98] ray-tracing software. An array of dipoles with half wavelength spacing was chosen for the initial array for testing purposes, which is only a very general approximation of arrays used in mobile networks. The frequency used throughout this study is 3.51GHz, to match the frequency of practical experiments conducted at the University of Bristol, for which it possesses a licence. The effective bandwidth was set initially at 3.51GHz. The waveform always originated from a sinusoidal source within this study.

It was decided to start with a small number of transmit antennas, and the smallest number that could still be considered Massive MIMO would be 64, so an 8x8 transmit array was used initially. (Figure 86)

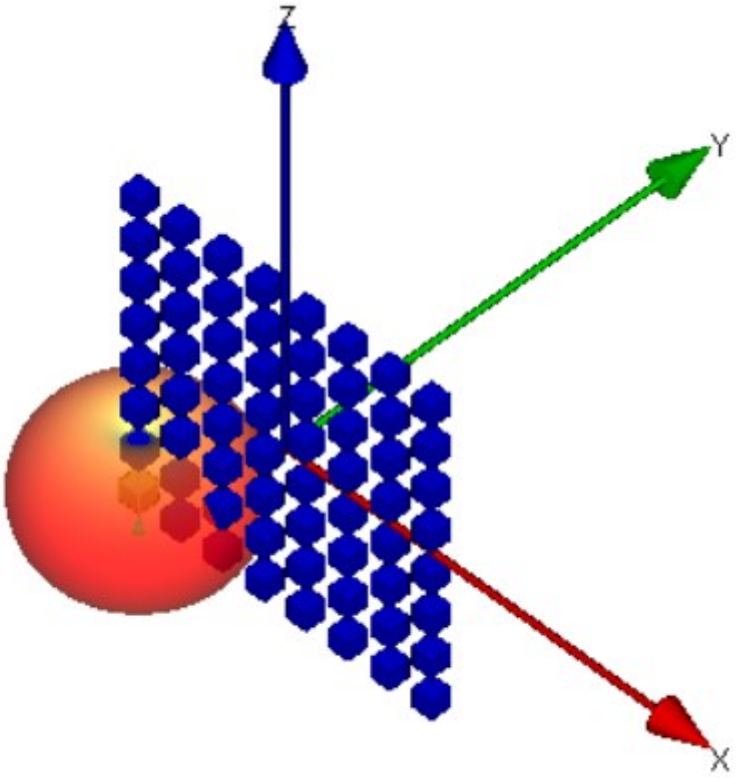

Figure 86: Initial 8x8 transmit array used for testing purposes

A 128 element 32x4 array was also used, which represents the dimensions of the patch antenna array that has been used for measurement campaigns at the University of Bristol (Figure 87).

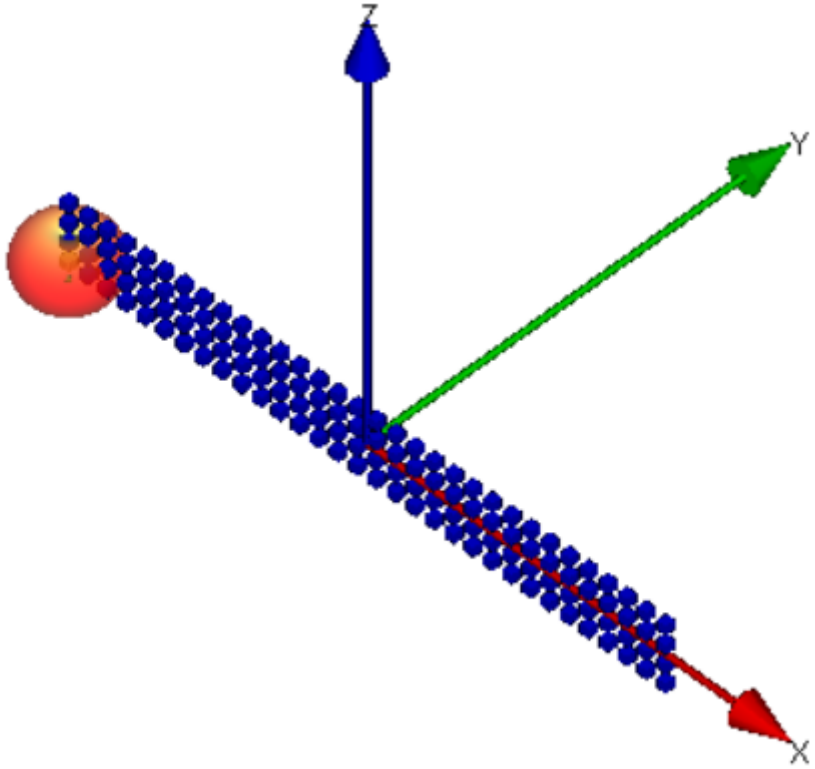

Figure 87: A 128 element 32x4 array representing the dimensions of the patch antenna array used for measurement campaigns at the University of Bristol.

5.2 Basic Scenarios and the Performance of the Propagation Model

Some basic propagation scenarios are considered in this section. The purpose of this presentation is to establish the plausibility of the propagation models used for the study and also to demonstrate how the comparisons between the different approaches to providing spatial divisions multiple access links are made. The section also provides practical examples of the analysis of the propagation channels after they have been generated.

The first basic scenario in this study consists of a one square kilometre flat terrain. A 50 metre high approximately rectangular metallic cuboid is placed near the upper edge of the terrain and has an approximate length of 250 metres and approximate width of 40 metres. The purpose of the cuboid is to act as a basic scatter in addition to the ground reflections, to provide some multipath propagation necessary for spatial division multiple access without beamforming.

A sinusoidal waveform is defined with a frequency of 3.51GHz and 20MHz of effective bandwidth. The 8x8 Massive MIMO array made of vertical half wave dipoles with half wavelength spacing is orientated so that all the elements lie on the north-south plane (using cartesian coordinates). The array is placed on the east side of the plane below the cuboid at 10 metres above the terrain. The power to the array elements in 30dBm of total array power, in other words the total power is divided equally across the whole of the array. The array is marked as ‘MIMO TX’ in the diagram.

Six mobile users are placed approximately in the north-south plane, approximately equal distance apart, to the west of the BS antenna and below the cuboid. Each UE is equipped with a single dipole antenna that is vertically polarised. As the elements in the BS are also vertically polarised, it is unnecessary to consider effects caused by different polarisations at the transmit and receive ends of the link. The noise figure at the receivers is set at 6dB, which is typical of many mobile telephones. The receivers are located at 1.5 metres above the terrain, which would be typical in such a scenario.

The study area for the simulation is placed at the perimeter around the mobile users, BS and cuboid. It is unnecessary for the study area to be larger, as there are no additional sources of reflections beyond the terrain and the cuboid, both of which are contained within the perimeter. Likewise, for this simple scenario, only two reflections need to be simulated for the multipath propagation, since each path will either be direct LoS with no reflection, or contain one reflection from either the terrain or the cuboid, or contain two reflections from the terrain and the cuboid before reaching the mobile user equipment. Diffraction is not simulated and is unnecessary as none of the users are located behind the cuboid from the perspective of the BS and therefore paths to the users will not be formed by diffractions over the cuboid. The default environmental parameters are selected with temperature at 22.2 degrees centigrade, 1013 millibars of air pressure and 50% humidity. Foliage models are not relevant for this simulation, as there are no trees or plants present. The complex impulse response is extracted from the ray-tracing simulation, containing magnitude and phase information for the channel. The three-dimensional setup for the simulation is summarised in Figure 88:

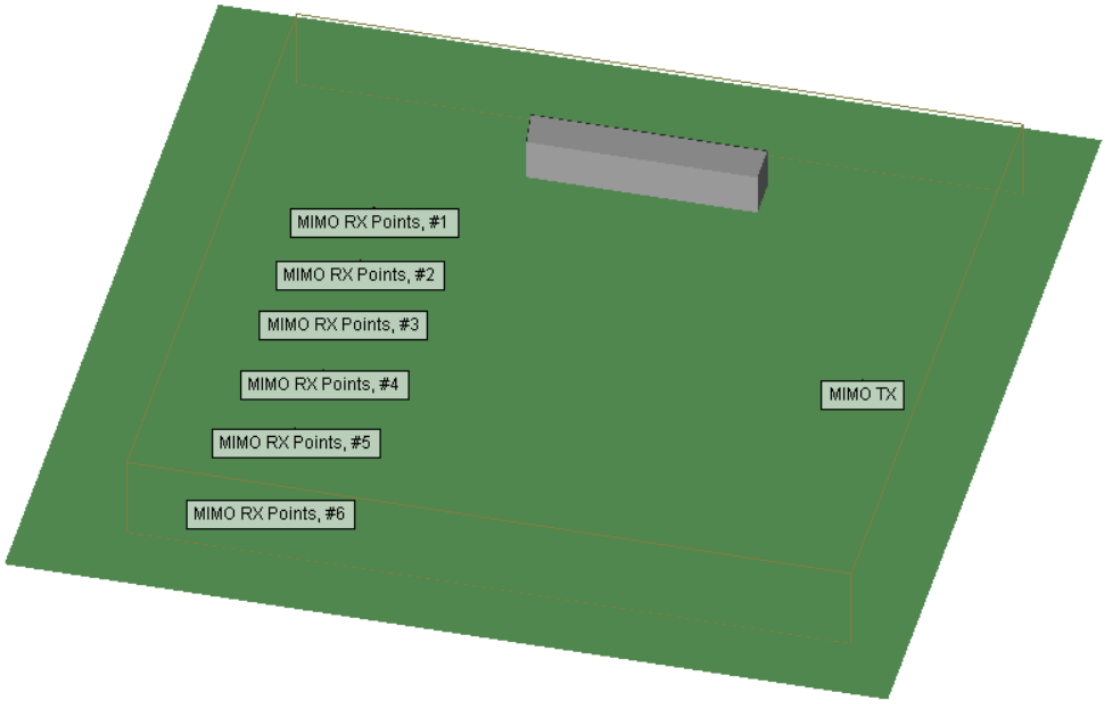

Figure 88: Three-dimensional setup for the simulation

The approximate X-Y coordinates of the BS are (844,523) metres. The approximate positions of the UEs with the angles toward the antennas from the BS are as follows (Table 2):

Table 2: Approximate positions of the UEs with the angles toward the antennas from the BSs

User	X	Y	X Displacement	Y Displacement	Angle
1	250	696	594	173	16.23798
2	256	604	588	81	7.843421
3	258	514	586	-9	-0.8799
4	262	410	582	-113	-10.9877
5	255	304	589	-219	-20.396
6	257	177	587	-346	-30.5167

It is possible, in order to demonstrate the possibility of the use of a grid of beams scenario using the propagation model, to use a directional antenna directed towards different points outward from the antenna location. This would create a coverage area, with the possibility of serving different users with different beams, depending on the quality of the receive signal from each of the beams at each user location. The quality of the received signal can be evaluated by setting up a communications system scenario, where reasonable parameters are chosen to simulate the effects of noise and other forms of interference. This process is described later in this section, after the description of the propagation scenario and antenna configuration.
A parabolic reflector can be placed within the scenario described above and the direction can be varied to effectively simulate a sweep across the coverage area. Given the location of the transmitter and the direction to the users described above, six beams were chosen for this example, each spaced ten degrees apart, so that the main lobe for the first beam points to -30 degrees, the second to -20 degrees, and so on up to the sixth beam that points to 20 degrees (with zero degrees being towards the west in this example). The transmit power is set to 30dBm with a maximum gain of approximately 10dBi.

In the basic scenario described in this section, the only interference considered is that from the noise, which is set at -174dbm, which is typical for thermal noise. The SINR metric used here refers to the signal level at each user relative to this noise.

Table 3 shows the simulated SINR in dBs at each user for each of the six candidate beams. The maximum SINR value obtained out of all six beams is shown, and the beam to which this maximum value corresponds is indicated in the final column.

Table 3: Simulated SINR in dBs at each user for each of the six candidate beams.

	Beam 1	Beam 2	Beam 3	Beam 4	Beam 5	Beam 6	Maximum SINR (dB)	Chosen Beam
User 1	7.85	20.04	8.99	28.86	39.06	40.61	40.61	6
User 2	13.56	9.91	24.26	34.94	39.47	30.75	39.47	5
User 3	14.42	17.10	25.82	31.80	23.44	15.50	31.80	4
User 4	19.06	26.90	27.59	21.30	14.47	19.46	27.59	3
User 5	20.75	37.63	12.31	3.11	18.18	13.45	37.63	2
User 6	32.16	13.47	-9.22	17.59	6.89	5.58	32.16	1

Given that the beams were chosen to point generally towards a specific user, with beam 1, for example, pointing roughly towards user 6, beam 2 towards user 5, etc, the maximum SINR value for each user is always, in this example, associated with the beam pointing most towards that user. The SINR value at each user is not always the same, because the main lobe of the beam has not been selected to point exactly at the users, but only in the approximate direction of the users, thus leading to variation. It may also be the case that some users are receiving more reflected power from the scatterer in this example.

5.3 Minimum Criteria for Successful Beamforming

In evaluating the performance of a Massive MIMO communications link, it is necessary to consider the interference between the data streams directed towards different UEs. It is intuitive that the more that the beams overlap, the greater the amount of interference from the point of view of the UEs. This would also be the case when the UEs are closer together, compared with when they are further apart. Therefore, it is necessary to consider these different types of user distributions as part of an analysis of the performance of beam steering Massive MIMO systems and their comparison with systems that do not rely on beamforming, as it could be the case that beamforming systems only work, for example, when the users are above a certain distance apart from one another, within certain types of environments. A standard list of how the SINR is related to the achievable code rate and the spectral efficiency is shown in Figure 89. These are standard values used in the design of LTE networks [128].

SINR and CQI mapping table in LTE

SINR [dB]	CQI code	Modulation	Code Rate	Spectral efficiency
-6.7	1	QPSK	0.076	0.15
-4.7	2	QPSK	0.12	0.23
-2.3	3	QPSK	0.19	0.38
0.2	4	QPSK	0.3	0.60
2.4	5	QPSK	0.44	0.88
4.3	6	QPSK	0.59	1.18
5.9	7	16QAM	0.37	1.48
8.1	8	16QAM	0.48	1.91
10.3	9	16QAM	0.6	2.41
11.7	10	64QAM	0.45	2.73
14.1	11	64QAM	0.55	3.32
16.3	12	64QAM	0.65	3.90
18.7	13	64QAM	0.75	4.52
21.0	14	64QAM	0.85	5.12
22.7	15	64QAM	0.93	5.55

Figure 89: Standard list of how the SINR is related to the achievable code rate and the spectral efficiency [129]

It should be noted that a standard way of addressing the issue of spatially correlated users accessing the network where, for example, two users are close together and it is not possible to serve each user with a separate beam from the BS, is to use Orthogonal Frequency-Division Multiple-Access. This method involves assigning sections of the subcarriers to specific users, allowing them to communicate with the BS by occupying different sections of the resource blocks. The use of this approach means that the sections of the subcarriers applied to a specific user cannot be used by other users while they are assigned to that user so, while the approach can still allow spatially correlated users to access the network successfully, this is at the expense of available bandwidth, since a portion of it cannot be reused.

5.4 Study of propagation environments

The remaining content of this study is based on the resources that are provided within the Remcom software and that can demonstrate the comparisons between the different approaches to beamforming and non-beamforming forms of multiplexing and their relative performance. The resources available, and that are used for the results presented in this chapter, include three broad elements. Firstly, basic beamforming can be investigated with the use of provided antenna patterns. This approach provides such parameters as received SNR and angles of arrival.

Secondly, the communications toolbox provides the ability to investigate multi-user MIMO without any specified beamforming, based on antenna patterns. Throughput data for the channel can be provided along with SINR data. It should be noted that 'multi-user' can mean a single user with multiple antennas using spatial multiplexing, from the perspective of the software. Thirdly, the same multi-user MIMO investigations can be combined with antenna weights to view multi-user MIMO performance with beamforming while employing standard pre-coding and combining methods.

The study can be broadly divided into three areas of study. These are: basic scenarios, formal scenarios and urban scenarios. It is important, in the interest of clarity concerning the results, to understand the basic performance of each of these features of the software as, although information is provided in the software documentation regarding each feature, the software itself is still closed source and so the precise techniques that are used for calculating the relevant figures of merit may not be obvious. Therefore, the first area of study, basic scenarios, is chosen primarily to provide an understanding and overview of the functionality available by using simple propagation environments with few users, or only one user, and either LoS only scenarios or scenarios with only a few scatterers (such as one metal structure in addition to a single ground reflection).

The second area of study, formal scenarios, provides an investigation of how the different approaches to spatial multiplexing in well-controlled environments. These environments include useful but unrealistic configurations of users within a well understood environment. The configurations of users include scenarios where the UEs are placed at equal distances apart before the antenna array. It also includes scenarios where users a lined-up perpendicular to the antenna array. Several simulations can be run with similar scenarios, but where the spacing between different users is altered. Running the simulations in this way helps in developing an understanding in how environmental changes affect general performance and in determining approximate threshold values for when one method may become superior to a different method.

The third area of study, urban scenarios, provides a broader investigation of the performance of the various spatial-multiplexing methods but in an environment that is both more realistic in terms of the forms of multipath propagation that are likely to

be found within modern cities. It also provides an understand of performance with more realistic user distributions, that is distributions that are not so formally controlled, and which do not have even spacing and distributions. The users can also be simulated to follow paths that are more realistic of the mobility features found within urban environments. When combined with the previous two areas of study, it is possible to begin to distinguish between the different phenomena present within the performance of MIMO systems within cities, and also to draw comparisons about comparative system performance, even though the scenarios are complex and it may not be possible to determine precise explanations for differences in performance.

5.4.1 Basic Scenarios

The first basic scenario is intended to observe the changes detected by the propagation model when a user is moving within the study area. The purpose of this is to determine how the propagation model responds to well understood variations within the environment. The environment consisting of a single scatterer and a ground reflection, as described previously, is used for this analysis. A simple directional antenna is used as a basic method for creating beams transmitting in a known direction. This is important, as beamforming is a key part of the analysis of Massive MIMO channels presented in this chapter, so it is necessary to understand how the propagation model processes beamforming scenarios. Firstly, the user is stationary and the azimuth of the BS antenna is varied so that it sweeps across the coverage area. Secondly, the BS antenna azimuth is stationary while the UE antenna moves across the study area.

To begin, a horn antenna is used to provide the directional beam as part of this scenario [130]. Standard parameters are obtained to provide the dimensions of the antenna according to the standard layout for such an antenna. Flann microwave defines the parameters for a horn antenna operating between 3.22 and 4.9GHz. The horn of the antennas is 290mm, the aperture width is 154mm and the aperture height is 114mm. The feeder width is 40mm and the feeder height is 20mm. These values for the feeder are not provided in the antenna documentation, but are obtained through adjusting the parameters to find a reasonable radiation pattern. These parameters are replicated for the simulation, with the resulting radiation pattern shown in Figure 90, according to the Remcom software. The radiation pattern has a

clear main beam and several side lobes. The side lobes are larger than what may be required, but are still significantly smaller than the main beam, which is the main area of focus within this section. The polarisation is set to vertical, as this is similar to the polarisation that would be expected at the UEs the majority of the time, if it is assumed that the UEs are mostly mobile telephones that are held vertically when in use. The main beam is projected in the X direction, and therefore the antenna should sweep across the half circle on the half plan in the negative X direction. As before, the antenna is placed in the centre and to the right hand side of the plane, at approximately the coordinates (840, 520). The height of the antenna is 10 metres, and this will be replicated at the UE end of the link, again, not because this would be expected but in order to verify the performance of the propagation model. The UE is located 600 metres to the west of the transmit antenna. The antenna at the UE is a vertically polarised dipole, to correspond with the vertical polarisation at the transmit end of the link.

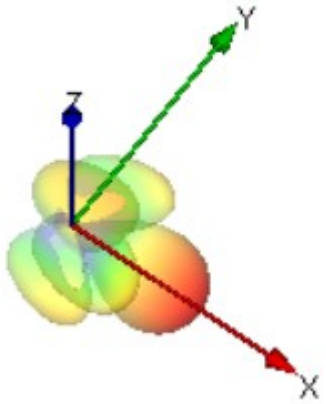

Figure 90: Radiation pattern showing a clear main beam and several side lobes.

The transmit power throughout this section is set to 30dBm. When directed away from the users, the antenna still provides some energy in the opposite direction from the main lobe, and the user also receives paths from the scatterer due to the side lobes providing paths in the relevant directions. When configured in the way described with the antenna pointing away from the user, with the ray-tracer set to provide a limited number of paths, most of the contribution at the user is provided by reflections from the scatterer, with paths being at approximately -88dBm. The path

directly from the antenna to the user is, by contrast, approximately -127dBm with the ground reflected component at approximately -159dBm. The total receiver power at the user is calculated to be approximately -87Bm (Figure 91).

```
# <Transmitter Set: Tx: 1 MIMO TX - Point 1>
# <Receiver Set: Rx: 2 MIMO RX Points >
# <number of receiver points>
# <receiver point number> <number of paths for this point>
# <path number> <arrival phi(deg)> <arrival theta(deg)> <received power(dBm)>
 1
1 3
1 41.4813 90 -87.5722
2 0.255211 91.8956 -127.133
3 0.255211 90 -158.808
```

Figure 91: Output with antenna pointing away from user

When the transmit antenna is orientated towards the user, and as expected, the receive power is higher at -55dBm. Much of this contribution, as before, is from the LoS path between the user and the BS and the associated ground reflection near this path, contributing approximately -52 and -55dBm respectively. There is a single path computed to and from the scatterer, with the path arriving at the user from the north-east (Figure 92).

```
# <Transmitter Set: Tx: 1 MIMO TX - Point 1>
# <Receiver Set: Rx: 2 MIMO RX Points >
# <number of receiver points>
# <receiver point number> <number of paths for this point>
# <path number> <arrival phi(deg)> <arrival theta(deg)> <received power(dBm)>
 1
1 3
1 0.255211 90 -52.7179
2 0.255211 91.8956 -55.7196
3 41.4813 90 -70.7031
```

Figure 92: Output with antenna pointing towards the user

It is now possible to test the propagation model by directing the main beam towards the reflector, which, from the point of view of the transmit antenna, is at an azimuth angle of approximately 135 degrees in the coordinate system used by the software. Again, the propagation model performs as expected, with the largest power contribution, of approximately -55dBm, originating from the path that arrives at the user from the reflector. The remaining two paths consist of the direct path from the transmitter and the ground reflected path, which are seen as side lobes from the

perspective of the user. These paths contribute -71 and -74dBm respectively (Figure 93).

```
# <Transmitter Set: Tx: 1 MIMO TX - Point 1>
# <Receiver Set: Rx: 2 MIMO RX Points >
# <number of receiver points>
# <receiver point number> <number of paths for this point>
# <path number> <arrival phi(deg)> <arrival theta(deg)> <received power(dBm)>
 1
1 3
1 41.4813 90 -55.334
2 0.255211 90 -71.2538
3 0.255211 91.8956 -74.2315
```

Figure 93: Output with antenna pointing towards the reflector

Finally for this section, the propagation model is tested with the main beam pointing south-west from the point of view of the transmit antenna (or 225 degrees in the software's coordinate system). Here, there is a direct path and a reflected ground path from the transmit to receive antenna, but with a much lower power contribution when compared with the scenario where the main beam is orientated directly towards the user. Here, the direct and ground reflected waves are approximately -71 and -74dBm respectively. There is also a ray that is reflected from the scatterer, however, since this ray originates from the direction of one of the side lobes, the contribution from this ray is also lower than the previous example, where the main beam was orientated directly towards the scatterer. Here, the contribution from the scattered ray is approximately -83dBm. The total received power, according to this simulation, is approximately -78dBm (Figure 94).

```
# <Transmitter Set: Tx: 1 MIMO TX - Point 1>
# <Receiver Set: Rx: 2 MIMO RX Points >
# <number of receiver points>
# <receiver point number> <number of paths for this point>
# <path number> <arrival phi(deg)> <arrival theta(deg)> <received power(dBm)>
 1
1 3
1 0.255211 90 -70.8288
2 0.255211 91.8956 -73.807
3 41.4813 90 -82.5485
```

Figure 94: Output with antenna pointing south-west

It is now possible to investigate the changes in received power observed by the user as it moves from the upper to lower part of the study area, but with the transmit antenna static, with its main beam orientated towards the west (or 180 degrees in the software's coordinate system). The north-south plane through the transmitter is transposed to the west by approximately 600m and a path traced with 0.5m spacing from the north to the south, from approximately 170m above the east-west plane through the transmitter to approximately 170m below the plane. The user follows this path during the simulation and records the received power, along with ray data including angles of arrivals for each of the points. This path was chosen so that there would be an equal distance above and below the transmit antenna, meaning that the received power value from the direct and ground reflected paths from the transmitter should peak at around the centre when the results are considered as a time series from north to south obtained by a user travelling at a constant velocity. This peak is observed clearly when no reflections are simulated by the software, and where only the direct path is considered (Figure 96). The shape of the curve corresponds with what would be expected as the received power level would be at its maximum when the UE is closest to the antenna, which is the mid-point of its journey, where it is directly opposite the BS antenna.

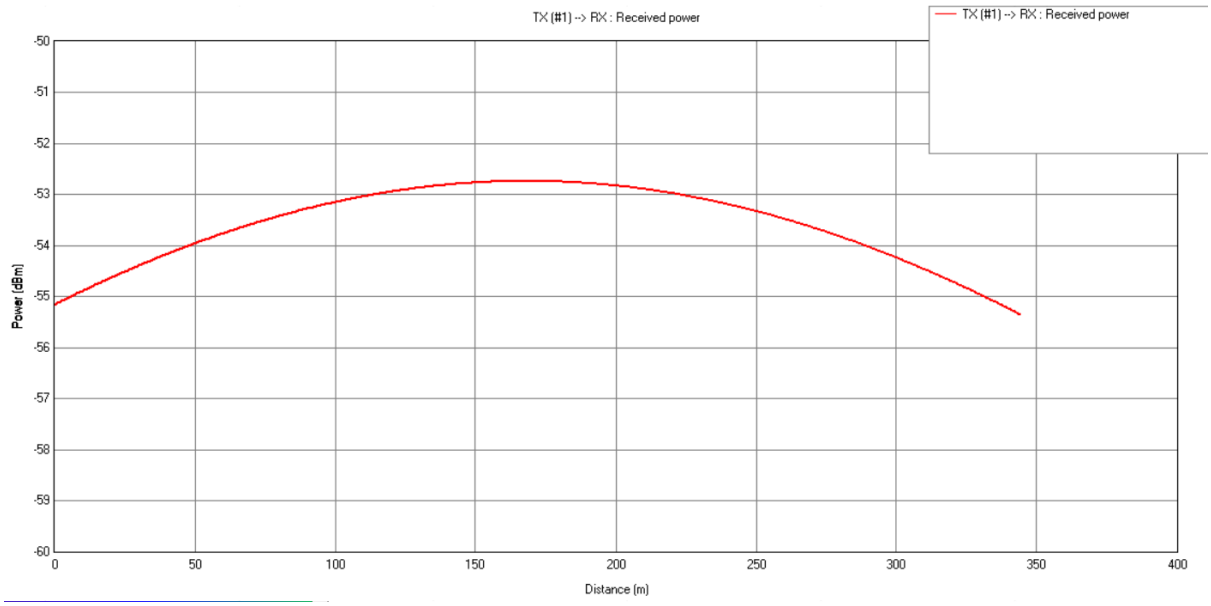

Figure 95: Variation in receive power

The effects of multipath propagation affects the receive power so as to distort the curve representing the effect of position on the receive power value. This is already apparent even when only two reflections are considered within the simple multipath environment described in this section. When the propagation model is set to include these two reflections, the receive power is more unpredictable, as shown in Figure 96.

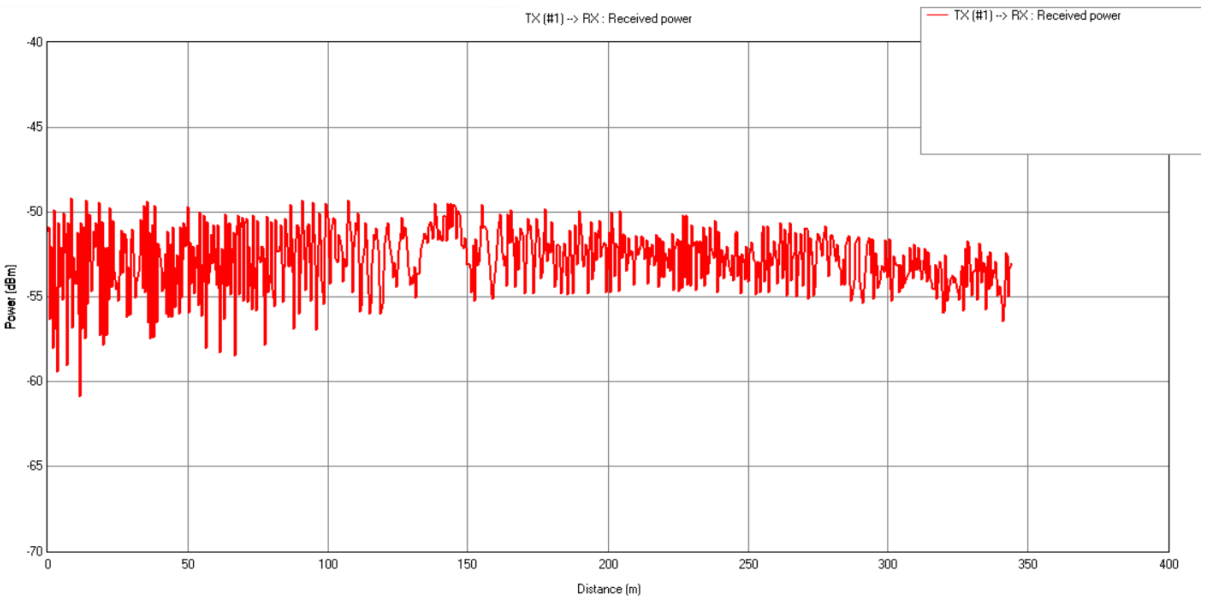

Figure 96: Fluctuating receive power resulting from setting the propagation model to include two reflections

If the route described here is repeated using the same antenna elements at both the receive and transmit end of the link, but using an 8x8 Massive MIMO array with no weights applied to the antenna elements, and therefore no beamforming, it can be seen that the receive power as the mobile user moves from north to south remains fairly stable, with a much smaller variation between the high and low values. When no reflections are simulated by the propagation model, the receive power still reaches a peak value near the centre of the route because, at this point, the user is closer to the BS. These effects can be seen in the spherical plot in Figure 97, which plots the receive power and the direction of arrival at the user of the LoS ray. The lower ray represents the direction of arrival when the user is to the north of the BS, or approximately 170m to the north from the centre of the route. The middle ray

represents the centre of the route, and the upper ray represents the direction of arrival when the user is to the south of the BS, or approximately 170m to the south from the centre of the route.

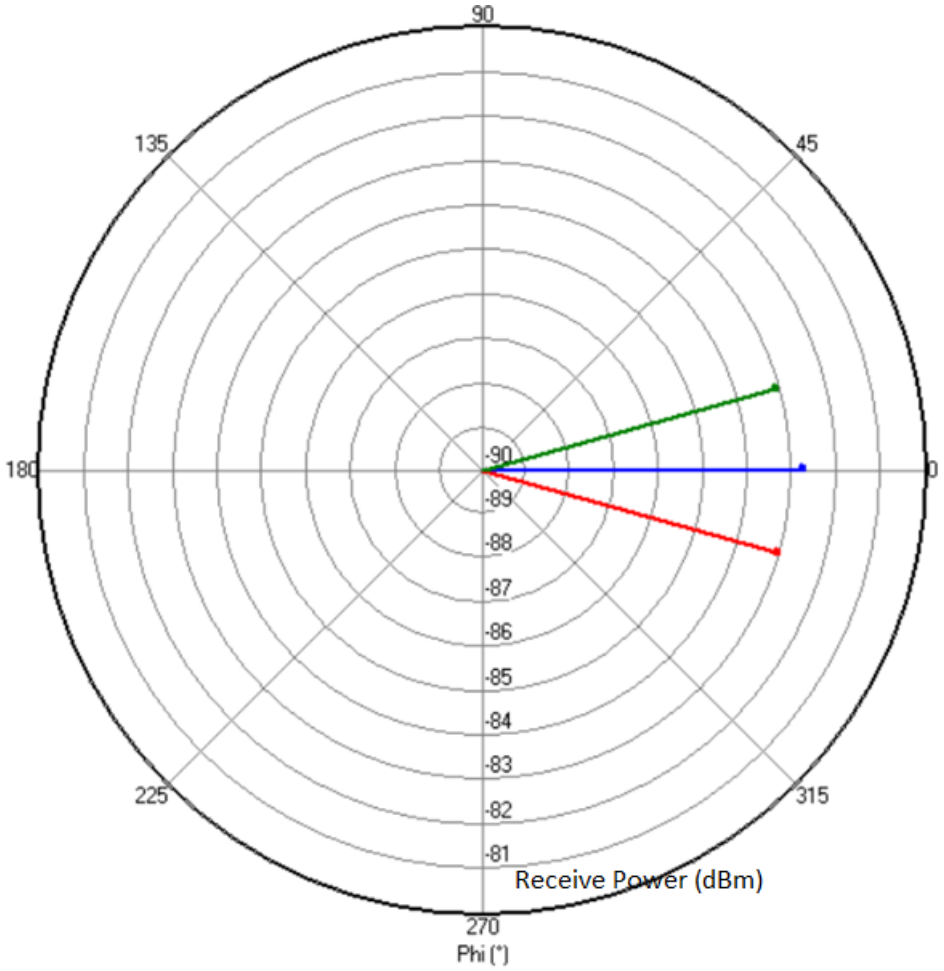

Figure 97: Spherical plot of receive power and the direction of arrival at the user of the LoS ray

The Remcom software provides the facility to implement the Maximum Ratio Transmission (MRT) method for beamforming [98]. This is a method for obtaining the weights to be applied to the elements within a Massive MIMO array such that that the main beam will be directed towards the receive antenna element or, in the case of multiple antennas elements, to the first element, as defined within the simulation. In the case of multipath environments, it is noticed that the beam may not represent a specific direction, but will be configured so as to take advantage of the multipath propagation, possibly through the use of side-lobes to maximise the receive power. The use of MRT for the beam to track the user in the propagation environment described for these basic scenarios, that is that the main beam will follow the user as

it moves from north to south. The SINR value can then be computed by the communications systems toolbox, making it possible to gauge the effect of adding beamforming, rather than relying only on the multipath properties present within the physical environment. Figure 98 shows the SINR value obtained for each of the points on the journey with beamforming with the weights obtained through the MRT method, and with only the main LoS component simulated by the propagation model.

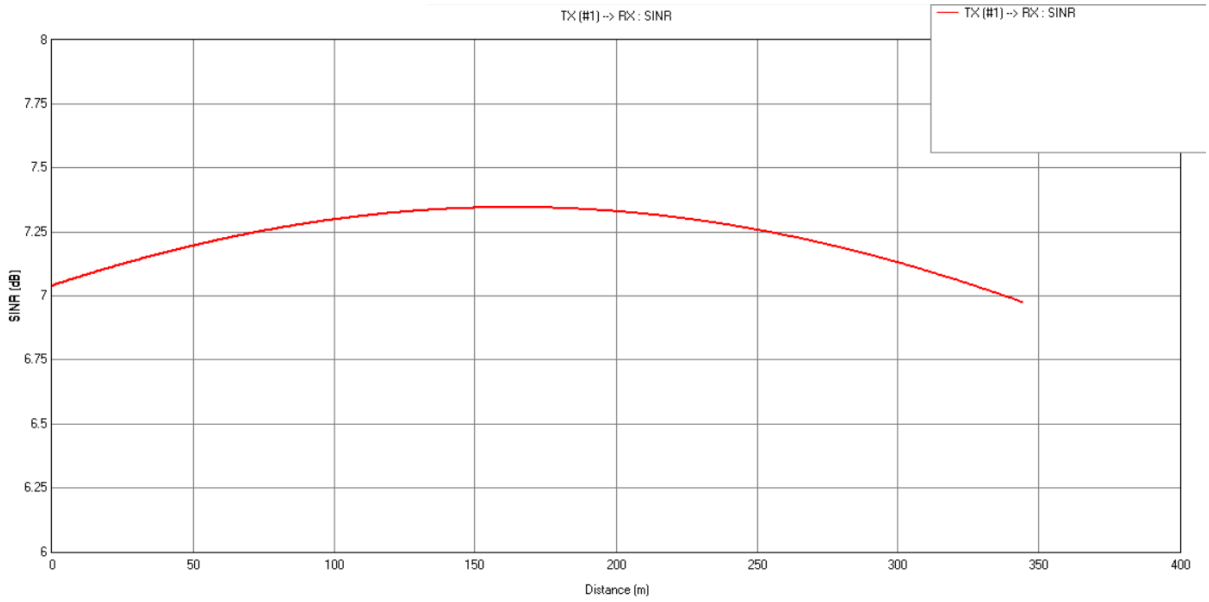

Figure 98: The SINR value obtained for each of the points on the journey with beamforming with the weights obtained through the MRT method, and with only the main LoS component simulated by the propagation model

This is in contrast with Figure 99 which shows the SINR value obtained at each point of the journey without any beamforming. With the exception of the area around the centre of the route, where the user antenna is closest to the transmit array, beamforming provides better performance at each user position. It also provides much more consistent performance, with all the SINR values being near 7dB. The non-beamforming scenario leads to variations of as much as 70dB in the SINR value.

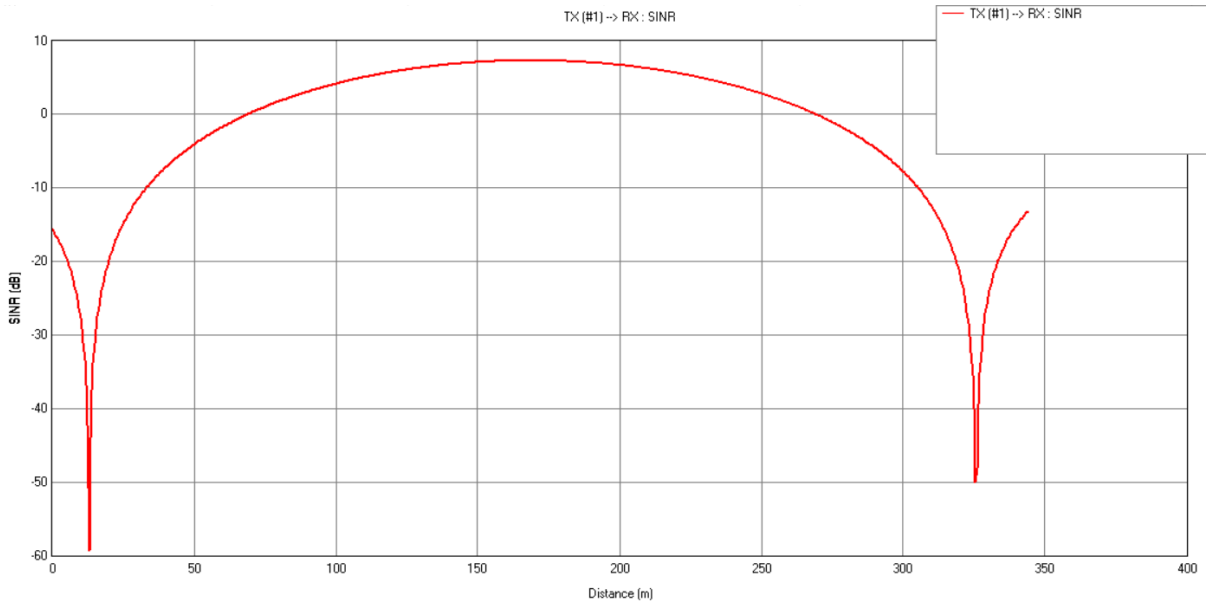

Figure 99: The SINR value obtained at each point of the journey without beamforming

5.4.2 Operational Scenarios

The previous examples were to verify and demonstrate how beamforming can be analysed within the Remcom software. These observations are now made more general by simulating more complex, but formally defined, scenarios. Firstly, the number of reflections is increased to investigate the effects of multipath environments with one scatterer and one ground reflection, and how these features can affect a single user's SINR value when a link is created with a Massive MIMO antenna array. Diffractions and terrain diffractions are also simulated by the propagation model. Without the use of beamforming, the SINR value varies by around 70dB (Figure 100), and there is some noise present within the SINR curve.

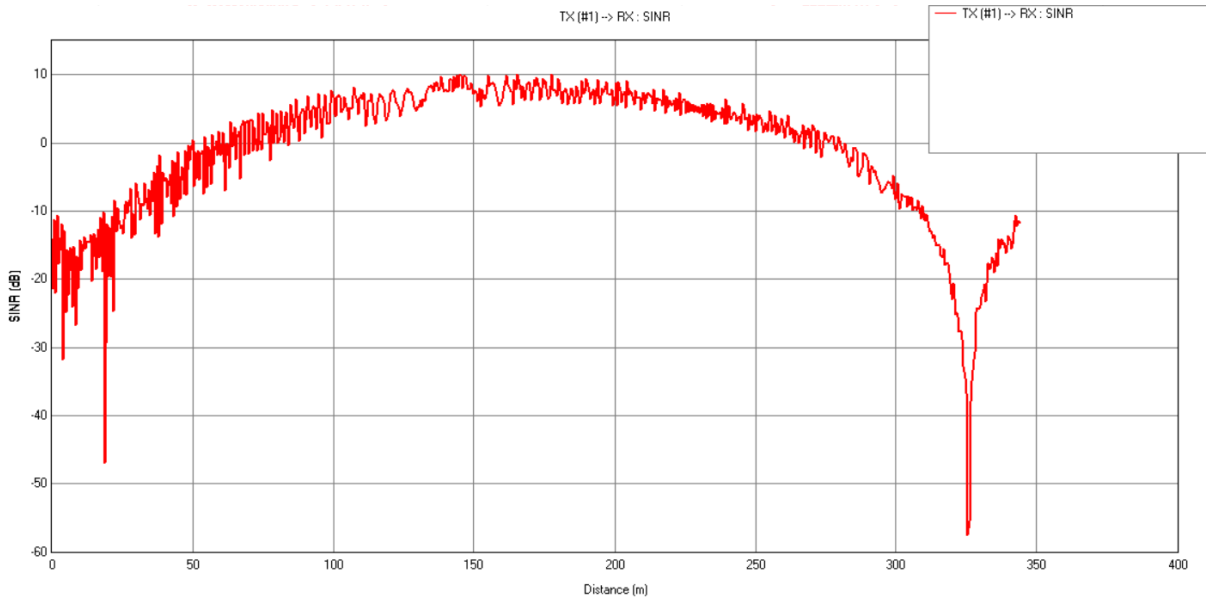

Figure 100: The SINR value without the use of beamforming

The SINR value with beamforming (Figure 101) is more consistent with most of the values within the range between 10 and 12.5 dBs and is, on average, always superior to not using beamforming. However, because of the noise present in both situations, there may be some instances in time where the non-beamforming system performs better than the beamforming system, at least momentarily.

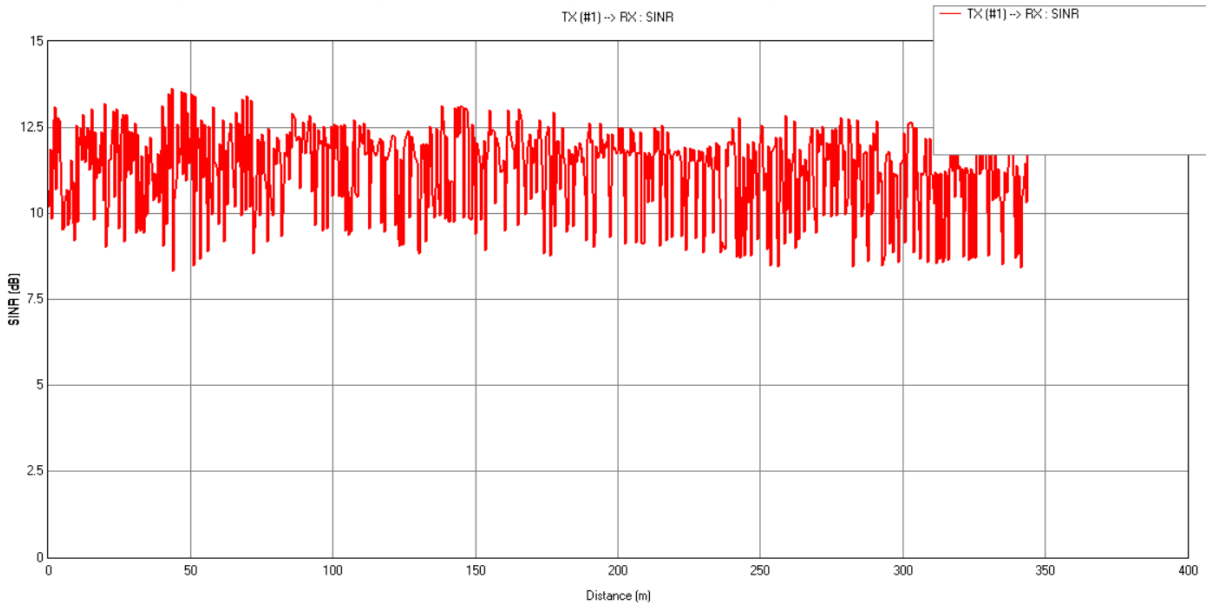

Figure 101: The SINR values with beamforming

Multi-user scenarios are now considered to understand how the spacing of users affects the relative performance of Massive MIMO without beamforming and Massive MIMO with beamforming. Initially, the users are positioned as shown in the diagram in Figure 88. The users are then re-positioned closer together, to determine if there is a point at which the distance between the users is such that it is not advisable to use MRT beamforming.

While the Remcom propagation software allows for the beamforming to be applied using the MRT method, it is limited in its ability to apply this simultaneously to many users. However, there are possible methods for addressing this lack of functionality within the software. The aim is to simulate the effect that nearby UEs have on the ability of the BS to serve the user that it is tracking. One would expect that, as users move closer together, it is more difficult for the BS to distinguish between the different users. In a beamforming scenario, this difficulty in distinguishing between users would be caused by overlap between the beams that are being used to serve the set of users, thus causing inter-beam interference. This inter-beam interference would gradually, as users moved closer together, increase the interference component within the SINR, thus causing its value to decrease. This decrease would lead to the reduction in the quality and complexity of the coding scheme that could be supported, thus reducing the data throughput that could be obtained within the channel.

Remcom does not provide the ability to calculate inter-beam interference directly within MIMO arrays; however, the types of effects described can be simulated by using a combination of transmitters and receivers within the study area. It is then possible to evaluate relative performance of different methods, for instance in determining how much better or worse the throughput gains are through beamforming compared with those of spatial multiplexing. As an example, consider the route in Figure 102 with its corresponding SINR obtained using MRT beamforming (Figure 103). This SINR plot implies that a similar coding scheme is achievable at all points along the route. However, if another receiver is added at the centre of the route, then it would be expected that the SINR value would decrease as the first user crosses paths with the second. This effect can be simulated by setting the second receiver to transmit mode, leading to the drop in SINR value observed in Figure 104.

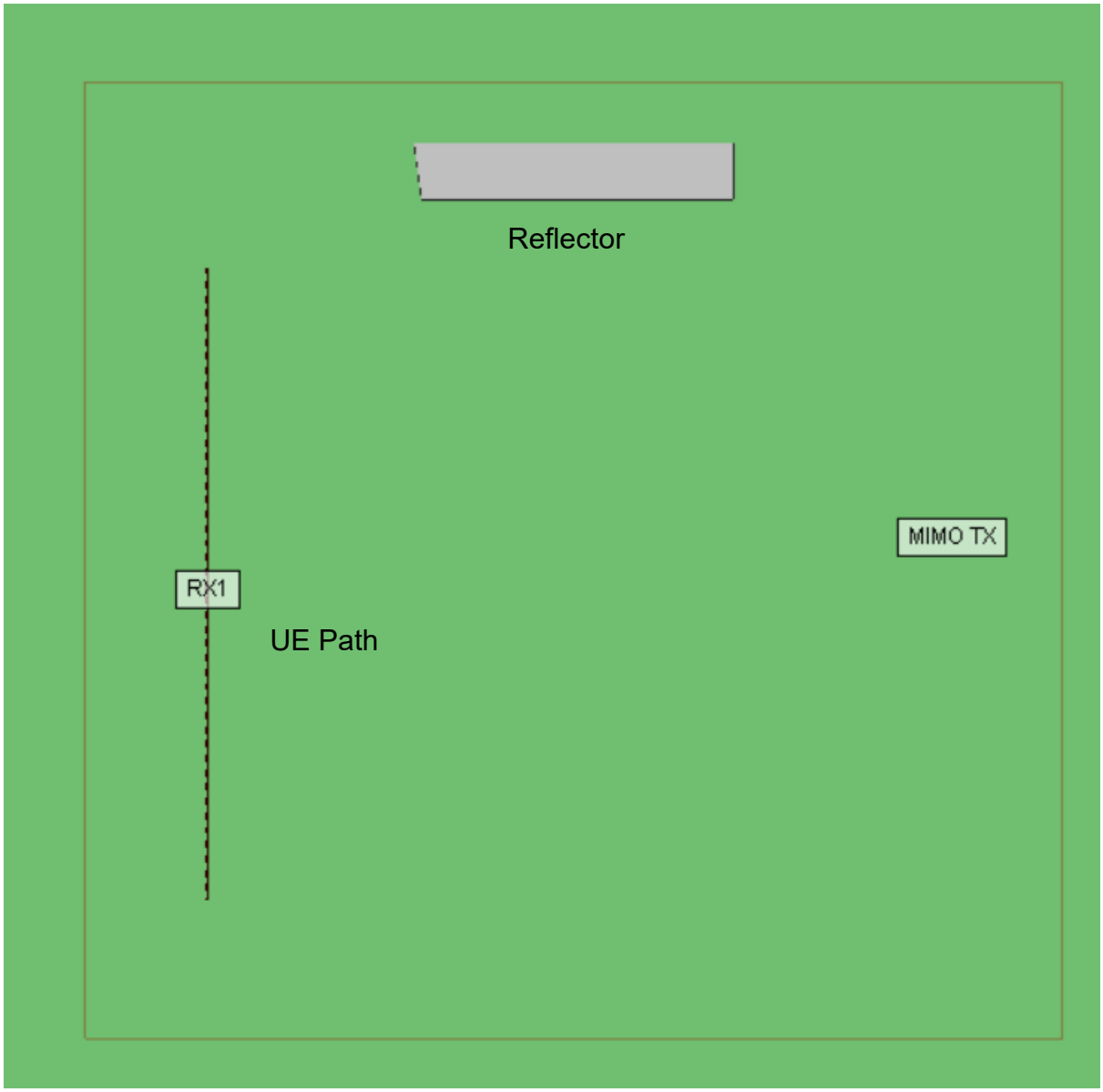

Figure 102: An 8x8 MIMO ray with the path of a single UE on a flat terrain with one reflector

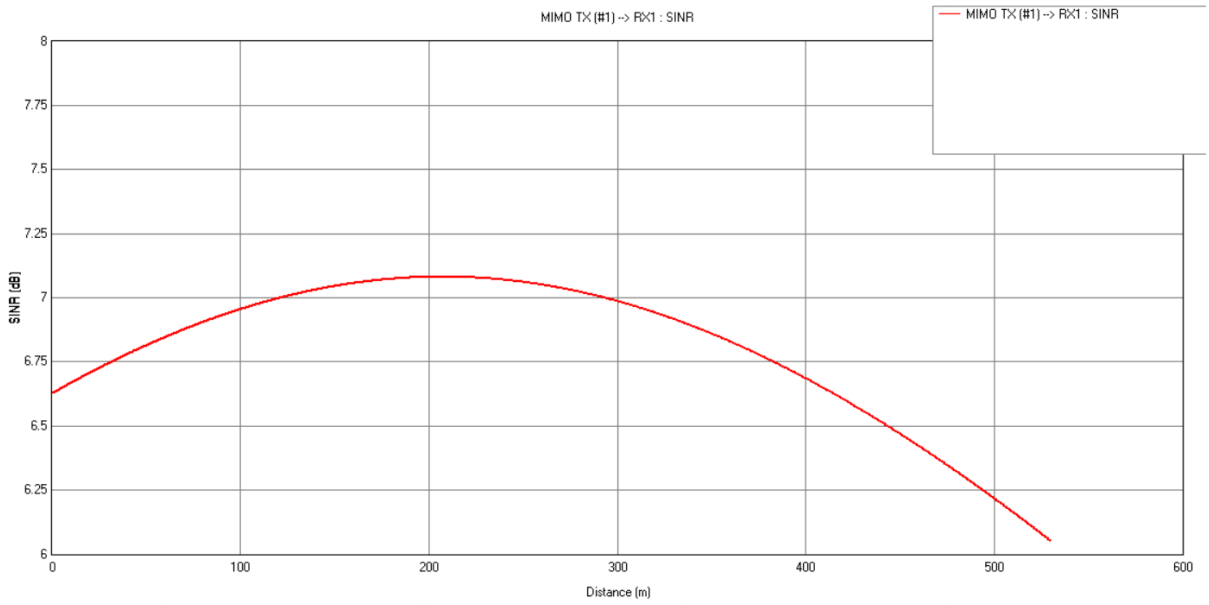

Figure 103: The route with its corresponding SINR obtained using MRT beamforming

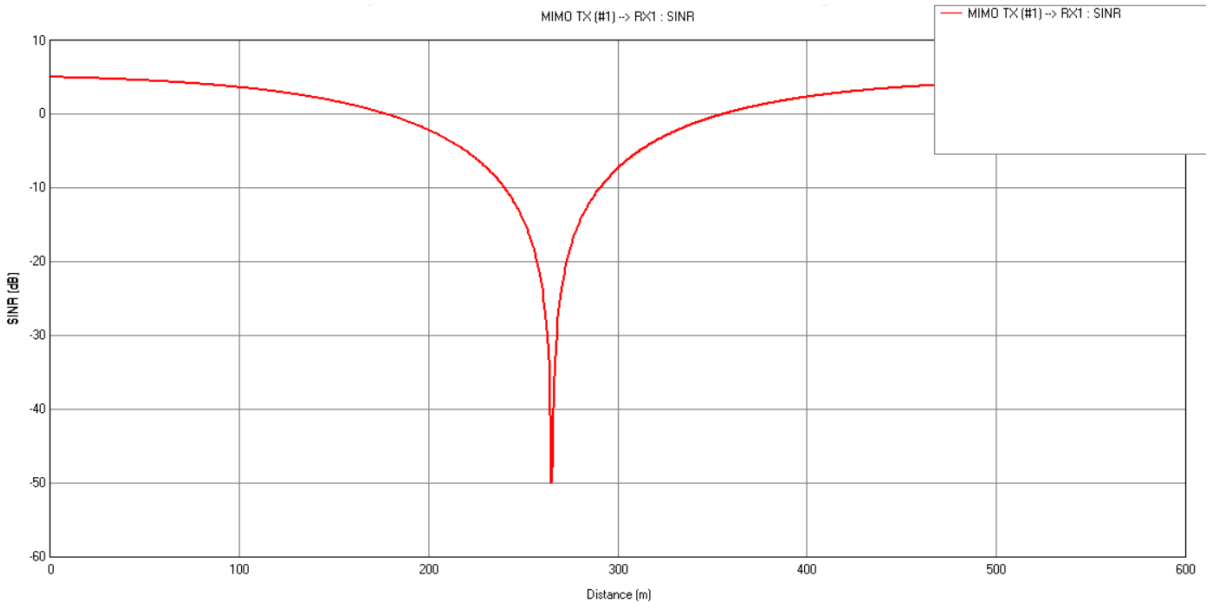

Figure 104: Drop in SINR value when another receiver is added at the centre of the route

These examples have been created using only direct path propagation, to illustrate the changes that are observed along the route. Figure 105 shows the effect of adding four more users distributed across the route, combined with increasing the number of reflections considered by the propagation model and addition diffraction to the model. It can be seen that there is more noise in the SINR curve compared with

the simpler propagation model, and that there are reductions in SINR of varying magnitudes.

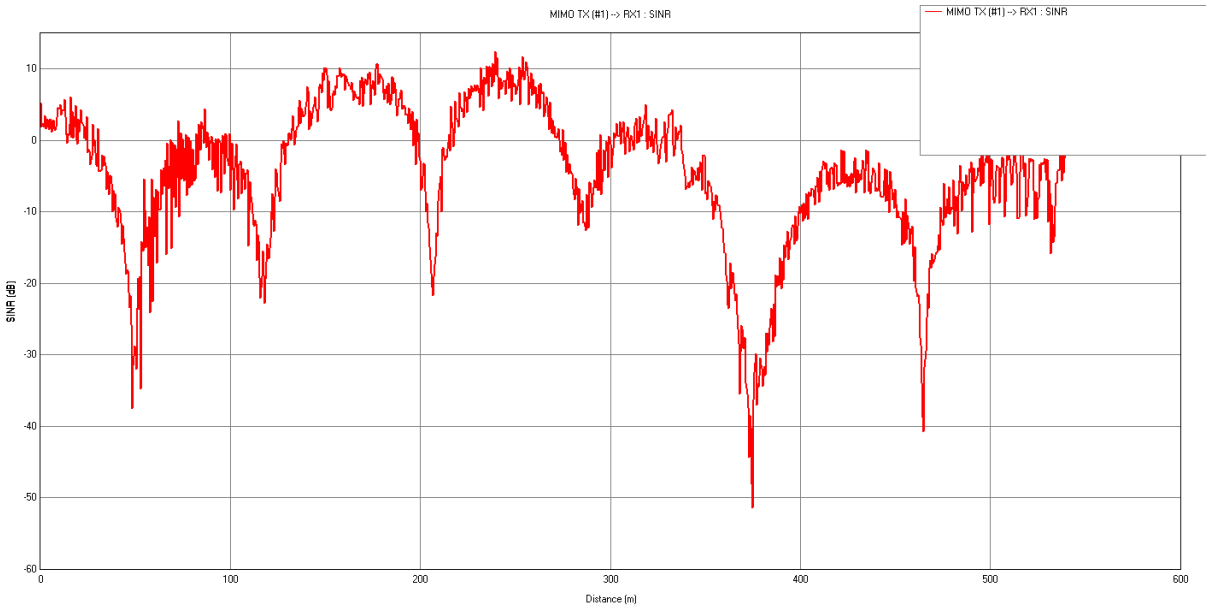

Figure 105: The effect of adding four more users distributed across the route, combined with increasing the number of reflections considered by the propagation model

Each of the approaches described here for simulating the comparison between spatial multiplexing and beamforming-based approaches to Massive MIMO communications have their strengths and limitations. The described technique of setting receivers in transmit mode, for example, provides a representation of the decrease in SINR value that would be expected when users are positioned close together, but this does not precisely simulate the width of the decrease. It may be possible to adjust the parameters, however, to increase the precision of the magnitude and width of the SINR decrease through further empirical observations.

In summary, it is possible to use the Remcom simulator to draw comparisons between beamforming and spatial multiplexing approaches to spectral efficiency gains. The methods for obtaining results for the beamforming approach include the use of MRT to track a user around a study area, which gives an indication of performance within different types of environments, but does not take into account the interference caused by the need to serve multiple nearby users. The second method for estimating beamforming performance is to repeat the first method, but

adding other antennas acting as ‘sinks’ that reduce the SINR performance as the user approaches them. The methods for obtaining results for spatial multiplexing are similar, but the closed singular value decomposition (SVD) method is used to generate multiple data streams, and no beamforming is used at the BS.

The use of SVD spatial multiplexing is of limited value when only one antenna is present at the UE end of the link, even if a Massive MIMO antenna is used at the BS. This can be illustrated with an example that compares a system where there are four dipole antennas used at the UE end of the link with a system where each UE has only one antenna.

The route considered in this example is shown in Figure 106, where the route taken by the UE is indicated by the dotted line. The total array power is 30dBm, with the array constructed from 8x8 dipole antennas at 3.4GHz with half-wavelength spacing. Both the UE and BS antennas are of the same vertical polarisation. The route taken by the UE has 5 metre spacing.

Figure 106: Route of UE in example to show the use of SVD spatial multiplexing with different numbers of UE antennas.

When the UE has four antenna elements in a 2x2 configuration, no pre-coding weights are applied at the BS and selection combining is used at the UE (where the antenna with the highest SINR value is selected), the SINR is simulated to appear as shown in Figure 107 when plotted against the distance around the route taken by the UE.

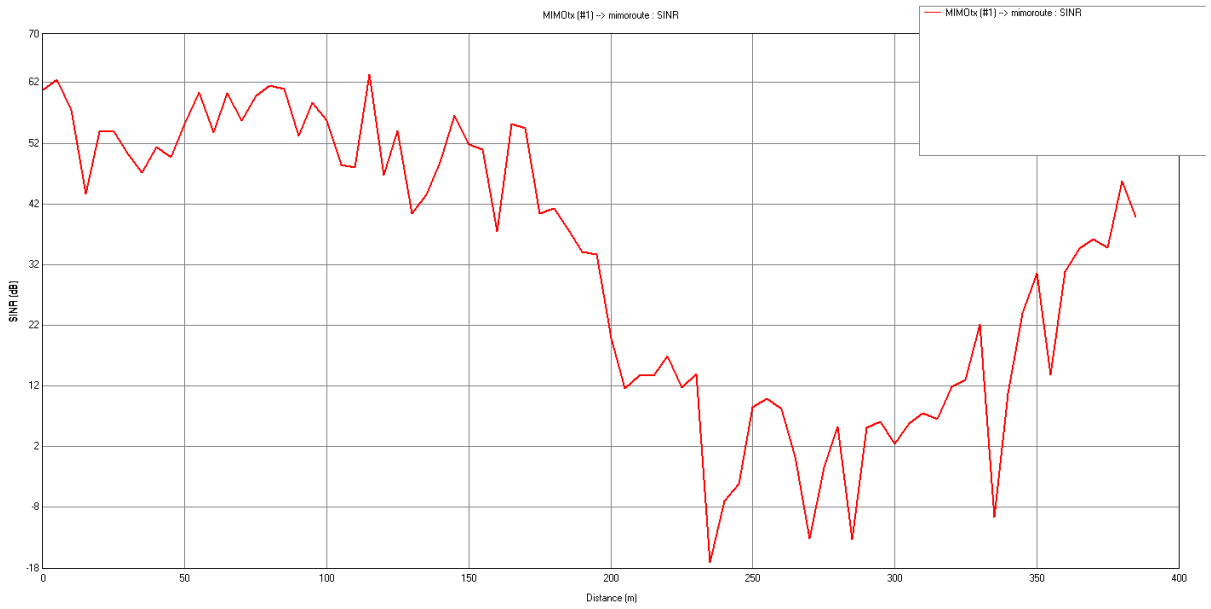

Figure 178: Simulated SINR for a UE travelling along the route shown in the previous figure with an array of four dipole antennas. No pre-coding weights are applied at the BS and Selection Combining is used for combining at the UE.

The graph in Figure 108 shows the same configuration with four UE antennas, but using SVD spatial multiplexing. Here it can be seen that, at several intervals, an improvement in SINR is recorded (although there are other intervals when the performance is inferior).

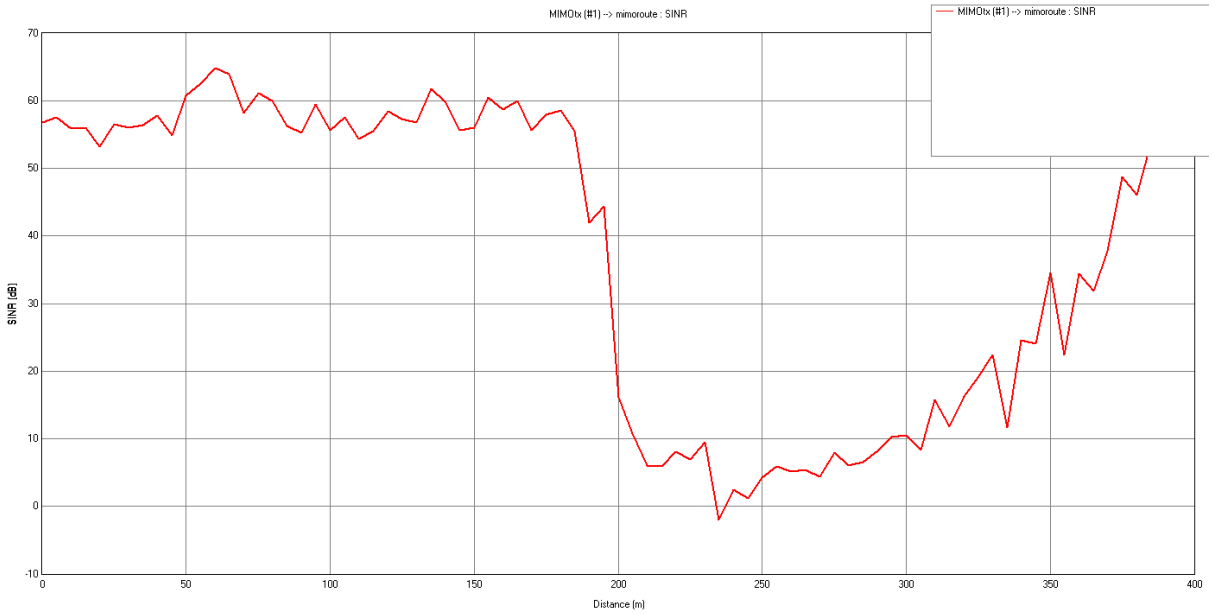

Figure 108: When compared with the SINR observed where only one antenna is used with SVD, the SINR is seen to be lower

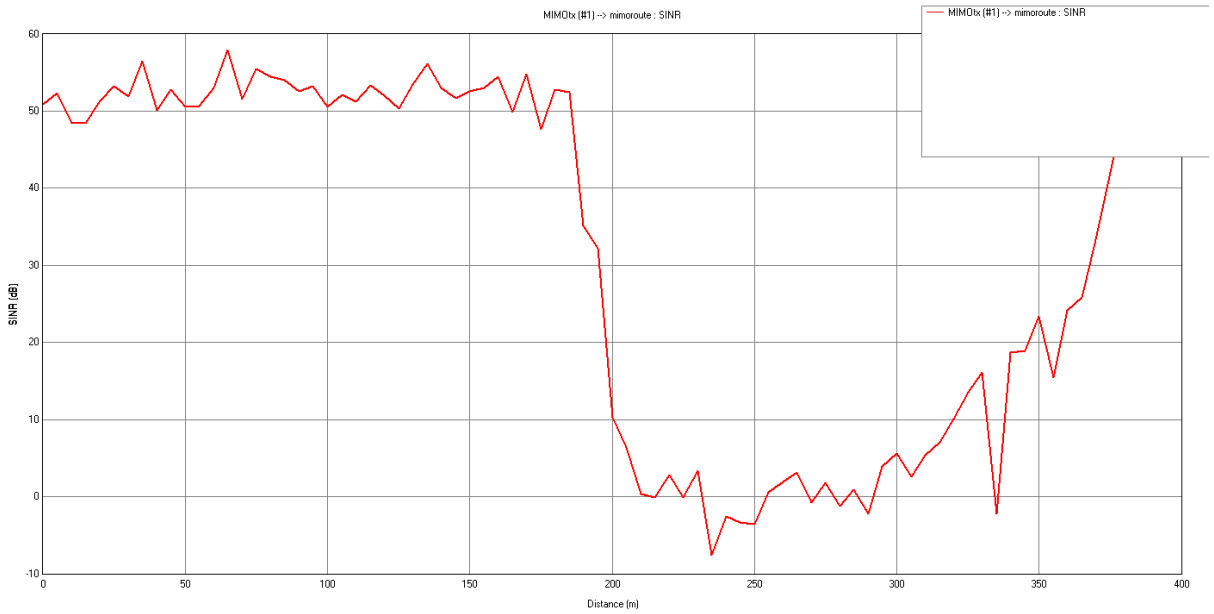

Figure 109: SINR when a single antenna is used at the UE set to SVD.

When compared with the SINR observed with no pre-coding weights and selection combining (Figure 109), not as much improvement is observed.

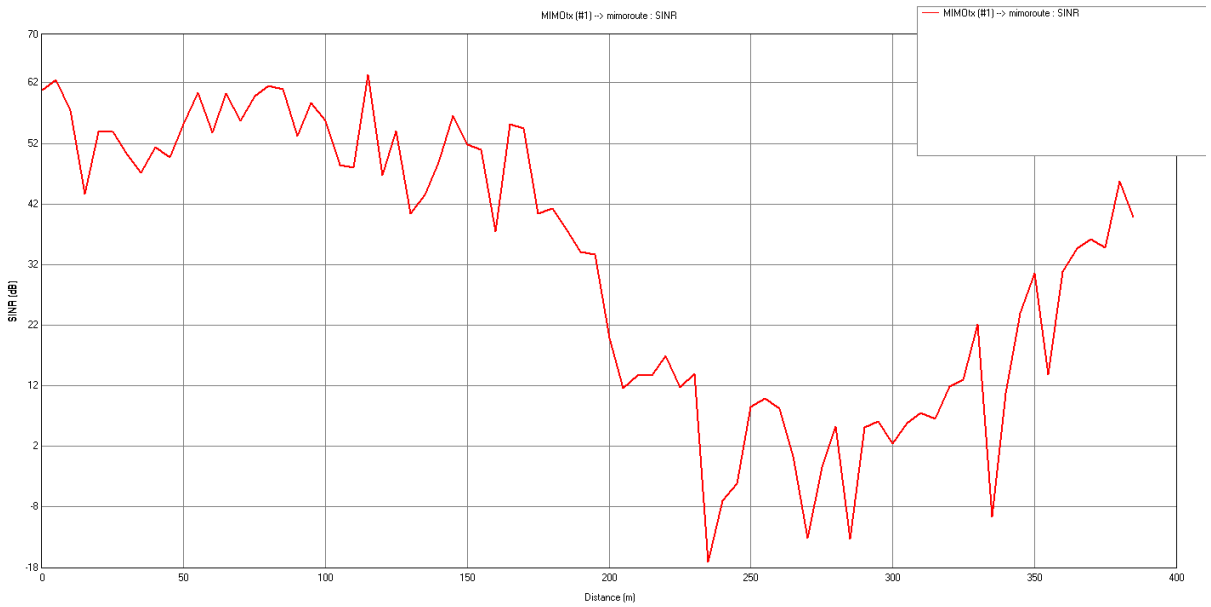

Figure 110: SINR when only one antenna is used, and no pre-coding weights are applied at the BS.

This is more apparent when considering the average SINR values when using four antennas at the UE and when using just one antenna at the UE (Figure 110). Figure 111 shows the average value (over five sample points) for the example where only one antenna is used at the UE for both the scenario where no pre-coding weights are used at the BS and where SVD spatial multiplexing is applied.

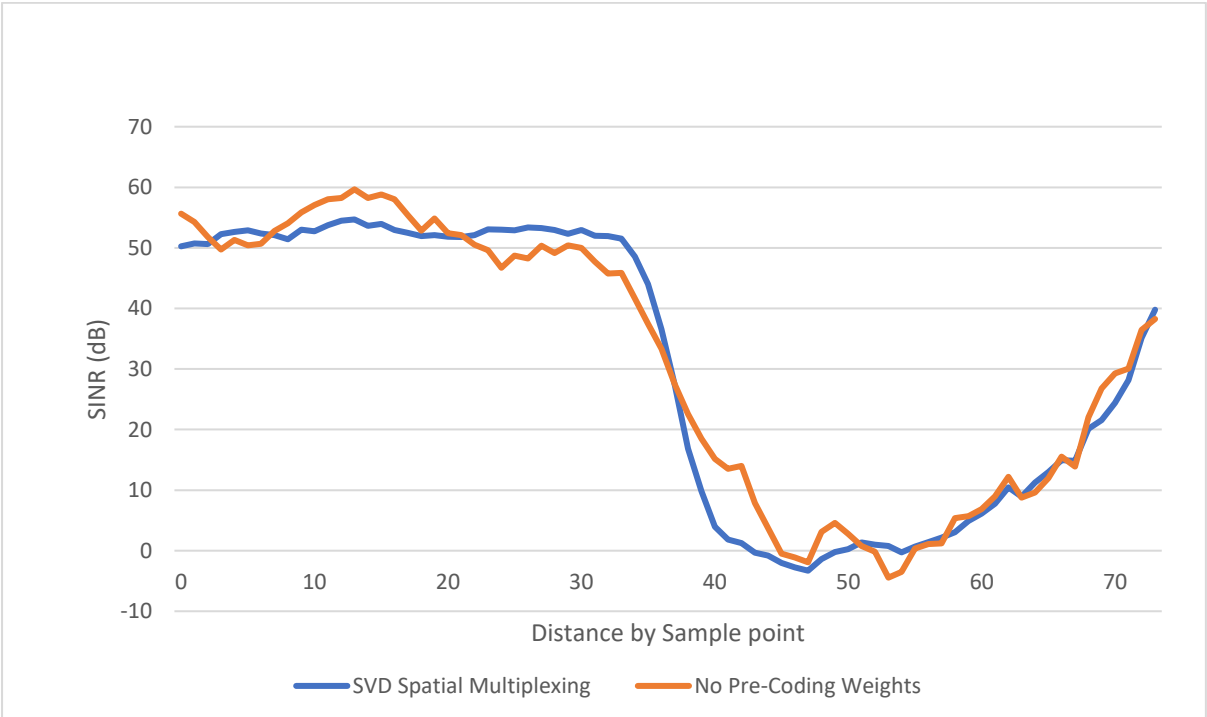

Figure 111: Simulated SINR values when one UE antenna is used.

When this is compared with the example that is set up in the same way, but with four UE antennas (Figure 112), it is apparent that the average SINR value when SVD spatial multiplexing is applied offers an improvement over the SINR value when no pre-coding weights are applied, more often than when only one antenna is used, as shown in Figure 111.

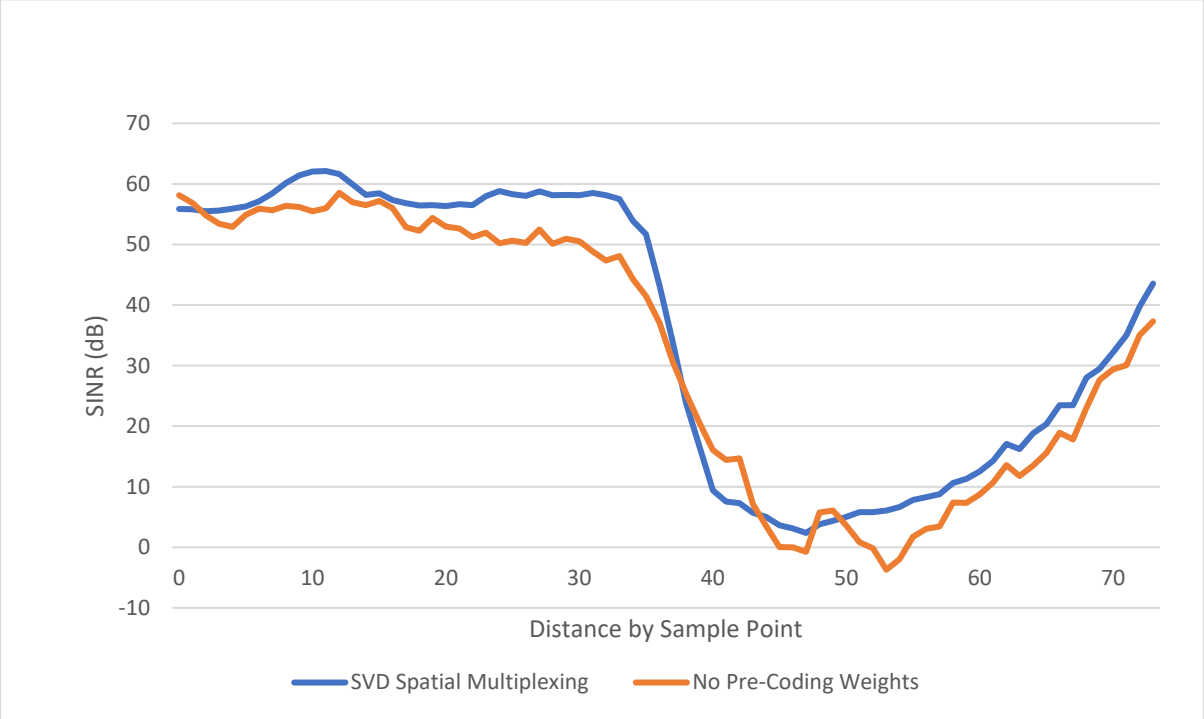

Figure 112: Simulated SINR values when four UE antennas are used.

These methods are shown in the following mobility example. Consider the route shown in Figure 113, where the user travels along a flat terrain from the south towards the reflector. It then makes a sharp turn to the right before taking a diagonal route towards the reflector. The user then travels behind the reflector so that it is obscured from view of the BS, before emerging from the other side. It is possible to view each of these stages when the SINR and Throughput are plotted. The BS array, once again, is an 8x8 array with vertically polarised dipoles, situated in parallel with the western and eastern edges of the terrain. The user antenna is a 2x2 array, also with vertically polarised dipoles.

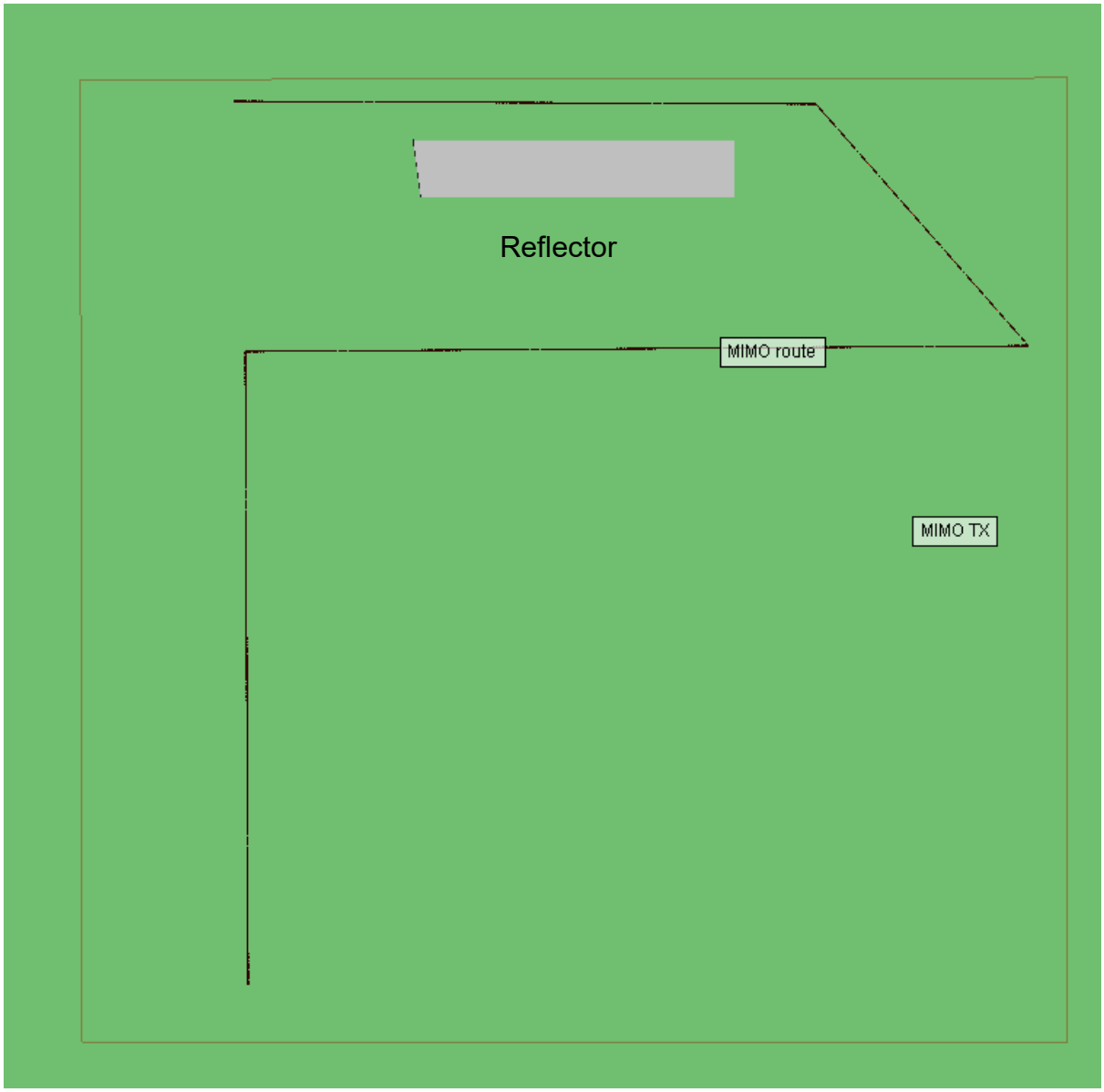

Figure 113: Mobility example: user travels in different directions along a flat terrain

The SINR plot when MRT beamforming is used is shown in Figure 114. This shows fairly consistent performance throughout the study area, with the exception of the region where the user travels behind the reflector, where the SINR falls off sharply and then recovers quickly as soon as the user emerges from behind the reflector. This can be compared to the situation where no beamforming is used, but where MRC is still used at the receiver (Figure 115). Here, the SINR values are similar, but there are several instances where the values drop along the path.

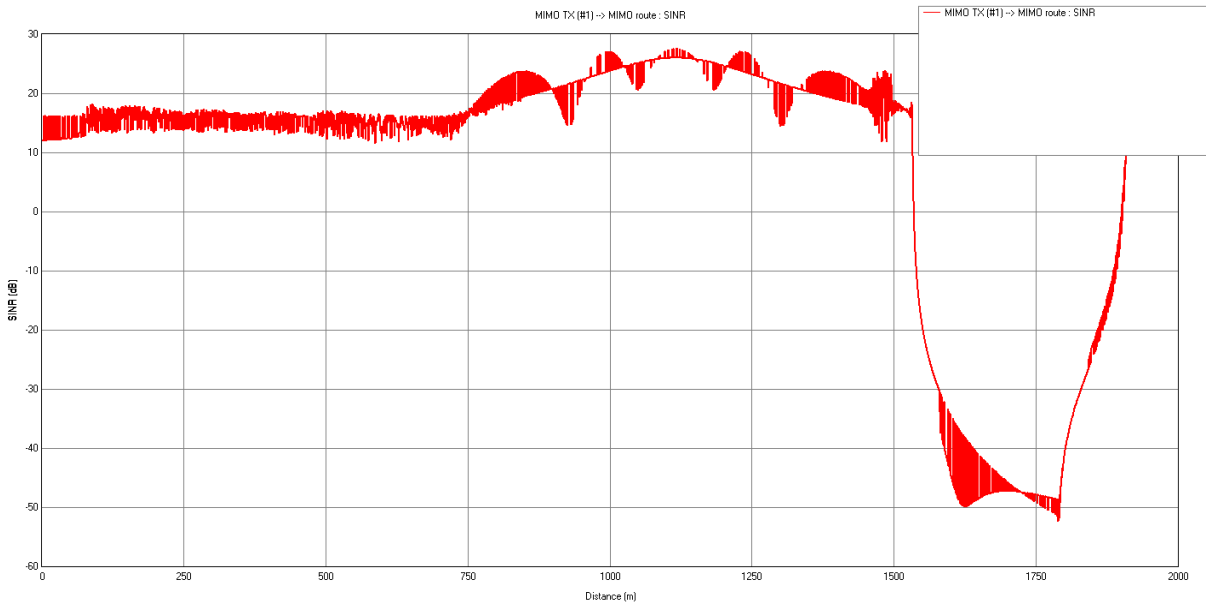

Figure 114: The SINR plot when MRT beamforming is used

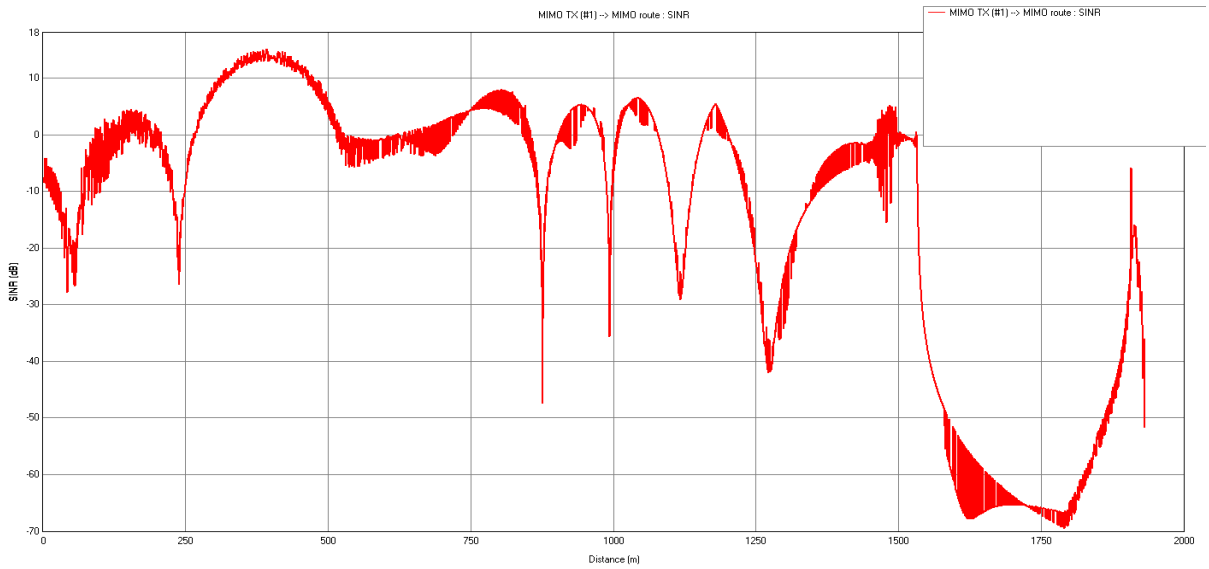

Figure 115: The SINR plot when no MRT beamforming is used

These results are broadly mirrored in the throughput graphs, where the beamforming example provides a generally consistent throughput, except when the user is located behind the reflector (Figure 116). As expected, the throughput for the scenario with no beamforming is much more variable, as shown in Figure 117. The bandwidth is set at 20MHz for these throughput examples, and the range of values shown are not much greater than what would be expected with a single antenna link when applying the Shannon-Hartley capacity formula. These values are also explained by the lack of complexity within the propagation environment, meaning that it is difficult to obtain values higher than for a single antenna link.

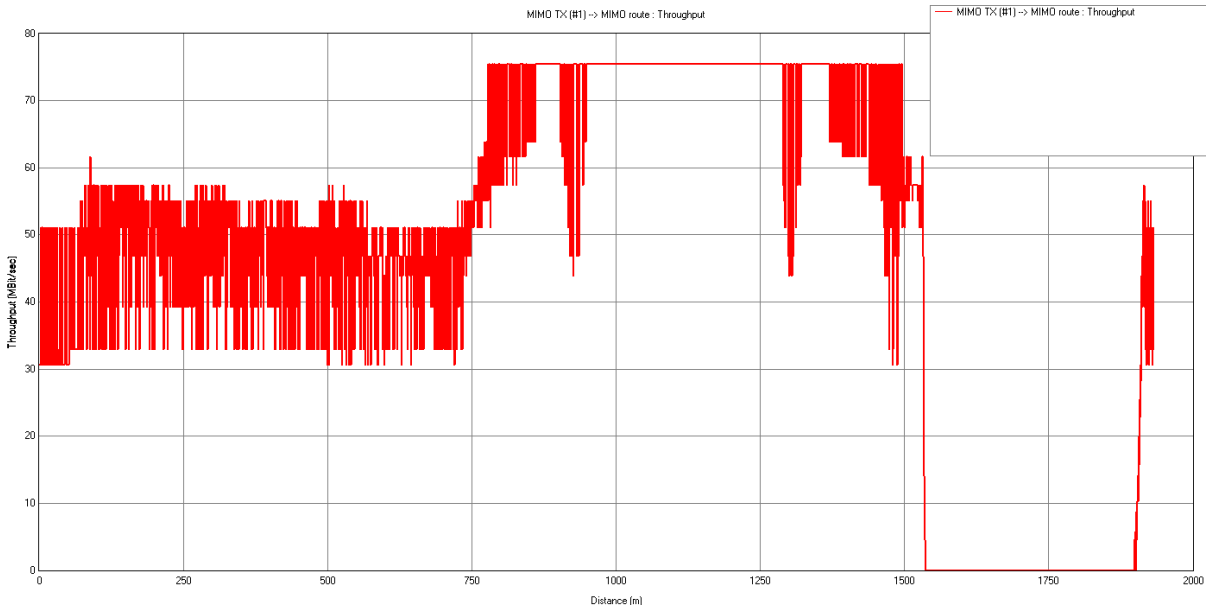

Figure 116: Throughput for scenario with beamforming

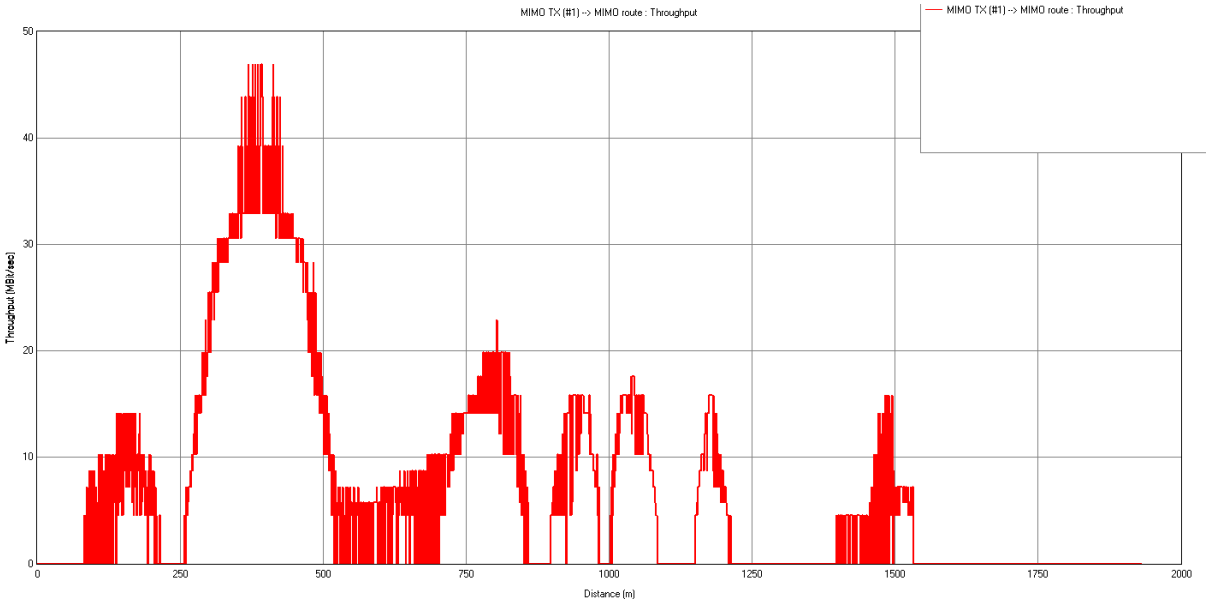

Figure 117: Throughput for scenario with no beamforming

These results can now be compared with the use of spatial multiplexing, as shown in Figure 119. Here it can be seen that, in some ways, the SINR variations within this spatial multiplexing scenario, largely mirror those of the beamforming example, although the SINR value is lower. This suggests that, in this scenario, beamforming outperforms spatial multiplexing, but either method is better than replying on diversity gain without beamforming. It also suggests that the process of beamforming does, in some situations, lead to results that resemble those of spatial multiplexing.

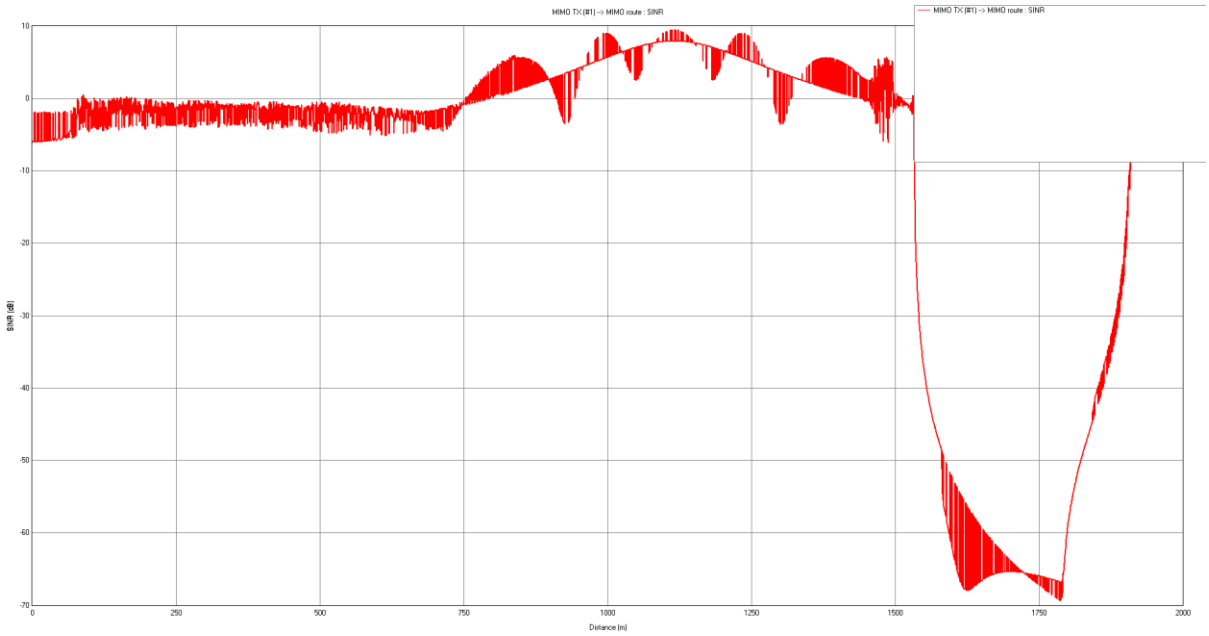

Figure 118: SINR for scenario with use of spatial multiplexing

It is now possible to compare the different methods when nearby users are present. For this, other users are placed along the route with the same MIMO antenna as used by the user following the route, providing transmitting interference as the user passes (Figure 119). Each of the additional users remain stationary throughout the simulation. The total array power for each of these stationary users is the same as the total array power of the BS (Figure 120).

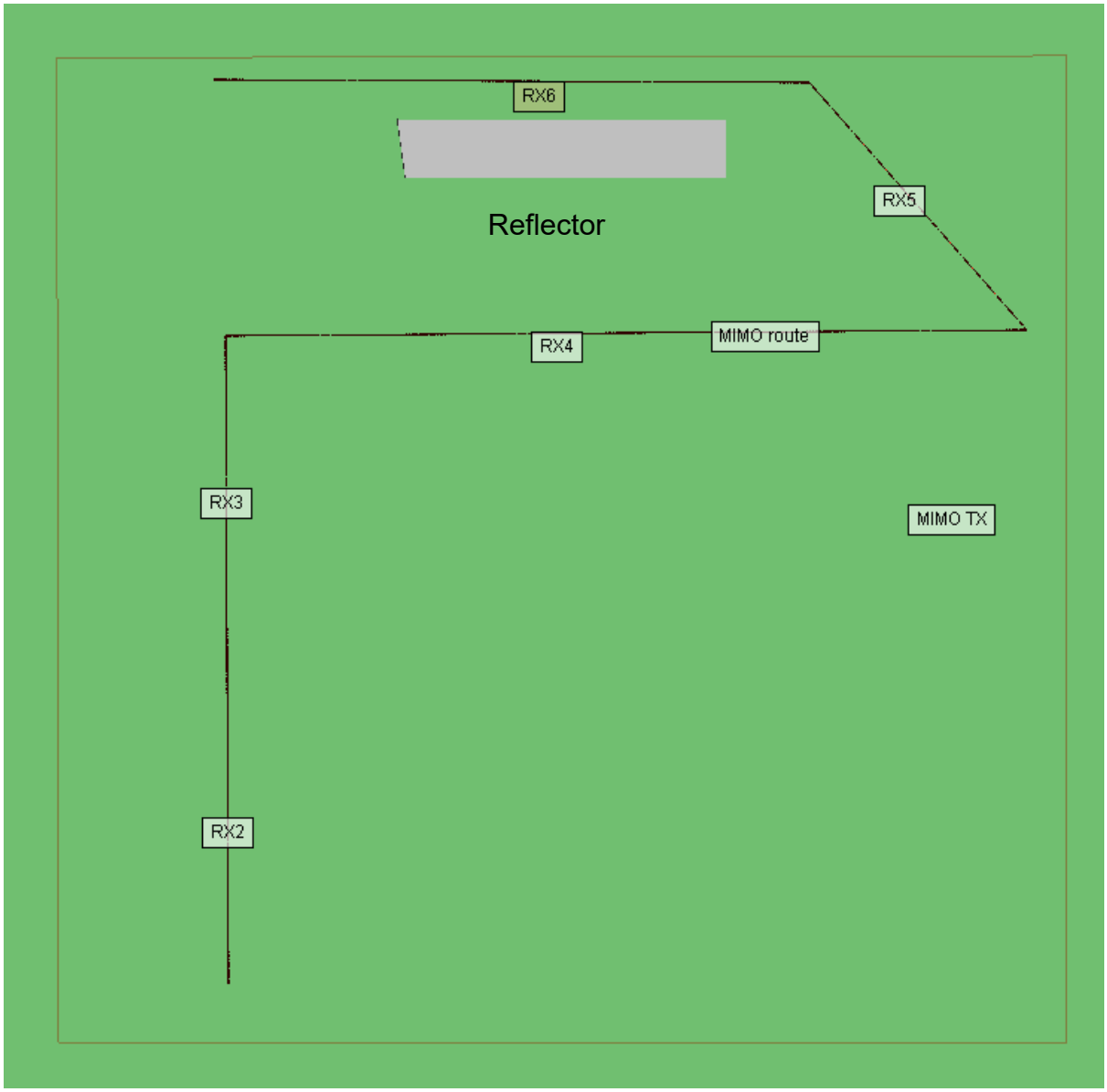

Figure 119: Route of user with other users placed along the route providing transmitting interference as the user passes

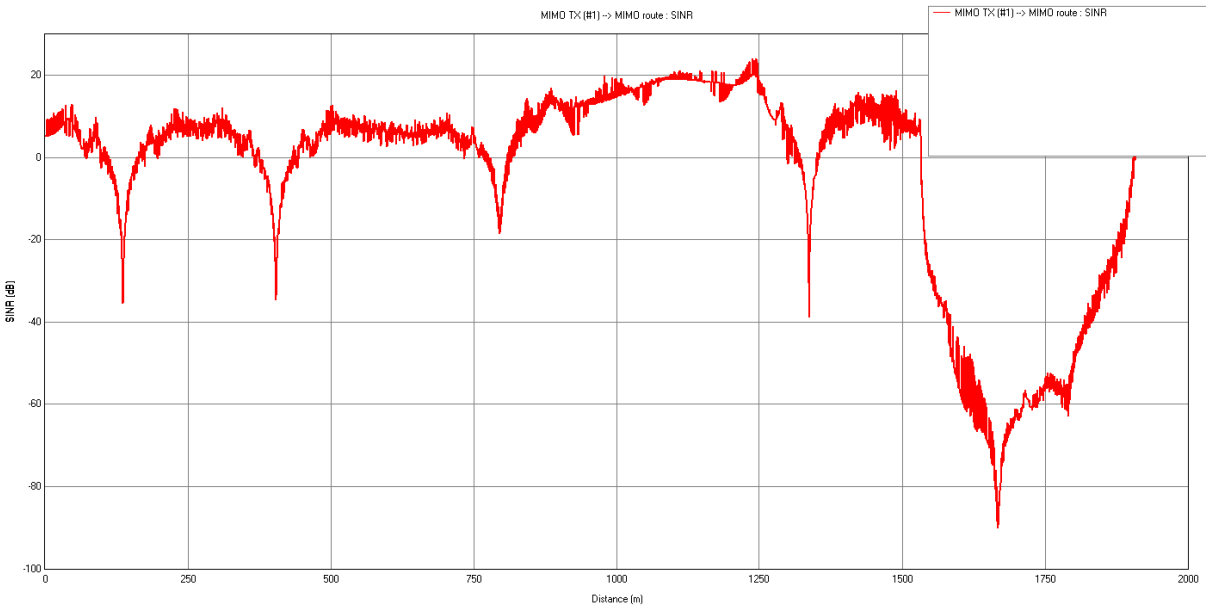

Figure 120: SINR with beamforming and the presence of interferers

It could be seen in the example without the presence of interfering antennas, that both the spatial multiplexing and beamforming approaches resulted in similar SINR characteristics, but that the beamforming approach led to SINR values that were approximately 20dB higher than the purely spatial multiplexing approach. This would be explained due to the gains obtained through beamforming as the user is tracked around the study area. A disadvantage of the use of beamforming is that the interference noise due to other users will be greater at some points in the study area, either due to inter-beam interference, or due to the inability of the beam to separate the different users, due to limitations in how narrow the beam can be. It would make sense, therefore, with the model for spatial multiplexing, to reduce the potential level of interference from the users that are placed along the route. The total array power is set to 10dB, 20dB lower than for the beamforming example. This leads to a similar SINR plot (Figure 121) with reductions due to the presence of other users. It is important to note here that, even though the spatial multiplexing performance in the described environment is generally inferior when compared with the beamforming approach, there are some instances where the spatial multiplexing method can result in SINR values that are higher than for beamforming. For example, at 804m, the beamforming method shows an SINR of about -20dB, but the spatial multiplexing method shows -18dB. These periods when the spatial multiplexing method performs better than the beamforming method are brief in this simulation setup, which would be expected given the relatively simple multipath environment. It is possible that, in

more complex multipath environments, the spatial multiplexing method may be superior for longer amounts of time. It is also significant that, even in a mostly LoS environment, there may still be times when spatial multiplexing is superior to beamforming, even if only briefly.

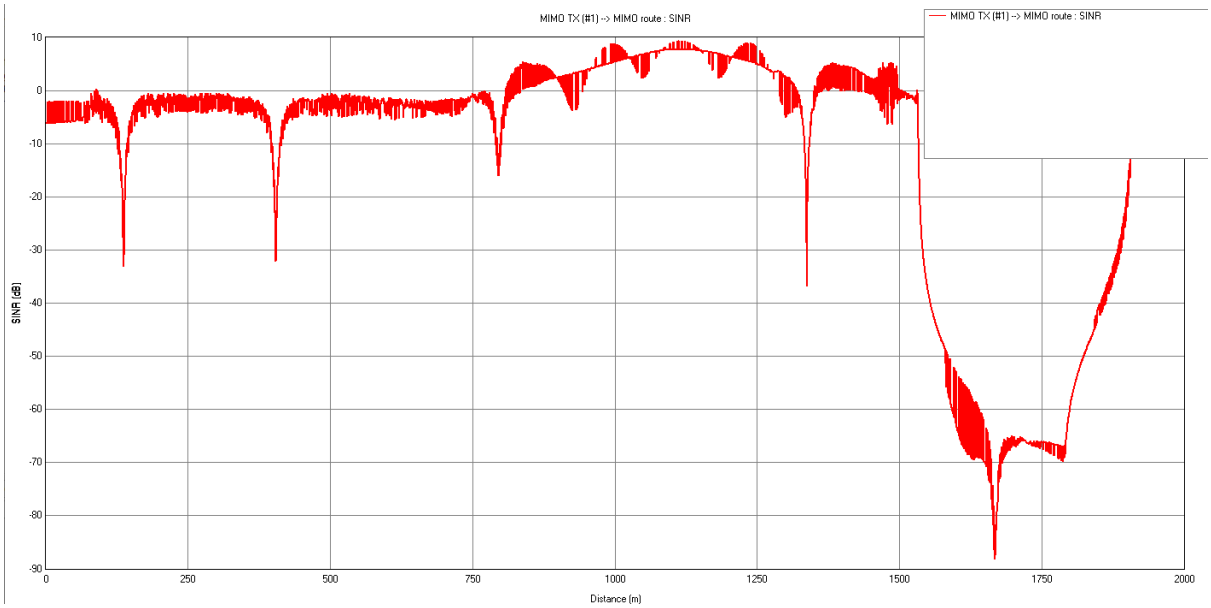

Figure 121: SINR without beamforming in the presence of interferers

5.4.3 Urban Scenarios

It is now possible to consider the urban scenario shown in Figure 123. A route is chosen, as in previous example, to provide a combination of LoS and Non-LoS environment from the perspective of different points of the route in relation to the Massive MIMO array at the BS.

Figure 122: Urban scenario with route of UE

As before, it is observed that the use of MRT beamforming with MRC combining methods (Figure 124) produces a result that is superior to that of spatial multiplexing (Figure 125), but that mirrors beamforming when there is only one user present in the environment, so that a variation of 1dB of the SINR obtained with beamforming corresponds to a variation of 1dB of the SINR when using SVD spatial multiplexing. However, unlike in the previous example, it makes less sense to compare the performance between the two methods by adding receive points to reduce the SINR values near other users. Doing so would lead to the same kind of result shown in the previous example with a broadly LoS environment, where, even though beamforming was shown to be superior in nearly all the locations studied, there were some times close to other users where the performance of a spatial multiplexing system was superior.

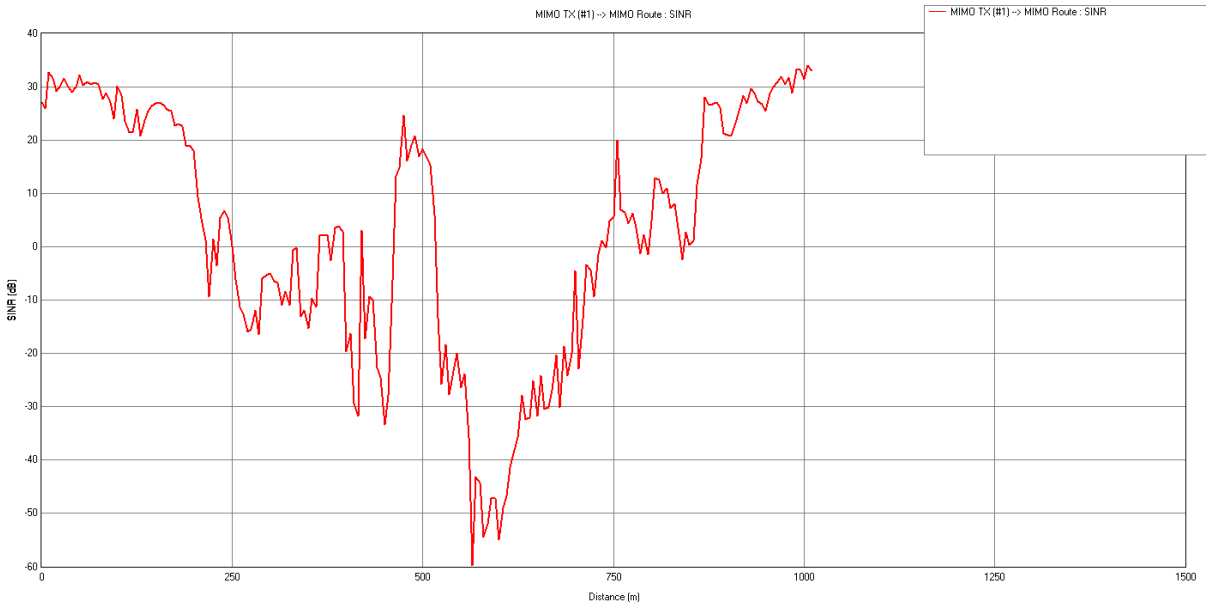

Figure 123: SINR from use of MRT beamforming with MRC combining methods

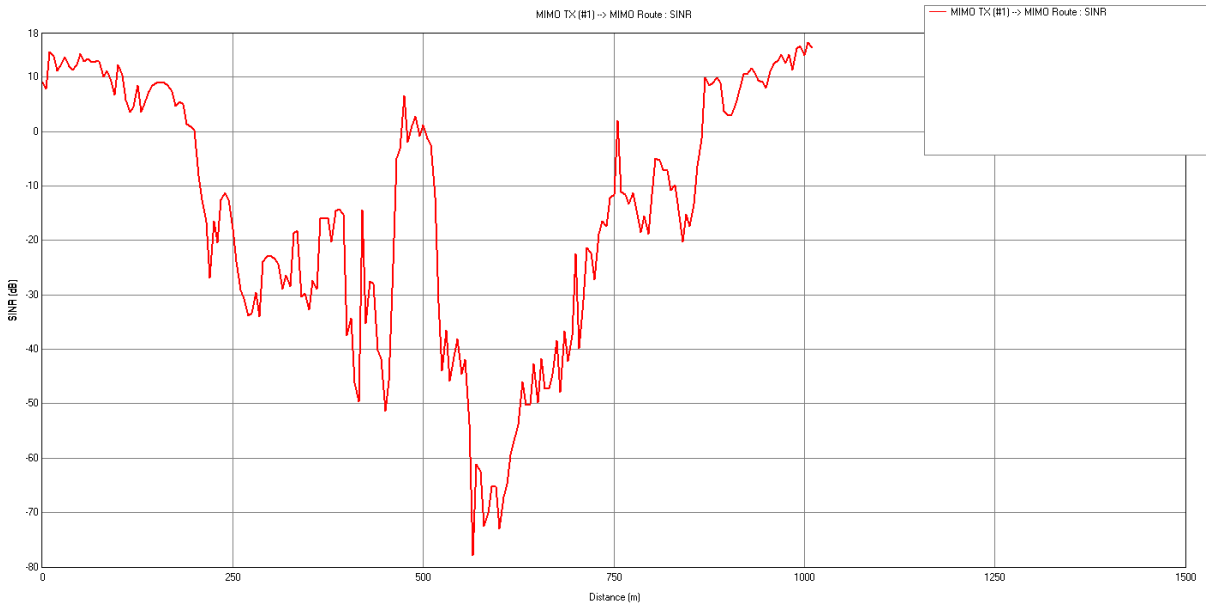

Figure 124: SINR from SVD spatial multiplexing

In this urban scenario, the rate at which the beam changes direction as the user moves around the scenario is different depending on the propagation characteristics at that time. Therefore, it is sometimes the case that, even though the user moves in a non-LoS section by a similar distance that it would move in an LoS section, the distance that the beam moves may be much less. This can occur when a reflector is responsible for providing the main component of the link between the user and BS

and can be illustrated by an example. The route described in this urban scenario begins at the north of the study area and begins by following a path in front of the Massive MIMO array. This leads to the array tracking the user in a similar way to the general Non-LoS environment in previous examples. The polar plots in Figure 125 and Figure 126 indicate the main components as they appear when the users are 50 metres apart and still visible to the BS array. The main components are separated by approximately 18.9 degrees.

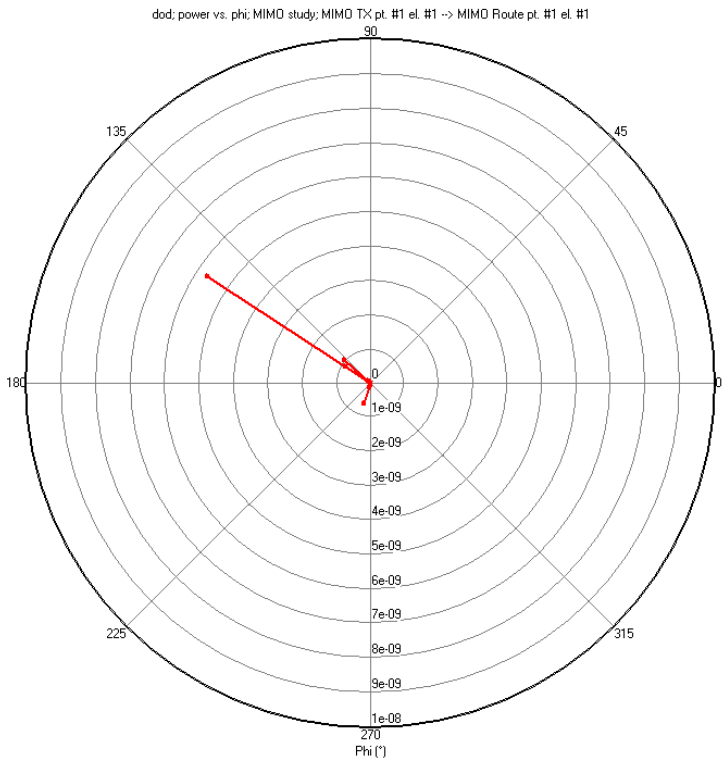

Figure 125: Polar plot showing the departure angles at BS from point 1 on the route

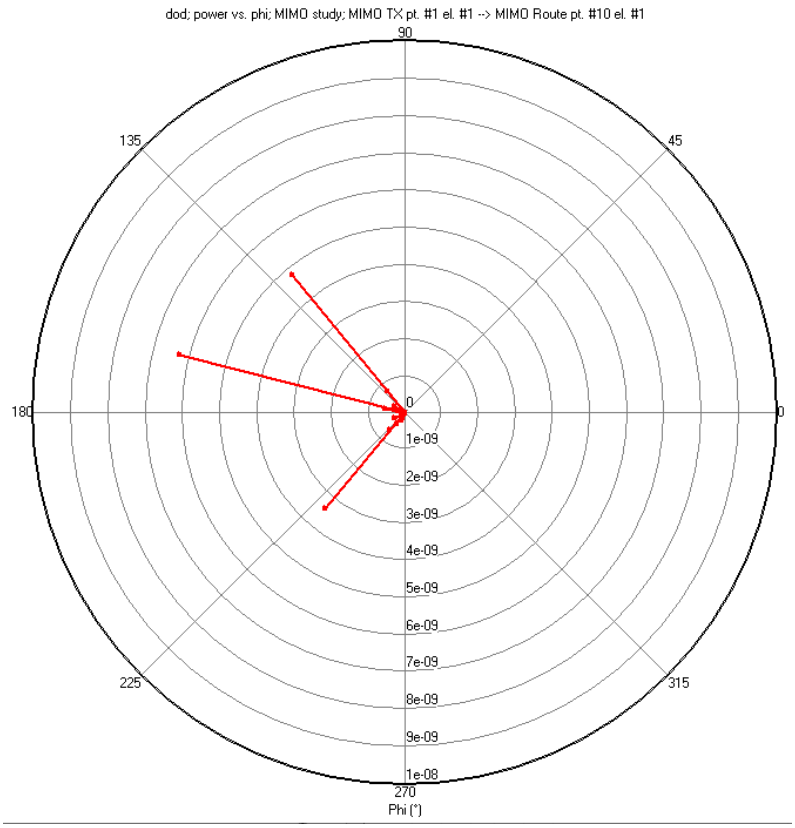

Figure 126: Polar plot showing the departure angles at BS from point 10 on the route

The route taken by the user then moves behind the council building from the south and travels northwards. Compared with a variation of 18.9 degrees corresponding to a move of 50 metres when the user is in front of the council building, a move of 100 metres behind the council building causes the main beam to move by only 4.3 degrees (Figure 128 and Figure 129). If these positions represented users, it would be much more difficult for the BS to avoid interference between the beams serving the users, even though they would be further apart.

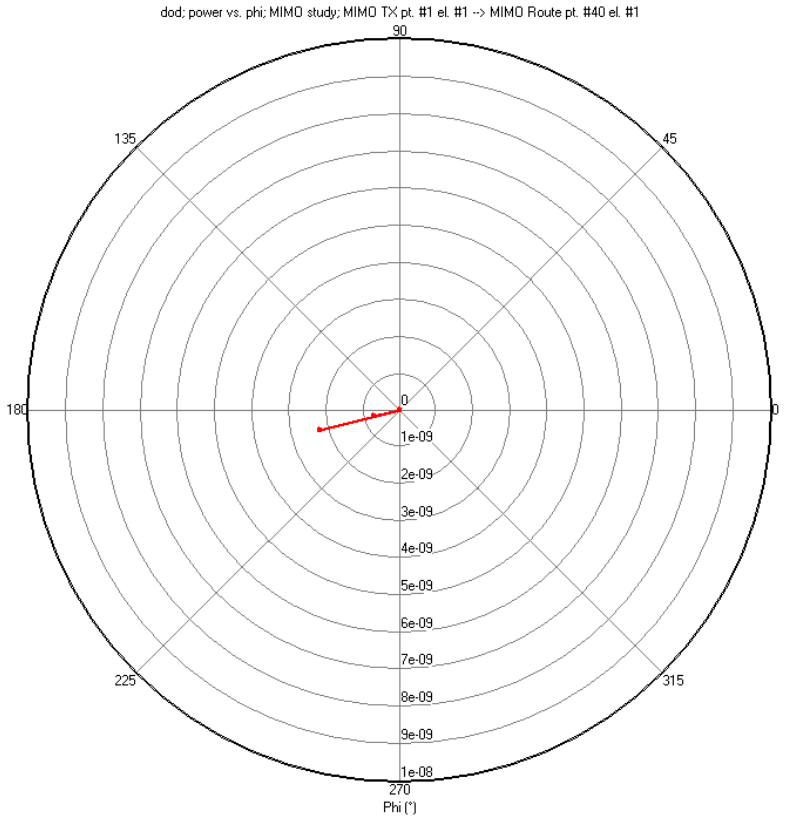

Figure 127: Polar plot showing the departure angles at BS from point 40 on the route

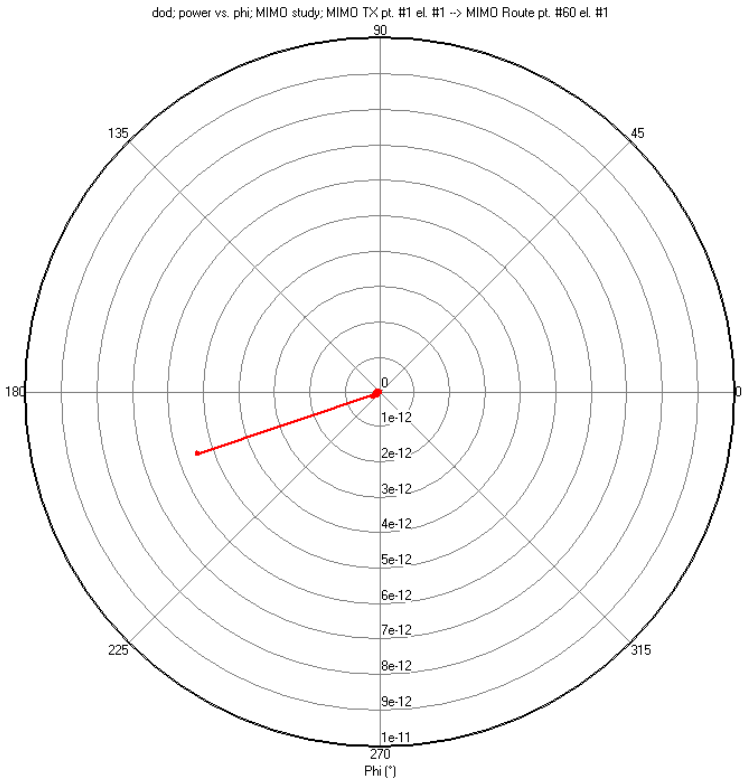

Figure 128: Polar plot showing the departure angles at BS from point 60 on the route

5.5 Conclusion

In an uncluttered environment with flat terrain, the use of beamforming with MRT and MRC almost always outperforms SVD spatial multiplexing without the application of beamforming. Generally, the MRT beamforming and SVD spatial multiplexing SINR values follow each other, with increases and decreases in SINR values being identical, but with the beamforming approach containing higher values.

However, there may be some instances in a flat terrain, uncluttered environment when spatial multiplexing is able to outperform MRT beamforming, although these instances would appear to be often brief in the case of a dynamic environment, which is to say an environment where users are passing each other only occasionally. These instances occur in the presence of nearby transmitters that cause interference, both by these transmitters causing interference during uplink, and also by the overlapping of beams required to serve these separate users. Although this process is not modelled precisely in the propagation software, it may be possible to approximate it by adding interferers to the propagation environment whose power levels are suitably matched to the gain obtained by the beamforming. Thus, these power levels would be lower for spatial multiplexing than with beamforming. It is then possible to determine the zone on the SINR plot where the SINR obtained with beamforming falls below that obtained using spatial multiplexing, at which point the spatial multiplexing performance would be superior. This implies that, although for open spaces a beamforming approach to data throughput in Massive MIMO is generally superior, there may still be occasions when spatial multiplexing should be used, for example where users are expected to be clustered closely together.

The approximation described for the flat propagation environments, however, does not apply to more complex urban environments where it is not always obvious how the main beam and sidelobes from the BS are directed. Here it is necessary to consider the separation between the beams that would be observed at the BS for each of the methods, and to considered whether the separation necessary to achieve the necessary throughput in attainable. It was shown that, when the UE is obscured from the BS, it is sometimes the case that a large physical separation between the users corresponds with only a small change in the main beams required

to serve the users simultaneously. In which case, it would not be advisable to use beamforming to serve the users, due to the increase in inter-beam interference.

6: Conclusion

This thesis has been concerned with the study of propagation environments and the features of the environments that are most relevant to systems employing Massive MIMO antenna systems. The study of such systems will be of importance to the future of wireless networks, since they form a key part of 5G and 6G networks and are likely to continue to be a part of existing and future networks for a considerable amount of time. The reason for this is the ability of Massive MIMO to increase spectrum efficiency within a system beyond what could be achieved using the facilities available to previous networks. In other words, Massive MIMO is able to increase capacity without increasing the bandwidth requirements within a network. Such an ability would continue to be appealing to mobile network operators due to the scarcity of free space within the radio spectrum, and thus the great expense of obtaining the rights to the use of radio spectrum from the regulatory authorities.

The study of the propagation environments that represent the types of settings in which such Massive MIMO communications systems operate is important. This importance applies both for the reasons associated with more established communication systems, such as the understanding of the level of coverage that can be expected with such a system within a certain geographic area, but also because the performance of a Massive MIMO system is affected in other ways by the propagation environment. These include the number of spatial streams that can be supported and the modulation schemes that can be used. Therefore, it is important to make sure that any propagation model used in the design of a network employing Massive MIMO technology takes account of the features within a propagation environment that affect the performance of the communications system. It is also important that these features are modelled in sufficient detail so that important features of the environment can be more accurately understood. Much of this thesis has been concerned with the study of the environment, a study which has led to several important observations and recommendations for Massive MIMO systems.

This study has been conducted largely with the aid of ray-tracing propagation modelling systems, including both an in-house system developed within the

University of Bristol, and a proprietary commercial ray-tracing system. Both systems are based on methods from Geometric Optics to provide realistic interpretations of the propagation environments using the study of rays that represent the paths between the BS and UE antennas. In addition, these methods for studying the environments have been combined with location data from Bristol, for example from lidar data and open source street map data, to provide an impression of expected locations and densities of features that lead to scattering within the environment. These systems are able to model the channels at both transmit and receive ends of a communications link principally by simulating the reflections off the scatterers (such as buildings and terrain features acting as reflectors), but also through the modelling of diffraction effects, as well as path losses in the presence of different types of materials. These types of simulations allow for the power delay profile to be formed at either end of the link by combining the different time delays associated with each path, which often varying depending on the route that the path takes, with the received power, which is obtained by applying the relevant path loss model, either relating to losses incurred with propagation in free-space or within other context, such as through foliage. When studying Massive MIMO channels, the links between each antenna element at both the BS and UE is considered. It is then possible to combine the power delay profile data to obtain the matrix representing the channel for the entire system. The elements at the BS are often located close together, and it is important to be able to model the differences between the elements, from the perspective of the UE, to obtain a reasonable channel matrix and to understand the effects present within the environment.

Although Massive MIMO can be implemented over a wide range of frequencies and is often associated with systems operating within mmWave frequencies, this thesis has been concerned exclusively with Massive MIMO systems operating below 7.125GHz and the multipath propagation effects present within the systems. The mmWave systems operate largely within LoS contexts, providing beamforming as part of the link. While there has been research related to the use of millimetre wave Massive MIMO at 5G BSs, in practice this has not yet been of significant interest to MNOs in terms of deployment.

The thesis began with an overview of Massive MIMO systems from the point-of-view of the information transferred within a system, the capacity of this type of system being defined according to typical Shannon Capacity observations using the concept of mutual information. This was followed by a review of some of the standard propagation models that have been applied within research and within the various wireless standards to MIMO communications. These included the purely geometry-based models where a selection of scatters are used to represent the physical locations of reflecting objects within the propagation environment. Hybrid models were also discussed, which are often applied in the wireless standards and feature scatterers combined with other statistical methods to model the propagation environment, but without reflecting exactly the physical layout of the environment. Purely correlative models that rely only on statistical techniques to model a MIMO channel were also discussed. Some of the limitations of these models as applied to Massive MIMO were also presented as a justification for much of the research in the following chapters. A summary of known measurement campaigns for Massive MIMO and the methodologies followed in obtaining the measurements was included to provide an overview of the information available for model validation. Some features of Massive MIMO systems have been especially relevant to the research presented in this thesis, and so the remainder of the chapter is concerned with some of these issues. Methods for detection within Massive MIMO systems were discussed, as the recovery of the transmit signal is relevant in some of the investigations that followed. Additionally, a summary of research related to spherical wavefronts has been included, an area that is especially relevant to chapter 3. The following chapters presented several key findings and recommendations, which are discussed in the following paragraphs along with a brief summary of the chapter contents.

The third chapter focussed on the use of ray-tracing systems to model specific propagation scenarios that would be common within Massive MIMO systems. The ray-tracing provided an example of spherical wavefront type model and served to demonstrate the advantages of the use of such a model for Massive MIMO systems.

Recommendation 1: It was shown in sections 3.3 to 3.7 that, even in fairly simple environments, the use of a spherical wavefront model can provide significant insights

into the nature of the channel that are not present within typical plane wave models. Examples include the variations in the power delay profile across the array in several different configurations. Therefore, it is likely that the use of a plane wave model will often lead to flawed analysis and conclusions in the design of Massive MIMO deployments. It is therefore recommended that the performance of any Massive MIMO propagation model should be assessed relative to a spherical wave model and not a plane wave model.

Recommendation 2: An even more significant effect in the differences in how the channel was seen by the UE was observed when slow fading was introduced across the array, as discussed in section 3.6. This makes the model choice more critical when deploying these systems in environments where slow fading is likely to occur and, in such cases, approximations should take these effects into account.

Recommendation 3: These effects were also observed when the UE was moving relative to the BS, and it was also observed that such effects led to changes in the correlation between the spatial streams at the UE. This was shown in the form of variation of the channel condition number, which provided an indication of the rank deficiency within the correlation matrix. Furthermore, it was shown that Massive MIMO channels have a tendency to enter various phases as the UE moves around the study area. These phases can be marked, for example, by greater variation in channel condition or by stages of consistently higher or lower values. Standard change detection methods were shown to successfully identify these changes within the Massive MIMO channel. The details are provided in sections 3.9 to 3.15. It is recommended that these methods should be applied within networks to identify significant changes that affect the spatial multiplexing performance of Massive MIMO systems. Further research may be conducted into how different anomaly detection methods may be able to detect or predict these changes.

Recommendation 4: Furthermore, it was shown in section 3.12 that, within the different phases of the channel condition, it was possible to develop time-series models to simulate the behaviour of the varying channel conditions, based on auto-regressive moving-average methods. Such methods would be useful in forecasting the state of a Massive MIMO channel, and it is recommended that these methods be used to provide approximations of expected variations in channel conditions. More

research is necessary to determine the accuracy of different time-series methods and which are the most useful to these applications.

Recommendation 5: The question of how to interpret the changes in channel conditions in terms of the physical location of users was also addressed. It was noted in section 3.15 that the changes in channel condition did indeed correspond to differing user configurations, but it is recommended that more research be conducted to provide a more formal explanation of how the user configuration and channel condition changes are linked.

The fourth chapter, in comparison with the previous chapter, was more focussed on beamforming with Massive MIMO systems than on propagation effects relevant to Massive MIMO in general. More specifically, it was concerned with how beams are selected for use within the synchronisation process within 5G networks. An overview of synchronisation within 5G was provided along with an overview of research topics within 5G beamforming optimisation.

Recommendation 6: It was apparent that it was possible to describe the problem of assigning beams formally as a mathematical combinatorial optimisation problem. An approach to define what the optimal combination of beams around any BS was also presented, along with a simplified propagation modelling approach that allowed for the effectiveness of a beam selection method to be effectively evaluated. This approach can provide a useful framework for investigating the application of beam selection and it is recommended that this framework be used as part of efforts to optimise coverage for synchronisation, as discussed in section 4.6.

Recommendation 7: A simulated annealing algorithm was presented, which was able to show that, by selecting the order in which beams were tested, it was possible to provide the most even coverage using significantly fewer iterations than would have been required if an exhaustive search was used to perform the optimisation, as discussed in sections 4.8 and 4.9. The deployment of such a technique within a 5G network could provide an operational advantage to an MNO by optimising the coverage during synchronisation and it is recommended that this approach be implemented in beam selection processes. Specific real-time implementations, for example, on open RAN architectures could be a topic for further research.

Recommendation 8: It is also possible to use methods for optimisation over longer time frames, for example by adjusting the types of beams used at different times of the day. It is recommended that this approach be incorporated into network planning when considering how user distributions vary throughout the day. This is discussed further in section 4.10. Further research may also be conducted on the performance of the method for specific user distributions and varying success criteria.

Recommendation 9: It was observed that the number of iterations required of an SA technique for beam selection varied depending on user clustering, as discussed in section 4.9. It is recommended that further research be conducted to develop a greater understanding of how clustering may affect the use of such methods.

While the fourth chapter focussed on the use of beamforming for synchronisation, the fifth chapter focussed more generally on the performance of Massive MIMO systems with different types of user configurations and propagation environments, and on how different methods for providing separate spatial streams compared within such environments. An overview of beamforming within these contexts was provided with explanations of how performance is measure. It was necessary to 220 conduct tests to determine the effectiveness of the ray-tracing propagation system when applied to such beamforming scenarios. This was achieved by reducing the number of paths simulated and using simple environments with few scatters, before scaling up to move complex simulations and scenarios.

Recommendation 10: It was shown that, compared with Singular Value Decomposition multiplexing, the use of basic beamforming methods often outperformed, however it is sometimes the case that closely overlapping beams make the use of such beamforming impractical, and other methods, such as those based on obtaining spatial multiplexing through multi-path within the propagation environments, may be preferred. Such scenarios can occur when users are located close together, in which case one would expect the performance of the system to dip as users pass one another. This is discussed in section 5.4. It is therefore recommended that a bias towards beamforming within a system be considered if it is predicted that users will generally be sufficiently separated for such an implementation to be advantageous.

Recommendation 11: A method was investigated in section 5.4 to simulate this decrease in performance by placing transmitters near the passing user, thus decreasing the effectiveness of the system. This method, however, is not based on computing the physics of the radio system, and thus it is recommended that more empirical investigation be conducted to determine threshold values that correctly match what would be observed within physical 5G systems.

Recommendation 12: Another method of investigating the closeness of the main MPCs was studied, also in section 5.4, to determine how close the beams from the BS would need to be. This method is more based on the physics of the radio environment, and it is possible to determine how far separated the main MPCs would need to be for effective performance. A major implication of the use of this model is that, in some scenarios, users can be placed far apart, but beamforming is still not an appropriate method to use because the beams would overlap to an extent that the spatial streams for the users could not be separated effectively. Further research could be conducted into how these different systems performed within different locations, allowing for more effective optimisation by MNOs. It is recommended that, when planning a network, zones where the possibility of overlap is present even when the users are physically separated should be identified so that the risks of reduced performance can be mitigated.

7: References

1. E. Godshalk, "Sparks save lives "CQD DE MGY" [Microwave Musings]," in *IEEE Microwave Magazine*, vol. 10, no. 4, pp. 176-174, June 2009

2. D. D. Hoolihan, "The radio act of 1912," in *IEEE Electromagnetic Compatibility Magazine*, vol. 5, no. 2, pp. 32-34, Second Quarter 2016.

3. M. Guarnieri, "The Age of Vacuum Tubes: The Conquest of Analog Communications [Historical]," in *IEEE Industrial Electronics Magazine*, vol. 6, no. 2, pp. 52-54, June 2012.

4. D. Consonni and M. T. M. Silva, "Signals in Communication Engineering History," in *IEEE Transactions on Education*, vol. 53, no. 4, pp. 621-630, Nov. 2010

5. Oswald, "Early History of Single-Sideband Transmission," in *Proceedings of the IRE*, vol. 44, no. 12, pp. 1676-1679, Dec. 1956

6. M. Schwartz, "Armstrong's invention of noise-suppressing FM [History of Communications]," in *IEEE Communications Magazine*, vol. 47, no. 4, pp. 20-23, April 2009

7. W. Gappmair, "Claude E. Shannon: the 50th anniversary of information theory," in *IEEE Communications Magazine*, vol. 37, no. 4, pp. 102-105, April 1999

8. J. Rothweller, "Turbo codes," in *IEEE Potentials*, vol. 18, no. 1, pp. 23-25, Feb.-March 1999

9. Y. Akaiwa, *Introduction to Digital Mobile Communication (2nd edn).* Oxford: Wiley, 2015.

10. Zola, “QAM (quadrature amplitude modulation)” techtarget.com https://www.techtarget.com/searchnetworking/definition/QAM#:~:text=The%20primary%20benefit%20of%20QAM,maps%204%20bits%20per%20carrier (accessed Jun 2, 2022)

11. M. Meraj ud in Mir and S. Kumar, “Evolution of Mobile Wireless Technology from 0G to 5G” in *International Journal of Computer Science and Information Technologies,* Vol. 6 (3), 2545-2551, 2015. Available from: https://ijcsit.com/docs/Volume%206/vol6issue03/ijcsit20150603123.pdf

12. . Frenkiel and M. Schwartz, "Creating cellular: A history of the AMPS project (1971-1983) [History of Communications]," in *IEEE Communications Magazine*, vol. 48, no. 9, pp. 14-24, Sept. 2010

13. Keysight, “LTE Technology Overview.” Keysight.com https://www.keysight.com/gb/en/lib/resources/technical-specifications/lte-technology-overview-1803101.html#:~:text=Long%2DTerm%20Evolution%20(LTE),an%20all%2DIP%20broadband%20network (accessed Jun 3, 2022)

14. S. O’Dea, “Mobile cellular subscriptions per 100 inhabitants in the United Kingdom (UK) from 2000 to 2020” Statista.com https://www.statista.com/statistics/468681/mobile-cellular-subscriptions-per-100-inhabitant-united-kingdom-uk/ (accessed Jun 3, 2022)

15. S. O'Dea. "Monthly mobile data traffic in the United Kingdom (UK) 2011-2020". Statista.com https://www.statista.com/statistics/277893/mobile-traffic-in-the-united-kingdom-uk-by-year/ (accessed Jun 3, 2022)

16. P. Demestichas et al., "5G on the Horizon: Key Challenges for the Radio-Access Network," in *IEEE Vehicular Technology Magazine*, vol. 8, no. 3, pp. 47-53, Sept. 2013

17. G. G. Raleigh and J. M. Cioffi, "Spatio-temporal coding for wireless communication," in *IEEE Transactions on Communications*, vol. 46, no. 3, pp. 357-366, March 1998, doi: 10.1109/26.662641

18. G. J. Foschini, "Layered space-time architecture for wireless communication in a fading environment when using multi-element antennas," in *Bell Labs Technical Journal*, vol. 1, no. 2, pp. 41-59, Autumn 1996, doi: 10.1002/bltj.2015.

19. S. M. Alamouti, "A simple transmit diversity technique for wireless communications," in *IEEE Journal on Selected Areas in Communications*, vol. 16, no. 8, pp. 1451-1458, Oct. 1998, doi: 10.1109/49.730453.

20. J. R. Hampton, *Introduction to MIMO Communications*. New York: Cambridge University Press, 2014.

21. T. Brown, P. Kyritsi and E. De Carvalho, *Practical Guide to MIMO Radio Channel: with MATLAB Examples*. Oxford: Wiley, 2012.

22. C. E. Shannon, "A mathematical theory of communication," in *The Bell System Technical Journal*, vol. 27, no. 3, pp. 379-423, July 1948, doi: 10.1002/j.1538-7305.1948.tb01338.x.

23. Y. Ren, X. Su, C. Qi and Y. Wang, "Channel Reconstruction for SVD-ZF Precoding in Massive 3D-MIMO Systems: Low-Complexity Algorithm," *2016 IEEE 83rd Vehicular Technology Conference* (VTC Spring), Nanjing, China, 2016, pp. 1-7, doi: 10.1109/VTCSpring.2016.7504159.

24. K. Abed-Meraim, A. Chkeif and Y. Hua, "Fast orthonormal PAST algorithm," in *IEEE Signal Processing Letters,* vol. 7, no. 3, pp. 60-62, March 2000, doi: 10.1109/97.823526.

25. E. Telatar, "Capacity of Multi-antenna Gaussian Channels," *European Transactions on Telecommunications,* vol. 10, no. 6, pp. 585-595, 1999.

26. K. R. Schaubach, N. J. Davis and T. S. Rappaport, "A ray tracing method for predicting path loss and delay spread in microcellular environments," [1992 Proceedings] *Vehicular Technology Society 42nd VTS Conference - Frontiers of Technology*, 1992, pp. 932-935 vol.2, doi: 10.1109/VETEC.1992.245274.

27. G. E. Athanasiadou, A. R. Nix and J. P. McGeehan, "A ray tracing algorithm for microcellular and indoor propagation modelling," *Antennas and Propagation, 1995., Ninth International Conference on (Conf. Publ. No. 407), Eindhoven,* 1995, pp. 231-235 vol.2.

28. K. H. Ng, E. K. Tameh, A. Doufexi, M. Hunukumbure and A. R. Nix, "Efficient Multielement Ray Tracing With Site-Specific Comparisons Using Measured MIMO Channel Data," in *IEEE Transactions on Vehicular Technology*, vol. 56, no. 3, pp. 1019-1032, May 2007, doi: 10.1109/TVT.2007.895606.

29. P. Almers *et al.*, "Survey of Channel and Radio Propagation Models for Wireless MIMO Systems," *EURASIP Journal on Wireless Communications and Networking,* vol. 2007, no. 1, p. 019070, 2007/02/26 2007, doi: 10.1155/2007/19070.

30. F. Molisch, A. Kuchar, J. Laurila, K. Hugl, and R. Schmalenberger, "Geometry-based directional model for mobile radio channels—principles and implementation," *European*

Transactions on Telecommunications, vol. 14, no. 4, pp. 351-359, 2003, doi: https://doi.org/10.1002/ett.928.

31. L. Liu *et al.*, "The COST 2100 MIMO channel model," in *IEEE Wireless Communications*, vol. 19, no. 6, pp. 92-99, December 2012, doi: 10.1109/MWC.2012.6393523.

32. X. Gao, M. Zhu, F. Tufvesson, F. Rusek and O. Edfors. "Extension of the COST 2100 channel model for massive MIMO," In *COST IC1004.* Dublin, Ireland, 2015. Available: https://lup.lub.lu.se/record/5114789

33. 3GPP Organisational Partners. "3GPP Technical Report: 3GPP TR 25.996 V12.0.0, 2014." https://www.arib.or.jp/english/html/overview/doc/STD-T63v11_30/3_T12/ARIB-TR-T12/Rel12/25/A25996-c00.pdf (accessed May 10, 2022).

34. D. S. Baum, J. Hansen, J. Salo, G. Del Galdo, M. Milojevic and P. Kyösti, "An interim channel model for beyond-3G systems: extending the 3GPP spatial channel model (SCM)," *2005 IEEE 61st Vehicular Technology Conference*, 2005, pp. 3132-3136 Vol. 5, doi: 10.1109/VETECS.2005.1543924

35. ETSI. "ETSI TR 138 901 V16.1.0 (2020-11)" [online] https://www.etsi.org/deliver/etsi_tr/138900_138999/138901/16.01.00_60/tr_138901v160100p.pdf (accessed June 17, 2023)

36. Kyösti, P et al. *WINNER II Channel Models D1.1.2 V1.2 IST-4–027756 WINNER II Deliverable*, February 2008. [online]. Available: http://www.ero.dk/93F2FC5C-0C4B-4E44-8931-00A5B05A331B?frames=no&

37. X. Gao, B. K. Lau, X. Wang and T. Bolin, "On simplifying WINNER II channel model for MIMO OTA performance evaluation," *Proceedings of the 5th European Conference on Antennas and Propagation (EUCAP), Rome,* 2011, pp. 2942-2946

38. X. Gao, "Massive MIMO in Real Propagation Environments", PhD dissertation, Lund University, 2016. [online]. Available: https://lucris.lub.lu.se/ws/files/3820621/8569798.pdf

39. Kosmowski, K., and Pawelec, J. (2010). A Stochastic Model of Channel Correlation in MIMO Systems. *Rozdział W: Concepts and Implementations for Innovative Military Communications and Information Technologies. Monografia pod redakcją Marka Amanowicza. Redakcja Wydawnictw Wojskowej Akademii Technicznej*.

40. V. Raghavan, J. H. Kotecha and A. M. Sayeed, "Why Does the Kronecker Model Result in Misleading Capacity Estimates?," in *IEEE Transactions on Information Theory*, vol. 56, no. 10, pp. 4843-4864, Oct. 2010, doi: 10.1109/TIT.2010.2059811.

41. J. W. Wallace and M. A. Jensen, "Modeling the indoor MIMO wireless channel," in *IEEE Transactions on Antennas and Propagation*, vol. 50, no. 5, pp. 591-599, May 2002.

42. T. Zwick, C. Fischer and W. Wiesbeck, "A stochastic multipath channel model including path directions for indoor environments," in *IEEE Journal on Selected Areas in Communications,* vol. 20, no. 6, pp. 1178-1192, Aug 2002.

43. G. Burr, "Capacity bounds and estimates for the finite scatterers MIMO wireless channel," in *IEEE Journal on Selected Areas in Communications,* vol. 21, no. 5, pp. 812-818, June 2003, doi: 10.1109/JSAC.2003.810291

44. M. Debbah and R. R. Muller, "MIMO channel modeling and the principle of maximum entropy," in *IEEE Transactions on Information Theory*, vol. 51, no. 5, pp. 1667-1690, May 2005.

45. M. Sayeed, "Deconstructing multiantenna fading channels," in *IEEE Transactions on Signal Processing,* vol. 50, no. 10, pp. 2563-2579, Oct 2002.

46. J. Aulin, "Benefits of variation of large scale fading across large antenna arrays," *2015 9th European Conference on Antennas and Propagation (EuCAP), Lisbon*, 2015, pp. 1-5.

47. Yang, Z. He, C. Xing, Z. Fei and J. Kuang, "The Role of Large-Scale Fading in Uplink Massive MIMO Systems," in *IEEE Transactions on Vehicular Technology,* vol. 65, no. 1, pp. 477-483, Jan. 2016.

48. J. -S Jiang and M. A. Ingram, "Spherical-wave model for short-range MIMO," in *IEEE Transactions on Communications*, vol. 53, no. 9, pp. 1534-1541, Sept. 2005, doi: 10.1109/TCOMM.2005.852842.

49. F. Bohagen, P. Orten and G. E. Oien, "Modeling of Line-of-Sight 2 × 2 MIMO Channels: Spherical Versus Plane Waves," *2006 IEEE 17th International Symposium on Personal, Indoor and Mobile Radio Communications*, 2006, pp. 1-5, doi: 10.1109/PIMRC.2006.254307.

50. Z. Zhou, X. Gao, J. Fang and Z. Chen, "Spherical Wave Channel and Analysis for Large Linear Array in LoS Conditions,"*2015 IEEE Globecom Workshops (GC Wkshps)*, 2015, pp. 1-6, doi: 10.1109/GLOCOMW.2015.7414041.

51. E. G. Larsson, O. Edfors, F. Tufvesson and T. L. Marzetta, "Massive MIMO for next generation wireless systems," in *IEEE Communications Magazine*, vol. 52, no. 2, pp. 186-195, February 2014, doi: 10.1109/MCOM.2014.6736761.

52. J. Wang, H. Zhu, L. Dai, N. J. Gomes and J. Wang, "Low-Complexity Beam Allocation for Switched-Beam Based Multiuser Massive MIMO Systems," in *IEEE Transactions on Wireless Communications*, vol. 15, no. 12, pp. 8236-8248, Dec. 2016, doi: 10.1109/TWC.2016.2613517.

53. S. Wu, C. -X. Wang, E. -H. M. Aggoune and M. M. Alwakeel, "A novel Kronecker-based stochastic model for massive MIMO channels," *2015 IEEE/CIC International Conference on Communications in China (ICCC)*, 2015, pp. 1-6, doi: 10.1109/ICCChina.2015.7448642.

54. Yi Xie, Bo Li, Xiaoya Zuo, Mao Yang and Zhongjiang Yan, "A 3D geometry based stochastic model for 5G massive MIMO channels," *Heterogeneous Networking for Quality, Reliability, Security and Robustness (QSHINE),* 2015 11th International Conference on, Taipei, 2015, pp. 216-222.

55. J. Weng, X. Tu, Z. Lai, S. Salous, and J. Zhang, "Indoor Massive MIMO Channel Modelling Using Ray-Launching Simulation," *International Journal of Antennas and Propagation,* vol. 2014, p. 279380, 2014/08/06 2014, doi: 10.1155/2014/279380.

56. X. Tu, H. Hu, Z. Lai, J. M. Gorce and J. Zhang, "Performance comparison of MR-FDPF and ray launching in an indoor office scenario," *Antennas and Propagation Conference (LAPC), 2013* Loughborough, UK, 2013, pp. 424-428 doi: 10.1109/LAPC.2013.6711934.

57. F. Bentosela, H. D. Cornean, A. Farhang and N. Marchetti, "On the Sublinear Behavior of Massive Multi-User MIMO Sum-Rates for Deterministic Channel Models," in *IEEE Transactions on Communications*, vol. 64, no. 10, pp. 4209-4223, Oct. 2016, doi: 10.1109/TCOMM.2016.2599877.

58. Q. U. A. Nadeem, A. Kammoun, M. Debbah and M. S. Alouini, "On the mutual information of 3D massive MIMO systems: An asymptotic approach," *2015 IEEE International Symposium on Information Theory (ISIT),* Hong Kong, 2015, pp. 2588-2592.

59. S. L. H. Nguyen and A. Ghrayeb, "Compressive sensing-based channel estimation for massive multiuser MIMO systems," *2013 IEEE Wireless Communications and Networking Conference (WCNC),* Shanghai, China, 2013, pp. 2890-2895.

60. J. Hoydis, C. Hoek, T. Wild and S. ten Brink, "Channel measurements for large antenna arrays," *2012 International Symposium on Wireless Communication Systems (ISWCS), Paris,* 2012, pp. 811-815.

61. W. Li, L. Liu, C. Tao, Y. Lu, J. Xiao and P. Liu, "Channel measurements and angle estimation for massive MIMO systems in a stadium," *2015 17th International Conference on Advanced Communication Technology (ICACT),* Seoul, 2015, pp. 105-108.

62. À O. Martínez, E. De Carvalho and J. Ø Nielsen, "Towards very large aperture massive MIMO: A measurement based study," *2014 IEEE Globecom Workshops (GC Wkshps)*, Austin, TX, 2014, pp. 281-286.

63. M. Gauger, J. Hoydis, C. Hoek, H. Schlesinger, A. Pascht and S. t. Brink, "Channel Measurements with Different Antenna Array Geometries for Massive MIMO Systems," *SCC 2015; Proceedings of 10th International ITG Conference on Systems, Communications and Coding*, Hamburg, Germany, 2015, pp. 1-6.

64. S. Sangodoyin et al., "Cluster-based analysis of 3D MIMO channel measurement in an urban environment," *Military Communications Conference, MILCOM 2015 - 2015 IEEE,* Tampa, FL, 2015, pp. 744-749.

65. V. Kolmonen *et al*., "A Dynamic Dual-Link Wideband MIMO Channel Sounder for 5.3 GHz," in *IEEE Transactions on Instrumentation and Measurement*, vol. 59, no. 4, pp. 873-883, April 2010, doi: 10.1109/TIM.2009.2026608.

66. Fang, C., Liu, E., & Ur Rehman, M. “Analysis of Sub-Channel Correlation in Dual-Polarised MIMO Systems via a Polarisation Diversity Scheme”. *IEEE Transactions on Antennas and Propagation, PP*, 1-1, 2017. doi:10.1109/TAP.2017.2673765

67. X. Gao, O. Edfors, F. Rusek and F. Tufvesson, "Massive MIMO Performance Evaluation Based on Measured Propagation Data," in *IEEE Transactions on Wireless Communications*, vol. 14, no. 7, pp. 3899-3911, July 2015.

68. P. Harris et al., "Performance Characterization of a Real-Time Massive MIMO System With LOS Mobile Channels," in *IEEE Journal on Selected Areas in Communications*, vol. 35, no. 6, pp. 1244-1253, June 2017, doi: 10.1109/JSAC.2017.2686678

69. L. Lu, G. Y. Li, A. L. Swindlehurst, A. Ashikhmin and R. Zhang, "An Overview of Massive MIMO: Benefits and Challenges," in *IEEE Journal of Selected Topics in Signal Processing*, vol. 8, no. 5, pp. 742-758, Oct. 2014, doi: 10.1109/JSTSP.2014.2317671.

70. J. Jose, A. Ashikhmin, T. L. Marzetta and S. Vishwanath, "Pilot Contamination and Precoding in Multi-Cell TDD Systems," in *IEEE Transactions on Wireless Communications*, vol. 10, no. 8, pp. 2640-2651, August 2011, doi: 10.1109/TWC.2011.060711.101155.

71. J. Hoydis, S. ten Brink, and M. Debbah, “Massive MIMO in the UL/DL of Cellular Networks: How Many Antennas Do We Need?,” *IEEE Journal on Selected Areas in Communications*, vol. 31, no. 2, pp. 160-171, 2013.

72. L. Yang, N. Young-Han, N. Boon Loong, and Z. Jianzhong, "A non-asymptotic throughput for massive MIMO cellular uplink with pilot reuse," in *2012 IEEE Global Communications Conference (GLOBECOM)*, 3-7 Dec. 2012 2012, pp. 4500-4504, doi: 10.1109/GLOCOM.2012.6503827.

73. K. Appaiah, A. Ashikhmin and T. L. Marzetta, "Pilot Contamination Reduction in Multi-User TDD Systems," *2010 IEEE International Conference on Communications*, 2010, pp. 1-5, doi: 10.1109/ICC.2010.5502810.

74. F. Rusek *et al*., "Scaling Up MIMO: Opportunities and Challenges with Very Large Arrays," in *IEEE Signal Processing Magazine*, vol. 30, no. 1, pp. 40-60, Jan. 2013, doi: 10.1109/MSP.2011.2178495.

75. G. J. Foschini, and M. J. Gans, “On Limits of Wireless Communications in a Fading Environment when Using Multiple Antennas,” *Wireless Personal Communications,* vol. 6, no. 3, pp. 311-335, 1998/03/01, 1998.

76. W. Yu, W. Rhee, S. Boyd and J. M. Cioffi, "Iterative water-filling for Gaussian vector multiple-access channels," in *IEEE Transactions on Information Theory*, vol. 50, no. 1, pp. 145-152, Jan. 2004, doi: 10.1109/TIT.2003.821988.

77. G. Caire and S. Shamai, "On the achievable throughput of a multiantenna Gaussian broadcast channel," in *IEEE Transactions on Information Theory*, vol. 49, no. 7, pp. 1691-1706, July 2003, doi: 10.1109/TIT.2003.813523.

78. M. Sharif and B. Hassibi, "On the capacity of MIMO broadcast channels with partial side information," in *IEEE Transactions on Information Theory*, vol. 51, no. 2, pp. 506-522, Feb. 2005, doi: 10.1109/TIT.2004.840897.

79. S. Vishwanath, N. Jindal and A. Goldsmith, "Duality, achievable rates, and sum-rate capacity of Gaussian MIMO broadcast channels," in *IEEE Transactions on Information Theory*, vol. 49, no. 10, pp. 2658-2668, Oct. 2003, doi: 10.1109/TIT.2003.817421.

80. H. Weingarten, Y. Steinberg and S. S. Shamai, "The Capacity Region of the Gaussian Multiple-Input Multiple-Output Broadcast Channel," in *IEEE Transactions on Information Theory*, vol. 52, no. 9, pp. 3936-3964, Sept. 2006, doi: 10.1109/TIT.2006.880064.

81. W. Yu and J. M. Cioffi, "Trellis precoding for the broadcast channel," *GLOBECOM'01. IEEE Global Telecommunications Conference (Cat. No.01CH37270)*, 2001, pp. 1344-1348 vol.2, doi: 10.1109/GLOCOM.2001.965707.

82. R. Zamir, S. Shamai and U. Erez, "Nested linear/lattice codes for structured multiterminal binning," in *IEEE Transactions on Information Theory*, vol. 48, no. 6, pp. 1250-1276, June 2002, doi: 10.1109/TIT.2002.1003821.

83. C. B. Peel, B. M. Hochwald and A. L. Swindlehurst, "A vector-perturbation technique for near-capacity multiantenna multiuser communication-part I: channel inversion and regularization," in *IEEE Transactions on Communications*, vol. 53, no. 1, pp. 195-202, Jan. 2005, doi: 10.1109/TCOMM.2004.840638.

84. L. Zheng, D. N. C. Tse and M. Medard, "Channel Coherence in the Low-SNR Regime," in *IEEE Transactions on Information Theory*, vol. 53, no. 3, pp. 976-997, March 2007, doi: 10.1109/TIT.2006.890777.

85. B. M. Hochwald, T. L. Marzetta, and V. Tarokh, “Multiple-antenna channel hardening and its implications for rate feedback and scheduling,” *IEEE Transactions on Information Theory,* vol. 50, no. 9, pp. 1893-1909, 2004.

86. [0nline] Available from: https://ieeexplore.ieee.org/mediastore_new/IEEE/content/media/5962382/8809239/8680715/cheng1-2909019-large.gif

87. E. G. Larsson, "MIMO Detection Methods: How They Work [Lecture Notes]," in *IEEE Signal Processing Magazine,* vol. 26, no. 3, pp. 91-95, May 2009.

88. J. Li et al., "On 3D Cluster-Based Channel Modeling for Large-Scale Array Communications," in *IEEE Transactions on Wireless Communications,* vol. 18, no. 10, pp. 4902-4914, Oct. 2019.

89. M. M. Tamaddondar and N. Noori, "Plane wave against spherical wave assumption for non-uniform linear massive MIMO array structures in LOS condition," *2017 Iranian Conference on Electrical Engineering (ICEE),* Tehran, 2017, pp. 1802-1805.

90. C. F. López, C. Wang and R. Feng, "A novel 2D non-stationary wideband massive MIMO channel model," *2016 IEEE 21st International Workshop on Computer Aided Modelling and Design of Communication Links and Networks (CAMAD),* Toronto, ON, 2016, pp. 207-212.

91. H. Jiang, Z. Zhang, J. Dang and L. Wu, "A Novel 3-D Massive MIMO Channel Model for Vehicle-to-Vehicle Communication Environments," in *IEEE Transactions on Communications,* vol. 66, no. 1, pp. 79-90, Jan. 2018, doi: 10.1109/TCOMM.2017.2751555.

92. J. Chen, S. Wang and X. Yin, "A Spherical-Wavefront-Based Scatterer Localization Algorithm Using Large-Scale Antenna Arrays," in *IEEE Communications Letters*, vol. 20, no. 9, pp. 1796-1799, Sept. 2016.

93. S. Wu. “Massive MIMO Channel Modelling for 5G Wireless Communication Systems.” https://core.ac.uk/download/pdf/77035819 .pdf 2015 (Accessed June 17, 2023)

94. S. Lu, H. T. Hui and M. Bialkowski, "Optimizing MIMO Channel Capacities Under the Influence of Antenna Mutual Coupling," in *IEEE Antennas and Wireless Propagation Letters*, vol. 7, pp. 287-290, 2008, doi: 10.1109/LAWP.2008.928474.

95. Z. Yun and M. F. Iskander, "Ray Tracing for Radio Propagation Modeling: Principles and Applications," in *IEEE Access,* vol. 3, pp. 1089-1100, 2015, doi: 10.1109/ACCESS.2015.2453991.

96. G. E. Athanasiadou and A. R. Nix, "Investigation into the sensitivity of the power predictions of a microcellular ray tracing propagation model," in *IEEE Transactions on Vehicular Technology*, vol. 49, no. 4, pp. 1140-1151, July 2000, doi: 10.1109/25.875221.

97. G. E. Athanasiadou and A. R. Nix, "A novel 3-D indoor ray-tracing propagation model: The path generator and evaluation of narrow-band and wide-band predictions," *IEEE Transactions on Vehicular Technology,* vol. 49, pp. 1152-1168, 08/01 2000, doi: 10.1109/25.875222.

98. Remcom. “High Fidelity Ray Tracing”. https://www.remcom.com/wireless-insite-models/high-fidelity-ray-tracing (Accessed May 31, 2022).

99. D. Tse and P. Viswanath, *Fundamentals of wireless communication*. New York: Cambridge University Press, 2005.

100. G. E. Athanasiadou, A. R. Nix and J. P. McGeehan, "A ray tracing algorithm for microcellular wideband propagation modelling," *1995 IEEE 45th Vehicular Technology Conference. Countdown to the Wireless Twenty-First Century*, 1995, pp. 261-265 vol.1, doi: 10.1109/VETEC.1995.504869.

101. F. Bohagen, “Design of capacity-optimal high-rank line-of-sight MIMO channels,” Submitted to IEEE Trans. Wireless Commun., Available from: http://www.unik.no/~frodbo/)

102. H. Q. Ngo, E. G. Larsson and T. L. Marzetta, "Aspects of favorable propagation in Massive MIMO," *2014 22nd European Signal Processing Conference (EUSIPCO)*, 2014, pp. 76-80.

103. C. Zhong, M. R. McKay, T. Ratnarajah and K. -K. Wong, "Distribution of the Demmel Condition Number of Complex Wishart Matrices," *2010 IEEE Global Telecommunications Conference GLOBECOM 2010*, 2010, pp. 1-5, doi: 10.1109/GLOCOM.2010.5684238.

104. H. Artes, D. Seethaler and F. Hlawatsch, "Efficient detection algorithms for MIMO channels: a geometrical approach to approximate ML detection," in *IEEE Transactions on Signal Processing*, vol. 51, no. 11, pp. 2808-2820, Nov. 2003, doi: 10.1109/TSP.2003.818210.

105. S. K. Sharma, S. Chatzinotas and B. Ottersten, "The effect of noise correlation on fractional sampling based spectrum sensing," *2013 IEEE International Conference on Communications (ICC)*, 2013, pp. 2589-2594, doi: 10.1109/ICC.2013.6654925.

106. R. W. Heath, S. Sandhu and A. Paulraj, "Antenna selection for spatial multiplexing systems with linear receivers," in *IEEE Communications Letters,* vol. 5, no. 4, pp. 142-144, April 2001, doi: 10.1109/4234.917094.

107. R. W. Heath and D. J. Love, "Multimode antenna selection for spatial multiplexing systems with linear receivers," in *IEEE Transactions on Signal Processing*, vol. 53, no. 8, pp. 3042-3056, Aug. 2005, doi: 10.1109/TSP.2005.851109.

108. T. Chan, M. Hamdi, C. Cheung, and M. Ma, "A link adaptation algorithm in MIMO-based WiMAX systems," *Journal of Communications,* vol. 2, 08/01 2007, doi: 10.4304/jcm.2.5.16-24.

109. N. Kita, W. Yamada, A. Sato, D. Mori and S. Uwano, "Measurement of Demmel condition number for 2/spl times/2 MIMO-OFDM broadband channels," *2004 IEEE 59th Vehicular Technology Conference*. VTC 2004-Spring (IEEE Cat. No.04CH37514), 2004, pp. 294-298 Vol.1, doi: 10.1109/VETECS.2004.1387961.

110. Roivainen, C. Ferreira Dias, N. Tervo, V. Hovinen, M. Sonkki and M. Latva-aho, "Geometry-Based Stochastic Channel Model for Two-Story Lobby Environment at 10 GHz," in *IEEE Transactions on Antennas and Propagation*, vol. 64, no. 9, pp. 3990-4003, Sept. 2016, doi: 10.1109/TAP.2016.2583460.

111. Y. Mlayeh, F. Rouissi, F. Tlili and A. Ghazel, "Performances of switching algorithm methods in MIMO-OFDM systems," *2011 18th IEEE International Conference on Electronics, Circuits, and Systems*, 2011, pp. 784-787, doi: 10.1109/ICECS.2011.6122391.

112. M S. Mukherjee, S. S. Das, A. Chatterjee and S. Chatterjee, "Analytical Calculation of Rician K-Factor for Indoor Wireless Channel Models," in *IEEE Access*, vol. 5, pp. 19194-19212, 2017, doi: 10.1109/ACCESS.2017.2750722.

113. S. K. Jayaweera and H. V. Poor, "Capacity of multiple-antenna systems with both receiver and transmitter channel state information," in *IEEE Transactions on Information Theory,* vol. 49, no. 10, pp. 2697-2709, Oct. 2003, doi: 10.1109/TIT.2003.817479. (See also corrigendum: K. Singh and C. Singh, "Comments and Corrections to “Capacity of Multiple-Antenna Systems With Both Receiver and Transmitter Channel State Information”," in *IEEE Transactions on Information Theory,* vol. 67, no. 8, pp. 5614-5622, Aug. 2021, doi: 10.1109/TIT.2021.3085248.)

114. H C. L. Holloway, D. A. Hill, J. M. Ladbury, P. F. Wilson, G. Koepke and J. Coder, "On the Use of Reverberation Chambers to Simulate a Rician Radio Environment for the Testing of Wireless Devices," in *IEEE Transactions on Antennas and Propagation,* vol. 54, no. 11, pp. 3167-3177, Nov. 2006, doi: 10.1109/TAP.2006.883987.

115. C. Lemoine, E. Amador, P. Besnier, J. Floc'h and A. Laisné, "Antenna Directivity Measurement in Reverberation Chamber From Rician K-Factor Estimation," in *IEEE Transactions on Antennas and Propagation,* vol. 61, no. 10, pp. 5307-5310, Oct. 2013, doi: 10.1109/TAP.2013.2272691.

116. J. Li and Y. Zhao, "Channel characterization and modeling for large-scale antenna systems," *2014 14th International Symposium on Communications and Information Technologies (ISCIT)*, 2014, pp. 559-563, doi: 10.1109/ISCIT.2014.7011977.

117. A. Asokan and J. Anitha, "Change detection techniques for remote sensing applications: a survey," *Earth Science Informatics,* vol. 12, no. 2, pp. 143-160, 2019/06/01 2019, doi: 10.1007/s12145-019-00380-5.

118. R. Chataut and R. Akl, "Massive MIMO Systems for 5G and beyond Networks—Overview, Recent Trends, Challenges, and Future Research Direction," *Sensors*, vol. 20, no. 10, p. 2753, May 2020, doi: 10.3390/s20102753.

119. M. Dryjański, Ł. Kułacz, and A. Kliks, "Toward Modular and Flexible Open RAN Implementations in 6G Networks: Traffic Steering Use Case and O-RAN xApps," *Sensors*, vol. 21, no. 24, p. 8173, Dec. 2021, doi: 10.3390/s21248173.

120. J. Wang, H. Zhu, L. Dai, N. J. Gomes and J. Wang, "Low-Complexity Beam Allocation for Switched-Beam Based Multiuser Massive MIMO Systems," in *IEEE Transactions on Wireless Communications*, vol. 15, no. 12, pp. 8236-8248, Dec. 2016, doi: 10.1109/TWC.2016.2613517.

121. J. Butler and R. Lowe, "Beam-forming Matrix Simplifies Design of Electrically Scanned Antennas," *Electronic Design*, April 1961.

122. R. Shafin, H. Chen, Y. H. Nam, S. Hur, J. Park, J. Zhang, J. Reed, and L. Liu. "Self-Tuning Sectorization: Deep Reinforcement Learning Meets Broadcast Beam Optimization," *IEEE Transactions on Wireless Communications,* vol. 19, no. 6, pp. 4038-4053, 2020, doi: 10.1109/TWC.2020.2979446.

123. S. Chen, S. Sun, G. Xu, X. Su and Y. Cai, "Beam-Space Multiplexing: Practice, Theory, and Trends, From 4G TD-LTE, 5G, to 6G and Beyond," in *IEEE Wireless Communications*, vol. 27, no. 2, pp. 162-172, April 2020.

124. A. Omri, M. Shaqfeh, A. Ali and H. Alnuweiri, "Synchronization Procedure in 5G NR Systems," in *IEEE Access*, vol. 7, pp. 41286-41295, 2019, doi: 10.1109/ACCESS.2019.2907970.

125. MathWorks. "5G Toolbox" https://uk.mathworks.com/products/5g.html (Accessed June 23, 2023).

126. S. P. Brooks and B. J. T. Morgan, "Optimization Using Simulated Annealing," *Journal of the Royal Statistical Society: Series D (The Statistician),* vol. 44, no. 2, pp. 241-257, 1995, doi: https://doi.org/10.2307/2348448.

127. S. Kirkpatrick, C. D. Gelatt, and M. P. Vecchi, "Optimization by Simulated Annealing," *Science,* vol. 220, no. 4598, pp. 671-680, 1983, doi: doi:10.1126/science.220.4598.671.

128. A. Ghosh and R. Ratasuk, *Essentials of LTE and LTE-A* (The Cambridge Wireless Essentials Series). Cambridge: Cambridge University Press, 2011.

129. Comtech. "Signal to Interference plus noise ratio." https://comtech.vsb.cz/qualmob/sinr_lte.html (Accessed May 15, 2023)

130. Flann Microwave. "Standard Gain Horns Series 240." https://flann.com/products/antennas/standard-gain-horns-series-240/ (Access June 23, 2023)